Mechanisms of co-stimulatory and inhibitory receptors in human cancer-specific cytotoxic T cells



Megat Hafizzuddin Bin Abd Hamid

Thesis Submitted for the Degree of Doctor of Philosophy

St Cross College

Trinity Term 2019

Supervisors

Professor Tao Dong

Dr Yanchun Peng

MRC Human Immunology Unit

Weatherall Institute of Molecular Medicine

Radcliffe Department of Medicine

University of Oxford

John Radcliffe Hospital

Oxford OX3 9DS

Mechanisms of co-stimulatory and inhibitory receptors in human cancer-specific cytotoxic T cells

Megat Hafizzuddin Bin Abd Hamid, St Cross College, Oxford

D. Phil Thesis, Trinity Term 2019

Abstract

Clinical studies have shown that the upregulation of immunocheckpoints such as PD-1 on tumor-infiltrating T lymphocytes (TILs) can impair the clinical outcome of cancer patients. However, current immunocheckpoints-targeting immunotherapies have failed to improve response in some patients and cancer types. This is likely due to the heterogeneity of the tumor immune composition, the overall complex TILs immunophenotype and the influence of the immunosuppressive tumor microenvironment. It is therefore important to assess the characteristics and mechanisms of TILs, especially cancer-specific cytotoxic $CD8^+$ T cells (CTLs), in order to develop more effective T cell immunotherapy strategies.

In this study, comprehensive assessment using paired tumor, paratumor and peripheral blood from cancer patients demonstrated concomitant upregulation of both inhibitory CD94/NKG2a receptor and its HLA-E ligand in tumor. Although their engagement has been described on NK cells, it remains unclear whether this interaction could constitute an additional immunocheckpoint of cancer-specific CTLs in cancer. We demonstrated that the engagement of NKG2a and HLA-E resulted in impaired anti-tumor cytotoxicity, cytokine production and proliferation of CTLs, which recovered following antibody-blockade treatment. In contrast, the antagonistic NKG2a and CD103 expression on TILs suggest a distinct anti-tumor role of CD103. The $CD103^+$ cancer-specific CTLs were found to self-produce TGF-β to sustain own CD103 expression, have improved TCR antigen sensitivity, faster cancer killing and elevated energy potential. However, they are more susceptible to apoptosis after prolonged cancer exposure. In addition, we demonstrated that a sizeable portion of cancer-specific CTLs lacks IFNγ expresssion and production, and discovered that this is contributed by CpG hypermethylation of its IFNγ promoter.

In summary, this study carried out in-depth investigation into the impacts of the inhibitory receptor NKG2a, costimulatory receptor CD103, and epigenetic DNA methylation, on anti-tumor T cell responses. The thorough understanding of these key factors in affecting cancer-specific CTL functions and their restoration potential, could be important for future designs of more effective cancer immunotherapy strategies.

Declaration

I declare that the work presented in this D.Phil thesis entitled “Mechanisms of co-stimulatory and inhibitory receptors in human cancer-specific cytotoxic T cells” is entirely my work, except for where the contributions of collaborators have been clearly acknowledged. No part of this thesis has been submitted for any other degree or other qualification in this University or elsewhere.

Megat Hafizzuddin Bin Abd Hamid

MRC Human Immunology Unit,

Weatherall Institute of Molecular Medicine,

Radcliffe Department of Medicine,

University of Oxford.

Trinity Term, 2019.

Acknowledgements

I would like to thank my supervisors, Professor Tao Dong and Dr Yanchun Peng for taking me under their supervision for the past four years of study. Their knowledge, advice, support, patience and guidance throughout the course of my D.Phil have been invaluable during this time. I would particularly like to thank Tao for the directions of the study given, her enthusiasm, thought-provoking ideas and patience throughout the years as well as providing the opportunities for the exciting and unforgettable summer and winter work travels in China. Importantly, thank you Tao for the support given especially during the personal and family matters that I experienced last year. Furthermore, I would also like to greatly thank Peng for all her advices, assistance, patience, clarifications on multitude of information and importantly, in passing on a wealth of knowledge about cell culture techniques and assays throughout the D.Phil journey. I would also like to thank Professor Andrew McMichael and Professor Alain Townsend for all their great advices and excellent ideas, especially as members of my Thesis Committee. I would further like to thank the Malaysian Government for providing me the King's Scholarship and in helping me to start pursuing my D.Phil study and dream here in Oxford.

Further thanks to Xuan Yao for all the help and support in the countless hours of optimizing and tirelessly working with me on the experiments undertaken, and importantly for all her encouragement, advices and supports both in Oxford and in China. Also, not to forget all current and past members of the Dong's group for the advices and support throughout the study process. I would also like to thank our collaborators for their assistance during this study. Special thanks to Professor Christopher Conlon and Professor Vincenzo Cerundolo for their assistance and advices, especially during the submission of the manuscripts for publications.

Thank you to Professor Rou-zheng Wang for all her support during my wonderful time in Xinjiang, and for Peiwen Fan, Xuimei Chang and Yaning Feng for making the experience in Xinjiang a wonderful, happy and excellent time. Huge thanks to Huw Colin-York and Marco Fritzsche, not only for their help on the *in vitro* imaging, but also for all the great ideas, help and thoughtful discussion. Thank you Jili Chen for providing some of the cancer-specific CTLs; Nasullah Alham, Molly Browne and Lucia Cerundolo for their help in tumor tissue IHC experiments and analysis; Clare Hardman and Janina Nahler on their knowledge on transwell migration assay and Djamila Ouaret for her huge knowledge on epithelial cancer cells. Further thanks to Professor Clare Verrill and her team, including David Maldonando-Perez, Emma Bowes and Stephanie Jones for providing us the precious cancer patients samples in Oxford. Lastly, huge thanks to the support staff of WIMM, especially Craig Waugh for all the long hours of cell sorting and idle but nice conversations to fill up the time. To Sally Ann-Clark for her additional FACS help, and to Tim Rostron and John Frankland for the help in huge numbers of sequencing performed. I would also like to thank my friends especially Marahaini, Huzaifah, Zarina, Samara, Ilham, Rabeah, Aslam, Hakimi and Adli, which have since completed or still pursuing their studies in Oxford or somewhere abroad, for all the good times and non-study related support and fun.

Last, but most importantly, I would like to thank my family, especially my mum (Mama), father (Abah) and sister (Ayong) as well as my five little cats back home in Malaysia for all their supports and patience during my D.Phil journey. Thank you for being there for all the good and hard times, for the endless moral and emotional supports, during the up and down in family matters especially last year. Thank you for making me the person that I am now, and I would not be here without my family. I love you guys so so much and this D.Phil is for you.

Publications and Awards

Publications

Abd Hamid M, Wang R, Yao X, Fan P, Li X, Chang X, Feng Y, Jones S, Maldonado-Perez D, Waugh C, Verrill C, Simmons A, Cerundolo V, McMichael A, Conlon C, Wang X, Peng Y, Dong T. Enriched HLA-E and CD94/NKG2a interaction limits antitumor $CD8^+$ tumor-infiltrating T lymphocytes responses. *Cancer Immunology Research*, 2019; 7(8):1293-306.

Abd Hamid M, Colin-York H, Alham NK, Browne M, Cerundolo L, Chen J, Y X, Rosendo-Machado S, Waugh C, Maldonado-Perez D, Bowes E, Verrill C, Cerundolo V, Conlon C, Fritszsche M, Peng Y, Dong T. Self-maintaining $CD103^+$ cancer-specific T cells are highly energetic with rapid cytotoxic and effector responses. *Cancer Immunology Research (early publication* November 2019*;* DOI:10.1158/2366-6066.CIR-19-0554).

Abd Hamid M, Yao X, Waugh C, Rosendo-Machado S, Li C, Rostron T, Frankland J, Peng Y, Dong T. Defective IFNγ production by tumor-specific $CD8^+$ T cells is associated with CpG hypermethylation of IFNγ promoter. *Manuscript accepted by Frontiers in Immunology*, January 2020.

Kanellakis NI, Asciak R, **Abd Hamid M**, Yao X, McCole M, McGowan S, Seraia E, Hatch S, Bedawi EO, Mercer R, Hallifax R, Jones S, Verrill, C, Dobson M, George V, Stathopoulos G, Peng Y, Ebner D, Dong T, Rahman NM, Psallidas I. Patient-derived malignant pleural mesothelioma cell cultures: A tool to advance biomarker-driven treatments. *Submitted.*

Awards

Malaysia's King Scholarship (Biasiswa Yang di-Pertuan Agong), Majlis Raja-Raja Melayu, Public Service Department of Malaysia.

WIMM Student Travel Fund, For attending (i) 2019 Keystone Conference C2: Cancer Immunotherapy: Mechanistic Insights to Improve Clinical Benefit, Vancouver, Canada, and (ii) 2019 17th International Congress of Immunology, Beijing, China.

Abstracts/Conferences

Poster presentation: Enriched HLA-E and CD94/NKG2a interaction attenuates tumor-infiltrating CD8^{+} T lymphocytes responses. Keystone Conference C2: Cancer Immunotherapy: Mechanistic Insights to Improve Clinical Benefit, Vancouver, Canada. 2019.

Poster presentation: Enriched HLA-E and CD94/NKG2a interaction limits anti-tumor CD8^{+} tumor-infiltrating T lymphocytes responses. 17th International Congress of Immunology, Beijing, China. 2019.

Poster presentation: Identifying HLA-E:CD94/NKG2a as a potential target for cancer immunotherapy. CRUK MRC Oxford Institute for Radiation Oncology, Wolfson College. 2018.

Poster presentation: Identification of HLA-E:CD94/NKG2a as a potential immune checkpoint receptor in cancer. WIMM Day, Said Business School. 2018.

Oral presentation: Identifying HLA-E and CD94/NKG2a as an inhibitory receptor-ligand in cancer. MRC Human Immunology Unit Friday Morning Talk, WIMM. 2019.

List of Abbreviations

2-DG	2-deoxy-glucose
7-AAD	7-aminoactinomycin D
ANOVA	analysis of variance
APCs	antigen-presenting cells
Akt	protein kinase B
APP	analysis protocol package
AP-1	activator protein-1
ATF	activating transcription factor
B_2m	beta-2-microglobulin
BCL	B cell lymphoblastoid
Bcl2	B cell lymphoma 2
BTLA	B and T lymphocytes associated
BIRC3	baculoviral IAP repeat containing 3
CCL-5	chemokine C-C motif ligand-5
CCR7	chemokine receptor 7
CD	cluster of differentiation
CDR	complementarity determining region

CFSE	carbocyflourescein succinimidyl ester
CMV	cytomegalovirus
CREB	cAMP response element binding protein
CSC	cancer stem cell
CTA	cancer-testis antigen
CpG	5’-methylcytosine-guanine dinucleotide
CTLA-4	cytotoxic T-lymphocytes-associated protein-4
CTLs	cytotoxic T cells
DAG	diacylglycerol
DMEM	Dulbecco Modified Eagle Media
DNA	deoxyribonucleic acid
DNMT3a	DNA methyltransferases 3a
DCs	dendritic cells
cDCs	conventional dendritic cells
dNTP	deoxynucleoside triphosphate
EBV	Epstein-Barr virus
ECAR	extracellular acidification rate
EGFR	epithelial growth factor receptor

ER	endoplasmic reticulum
ERK	extracellular signal-related kinase
EZH2	enhancer of zester homolog 2
FACS	flow cytometry cell sorting
Fas-L	Fas ligand
FCCP	carbonyl cyanide-p-triflouromethoxyphenylhydrazone
FDA	Food and Drugs Administration
gDNA	genomic deoxyribonucleic acid
GLOBOCAN	Global Cancer Incidence, Mortality and Prevalence
HLA	human leukocyte antigen
HIV-1	Human Immunodeficiency virus-1
HSV	herpes simplex virus
ICOS	inducible co-stimulator
IFNγ	Interferon gamma
IL-2	Interleukin 2
IL-2R	Interleukin 2 receptor
IFNGR	interferon gamma receptor
IP_3	inositol triphosphate

ITAM	immunoreceptor tyrosine-based activating motif
ITIM	immunoreceptor tyrosine-based inhibitory motif
IS	immunological synapse
JAK	janus tyronsine kinase
LAMP-1	lysosome-associated membrane protein-1
LAT	linker for the activation of T cells
KIRs	killer-cell immunoglobulin-like receptors
KLF2	krupper like factor 2
KLRG-1	killer cell lectin-like receptor subfamily G member-1
MAPK	mitogen activated protein kinase
MHC	major histocompatibility complex
mRNA	messenger ribonucleic acid
Mtb	Mycobacterium tuberculosis
NFAT	nuclear factor of activated T cells
NF-κB	nuclear factor-kappa B
NK cells	natural killer cells
NKT cells	invariant natural killer T cells
NY-ESO-1	New York-esophageal squamous cell carcinoma-1

ORB	Oxford Radcliffe Biobank
OCR	oxygen consumption rate
PBMC	peripheral blood mononuclear cells
PCR	polymerase chain reaction
PD-1	programmed cell death protein-1
PI3K	phosphoinositide-3
PDL	programmed cell death ligand
PKCθ	protein kinase C theta
PLCγ1	phospholipase Cγ1
$PI(4,5)P_2$	phospholipid phosphatidylinositol 4,5 biphosphate
RNA	ribonucleic acid
RPMI	roswell park memorial institute
ROI	region of interest
S1PR1	sphingosine-1-phosphate receptor 1
SEB	staphylococcal enterotoxin B
SIV	simian immunodeficiency virus
SHP	SH2-domain containing tyrosine phosphatase
STAT	signal transducer and activator of transcription

SLP-76	SH2 domain-containing leukocyte phosphoprotein of 76 kDA
SSX-2	synovial sarcoma X-2
TAA	tumor-associated antigen
TAP	transporter-associated protein
TCR	T cell receptor
TGF-β	tumor growth factor-beta
TGF-βR	tumor growth factor-beta receptor
TILs	tumor-infiltrating T lymphocytes
Tim3	T cell immunoglobulin and mucin-domain containing 3
TIGIT	T cell immunoreceptor with immunoglobulin and ITIM domains
TNFα	Tumor necrosis factor alpha
TNFR	tumor necrosis factor receptor
TNM	tumor, node, metastasis
TRA/TRB	T cell receptor alpha/beta chain
TRAF	TNF receptor associated factor
TRAIL	tumor necrosis factor-related apoptosis inducing ligand
Trm	Tissue-resident memory T cells
ZAP-70	zeta-chain-associated protein kinase-70

Table of Contents

Chapter 1: Introduction 26

1.1 Cancer and human health 26

1.2 Immunity and cancer 26

1.3 Interplay between innate and adaptive immunity 29

1.4 Antigen processing and presentation 31

1.4.1 Human Leucocyte Antigen (HLA) 31

1.4.2 Antigen processing for MHC Class I presentation 34

1.4.3 Antigen presentation by APCs 36

1.5 T cell receptor (TCR) and signaling 38

1.5.1 TCR development 38

1.5.2 TCR signaling 40

1.6 Functions of $CD8^+$ cytotoxic T cells (CTLs) 42

1.6.1 Cytotoxic-mediated responses of CTLs 42

1.6.2 Effector responses of CTLs 44

1.6.3 Proliferation of activated CTLs 46

1.7 Evasion of anti-tumor immunity by dysregulating MHC Class I expression 47

1.7.1 Downregulation of MHC Class Ia surface expression 47

1.7.2 HLA-E in cancer 47

1.7.3 HLA-E recognition by inhibitory CD94/NKG2a receptor 49

1.8 Evasion of anti-tumor immunity by elevating inhibitory receptors expression.....50

1.8.1 CTLA-4 50

1.8.2 PD-1 53

1.8.3 Tim3..... 54

1.8.4 Other related immune checkpoints 55

1.9 Co-stimulatory molecules in aiding T cell immunity 56

1.9.1 CD28 56

1.9.2 4-1BB 57

1.9.3 ICOS 58

1.10 CD103 as a potential co-stimulator of cancer-specific CTLs.....58

1.10.1 CD103 as a T cell surface molecule..... 58

1.10.2 CD103 expression during T cell development 59

1.10.3 Identification of CD103^{+} Trm cells 59

1.10.4 The role of CD103 in healthy setting and disease..... 61

1.11 Evasion of anti-tumor immunity by dysregulating epigenetic processes 62

1.12 The aims of the study.....64

Chapter 2: Materials and Methods..... 65

2.1 Study subjects 65

2.2 Isolation of mononuclear cells from blood and tissues.....65

2.3 Generating antigen-specific T cells in vitro.....65

2.4 Target cell lines used for in vitro functional assays.....69

2.5 Generating HLA-E^{high} EBV-transformed B cell lymphoblastoid (BCL).....70

2.6 Ex vivo flow cytometry staining.....71

2.7 T cell proliferation assay.....74

2.8 Cytokine production assessment.....74

2.9 Intracellular cytokine staining 75

2.10 CFSE-based CTL killing assay.....76

2.11 TCR sequencing.....76

2.12 Migration transwell assay 77

2.13 Mitochondrial and glycolytic analysis.....77

2.14 Live cell imaging 78

2.15 Immunohistochemical analysis.....79

2.16 mRNA expression analysis.....80

2.17 Bisulphite treatment, PCR and methylation sequencing 81

2.18 Statistical analysis.....83

Chapter 3: Enriched HLA-E and CD94/NKG2a interaction limits antitumor CD8^{+} tumor-infiltrating T lymphocytes responses 84

3.1 Introduction.....84

3.2 Results.....86

3.2.1 HLA-E expression is upregulated on specific cell populations in tumor 86

3.2.2 Inhibitory CD94/NKG2a ligand is upregulated on CD8$^+$ TILs 93

3.2.3 CD94/NKG2a and PD-1 are co-expressed on CD8$^+$ TILs 106

3.2.4 CD94/NKG2a$^+$ TILs lack intratumoral CD103 expression 111

3.2.5 CD94/NKG2a$^+$ antigen-specific T cells have impaired proliferation capacity 111

3.2.6 Impaired effector and cytotoxic responses recovered after CD94/NKG2a antibody blockade *in vitro* 115

3.2.7 Recovery of T cell functions after CD94/NKG2a antibody blockade *ex vivo* . 119

3.3 Discussion 122

Chapter 4: Self-maintaining CD103$^+$ cancer-specific CTLs are highly energetic with rapid cytotoxic and effector responses 129

4.1 Introduction 129

4.2 Results 131

4.2.1 Cancer-specific CTLs self-regulate CD103 expression by producing activated TGF-β1 131

4.2.2 CD103 helps to improve tumor antigen sensitivity of CTLs 139

4.2.3 Rapid and accumulating cytotoxicity by CD103$^+$ CTLs 142

4.2.4 CD103$^+$ cancer-specific CTLs have high energetic potential 146

4.2.5 CD103$^+$ CTLs have better homing capacity and localise on E-Cadherin rich tumor cells 151

4.2.6 Prolonged exposure of CD103$^+$ T cells to cancer contributes to T cell death . 158

4.3 Discussion 162

Chapter 5: Defective IFNγ production by cancer-specific CTLs is contributed by CpG hypermethylation of the IFNγ promoter 168

5.1 Introduction.....168

5.2 Results.....170

5.2.1 Several cancer-specific CTL clones have reduced IFNγ expression and impaired cytotoxicity 170

5.2.2 CpG hypermethylation of the IFNγ promoter contributes to the IFNγ defect175

5.2.3 The IFNγ defect is unique to cancer-specific CTLs 175

5.2.4 CpG hypermethylation is associated with reduced IFNγ transcription..... 179

5.3 Discussion..... 183

Chapter 6: Summary and Future Directions 187

References..... 196

List of Figures

Chapter 1

Figure 1.1 Mortality by cancer in 2018.

Figure 1.2 Interplay between innate and adaptive immunity.

Figure 1.3 HLA alleles locations in the chromosome 6p21.31.

Figure 1.4 The antigen processing and presentation on HLA Class I molecule.

Figure 1.5 The domains/regions of T cell receptor of alpha and beta chains.

Figure 1.6 The process of TCR triggering.

Figure 1.7 CpG methylation positions within IFNγ promoter sequence.

Figure 1.8 The Il-2/IL-2-recetor signaling loop.

Figure 1.9 CD94/NKG2a influence on T cells.

Figure 1.10 Known inhibitory and co-stimulatory receptors on T cells and associated ligands on antigen-presenting cells or tumors.

Figure 1.11 CD103 influence on T cells.

Figure 1.12 Known phenotype of $CD103^{+}$ Trm cells in human.

Chapter 2

Figure 2.1 Flowchart of identification, sorting and cloning of HLA-A2-restricted cancer-specific CTLs.

Figure 2.2 HLA-E^{high} BCL generation.

Chapter 3

Figure 3.1 Gating strategy to identify EpCAM-specific cells.

Figure 3.2 EpCAM expression on cells derived from tumor, paratumor and peripheral blood of a patient.

Figure 3.3 HLA-E and MHC Class Ia expression on EpCAM-expressing cells.

Figure 3.4 HLA-E and MHC Class Ia expression on EpCAM-expressing cells in different cancer types.

Figure 3.5 Gating strategy for APC subsets.

Figure 3.6 HLA-E and MHC Class Ia expression different APC subsets.

Figure 3.7 Correlative analysis between HLA-E expression and frequency of APC subsets.

Figure 3.8 HLA-E and MHC Class Ia expression on non-professional APC, B cells.

Figure 3.9 HLA-E expression on different APC subsets derived from paired tumor, paratumor and peripheral blood samples, in different cancer types.

Figure 3.10 CD94/NKG2a expression on tumor-infiltrating T cells.

Figure 3.11 Activating CD94/NKG2c^{+} T cells in paired samples.

Figure 3.12 Correlation between HLA-E and CD94/NKG2a expression in tumor.

Figure 3.13 Frequency of CD94/NKG2a^{+} immune cell populations in paired samples.

Figure 3.14 Frequency of CD94/NKG2a^{+} CD^{+} T cell populations in paired samples of different cancer types.

Figure 3.15 Frequency of CD94/NKG2a^{+} and CD94/NKG2a^{-} CD8^{+} TILs according to TNM stages of cancer.

Figure 3.16 Differentiation phenotype of CD94/NKG2a^{+} and CD94/NKG2a^{-} CD8^{+} TILs in tumor.

Figure 3.17 Differentiation phenotype of CD94/NKG2a^{+} and CD94/NKG2a^{-} CD8^{+} TILs in paired paratumor and peripheral blood.

Figure 3.18 Gating strategy for inhibitory receptors and tissue-resident marker expression.

Figure 3.19 CD94/NKG2a^{+} TILs co-expression with PD-1.

Figure 3.20 CD94/NKG2a^{+} TILs co-expression of different inhibitory receptors.

Figure 3.21 CD94/NKG2a^{+} Tils lack tissue resident CD103 marker.

Figure 3.22 CD94/NKG2a^{+} TILs frequency increased as tumor progress while CD103^{+} TILs decreased.

Figure 3.23 Proliferation of CD94/NKG2a^{+} HLA-A2-restricted antigen-specific CTLs *in vitro*.

Figure 3.24 IL-2 receptor alpha (CD25) expression on CD94/NKG2a^{+} HLA-A2-restricted antigen-specific CTLs following antibody-mediated blocking treatment *in vitro.*

Figure 3.25 IL-2 production and expression on CD94/NKG2a^{+} HLA-A2-restricted antigen-specific CTLs following antibody-mediated blocking treatment *in vitro*.

Figure 3.26 Cytotoxicity by CD94/NKG2a^{+} HLA-A2-restricted antigen-specific CTLs *in vitro*.

Figure 3.27 IFNγ response by CD94/NKG2a^{+} HLA-A2-restricted antigen-specific CTLs *in vitro*.

Figure 3.28 Cytokines by CD94/NKG2a^{+} HLA-A2-restricted antigen-specific T cells which recovers following antibody-mediated blocking treatment *in vitro*.

Figure 3.29 Recovery of CD8^{+} TILs IFNγ following anti-CD94/NKG2a-mediated blocking treatment *ex vivo*.

Figure 3.30 Recovery of CD8^{+} TILs IL-2-dependent proliferation following anti-CD94/NKG2a-mediated blocking treatment *ex vivo*.

Figure 3.31 Effects of CD94/NKG2a on T cell functions.

Chapter 4

Figure 4.1 Phenotype of paired CD103^{+} and CD103^{-} cancer-specific T cells**.**

Figure 4.2 TGF-β1 production by CD103^{+} cancer-specific T cells.

Figure 4.3 T cell-mediated response of cancer-specific T cells without external antigen stimulation.

Figure 4.4 TGF-β1 production by CD103^{+} cancer-specific T cells following interference of CD103.

Figure 4.5 TGF-β1 intracellular expression by CD103^{+} cancer-specific T cells.

Figure 4.6 Membrane β8 surface expression by CD103^{+} cancer-specific T cells.

Figure 4.7 TCR antigen sensitivity by evaluating IFNγ and degranulation CD107a on CD103^{+} cancer-specific T cells.

Figure 4.8 TCR tumor antigen sensitivity measured by cytotoxicity on $CD103^+$ cancer-specific T cells.

Figure 4.9 TCR antigen sensitivity by evaluating the need of CD103 and E-Cadherin interaction by $CD103^+$ cancer-specific T cells.

Figure 4.10 The timing of $CD103^+$ cancer-specific T cells cytotoxicity.

Figure 4.11 The $CD103^+$ cancer-specific T cells cytotoxicity across 12-hours period.

Figure 4.12 The target cells death over time by $CD103^+$ cancer-specific T cells cytotoxicity.

Figure 4.13 T cell cytotoxic events.

Figure 4.14 Anti-tumor T cells cytotoxicity E-Cadherin-negative THP-1.

Figure 4.15 Glycolytic activities of $CD103^+$ cancer-specific T cells.

Figure 4.16 Mitochondrial activities of $CD103^+$ cancer-specific T cells.

Figure 4.17 CD103 expression on T cells enables faster migration *in vitro.*

Figure 4.18 CD103+ or CD103- cancer-specific T cells migration towards E-Cadherin-negative THP-1.

Figure 4.19 $CD103^+$ $CD8^+$ TILs localisation in tumors.

Figure 4.20 *Ex vivo* $CD103^+$ TILs subpopulations analysis.

Figure 4.21 *Ex vivo* $CD103^+$ TILs inhibitory receptors expression.

Figure 4.22 *Ex vivo* $CD103^+$ TILs inhibitor receptors co-expression phenotype.

Figure 4.23 *In vitro* analysis of T cell death during prolonged cancer exposure.

Figure 4.24 Effects of CD103 on CTLs functions.

Chapter 5

Figure 5.1 A high frequency of tumor-specific $CD8^+$ T cell clones do not express or secrete IFNγ.

Figure 5.2 The IFNγ-negative T cell clones have reduced cytotoxicity.

Figure 5.3 Surface phenotype of SSX-2-specific T cell clones.

Figure 5.4 $IFN\gamma^-$ T cell clones have CpG methylation in the IFNγ promoter.

Figure 5.5 Correlation of IFNγ expression by different T cell clones with CpG methylation in the IFNγ promoter.

Figure 5.6 IFNγ methylation, in short-term expanded bulk antigen-specific CTLs.

Figure 5.7 IFNγ methylation, and correlation to IFNγ production and T cell cytotoxicity of short-term expanded bulk antigen-specific CTLs.

Figure 5.8 IFNγ kinetics of SSX-2-specific T cell clones.

Figure 5.9 TNFα kinetics of SSX-2-specific T cell clones.

Figure 5.10 IFNγ kinetics comparison between short-term expanded bulk antigen-specific CTLs.

Chapter 6

Figure 6.1 As tumor progresses, the frequency of NNKG2a+ TILs increased while the CD103+ TILs decreased.

Figure 6.2 General summary of the study.

List of Tables

Chapter 1

Table 1.1 Top five cancer types, with number of new cases and mortality in 2018, as per recorded by WHO.

Table 1.2 HLA-E polymorphic distribution across different populations.

Chapter 2

Table 2.1 General clinical parameters of cancer patients.

Table 2.2 Flow cytometry surface antibodies.

Chapter 4

Table 4.1 The TCR alpha and beta chain of each CTL pairs.

Chapter 5

Table 5.1. The T cell receptor sequence of SSX-2-specific T cell clones.

Table 5.2 CpG locations within IFNγ promoter sequence.

Chapter 1: Introduction

1.1 Cancer and human health

Cancer is one of the leading causes of mortality worldwide, with an estimated 9.6 million deaths just in 2018. The Global Cancer Incidence, Mortality and Prevalence (GLOBOCAN) study reported that around 60% of cancer-related death were reported in Asia while a sizeable 20% were reported in Europe **(Figure 1.1)** (Bray et al., 2018). Among the most common cancers with more than 500 thousand death reported per year include lung, colorectal and stomach cancers **(Table 1.1)** (Bray et al., 2018; Ferlay et al., 2015). In the United Kingdom alone, lung cancer accounts for 21% of all cancer-related mortality (Bray et al., 2018). As cancer is highly prevalent and affects people across the world, it highlights the need of developing effective therapy regiments to treat cancer.

1.2 Immunity and cancer

In the past, the principal focus of cancer research has been on cancer cells themselves and how to inhibit their tumorigenesis. However, this neglect other components of the tumor microenvironment such as endothelial, stroma and infiltrating immune cells, as well as their roles in mediating or combating malignancies. In the last two decades, increasing number of studies have demonstrated the significant anti-tumor role, particularly of tumor-infiltrating T lymphocytes (TILs) against cancer. Clinical studies have shown that the presence and enrichment of TILs in tumor is highly associated with better clinical outcome in patients of varying cancer types, including melanoma, colorectal and lung cancers (Azimi et al., 2012; Burton et al., 2011; Ferrone and Dranoff, 2010; Galon et al., 2006; Kawai et al., 2008). Furthermore, adoptive transfer of T lymphocytes to tumor-induced murine model as well as in

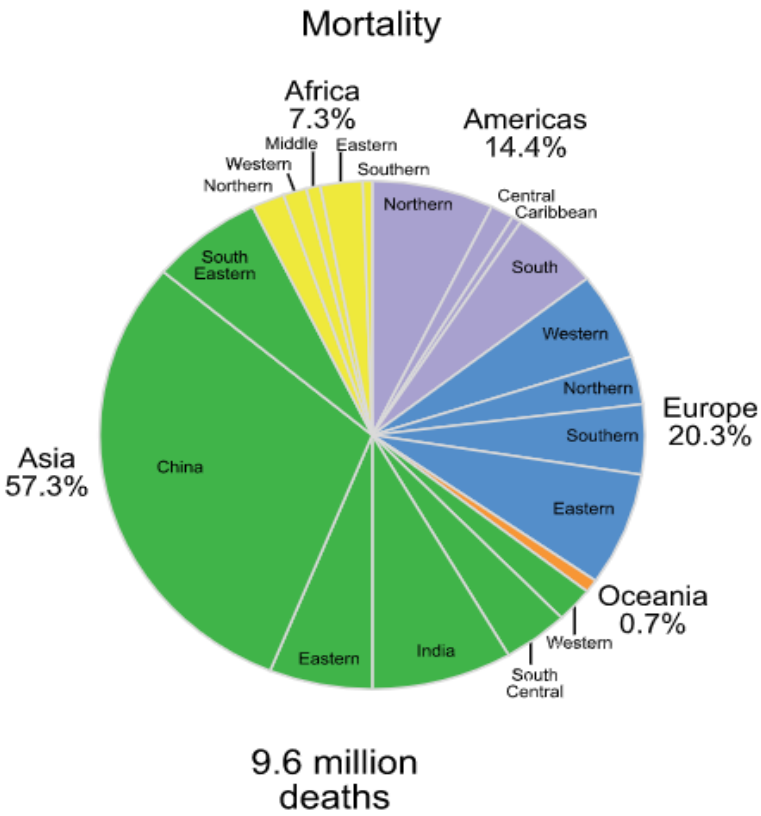


Figure 1.1 Mortality by cancer in 2018. Pie chart illustrating the incidence of cancer-related deaths reported to WHO, according to continents and regions. Adapted from Bray *et al.*, CA Cancer J Clin, 2018.

Table 1.1 Top five cancer types, with number of new cases and mortality in 2018, as per recorded by WHO. (adapted from Bray *et al.*, *CA Cancer J Clin, 2018).*

Cancer type	Percentage of total cancer mortality (%)	Number of new cases (million)	Number of mortality (million)
Lung	18.4	2.09	1.76
Colorectal	9.2	1.1	0.55
Stomach	8.2	1.03	0.78
Liver	8.2	0.84	0.78
Breast	6.6	2.09	0.63
Esophagus	5.3	0.57	0.51

cancer patients have demonstrated significant tumor regression (Besser et al., 2013; Boni et al., 2008; Klebanoff et al., 2011; Radvanyi et al., 2012). Altogether, these observations reinforce the necessity of TILs and the need to fully comprehend anti-tumor T cell-mediated immunity in cancer patients.

1.3 Interplay between innate and adaptive immunity

Host immunity involves primarily the innate and adaptive immunity. The innate immunity comprises of two components; (i) the effector-based immune cells, such as natural killer cells (NK cells) and invariant natural killer-T cells (NKT cells), as well as (ii) the antigen-presenting-based immune cells, such as macrophages and dendritic cells (DCs). NK and NKT cells form the primary front line of defense against cancer or pathogenic infection. They do not require prior specific-activation before inducing cell killing. However, in order to prevent randomised killing, NK and NKT cells activity are highly dependent on the balance of signals between its activating receptors such as NKG2c and its inhibitory receptors such as NKG2a and killer-cell immunoglobulin-like receptors (KIRs).

Antigen-presenting cells (APCs) such as DCs are vital for the primary activation of adaptive immune cells, such as T cells and B cells **(Figure 1.2)**. APCs process and present tissue-localised antigens on its cell surface through the human leukocyte antigen (HLA). Its subsequent migration to the draining lymph nodes resulted in the recognition, priming and initial activation of T cells and B cells. Following antigen priming by DCs, naive immune cells differentiated and acquired homing molecules to mediate its movement through the circulation onto the site of disease. Adaptive immune cells with matured T cell receptor or B cell receptor can recognise HLA molecules presented with specific antigens on the surface of infected cells

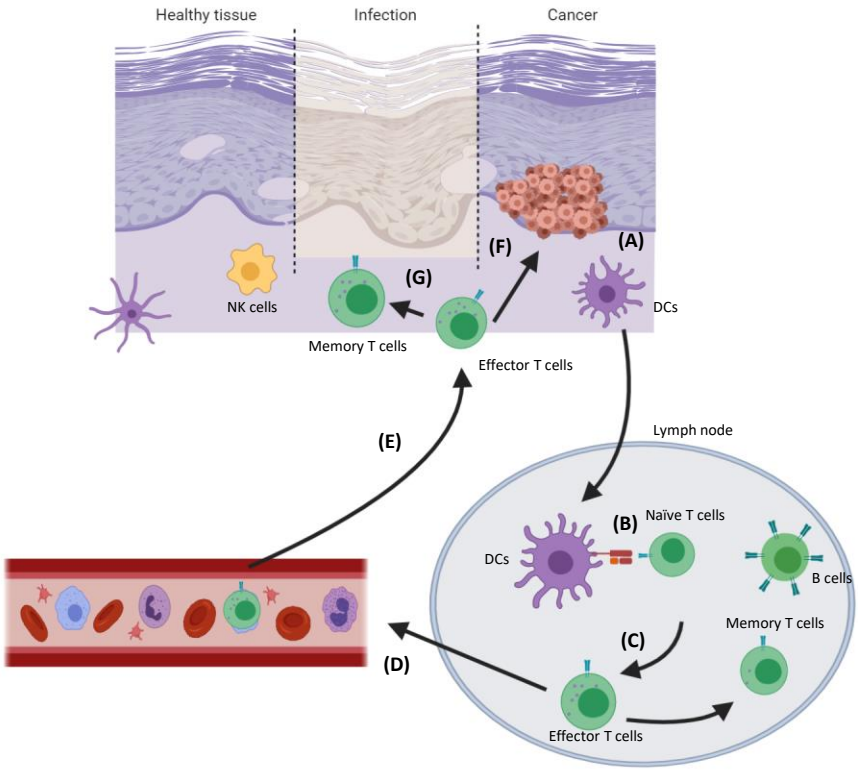


Figure 1.2 Interplay between innate and adaptive immunity. (A) Antigen-presenting cells such as dendritic cells (DCs) phagocytose dead cells and present antigens on their cell surface. (B) Movement of DCs into draining lymph nodes of tissues enable presentation of antigens to adaptive immune cells such as T cells. Recognition by naïve T cells leads to antigen-specific T cells activation and proliferation. (C) Activated T cells are known as effector cells, with some differentiating further into memory T cells in nodes, while (D) others move into circulation. (E) Antigen-specific T cells with homing molecules enables migration into specific tissue. (F) Presence of effector T cells in inflammatory condition such as infected tissue or cancer leads to antigen-specific T cells immune response, while some (G) further differentiate into memory T cells. (Adapted from Garland, The Immune System, 3rd Edition, 2009)

or cancer. This specific-activation acts as the primary mechanism in the cytotoxic and effector responses of adaptive immune cells, helping to clear virus infection and cancer.

1.4 Antigen processing and presentation

1.4.1 Human Leucocyte Antigen (HLA)

Antigenic peptides are presented via the MHC molecules that include the MHC Class I, Class II and Class III. The MHC gene locus on chromosome 6p21.31 comprise of the most polymorphic genes in the human genome, known as the HLA. Polymorphism of the HLA is driven by the selection of advantageous HLA genes that can mediate antigenic recognition and effective immune responses in host (Doherty and Zinkernagel, 1975). It is now well-established that MHC Class I gene locus has numerous functional gene products that can be synthesised as the heavy chain of MHC Class I molecule (such as HLA-A: 1448 proteins; HLA-B: 1998 proteins and HLA-C: 1119 proteins) (Robinson et al., 2000). The locus also consists of MHC genes encoding the non-classical MHC Class I molecules (such as HLA-E, HLA-F and HLA-G) **(Figure 1.3)**.

1.4.1.1 Non-classical HLA-E

HLA-E is the least polymorphic of the MHC family with only two known functional alleles, HLA-E0101 and HLA-E0103. Both alleles are found to have similar distribution across different populations, being it Eurasian, Asian, African or native American populations **(Table 1.2).** HLA-E0101 and HLA-E0103 differs only at a single nucleotide polymorphism (SNP) location rs1264457. The difference in SNP leads to a change of amino acid at position 107 located outside of the peptide binding groove of the translated heavy chain (Strong et al., 2003). However, the single amino acid difference does not affect the variation of peptide that can be loaded on each allele but does affect the thermostability of bound peptides.

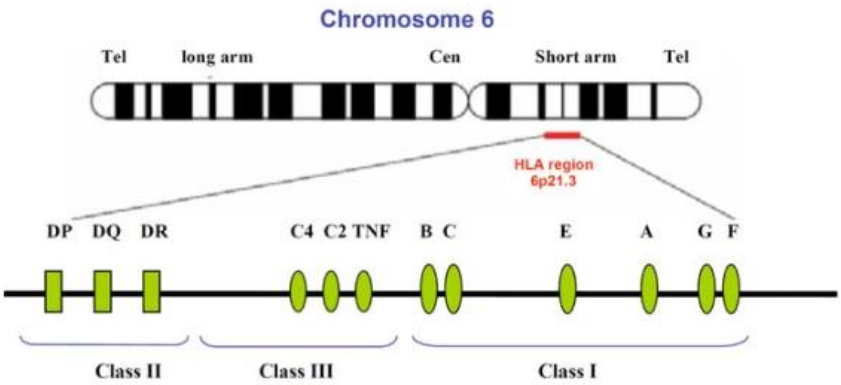


Figure 1.3 HLA alleles location in the chromosome 6p21.31. The MHC Class I gene locus comprise of three classical MHC (HLA-A, HLA-B and HLA-C) and three non-classical MHC (HLA-E, HLA-F and HLA-G). (Adapted from LI *et al.*, Current Molecular Medicine, 2009)

Table 1.2 HLA-E polymorphic distribution across different populations. (adapted from Liu *et al., Tissue Antigens, 2012)*.

	This study																		
	HNH (2*n* = 638)	IMH (2*n* = 208)	IMM (2*n* = 320)	GDH (2*n* = 214)	Japanese (2*n* = 100) (6)	Euro-Caucasoid (2*n* = 446) (7)	Afro-Caribbean (2*n* = 120) (7)	Indo-Asian (2*n* = 104) (7)	Mazatecan (2*n* = 172) (9)	Wayu (2*n* = 94) (9)	Mapuche (2*n* = 68) (9)	French (2*n* = 110) (8)	Congolese (2*n* = 182) (8)	Pygmies (2*n* = 146) (8)	African Shona (2*n* = 216) (24)	Thai (2*n* = 200) (13)	North Indian (2*n* = 400) (25)	Korean (2*n* = 972) (12)	Brazilian (2*n* = 208) (26)
*E*01:01*	0.3229	0.4375	0.5344	0.3832	0.32	0.558	0.533	0.567	0.6258	0.3144	0.7571	0.5	0.5769	0.5867	0.5093	0.425	0.6475	0.4907	0.625
*E*01:03*	0.6771	0.5625	0.4656	0.6168	0.68	0.442	0.467	0.433	0.3649	0.5934	0.2841	0.5	0.4231	0.409	0.4907	0.575	0.3525	0.5093	0.3365
Comparison[a]																			
HNH	—	—	—	—	1	**0.0001**	**0.0001**	**0.0001**	**0.0001**	0.7131	**0.0001**	**0.0007**	**0.0001**	**0.0001**	**0.0001**	0.0089	**0.0001**	**0.0001**	**0.0001**
IMH	**0.0033**	—	—	—	0.0616	0.0041	0.1097	0.0407	**0.0006**	0.1942	**0.0002**	0.3475	0.0068	0.0074	0.1477	0.8458	**0.0001**	0.1708	**0.0001**
IMM	**0.0001**	0.0339	—	—	**0.0001**	0.5513	1	0.5763	0.0452	0.0024	0.0042	0.5816	0.4016	0.3159	0.6008	0.0221	0.0024	0.1751	0.0114
GDH	0.1096	0.2745	**0.0008**	—	0.3258	**0.0002**	0.0071	0.0016	**0.0001**	0.6019	**0.0001**	0.0555	**0.0003**	**0.0003**	0.0085	0.4273	**0.0001**	0.0054	**0.0001**

GDH, Guangdong Han population; HLA, human leukocyte antigen; HNH, Hunan Han population; IMH, Inner Mongolia Han population; IMM, Inner Mongolia Mongol population.

HLA-E was first discovered to bind to the HLA signal peptides such as HLA-A2 (VMAPRLTVL) or HLA-Cw03 (VMAPRLTIL), as a mechanism for host immune cells recognition of healthy self-cells and to prevent spontaneous cytotoxic activity by NK cells (Braud et al., 1998; Lee et al., 1998). Interestingly, in the last decade, emerging number of studies have demonstrated HLA-E association with anti-bacterial and anti-viral immunity. For example, 65 *Mycobacterium tuberculosis* ***(****Mtb.)* antigenic peptides were able to bind to the HLA-E binding groove, with several able to be recognised by HLA-E-restricted *Mtb*-specific T cells, through TCR binding (Caccamo et al., 2015; van Meijgaarden et al., 2015). Furthermore, simian immunodeficiency virus (SIV)-infected rhesus macaques immunised with rhesus CMV vector was also found to induce broad HLA-E-restricted T cell responses (Hansen et al., 2016).

1.4.2 Antigen processing for MHC Class I presentation

A complete MHC Class I molecule consist of (i) the glycosylated HLA heavy chain, (ii) the non-covalently associated beta-2-microglobulin (β2m) and (iii) the bound antigenic peptide (Cresswell et al., 1973; Grey et al., 1973). Structural resolution study of the first MHC Class I crystals identified the extracellular folded distal domains α1 and α2 of two anti-parallel alpha helices laying on eight anti-parallel beta pleated sheets, to create a specific groove and to accommodate the antigenic peptide binding on the HLA heavy chain (Bjorkman et al., 1987a; Bjorkman et al., 1987b).

The loading of antigenic peptides on the binding groove involves an initial proteolytic digestion of a whole protein in the cytosol by proteasome to create shorter polypeptide sequences **(Figure 1.4)** (Kloetzel, 2004). Degraded hydrophobic or basic COOH-terminus αα residues polypeptides are then transported by transporter-associated protein (TAP) into the endoplasmic reticulum (ER) to be further trimmed by ER endopeptidases into 8-11 amino acids

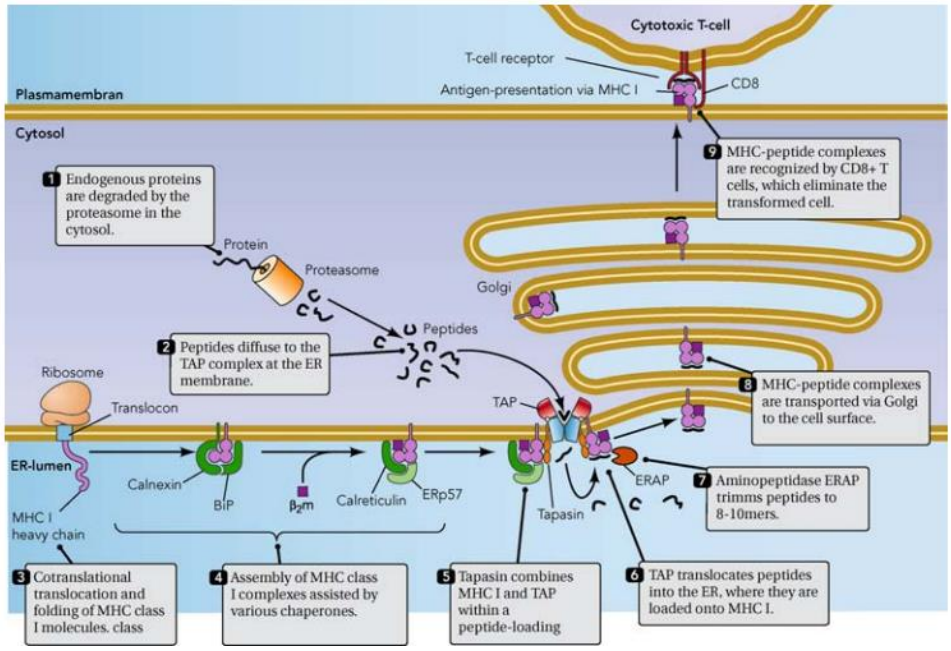


Figure 1.4 The antigen processing and presentation on HLA Class I molecule. Protein are originally degraded by proteasome in the cytosol before entering the endoplasmic reticulum for further trimming into 8-11 amino acids long. HLA Class I molecule is refolded in the ER and originally bind to calnexin. Presence of trimmed peptide and loading onto the binding groove of HLA molecule remove the calnexin, and stabilises the molecule. Stabilised MHC are then transported to the golgi apparatus to be transported to the cell surface. (Adapted from Loch *et al.,* Eur J Physiol, 2005)

long (Yewdell and Haeryfar, 2005). In parallel, the synthesised HLA heavy chain is folded and glycosylated in the ER to allow the non-covalent association with β2m, with the help of the chaperon protein calnexin (Danilczyk et al., 2000; Diedrich et al., 2001). In the presence of trimmed peptides in the ER, calnexin dissociates from the HLA heavy chain to enable docking of the peptide onto the HLA binding groove. The now stabilised MHC/peptide complex is then processed onto the Golgi apparatus to be transported to the cell surface.

The first HLA-A2 structure highlighted six pockets within the HLA binding groove that determines the specificity of the peptide loading for each HLA allele (Bjorkman et al., 1987b). The antigenic peptide with correct motif is anchored onto the groove via the amino acid residue filing into the pockets. Other exposed amino acid side chains protruding from the MHC/peptide complex are able to interact with $CD8^+$ cytotoxic T cells (CTLs), specifically by direct contact with the CDR3 loop of the T cell receptor (TCR) (Madden et al., 1992).

1.4.3 Antigen presentation by APCs

MHC molecule was first described in transplantation study as to present 'self' antigens and to explain graft rejection in patients. This involves utilising self-producing proteins to be presented on the MHC molecules of the cell surface, known as the antigen direct-presentation. MHC was later well-established as the major presenter of foreign antigens, especially by APCs (Benacerraf and McDevitt, 1972). APCs such as DCs and to a certain extend macrophages play a significant role in the initial pathogenic antigen presentation for the priming, activation and maintenance of T cell responses.

DCs primarily present pathogenic antigens through the antigen cross-presentation mechanism, in which exogenous antigens are endo-phagocytosed to be cytosolically processed and presented onto the MHC Class I molecules (Embgenbroich and Burgdorf, 2018). Among

the first evidences of DC cross-presentation capacity was observed in transplantation studies, whereby grafted murine cell proteins were cross-presented by host DCs, which in turn activated the host CTL immune responses (Bevan, 1976; Carbone and Bevan, 1990). Subsequent studies demonstrated that engulfment of dead cells by murine macrophages and human monocyte-derived DCs led to the acidification of endosomes, helping the proteo-degradation of endocytosed proteins into shorter peptides that can be mounted on the MHC Class I molecules of APCs (Albert et al., 1998; Bellone et al., 1997).

This cross-presentation mechanism enables APCs to present foreign antigens such as viral antigens for more effective activation and immune responses of CTLs. For example, skin migratory DC transport herpes simplex virus (HSV) antigen from infected murine skin tissue to the lymph nodes where the antigen are subsequently transferred to lymphoid DCs to induce initial priming of CTLs (Allan et al., 2006). In another study, increased population of migratory DCs are present in the lung draining lymph nodes following murine lung influenza infection. This contributed to the subsequent activation, killing and the clearance of lung infected tissue by influenza-specific CTLs (GeurtsvanKessel et al., 2008). In human, $CD141^+$ conventional DCs (cDCs) were found to be better at cross-presentation of human cytomegalovirus (hCMV) infected necrotic fibroblast culture *in vitro* (Jongbloed et al., 2010). Furthermore, prolonged tumor recognition and T cell maintenance by tumor tissue-localised $CD141^+$ cDC was highlighted to help in maintaining continual immune activities of tissue-localised CTLs (Roberts et al., 2016). Thus, DCs have significant role as the core antigen presenter and in the priming and activation of CTLs, by engaging with the TCR of T cells.

1.5 T cell receptor (TCR) and signaling

1.5.1 TCR development

T cells utilise TCR to sense surrounding cells for immunosurveillance and antigenic immune responses. The most common TCR used in human is the αβ TCR, which is a heterodimer of two glycosylated polymorphic polypeptides known as the alpha chain (TRA) and beta chain (TRB), that are covalently linked by a disulphide bond (Meuer et al., 1983; Rabbitts et al., 1985). Each TCR chain comprise of two extracellular domains known as the membrane proximal constant (C) region and the membrane distal variable (V) region (Acuto et al., 1983; Early et al., 1980; Seidman et al., 1979). The V region with three hypervariable loops in its uppermost part form the antigen binding/recognition site, known as the complementarity determining region 1, 2 and 3 (CDR1, CDR2 and CDR3) **(Figure 1.5)**.

CDRs are highly variable and arise from somatic DNA rearrangement of the whole *TRA* and *TRB* gene loci, during T cell development. This process involves a random selection of two (for *TRA*) or three (for *TRB*) gene segments; of a variable (V) segment, a joining (J) segment and a diversity (D) segment (for *TRB* only). Subsequent DNA recombination process and base pairing editing by exonucleases allow the selected gene segments to be imprecisely joined which further increase the variable numbers of DNA template palindromic nucleotides (Oettinger, 2004). Additional variations in the α and β chains pairing in different individual T cells further increase the total number of possible TCR combinations up to $>10^{18}$. The diverse TCR repertoire is selected through thymic positive and negative selections to ensure only MHC-recognising $CD8^+$ or $CD4^+$ T cells that recognises non-self-peptides are maintained in the host body (Kisielow et al., 1988; Liston et al., 2003; Surh and Sprent, 1994). Following disease condition such as viral infection, T cells with specific MHC/peptide recognition and restriction

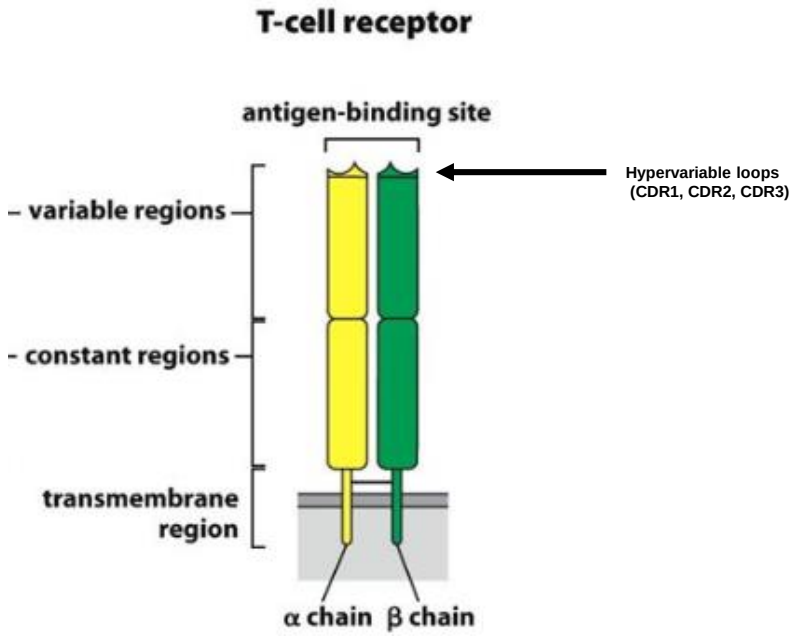


Figure 1.5 The domains/regions of T cell receptor of alpha and beta chains. Both chains comprise of transmembrane region and constant region. The variable region contain the hypervariable loops (CDR1, CDR2, CDR3) at the uppermost part of the receptor, which acts as the antigen-binding site. (Adapted from Garland, The Immune System, 3rd edition, 2009)

will be primed and undergo activation, differentiation and proliferation which will dominate the T cell pool during the inflammation period (Berger et al., 2011; Chen et al., 2012; Price et al., 2009).

1.5.2 TCR signaling

A functional TCR consists of the disulphide bond, non-covalently associated TRA-TRB chains and the non-polymorphic CD3 protein present on the T cell surface. The TCR engagement with MHC/peptide complex known as 'TCR triggering', mediates the phosphorylation of the tyrosine residues on the immunoreceptor tyrosine-based activation motifs (ITAMs) of the CD3 cytoplasmic domain **(Figure 1.6)** (Reth, 1989; Smith-Garvin et al., 2009). Activated ITAMs on the CD3 chains then recruit ZAP-70 protein that activates downstream scaffold proteins such as linker for the activation of T cells (LAT) and SH2 domain-containing leucocyte phosphoprotein of 76 kDa (SLP-76), which nucleates TCR signal propagation (Bubeck Wardenburg et al., 1996; Herndon et al., 2001; Shim et al., 2011).

In parallel, another CD3-associated protein known as phospholipase Cγ1 (PLCγ1) hydrolyses phospholipid phosphatidylinositol 4,5 biphosphate ($PI(4,5)P_2$) to induce activation of inositol triphosphate (IP_3) and diacylglycerol (DAG) proteins. DAG activates the mitogen activated protein kinase (MAPK) pathway that upregulates the extracellular signal-related kinase (ERK) and protein kinase C theta (PKCθ), which are important in regulating nuclear factor-κB (NF-κB) transcription factor activity (Roose et al., 2005; Teixeira et al., 2003). NF-κB is involves in variety of downstream signaling including of T cells effector genes transcription, calcium influx and homeostasis. Activation of DAG also protects some phosphorylated proteins such as ZAP-70 from the inhibitory action of the SH2-domain containing tyrosine phosphatase-1 (SHP-1) (Altan-Bonnet and Germain, 2005).

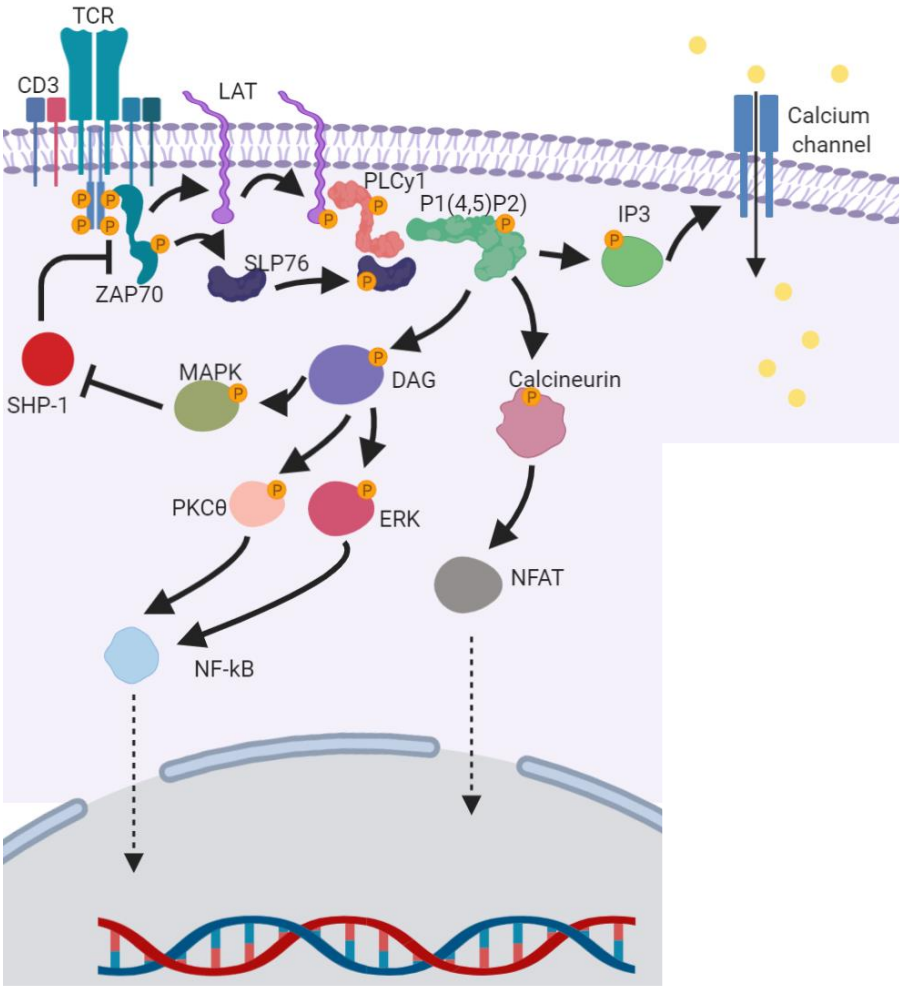


Figure 1.6 The process of TCR triggering. TCR triggering involves activated TCR/CD3 complex phosphorylating ZAP70 molecule that leads to activation of LAT and SLP76. The subsequent phosphorylation of PLCγ1 leads to the activation of P1(4,5)P2 molecule that contribute to (i) IP3 phosphorylation that result in calcium influx, and (ii) the activation of DAG and calcineurin. Calcineurin activates the transcription factor NFAT which translocate into the nucleus to initiate effector genes transcription. In parallel, activation of DAG proteins leads to activation of PKCθ and ERK proteins that subsequently activates the NF-κB transcription factor, which translocate into the nucleus for genes transcription. Phosphorylation of MAPK by DAG further stop the inhibitory action of SHP-1 upon ZAP70.

In contrast to DAG, activation of IP_3 results in its ligation to the endoplasmic IP_3 receptor and contribute to the release of calcium stored in the endoplasmic reticulum (ER). This action further triggers the calcium ions influx across the plasma membrane, which helps cytolytic degranulation process of CTLs (Imboden and Stobo, 1985). In tandem with the calcium flux, downstream TCR signaling propagation increase the activities of calcineurin and to translocate the nuclear factor of activated T cells (NFAT) into the nucleus, which further aid the effector-associated genes transcription and protein synthesis (Lyubchenko et al., 2001). Taken altogether, a robust TCR signaling mediated through the TCR/CD3 interaction with MHC/peptide complex is essential for efficient immune responses by T cells.

1.6 Functions of $CD8^+$ cytotoxic T cells (CTLs)

CTLs are one of the key components of adaptive immunity. It is well-established to induce highly specific effector and cytotoxic responses against infection and cancer. The main features of CTLs are (i) its cytolytic activities via immune killing and (ii) the secretion of cytokines and chemokines to the immediate tissue milieu to further aid the immunogenicity of T cell responses.

1.6.1 Cytotoxic-mediated responses of CTLs

1.6.1.1 Granzyme-mediated cytotoxicity

One of the major killing mechanism of CTLs is through the granzyme-mediated cytotoxicity. It is specifically mediated via the TCR recognition of the MHC/peptide complex on target cells. Upon TCR triggering, the cytolytic granules-containing lysosomes are polarised to the cell membrane by the cytoskeleton movement of T cells. The polarisation to the membrane leads to the lytic degranulation and secretion of perforin and granzyme B among others into the immunological synapse (IS) (Jenkins et al., 2009). Degranulation is an important component of

granules-aided killing and is detected by the presence of lysosome-associated membrane protein-1 (LAMP-1) or better known as CD107a, on the T cell membrane. CD107a is originally present on membrane of the lysosomal granules and becomes incorporated on the cell membrane following T cell activation and TCR-initiated killing (Shen et al., 2006).

Presence of perforin in the IS mediate the formation of transient pores in the cell membrane of target cell that allows direct movement of granule serine proteases into the cytosol (Thiery et al., 2011). As one of the key cytotoxic molecules of the protease family, granzyme B activates aspartic acid-specific cysteine proteases pathways in the target cells. The protease pathways include the activation of caspase-3, which is a key apoptotic protein that can induce target cell death (Chowdhury and Lieberman, 2008). The granzyme-mediated cytotoxicity of CTLs is known to be efficient, with the apoptotic process taking between 5 to 10 minutes upon T cells engagement (Matter, 1979; Rothstein et al., 1978).

1.6.1.2 Fas-mediated and TRAIL-mediated cytotoxicity

Other cytotoxic mechanisms that can be employed by CTLs include the Fas/Fas-ligand (Fas-L)-mediated cytotoxicity and the TRAIL-mediated cytotoxicity. In a perforin knock-out mice study, perforin$^-$ CTLs can induce residual killing *in vitro* by expressing Fas-L (Kagi et al., 1994). Its engagement with Fas on target cells can induce apoptosis of target cells, though with lower efficiency (Lowin et al., 1994). The Fas-L expression on T cell membrane is regulated by two mechanisms; the first condition involve exporting Fas-L-containing vesicles to the cell membrane, while the second condition involves transcriptional synthesis of Fas-L as early as two hours post T cells activation (He et al., 2010). In contrast, tumor necrosis factor-related apoptosis inducing ligand (TRAIL)-mediated cytotoxic response induces TRAIL-to-death receptors interaction, namely to R1/DR4 and R2/RD5 (Chaudhary et al., 1997; Schneider et al.,

1997). It is believed that the TRAIL-mediated pathway is primarily used in the maintenance of peripheral tolerance, to prevent over-stimulation and over-response by matured T cells (Kayagaki et al., 1999; Martinez-Lorenzo et al., 1998).

1.6.2 Effector responses of CTLs

In addition, CTLs induce secretion of cytokines such as tumor necrosis factor alpha (TNFα) and interferon gamma (IFNγ) that further mediates immune response against pathogens and cancer.

1.6.2.1 IFNγ

IFNγ is a type II interferon family member that was first discovered to interfere with viral replication (Isaacs and Lindenmann, 1957). It mediates biological effects by binding to the IFNγ receptor complex, a heterodimer of IFN gamma receptor 1 and 2 (IFNGR1 and IFNGR2). The ligation phosphorylates the janus tyrosine kinase-1-signal transducer and activator of transcription-1 (JAK-1/STAT-1) cellular pathway. This pathway enables the formation of immunoproteasome and the induction of antigen processing machinery-associated genes such as tapasin and transporter-associated with antigen processing (TAP) proteins (Dick et al., 1996; Farrar et al., 1991; Groettrup et al., 2001; Seliger et al., 2001). Most importantly, IFNγ mediates the induction of intrinsic viral defense factors that further helps the activities of anti-viral T cell-mediated immunity (Adams et al., 2004; Trilling et al., 2009). The induction of IFNγ expression is first mediated through the acetylation process of the histone containing the IFNγ gene locus. Acetylation enables accessibility to the IFNγ promoter sequence, which enables activating transcription factor (ATF), cAMP response element binding protein (CREB) and activator protein-1 (AP-1) transcription factors to be recruited and dock onto the promoter **(Figure 1.7)** (Penix et al., 1996; Samten et al., 2008). Employment of these factors form the eukaryotic

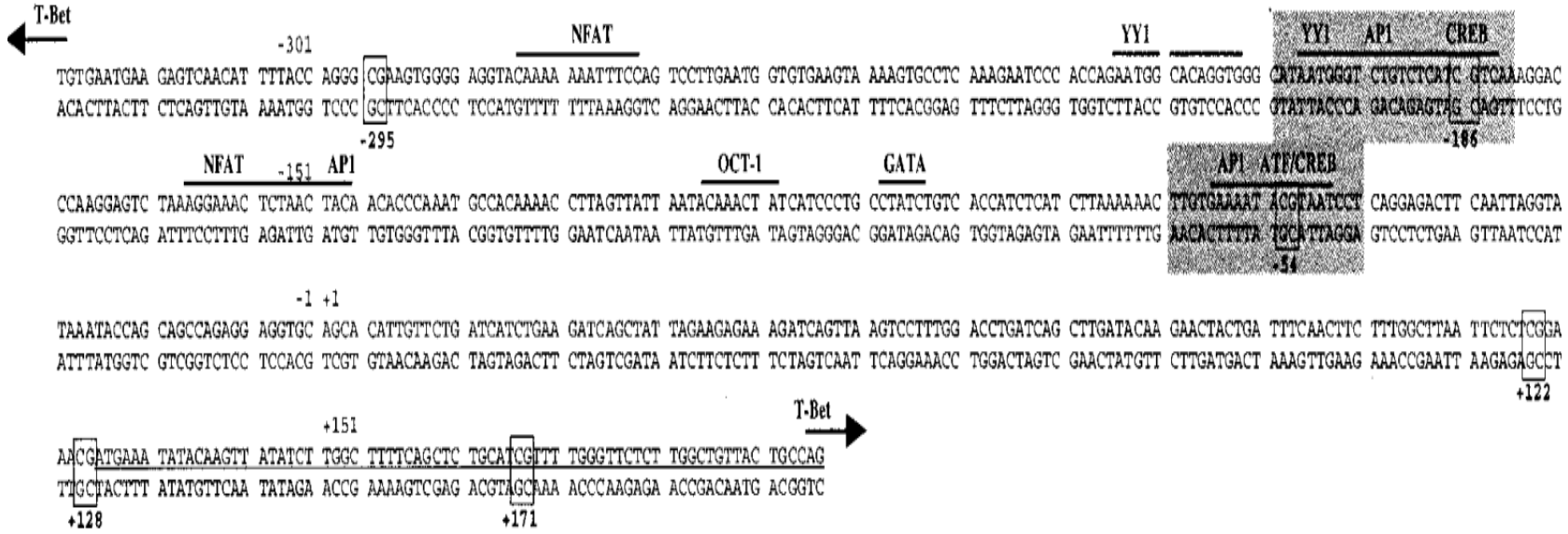


Figure 1.7 CpG methylation positions within IFNγ promoter sequence. Two CpG positions are located within transcription factor binding regions, namely position -186 and -54. (Extracted from White *et al., J Immunol*, 2002)

transcription assembly complex, that allows efficient docking of RNA polymerase II to start the transcription process (Eivazova et al., 2007). In turn, transcribed IFNγ mRNA are then translated and processed into IFNγ protein in the ribosomes and later packaged in the Golgi apparatus for subsequent secretion into the surrounding milieu during inflammation condition.

1.6.2.2 TNFα

TNFα is a pleiotropic cytokine that contributes to the defense against viruses and tumor growth. Its ligation to the TNF receptor 1 and 2 (TNFR1 and TNFR2) promotes apoptosis and prevents the expression of anti-apoptotic factors (Grell et al., 1999; Wajant et al., 2003). TNFR1 has a cytoplasmic death-domain that can activates caspases in target cells, which are known to initiate the process of cellular death. TNFα is induced in different immune cells. For example, macrophages produce TNFα in response to lipopolysaccharides recognition, while CTLs produce TNFα upon activation by pathogenic MHC/peptide complex recognition. In tandem with the secretion of IFNγ and other cytokines, these molecules help to enhance T cell-mediated immunity.

1.6.3 Proliferation of activated CTLs

In addition to effector cytokines, activated T cells also upregulate their proliferation-associated genes such as interleukin-2 (IL-2). IL-2 is an alpha helical protein that is produced by antigen-activated T cells, which binds to the IL-2 receptor complex comprising of three subunits; IL-2 receptor alpha, (IL-2Rα (CD25), beta (IL-2Rβ (CD122)) and a common gamma chain (γc (CD132)). While both CD122 and CD132 are also part of other interleukins receptor complexes such as IL-15 and IL-4, CD25 binds specifically to IL-2 cytokine (Depper et al., 1985; Giri et al., 1994; Russell et al., 1993). IL-2 cytokine binding to CD25 helps to recruit CD122 and CD132 to form a high affinity IL-2R complex to significantly induce efficient IL-2-dependent

proliferation signaling in T cells (Stauber et al., 2006; Takeshita et al., 1992). As further shown in **Figure 1.8**, the ligation phosphorylates JAK-3 which activates the downstream STAT-5 transcription factor that enters the nucleus and bind to the promoter region of IL-2 gene, enabling its DNA transcription and protein synthesis (Friedmann et al., 1996; Miyazaki et al., 1994). The resulting IL-2 production and secretion by T cells into the surrounding milieu contributes further to the CD25 continual ligation, therefore allowing a positive feedback mechanism of IL-2-IL2R signaling loop, especially in inflammation condition (Busse et al., 2010).

1.7 Evasion of anti-tumor immunity: dysregulation of MHC Class I expression

1.7.1 Downregulation of MHC Class Ia surface expression

Cancer is known to employ diverse mechanisms to avoid anti-tumor T cell immunity. For example, cancer of various types such as melanoma and lung carcinoma can downregulate its MHC Class Ia cell surface expression (Koopman et al., 2000; Leone et al., 2013). The MHC Ia downregulation involves limiting the efficiency of the antigen processing machinery, in which processing proteins such as TAP, tapasin and calnexin were dysregulated in their expression and normal functioning. This in turn can result in reduced MHC presentation of tumor antigens on the cancer cell surface. Therefore, cancer-specific T cells are less efficient in detecting, recognising and killing cancer cells, as the MHC downregulation can masks the dysregularity and presence of tumorigenic cells.

1.7.2 HLA-E in cancer

In contrast to classical MHC Ia molecules, emerging number of studies have now reported that the non-classical MHC Class Ib molecules such as HLA-E can also be enriched in various cancer types (Bossard et al., 2012; de Kruijf et al., 2010).

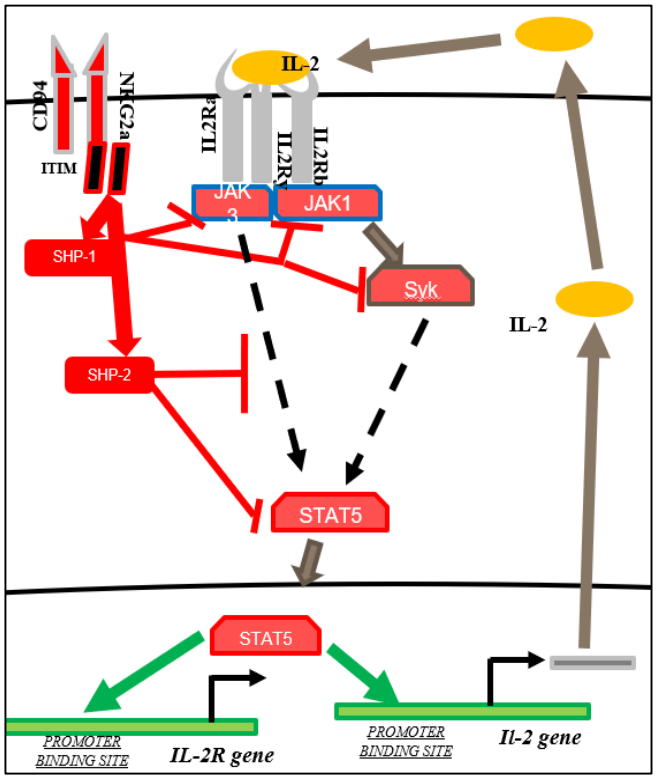


Figure 1.8 The IL-2/IL-2 receptor signalling loop. Binding of IL-2 to IL-2 receptor α (IL-2Rα) subsequently recruites IL-2Rβ and γc receptors to form a high affinity IL-2 receptor complex. Activation will phosphorylate JAK3 and JAK1 on the cytoplasmic domain of IL-2Rα. Subsequent downstream signalling activates the STAT5 transcription factor, which are translocated into the nucleus and bind to the IL-2 and IL-2Rα promoter binding site. This will stimulate the transcription and translation process of IL-2 and IL-2Rα. Synthesised IL-2 are secreted into the cell milieu and can interact back with the IL-2 receptor complex on T cell surface. It is likely that presence of inhibitory receptor such as CD94/NKG2a could negatively affect T cell proliferation at different part of the IL-2/IL-2R-dependent proliferation pathway, through activation of SHP-1/SHP-2 molecules.

HLA-E has been associated with poorer clinical outcome in patients such as with melanoma or lung cancer (Bossard et al., 2012; de Kruijf et al., 2010; Gooden et al., 2011; Levy et al., 2008). Importantly, preclinical studies in lymphoma Qa-1b (murine homologue of human HLA-E) knockout mice demonstrated better tumor regression in these mice (Andre et al., 2018; van Montfoort et al., 2018). It is therefore likely that cancer can manipulate HLA-E expression as another mechanism to induce immune evasion in the tumor microenvironment.

1.7.3 HLA-E recognition by inhibitory CD94/NKG2a receptor

HLA-E was first discovered to be recognised by the inhibitory CD94/NKG2a receptor complex present on NK cells and a subset of T cells (Braud et al., 2003; Braud et al., 1998). The interaction between HLA-E and CD94/NKG2a is well-established to inhibit NK cell cytotoxicity and prevents autoimmunity in healthy tissue condition. This is as NKG2a has two immunoreceptor tyrosine-based inhibitory motifs (ITIMs) on its cytoplasmic domain that can phosphorylate downstream SHP-1 and SHP-2 inhibitory molecules. Similar to the downstream effect of PD-1, the activation of SHP-1 and SHP-2 can lead to an overall inhibitory effect on immune cell functions (Kabat et al., 2002; Rota et al., 2018; Sheppard et al., 2004).

The inhibitory HLA-E and CD94/NKG2a interaction are known to be exploited by hCMV to evade anti-viral NK and T cell immunity. Two strains of hCMV; Toledo and AD169 CMV strains can synthesise UL40 glycoprotein that contains similar sequence as that of the classical HLA signal peptides (Lee et al., 1998). Proteolytic degradation of UL40 by CMV-infected cells contribute to the loading of CMV peptides (signal peptide homologues) onto HLA-E binding groove. With its known high affinity binding, the stabilised HLA-E/peptide complex on the infected cells surface can masks the dysregularity of the infected cells and present ‘don’t eat me’ signal to the immune cells to prevent anti-CMV immune responses.

In the case of cancer, whether HLA-E and CD94/NKG2a inhibitory mechanism could also be exploited to evade anti-tumor T cell immunity in different cancer types remains unclear **(Figure 1.9)**. Despite this ambiguity, recent clinical study have shown that combinatory anti-NKG2a with anti-epithelial growth factor receptor (EGFR) treatment in head-and-neck cancer patients mediated significant improvement in the clinical recovery of these patients (Andre et al., 2018). This highlighted a potentially new target that could be utilised for future immune checkpoints combinatory blockade treatment, such as with anti-PD-1. Therefore, further understanding of the HLA-E and CD94/NKG2a inhibitory effects on anti-tumor T cell effector responses and cytotoxicity is urgently required.

1.8 Evasion of anti-tumor immunity: elevated inhibitory receptors expression

In the last two decades, increasing evidences have demonstrated that cancer can manipulate expression of inhibitory molecules such as CTLA-4, PD-1 and Tim3 in the tumor microenvironment to further impair and limit anti-tumor T cell immunity. **Figure 1.10** highlighted the current known inhibitory and co-stimulatory receptors of T cells.

1.8.1 CTLA-4

Cytotoxic T-lymphocyte-associated protein-4 (CTLA-4) is an inhibitory receptor that can be induced on T cell upon antigen activation. CTLA-4 binds to B7-1 (CD80) and B7-2 (CD86), the same ligands that can be recognised by the co-stimulatory receptor CD28. In contrast to CD28, CTLA-4 negatively regulates the activation of T cells. Among the first known function of CTLA-4 is to inhibit spontaneous T cell reaction against self-antigens in healthy tissue (Friedline et al., 2009; Sansom, 2000; Takahashi et al., 2000).

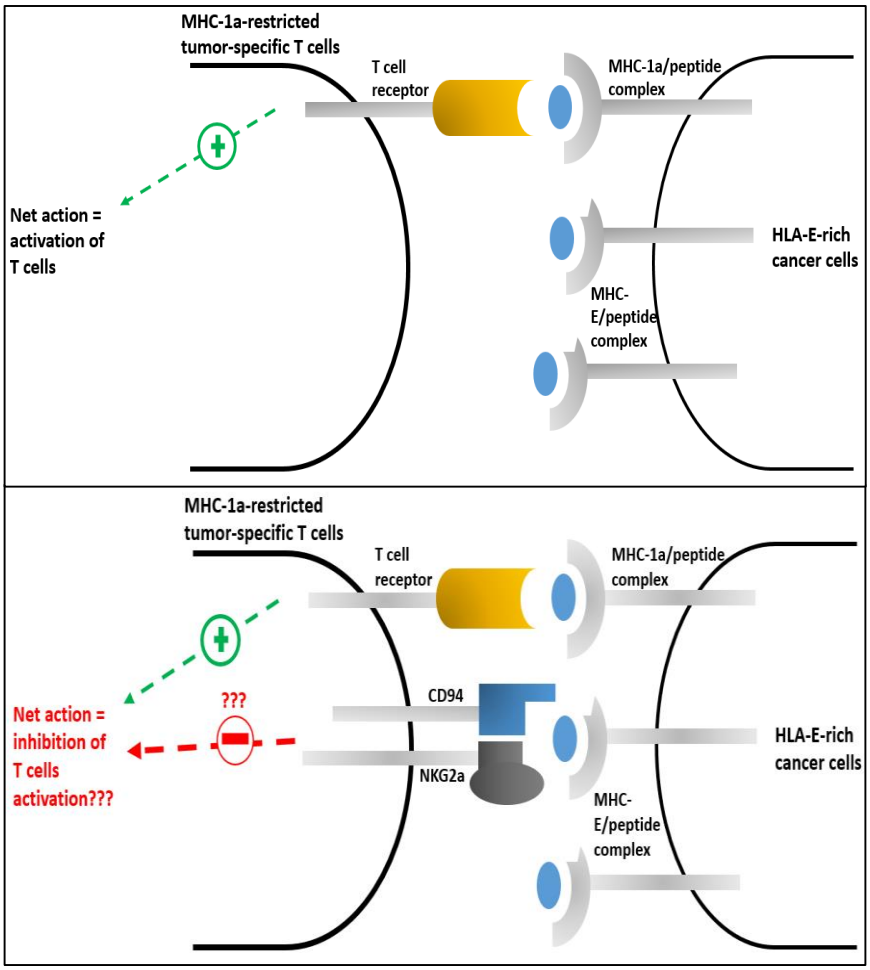


Figure 1.9 CD94/NKG2a influence on T cells. Recognition of MHC/peptide by classical MHC-restricted tumor-specific T cells will lead to net activation of T cells. However, the presence of CD94/NKG2a on classical MHC-restricted T cells could potentially inhibit normal T cell functioning.

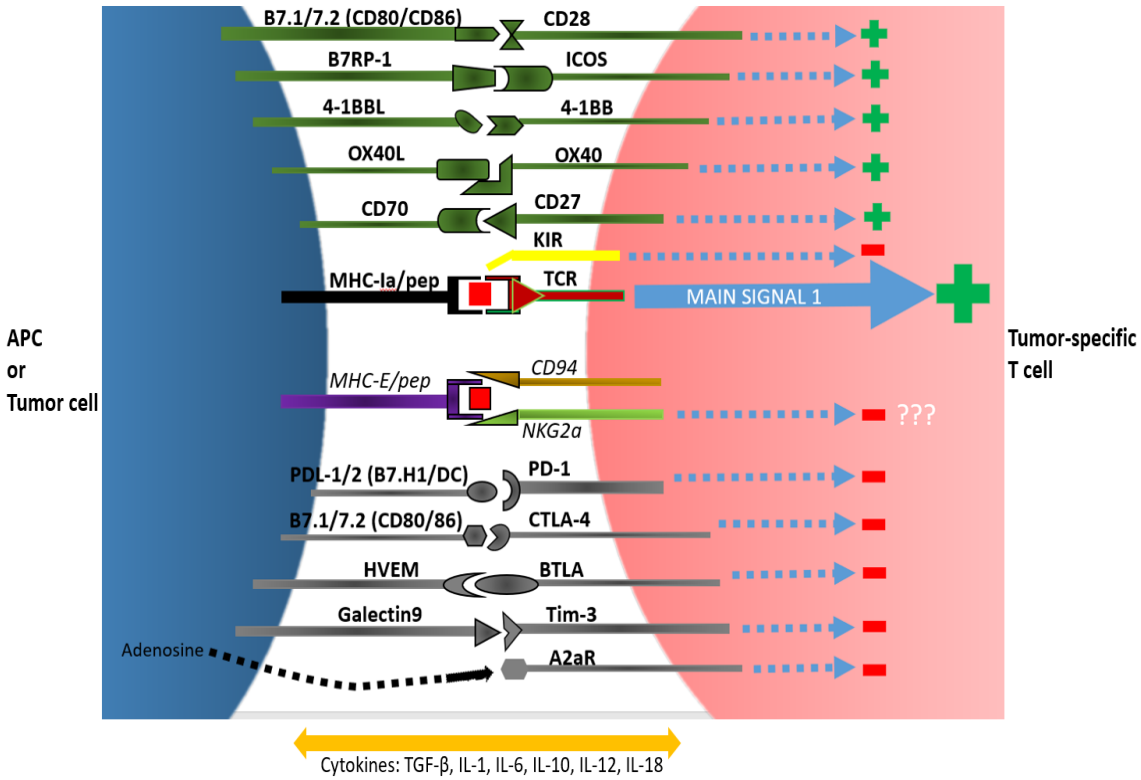


Figure 1.10 Known inhibitory and co-stimulatory receptors on T cells and associated ligands on antigen-presenting cells or tumors. Inhibitory molecules such as PD-1/PDL-1, CTLA-4/B7.1. BTLA/HVEM, Time-3/Galectin axes are known to induce inhibitory signalling on T cells and leads to inhibition of anti-tumor T cell responses and survival. It still remains unclear if NKG2a/MHC-E axis can negatively effect tumor-specific T cells functions. In contrast, co-stimulatory molecules such as CD28/B7.1, ICOS/B7RP-1, 4-1BB/4-1BB-L axes are known to help efficient TCR-mediated signalling for proper activation and T cell immune responses.

In cancer, several preclinical studies of CTLA-4 blocking antibody treatment in mouse models have successfully demonstrated prevention of tumor establishment and the promotion of tumor rejection (Kwon et al., 1997; Leach et al., 1996). However, in human clinical studies, fully humanised anti-CTLA-4 treatment such as ipilimumab in certain cancers have been shown to increase the risk of autoimmune side effects such as colitis in treated cancer patients (Hodi et al., 2003; Hodi et al., 2010; Hoos et al., 2010; Phan et al., 2003).

1.8.2 PD-1

Programme cell death protein-1 (PD-1) was first discovered as a transmembrane protein expressed on T cells following antigen stimulation. In healthy setting, PD-1 induced self-tolerance by phosphorylating its ITIMs motif on its cytoplasmic domain to activate the inhibitory SHP-1 protein (Sheppard et al., 2004). Activation of both SHP-1 and SHP-2 are known to interfere with the phosphorylation of the TCR downstream signaling molecules such as ZAP70, PCKθ and ERK1/2, which can impair among others the calcium utilisation by T cells (Zaugg et al., 2011). It was further shown that PD-1 expression can contribute to T cell exhaustion (Barber et al., 2006; Ishida et al., 1992). Upon its ligation to programme cell death ligand 1 or 2 (PDL-1 and PDL-2), this interaction can mediates epigenetic and transcriptional transformation on T cells, thus creating hypo-responsive T cell phenotype that resemble senescence (Agata et al., 1996; Pauken and Wherry, 2015). In addition, PD-1 activation on T cells can lead to cell cycle arrest and reduced cytolytic mediators activities, subsequently impairing the inflammatory responses and cytotoxicity of CTLs (Patsoukis et al., 2015).

Importantly in cancer, both PD-1 and PDL-1 can also be upregulated on tumor-derived myeloid cells and malignant cells themselves. Through this discovery, preclinical studies have shown that blocking the PD-1/PDL-1 axis can increase the overall T cell activation, anti-tumor

immune responses and inhibition of tumor growth in murine models (Kuang et al., 2009; Zhang et al., 2009). In human studies, fully humanised anti-PD-1 such as pembrolizumab and anti-PDL-1 such as atezolizumab demonstrated tumor regression in melanoma, non-small cell lung carcinoma and renal carcinoma patients (Hamid et al., 2013; Powles et al., 2014; Topalian et al., 2012). Furthermore, metastatic melanoma patients treated with pembrolizumab exhibited active proliferation of cytotoxic TILs that is associated with decreasing tumor size, especially in patients with high PDL-1 levels of expression (Tumeh et al., 2014). It is therefore not surprising that pembrolizumab was successfully certified by Food and Drug Administration (FDA), US in 2014 for the treatment of metastatic and late stage cancer patients. However, it is worth to note that treatment with anti-PD-1 or anti-PDL-1 failed to improve clinical outcome in some cancer patients and cancer types, indicating that other mechanisms could also be contributing to the tumor immune evasion.

1.8.3 Tim3

T cell immunoglobulin and mucin-domain containing 3 (Tim3) is a transmembrane inhibitory receptor of the immunoglobulin superfamily that was first discovered to mark IFNγ-producing Th1 T cells (Monney et al., 2002). It was later found that Tim3 expression can lead to the suppression of effector Th1 responses in mouse models of multiple sclerosis (Koguchi et al., 2006). While Tim3 expression is believed to be transient in healthy setting, its persistent expression has been found following chronic infection. In viral infection, high levels of Tim3 has been associated with T cell exhaustion and was first identified in human immunodeficiency virus-1 (HIV-1) patients. It was found that Tim3 can acts as an inhibitory checkpoint receptor controlling HIV-1-specific T cell responses in these patients (Jones et al., 2008).

In cancer, Tim3 has been associated with TILs exhaustion in mouse and human tumors. Importantly, co-expressed $Tim3^+$ $PD\text{-}1^+$ TILs were demonstrated to represent a deeply exhaustive T cell population with strong association to tumor progression such as in prostate, colon and hepatocellular carcinoma (Japp et al., 2015; Sakuishi et al., 2010). In addition, around 30% of New York-esophageal squamous cell carcinoma-1 (NY-ESO-1)-specific CTLs expressed Tim3 in advanced melanoma patients. Furthermore, $Tim3^+$ TILs in lung tumors were found to have large defects in anti-tumor cytokine productions and T cell proliferation (Fourcade et al., 2010; Gao et al., 2012).

1.8.4 Other related immune checkpoints

Other known inhibitory receptors of T cells include killer cell lectin-like receptor subfamily G member-1 (KLRG-1), B and T lymphocyte associated (BTLA) and T cell immunoreceptor with immunoglobulin and ITIM domains (TIGIT). BTLA activation on T cells was known to activate the inhibitory SHP-1 protein that impairs the downstream TCR-mediated signaling cascade (Sedy et al., 2005). KLRG-1 is an inhibitory C-type lectin with ITIM motifs on its cytoplasmic domain that was also found to mediate inhibition of T cell activation via SHP-1 (Tessmer et al., 2007). TIGIT, also with its cytoplasmic ITIM motifs can be expressed on activated and memory T cells and was first discovered to inhibit spontaneous T cells activation (Yu et al., 2009). However, in a recent study in our group, the expression of these three receptors were not found to be enriched on TILs compared to their counterparts in peripheral blood (Li *et al.,* under revision). It therefore suggests the possibility that the three inhibitory receptors might not be under the influence of immunosuppressive tumor microenvironment but rather as a constant marker of T cell activation, in comparison to Tim3 and PD-1.

1.9 Co-stimulatory molecules in aiding T cell immunity

In contrast to inhibitory receptors, co-stimulatory receptors of T cells act as a secondary signal for an effective TCR-mediated T cell activation and responses. It is well-known that an overall activation of T cells without co-signal can induce T cell anergy, a state of hypo-responsiveness and growth arrest state that leads to dysregulated immune tolerance and an impaired proliferation and effector T cell responses (Chen and Flies, 2013). Among the well-established and known co-stimulatory receptors of T cells include CD28, 4-1BB and inducible co-stimulator (ICOS) **(Figure 1.10)**.

1.9.1 CD28

CD28 is the best characterised co-stimulatory receptor of activated T cells. A member of the immunoglobulin superfamily, its ligation to CD80 and CD86 promotes T cell proliferation, cytokine production, cell survival and stabilisation of cytokine mRNAs (Boise et al., 1995; Lindstein et al., 1989; Linsley et al., 1991). Studies in CD28 knockout murine model further exemplify the necessity of CD28 on T cell responses. It is such that the absence of CD28 leads to T cells failure to induce efficient effector response and total clearance of viral infection (Cook et al., 2009; Mittrucker et al., 1999). As CD28 and CTLA-4 shares the same ligands of CD80 and CD86, it has been demonstrated that these two receptors heavily competes for the ligands recognition (Sansom, 2000). This in turn can define the activation or inhibition outcome of T cell activities.

Activation of CD28 was demonstrated to amplify the TCR-mediated downstream cascade pathways (Smith-Garvin et al., 2009). For example, activated CD28 cytoplasmic domain enhanced the TCR-mediated PI3K and Akt triggering of calcium signaling as well as promoting prolonged activation of AP-1 transcription factor expression. In addition, the ligation

of CD28 to CD80 can promote increased IL-2 receptor α chain expression and enhanced IL-2 transcription and mRNA stability (Linsley et al., 1991; Mueller et al., 1996). In cancer, the presence of CD80-transfectant tumor cells in murine models were observed to sufficiently induce CD28-responsive CTL-mediated activation and tumor rejection (Douin-Echinard et al., 2000).

1.9.2 4-1BB

4-1BB is a member of the TNF receptor superfamily, primarily expressed by activated T cells. Its ligation to 4-1BB ligand (4-1BBL) expressed mainly by DCs are highly responsive towards $CD8^+$ T cells effector responses (Shuford et al., 1997; Vidric et al., 2005). A key downstream signaling molecule of 4-1BB is known as the TNF receptor associated factor 1 (TRAF1). TRAF1 acts as an important inducer of immune-stimulatory genes, which are found to be downregulated during chronic viral infection (Wang et al., 2012). In a preclinical study, 4-1BB agonist combinatory treatment with anti-PDL-1 in acute CMV infected mice model demonstrated increased cytotoxicity and cytokine production by virus-specific $CD8^+$ T cells (Vezys et al., 2011). In addition to elevated killing capacity, 4-1BB agonist with IL-7 agonist treatment on chronic CMV infected mice showed significant reversal of T cell exhaustion, enabling better T cell survival and memory development.

In cancer, treatment using 4-1BB agonist and anti-PD-1 combinatory treatment of tumor mice model *in vivo* and human melanoma cells *in vitro* demonstrated elevated IFNγ-response, mediated primarily by the effector memory CTLs (Chen et al., 2015). Furthermore, treatment of 4-1BB agonist (utomilumab) in phase I clinical trial not only demonstrated its safety in treated cancer patients, but also highlighted a higher response rate in melanoma patients.

However, only 3.8% of the overall solid tumor cancer patients treated exhibited better response to this treatment (Segal et al., 2018).

1.9.3 ICOS

ICOS, also known as CD278 is present on activated T cells and interacts with ICOS-ligand (ICOS-L), which is mainly expressed on APCs. Activation of ICOS can phosphorylate PI3K of the TCR downstream signaling and lead to an enhanced T cell proliferation (Dong et al., 2001; Fos et al., 2008). In disease setting, it was first demonstrated in murine model that ICOS-allo-reactive CTLs exhibited enhanced graft-versus-host disease (GVHD) morbidity, with accelerated mortality. (Taylor et al., 2005). Interestingly, preclinical studies demonstrated that ICOS were upregulated following anti-CTLA-4 treatment (Chen et al., 2009; Fu et al., 2011). Taken altogether, the presence and possible enrichment of co-stimulatory molecules on TILs may help to improve anti-tumor functionality and responses.

1.10 CD103 as a potential co-stimulator of cancer-specific CTLs

Each of the well-known co-stimulatory receptors are either expressed during T cell activation and/or require ligands expressed on matured APCs. However, tumor-infiltrating APCs are known to be limited in numbers and are highly dysregulated in the tumor microenvironment (Laoui et al., 2016; Ruffell et al., 2014; Scarlett et al., 2012; Spranger et al., 2015). Therefore, a co-stimulatory molecule that have its ligand presented by cancer cells are vital for an efficient tumor-localised anti-tumor T cell immunity.

1.10.1 CD103 as a T cell surface molecule

CD103, also known as integrin alpha E, is first discovered as a T cell marker for tissue retention and residency, especially in the gut and lung. The heterodimeric integrin alpha E pairing with

integrin beta 7 subunit form a complex that can be recognised by E-Cadherin, a molecule that is usually expressed on epithelial cells. E-Cadherin is also known to be expressed on epithelial-derived cancer cells. The ligation of CD103 to E-Cadherin enables the attachment of $CD103^+$ T cells to E-$Cadherin^+$ cells (Kutlesa et al., 2002; Pauls et al., 2001). This T cell population is also termed as the $CD103^+$ tissue resident memory T cells ($CD103^+$ Trm cells), that lacks tissue exit markers such as CD62L (El-Asady et al., 2005; Sathaliyawala et al., 2013; Suffia et al., 2005).

1.10.2 CD103 expression during T cell development

CD103 expression is generated during naïve T cell development and differentiation. Its induction on naïve T cell requires (i) prior antigenic MHC/peptide complex recognition by TCR, and (ii) the presence of transforming growth factor beta-1 (TGF-β1) and its ligation to the TGF-β receptor (TGFBR). Notably, Batf3-dependent murine DC and human $CD1c^+$ cDC were defined to be the primary generator of TGF-β1 during this process (Enamorado et al., 2017; Graham et al., 2014; Yu et al., 2013). Importantly, the blocking of TGF-β/ TGF-βR ligation in wildtype murine model demonstrated significant impacts on the Trm cell generation in healthy tissues (Nizard et al., 2017).Other studies has further suggested that IL-33, IL-15 receptor and/or TNF could also support the induction of naïve to Trm differentiation (Liu et al., 2018; Mackay et al., 2013; Skon et al., 2013).

1.10.3 Identification of $CD103^+$ Trm cells

In addition to the CD103 expression, $CD103^+$ Trm cells can also be identified by the CD69 co-expression, elevated especially during the differentiation process (Mackay et al., 2013). Other known $CD103^+$ Trm phenotype is as described in **Figure 1.11.** At the genetic level, upregulation of the transcription factor Notch and Runx3 activities were identified as the genetic regulator of

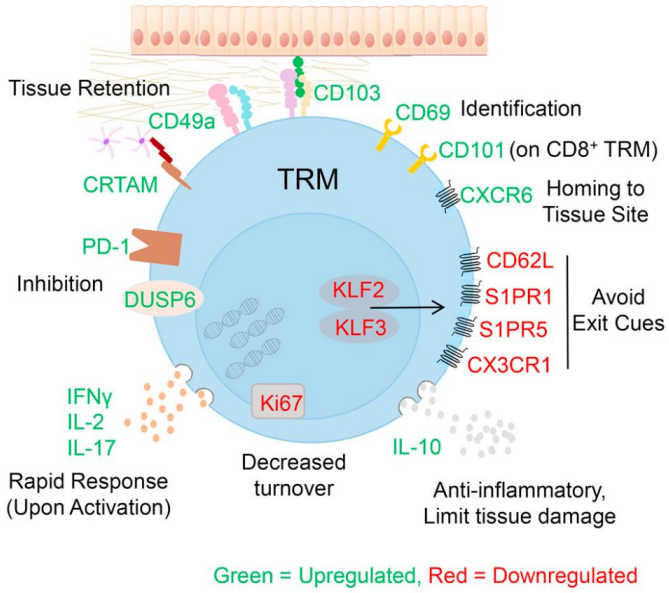


Figure 1.11 Known phenotype of CD103+ Trm cells in human. CD103+ Trm cells express CD103 and CD69, with some Trm cells also expressing CD49a. They do not express CD62L and S1PR1, which are tissue exit markers. (adapted from Kumar *et al.*, *Cell reports*, 2017).

Trm induction (Hombrink et al., 2016; Milner et al., 2017). Chromatin re-modification during Trm induction can result in genes associated with T cell recirculation such as *Klf2* and *S1pr1* to become more restricted and non-accessible (Hombrink et al., 2016; Skon et al., 2013). As a result of this genetic process, $CD103^+$ Trm cells lack CCR7, CD62L and S1PR1 surface expression, which are the key tissue exit markers (Djenidi et al., 2015; Ganesan et al., 2017). $CD103^+$ Trm cells was also believed to further maintain its prolonged viability in healthy tissue by increasing the expression of pro-survival and anti-apoptotic molecule such as Bcl-2 and BIRC3 (Djenidi et al., 2015; Hombrink et al., 2016).

1.10.4 The role of CD103 in healthy setting and disease

$CD103^+$ Trm cells help to mediate better immune surveillance in localised tissue and act as an important first defender against secondary viral infection. For example, the enrichment of Trm cells in murine lung tissue following primary infection resulted in even faster virus clearance following subsequent secondary influenza infection (Piet et al., 2011). In addition, $CD103^+$ Trm cells has been associated with better skin virus clearance following murine skin injection of herpes simplex virus (HSV) (Mackay et al., 2013). These observations thus demonstrated the critical significance of $CD103^+$ residential T cells in immunity, especially during localised virus infection. In recent years, emerging number of studies have associated the enrichment of $CD103^+$ TILs with improved clinical outcome, such as in melanoma, colorectal and lung cancer patients (Djenidi et al., 2015; Ganesan et al., 2017; Malik et al., 2017; Quinn et al., 2003; Wang et al., 2015). Specifically, the $CD103^+$ T cells contributed to an elevated T cells infiltration into tumor islets, with better tumor control observed in mice model (Sandoval et al., 2013; Webb et al., 2014). As E-Cadherin is vital for the ligation of CD103, the lack of E-Cadherin expression

by some melanoma cells can impair the overall anti-tumor responsiveness of murine Trm TILs, even after anti-CTLA-4 and anti-PD-1 treatments (Shields et al., 2019).

In terms of T cell functions, previous works have interestingly demonstrated accumulation of the CD103 molecules within the immunological synapse, following $CD103^+$ T cells interaction with autologous E-$Cadherin^+$ cancer cells (Le Floc'h et al., 2011; Le Floc'h et al., 2007). Importantly, the CD103 accumulation overlap with the enriched granzyme B presence in the synapse (Le Floc'h et al., 2007), suggesting the possibility that CD103 could provide an additional co-stimulatory signal for CTLs cytotoxic responses. However, it remains unclear the possible anti-tumor CD103-mediated mechanisms and the characteristics of $CD103^+$ cancer-specific CTLs, which merits in-depth investigation **(Figure 1.12)**.

1.11 Evasion of anti-tumor immunity by dysregulating epigenetic processes

Epigenetic is a cellular process that helps regulate gene expression, in healthy and disease conditions. Epigenetic regulation processes include histone modification and DNA methylation. As a significant part of the methylation process, DNA CpG methylation in normal setting is vital to prevent hyperactivities of immune cells. It primarily involves addition of a methyl group to the pyrimidine ring of the cytosine nucleotide, creating 5'methylcytosine-guanine dinucleotide. CpG methylation on the promoter of genes prevents accessibility of transcription factor molecules to assemble on the promoter and induce transcription of specific development and effector genes (Komori et al., 2015; Moore et al., 2013).

Cancer tissue, such as cervical cancer cells is known to have hypermethylated IFNγ promoter that promote tumorigenesis, by impairing the overall IFNγ presence in the tumor microenvironment (Ma et al., 2014). As previously mentioned, presence of IFNγ is important

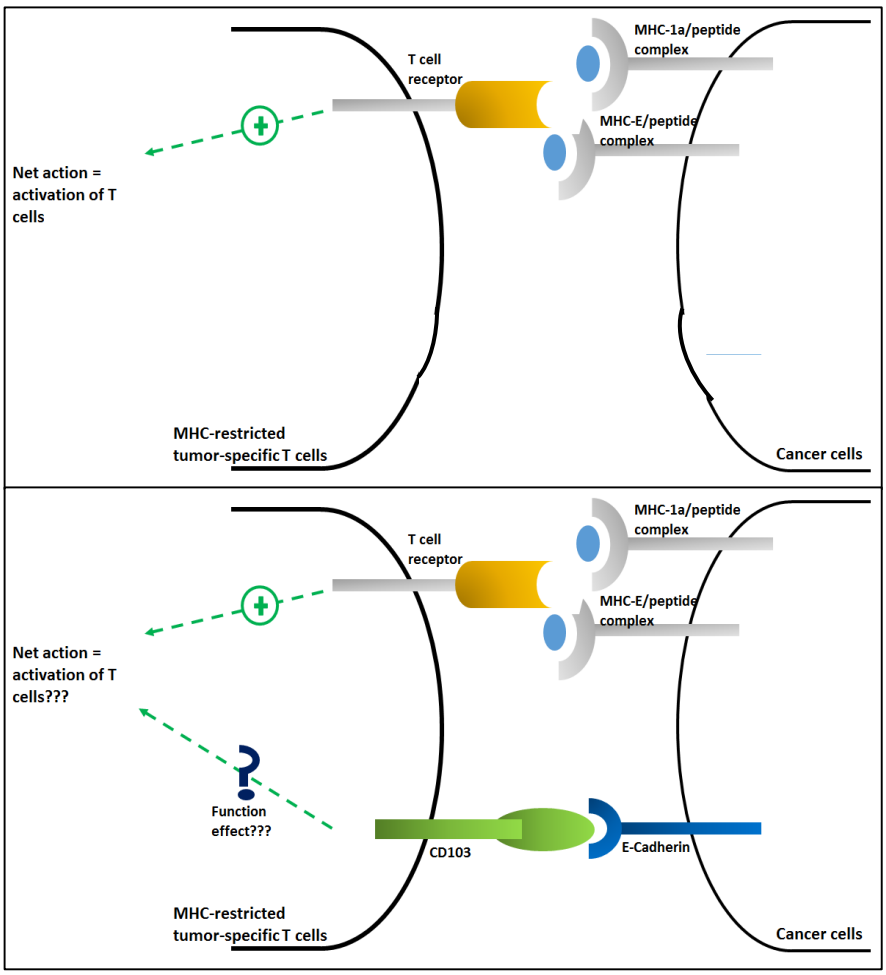


Figure 1.12 CD103 influence on T cells. TCR interaction with MHC/peptide complex enables net activation of classical MHC-restricted tumor-specific T cells. However, it remains unclear whether the presence of CD103 on classical MHC-restricted tumor-specific T cells will have any effects on T cells activation, functions and activities.

for effective anti-tumor T cell responses and the impaired presence in the tumor microenvironment could have negative effect on the immunogenicity of cancer cells. Although cancer cells themselves are known to dysregulate its IFNγ production in the tumor microenvironment, it remains unclear whether cancer-specific CTLs in tumor could also be dysregulated, especially at the methylation level.

1.12 The aims of the study

Overall, the aims of this study are to acquire a detailed understanding of the underlying characteristics and mechanisms of inhibitory and co-stimulatory receptors and their less-understood effects on cancer-specific CTL functions. Furthermore, to assess the effects of the tumor microenvironment on the immune responses of cancer-specific CTLs. Therefore, specific assessments were carried out in this study, which includes:

1. As described in **Chapter 3,** the characterisation of HLA-E and CD94/NKG2a on tumor-derived cells and the effects of enriched HLA-E and CD94/NKG2a interaction on anti-tumor T cell functions, using *ex vivo* phenotypic analysis of CD94/NKG2a^{+} immune cells and *in vitro* T cell functional assays.
2. As described in **Chapter 4,** the characterisation of CD103^{+} cancer-specific CTLs, specifically of its contribution to CTLs effector functions, self-maintenance capacity, antigen sensitivity, cytotoxic capacity, homing and localization and its features in prolonged cancer exposure, using *in vitro* T cell functional assays and *ex vivo* co-localisation and immune checkpoints phenotypic analysis. And lastly,
3. As described in **Chapter 5,** the CpG methylation of IFNγ promoter and its effect on IFNγ production by cancer-specific CTLs, using bisulphite treatment for methylation sequencing and *in vitro* T cell functional assays.

Chapter 2: Materials and Methods

2.1 Study subjects

Human study was approved by the Oxford Radcliffe Biobank (ORB) research ethics committee (reference number: 09/H0606/5+5) and the Ethics Committee of the Third Affiliated Tumor Hospital of Xinjiang Medical University (reference number: K-201403), based on the guidelines of the Declaration of Helsinki. The average age of the patients was 58.18 years (range of 39 to 81 years). Inclusion criteria include: (i) sizes of tissue samples collected were kept consistent between each patient (resection volume of no less than 0.5*0.5*0.5cm), (ii) no indication of metastatic disease. The tumors were confirmed using immunohistopathology. Written informed consent was obtained from all subjects prior to the inclusion in the study. General stratification of patients used in this study is described in **Table 2.1.**

2.2 Isolation of mononuclear cells from blood and tissues

Peripheral blood mononuclear cells (PBMC) were isolated from fresh heparinised blood using Ficoll-Hypaque density gradient centrifugation. Cells were resuspended from tumor and paratumor tissues using Miltenyi tumor dissociation kit (Miltenyi, UK), as commercially described, before isolated using Ficoll-Hypaque density gradient centrifugation.

2.3 Generating antigen-specific T cells in vitro

All *in vitro* functional experiments were performed with short-term expanded antigen-specific CTLs derived from cancer patients, using well-established human antigen-specific T cells generation technique as previously described (Dong et al., 2004; Zhang et al., 2018). A detailed flow chart of generating human cancer-specific CTLs is shown in **Figure 2.1.**

Table 2.1 General clinical parameters of cancer patients

Clinical parameters of cancer patients		
Age	≤39	1
	40-59	24
	60-69	7
	70-79	5
	≥80	1
	average (range)	58.18 (39-81)
	TOTAL	*38*
Sex	Male	24
	Female	14
Identification of cancer	Carcinoma	38
Tumor type	Esophageal	8
	Gastric	9
	Colorectal	8
	Lung	8
	Kidney	5
Tumor origin	metastatic	0
	non-metastatic	38
Clinical tumor TNM stage	T1N0M0	4
	T2N0M0	3
	T2N1M0	3
	T3N0M0	6
	T3N1M0	14
	T4N0M0	8

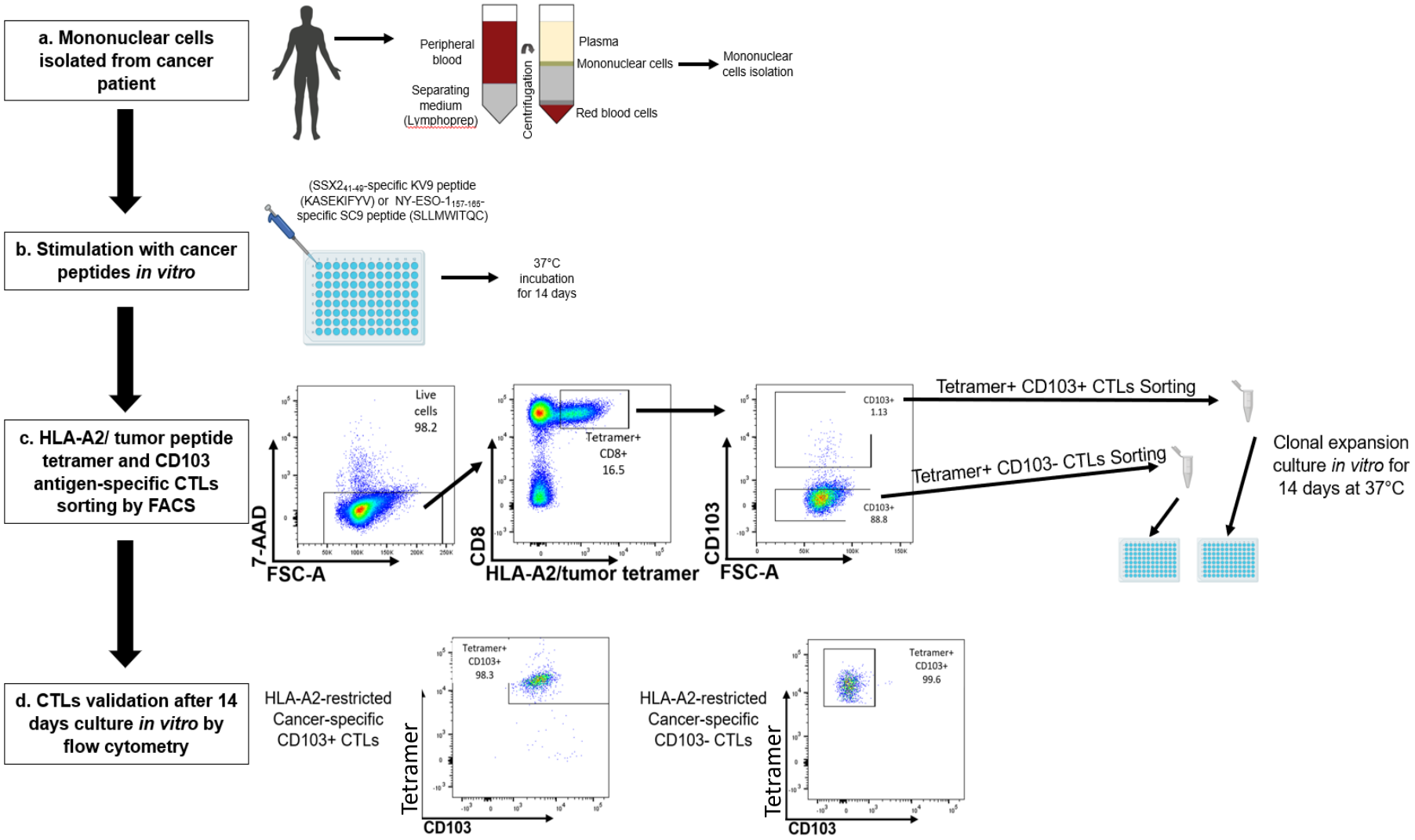

a. Mononuclear cells isolated from cancer patient
Peripheral blood
Separating medium (Lymphoprep)
Centrifugation
Plasma
Mononuclear cells
Red blood cells
Mononuclear cells isolation
b. Stimulation with cancer peptides in vitro
(SSX2 41-49-specific KV9 peptide (KASEKIFYV) or NY-ESO-1 157-165-specific SC9 peptide (SLLMWITQC)
37°C incubation for 14 days
c. HLA-A2/ tumor peptide tetramer and CD103 antigen-specific CTLs sorting by FACS
Live cells 98.2
7-AAD
FSC-A
Tetramer+ CD8+ 16.5
CD8
HLA-A2/tumor tetramer
CD103+ 1.13
CD103+ 88.8
CD103
FSC-A
Tetramer+ CD103+ CTLs Sorting
Tetramer+ CD103- CTLs Sorting
Clonal expansion culture in vitro for 14 days at 37°C
d. CTLs validation after 14 days culture in vitro by flow cytometry
HLA-A2-restricted Cancer-specific CD103+ CTLs
Tetramer+ CD103+ 98.3
Tetramer
CD103
HLA-A2-restricted Cancer-specific CD103- CTLs
Tetramer+ CD103+ 99.6
Tetramer
CD103

Figure 2.1 Flowchart of identification, sorting and cloning of HLA-A2-restricted cancer-specific CTLs. Mononuclear cells from cancer patient was initially isolated and stimulated with cancer peptides *in vitro* for 14 days at 37℃. After 14days, mononuclear cells were stained with HLA-A2/tumor peptide tetramer and CD103 and sorted for CD103+ and CD103- cancer-specific CTLs by FACS. Sorted cells were then clonally expanded *in vitro* for 14 days at 37°C. After 14 days, CD103 and tetramer specificity is validated using flow cytometry. Clonality of CTLs were determined by RNA transcript extraction, cDNA generation and subsequent TCR sequencing.

Briefly, mononuclear cells (consisting of a mixture of T cells, B cells and antigen-presenting cells) isolated from individual cancer patient were stimulated with either tumor antigen-specific $SSX2_{41-49}$ KV9 peptide (KASEKIFYV), NY-ESO-$1_{157-165}$ SC9 peptide (SLLMWITQC), CMV-specific $pp65_{495-503}$ NV9 peptide (NVLPMVATV) or Influenza-specific CY9 peptide (CTELKLNDY) and cultured in RPMI-1640 supplemented with 10% v/v heat-inactivated human AB serum (National Blood Service, UK), 2mM L-Glutamine, 1% v/v (500U/ml) penicillin streptomycin (Sigma-Aldrich, UK) and recombinant human IL-2 (Peprotech, UK) (H10) at 37°C. The B cells and antigen-presenting cells within the isolated mononuclear cells mixture will present the peptides to the T cells for T cell's activation and proliferation.

After 14 days, antigen-specific T cells were FACS sorted with peptide-MHC Class I tetramer (HLA-A2 KV9, HLA-A2 SC9, HLA-A2 NV9 or HLA-A2 CY9) conjugated with PE, using BD Aria Illu (BD Biosciences). Peptide-MHC Class Ia tetramers were prepared in-house by Dr. Yanchun Peng and Dr. Xuan Yao. Sorting of antigen-specific T cells with specific surface markers were carried out using BV711-CD103 (clone: Ber-ACT8, Biolegend; RRID: AB_2629650) or APC-NKG2a (131411; R&D Systems; RRID:AB_356987). Sorted cells were either clonally expanded or short-term population expanded *in vitro.* The T cells were confirmed for antigen-specificity using tetramer and surface marker staining by flow cytometry. T cells were tested for mycoplasma monthly.

2.4 Target cell lines used for in vitro functional assays

All *in vitro* functional assays were performed by culturing CTLs with target cells, either with HCT116 (CCL-247; ATCC), THP-1 (TIB-202; ATCC) or Epstein-Barr virus (EBV)-transformed B cell lymphoblastoid (as described below). Briefly, target cells were preincubated

with specific peptide concentrations (2μg/ml, 1μg/ml, 0.4μg/ml, 0.08μg/ml or 0μg/ml) at 37°C for 1 hour to enable the loading and presentation of peptide on the MHC complex on the target cell surface. HCT116 is a commercially available cancer cell line that is known to be HLA-A2^{+}, E-Cadherin^{+} (the ligand for CD103) and does not express SSX-2 and NY-ESO-1 proteins (Gjerstorff et al., 2014; Greve et al., 2014; Purbhoo et al., 2006; Saias et al., 2015). THP-1 is a commercially available cancer cell line that is E-Cadherin^{-} HLA-A2^{+} SSX-2^{-} NY-ESO-1^{-}. A HLA-A2^{+} EBV-transformed B cell lymphoblastoid (BCL) is generated from a healthy donor, generated in-house in 2005 by Dr. Yanchun Peng. The BCL used in this study is E-Cadherin^{-} HLA-A2^{+} SSX-2^{-} NY-ESO-1^{-}. Preparation of HLA-E^{high} BCL is described below.

2.5 Generating HLA-E^{high} EBV-transformed B cell lymphoblastoid (BCL)

To assess the contribution of HLA-E and its interaction with CD94.NKG2a on T cell responses, we first generated HLA-E-high-expressing EBV-transformed B cell lymphoblastoid (BCL) *in vitro*. HLA-E0101 or HLA-E0103-pHR plasmid construct were first generated on the backbone of HLA-A2-pHR plasmid, provided previously by Dr. Yanchun Peng. HLA-E sequence was first generated as PCR product from gDNA of a healthy donor (provided by Dr. Xuan Yao). HLA-E plasmid was then generated by double digestion of HLA-A2-pHR to remove HLA-A2 sequence and ligation to insert the HLA-E sequence. pHR plasmid was then transformed and grown using TOP10 bacteria transformation kit (ThermoFisher) and colonies were grown and miniprep to isolate plasmids and send for sequencing by John Frankland (WIMM). With the correct HLA-E-pHR plasmid **(Figure 2.2A),** HLA-E lentiviruses expressing either HLA-E0101 or HLA-E0103 allele were generated using the three plasmids system by co-transfection of 293T cell line cultured in DMEM supplemented with 10% v/v fetal calf serum (Sigma Aldrich), 2mM L-Glutamine and 1% v/v (500U/ml) penicillin streptomycin (Sigma-Aldrich, UK) at

37°C, as previously described (Zhang et al., 2018). After 48hours, supernatant containing HLA-E lentiviruses were collected, filtered and later concentrated using Lenti-X^{TM} Concentrator (ClonTech) according to manufacturer's instruction.

The HLA-A2^{+} BCL was then transduced with either HLA-E0101 or HLA-E0103 lentivirus and cultured for 5 days at 37°C in 24-well plate before sorted for HLA-E high expression using BD Aria II (BD Biosciences) and grown in complete media at 37°C. HLA-E enriched expression was confirmed, as shown in **Figure 2.2B**. The BCLs were maintained in RPMI-1640 supplemented with 10% v/v fetal calf serum (Sigma Aldrich), 2mM L-glutamine and 1% v/v (500U/ml) penicillin streptomycin (Sigma-Aldrich, UK) at 37°C. After 7 days, HLA-E expression was confirmed using flow cytometry, with wild-type HLA-A2^{+} BCL as negative control. Mycoplasma testing was carried out with all the cell lines monthly. Surface expression of CD19, HLA-E and HLA-A2 on the BCL were assessed by flow cytometry staining regularly.

2.6 Ex vivo flow cytometry staining

Cells were initially stained with LIVE/DEAD Fixable Aqua Dead Cell Stain kit (ThermoFisher, UK), using manufacturer's instructions. Tetramer staining was performed as previously described (Dong et al., 2004; Zhang et al., 2018). Briefly, cells were stained with tetramer for 20 minutes at 37°C before the surface staining was performed, with incubation at each step for 20 minutes at 4°C. Antibody specificities and coupled labels used for surface staining are as described in **Table 2.2**. All samples were acquired on BD LSR Fortessa (BD Biosciences) flow cytometer or BD LSR Symphony (BD Biosciences) and analyzed using FlowJo v.10 software (Tree Star Inc.).

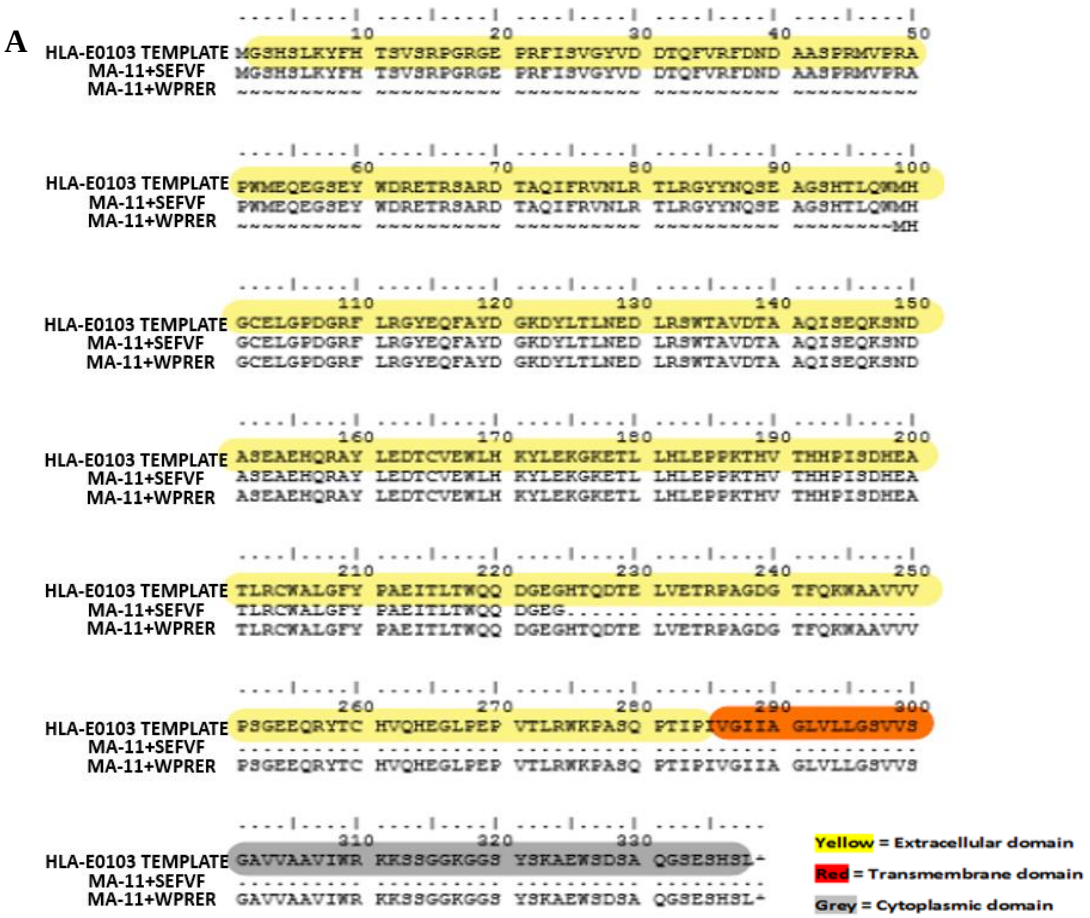


Figure 2.2 HLA-E^{high} BCL generation. (A) The HLA-E0103-pHR plasmid construct with correct sequence of extracellular, transmembrane and cytoplasmic domains. (B) HLA-E MFI expression comparison between HLA-E^{high} BCL, HLA-E^{wt} BCL (negative control), HLA-E^{high} BCL stained with isotype control, and HLA-E^{high} BCL without antibody stain.

Table 2.2 Flow cytometry surface antibodies

Marker	Flourophore	Clone	Source	RRID Identifier
MHC-Ia	Alexa Flour488	W6/32	BioRad	RRID:AB_322094
HLA-E	PE	3D12	Biolegend	RRID:AB_1659249
EpCAM	BV421	EBA-1	BD Biosciences	RRID:AB_2738050
CD163	PerCP/Cy5.5	GHI/61	Biolegend	RRID:AB_2228986
CD123	BV650	6H6	Biolegend	RRID:AB_2563827
CD1c	BV421	L161	Biolegend	RRID:AB_10962909
CD141	BV605	M80	Biolegend	RRID:AB_2572199
CD14	BV711	M5E2	Biolegend	RRID:AB_2562909
CD20	PE/Cy5	2H7	Biolegend	RRID:AB_314256
HLA-DR	BV785	L243	Biolegend	RRID:AB_2563461
CD11b	APC/Cy7	ICRF44	Biolegend	RRID:AB_2563395
CD3	BV510	OKT3	Biolegend	RRID:AB_2561943
CD163	BV510	3G8	Biolegend	RRID:AB_2561944
CD19	BV510	HIB19	Biolegend	RRID:AB_2561668
CD141	BV510	1A4	BD Biosciences	RRID:AB_27828103
CD14	BV510	M5E2	Biolegend	RRID:AB_2561946
CD1c	BV510	L161	Biolegend	RRID:AB_2566119
CD163	BV510	GHI/61	Biolegend	RRID:AB_2650632
CD123	BV510	6H6	Biolegend	RRID:AB_2562068
CD3	BV785	OKT3	Biolegend	RRID:AB_2563507
CD8	PerCP/Cy5.5	SK1	BD Biosciences	RRID:AB_2687497
CD4	APC/H7	SK3	BD Biosciences	RRID:AB_1645732
CD56	PE Texas Red	HCD56	Biolegend	RRID:AB_2563564
CD94	FITC	HP-3D9	BD Biosciences	RRID:AB_396200
NKG2a	APC	131411	R&D Systems	RRID:AB_356987
CD27	PE/Cy7	M-T271	Biolegend	RRID:AB_2562258
CCR7	BV421	G043H7	Biolegend	RRID:AB_11203894
CD45RA	BV605	HI100	Biolegend	RRID:AB_2563814
CD4	PE	SK3	BD Biosciences	RRID:AB_400079
PD-1	BV650	EH12.2H7	Biolegend	RRID:AB_2566362
KLRG-1	BV711	2F1/KLRG-1	Biolegend	RRID:AB_2629721
BTLA	APC	MIH26	Biolegend	RRID:AB_10613101
CD16	BV510	2G8	Biolegend	RRID:AB_2562085
CTLA-4	PE/Cy7	L2D10	Biolegend	RRID:AB_2563097
CD160	PE/Cy7	BY55	Biolegend	RRID:AB_2562875
Tim3	BV421	7D3	BD Biosciences	RRID:AB_2744369
2B4	APC	C1.7	Biolegend	RRID:AB_2702861
TIGIT	FITC	MBSA43	TermoFisher	RRID:AB_2572530
CD3	BUV395	SK7	BD Biosciences	RRID:AB_2744382
CD4	BUV737	SK3	BD Biosciences	RRID:AB_2713927
CD56	PE	MEM-188	Biolegend	RRID:AB_314447
CD39	PE-Texas Red	A1	Biolegend	RRID:AB_2564318
CD103	BV785	Ber-ACT8	Biolegend	RRID:AB_ 2734364
Tim3	BB515	7D3	BD Biosciences	RRID:AB_ 2744368
TIGIT	APC-R700	1G9	BD Biosciences	RRID:AB_2739254
CD28	FITC	CD28.2	BD Biosciences	RRID:AB_396071
Integrin β8	APC	416922	R&D Systems	RRID:AB_2044685

2.7 T cell proliferation assay

Target cells were peptide-loaded at four different concentrations (2μg/ml, 1μg/ml, 0.4μg/ml, 0.08μg/ml, 0μg/ml). T cells were stained with 0.5μM CFSE before co-cultured with peptide-loaded target cells at E:T ratio of 1:1 at 37°C. For e*x vivo* assay, TILs (with confirmed presence of CD94/NKG2a$^+$ T cell population) were stimulated with 1μM *Staphylococcal enterotoxin B* (SEB; Sigma Aldrich) for one hour at 37°C, before stained with CFSE and cultured at 37°C. For analyzing the IL-2 receptor expression, cells were stained with PE-anti-CD25 (M-A251; Biolegend; RRID: AB_2561861) after 30 hours incubation. To analyse the proliferation, cells were measured for CFSE fluorescence after 72 hours. To evaluate the change in response following blocking antibody treatment, T cells were treated with either Ultra-LEAF purified mouse IgG1 kappa isotype Control (MG1-45; Biolegend; RRID:AB_11148942) or 15ug/ml purified anti-CD94 antibody (DX22; Biolegend; RRID:AB_314532) plus 5ug/ml purified anti-NKG2a antibody (Z199; Beckman Coulter; RRID:AB_131495) for 15 minutes at 37°C before stimulated and prolonged culture.

2.8 Cytokine production assessment

To assess cytokine production, target cells were peptide-loaded at five different concentrations (2μg/ml, 1μg/ml, 0.4μg/ml, 0.08μg/ml, 0μg/ml) and co-cultured with T cells at either E:T ratio of 1:10 (for **Chapter 5 and 6)** or E:T ratio of 1:1 (for **Chapter 3)** at 37°C for 6 hours. Supernatant of T cells was collected after 48 hours co-culture and quantified using Bio-Plex Pro^{TM} Human cytokine Assay (BioRad) for IFNγ, CCL-5 and TNFα production. For assessing the effect of blocking treatment on cytokine production, T cells were initially treated with blocking antibody at 37°C for 20 minutes before co-cultured with target cells for 48 hours. For CD103 assay: 15μg/ml anti-CD103 antibody (Ber-ACT-8, Biolegend) or isotype control were

used. For NKG2a assay: 15ug/ml purified anti-CD94 antibody, plus 5ug/ml purified anti-NKG2a antibody or isotype control were used. TGF-β1 presence in the supernatant was evaluated using the Human TGF-beta1 Quantikine ELISA kit (R&D Systems), according to manufacturer's instructions.

Supernatant of *ex vivo* SEB-stimulated $CD8^+$ TIL mixture (with confirmed presence of CD94/$NKG2a^+$ T cell population) were evaluated using Quantikine human IFNγ or IL-2 ELISA kits (R&D Systems), according to manufacturers' instruction.

2.9 Intracellular cytokine staining

T cells were treated with Monensin and Brefeldin A (BD Biosciences) prior to co-culture with peptide-loaded target cells for 5 hours at 37°C. Cells were then fixed with Cytofix/Cytoperm™ (BD Biosciences) and stained with conjugated antibodies including Alexa Flour488-IFNγ (B27; BD Biosciences; RRID:AB_396827), APC-TNFα (Mab-11; Biolegend; RRID:AB_315264), BV421-IL2 (MQ1-17H12, Biolegend; RRID:AB_315264), PE-MIP-1β (D21-1351; BD Biosciences; RRID:AB_10564091), APC-CD107a (H4A3; BD Biosciences; RRID:AB_1727417) and PE-TGF-beta1 (TW4-6H10; Biolegend; RRID:AB_10639862). For assessing the effect of blocking treatment, T cells were initially treated with blocking antibody at 37°C for 20 minutes before co-culture with target cells. For CD103 assay: 15μg/ml anti-CD103antibody or isotype control were used. For NKG2a assay: 15ug/ml purified anti-CD94 antibody, plus 5ug/ml purified anti-NKG2a antibody or isotype control were used. Samples were acquired on Attune Nxt flow cytometer (ThermoFisher Inc.) and analysed using FlowJo™ v.10 software (Tree Star Inc.).

2.10 CFSE-based CTL killing assay

Target cells were initially stained with 0.5μM CFSE (ThermoFisher, UK) before peptide-loaded at five different concentrations (2μg/ml, 1μg/ml, 0.4μg/ml, 0.08μg/ml, 0μg/ml), and co-cultured with CTLs at either E:T ratio of 1:10 (for **Chapter 5 and 6)** or E:T ratio of 1:1 (for **Chapter 3)** at 37°C for 6 hours. For assessing the effect of blocking treatment, T cells were initially treated with blocking antibody at 37°C for 20 minutes before co-culture with target cells. For CD103 assay: 15μg/ml anti-CD103 antibody or isotype control were used. For NKG2a assay: 15ug/ml purified anti-CD94 antibody, plus 5ug/ml purified anti-NKG2a antibody or isotype control were used. For the prolonged duration of cancer exposure assay, target cells were co-cultured with CTLs hourly for up to 12 hours. Cells were then stained with 7-AAD (BD Biosciences) and either APC-E-Cadherin (67A4, Biolegend; RRID:AB_756069) for HCT116 or APC-CD33 (WM53; Biolegend; RRID:AB_314352) for THP-1. Assessment of cell death was based on the $CFSE^{-}$ $7\text{-}AAD^{+}$ population present. Apoptosis-induced death was measured hourly by the presence of activated caspase-3 in CTLs following 12 hours' exposure to target cells, using the FITC-active caspase-3 apoptosis kit (BD Biosciences). Samples were acquired on Attune Nxt flow cytometer (ThermoFisher Inc.).

2.11 TCR sequencing

Briefly, the T cell receptor was sequenced by isolating mRNA from CTLs using RNAeasy Mini Kit (Qiagen, Germany) and cDNA was synthesised using SMARTer RACE cDNA Amplification kit (Takara). Following cDNA generation, TCR sequences were PCR-amplified using PCR Advantage 2 Kit (Takara) and run on 1.2% agarose gel for PCR band confirmation. PCR products were then purified and transform with TOP10 competent cells (ThermoFisher, UK) and plated on LB agar plate. Bacterial colonies were used to perform colony PCR to

confirm correct PCR product. The correct colony was then amplified with LB medium before plasmid DNA was isolated using Spin Miniprep kit (Qiagen, Germany). The purified plasmid DNA was then sent for sequencing at 100nM concentration. Plasmid was sequenced by Timothy Rostron and John Frankland (WIMM).

2.12 Migration transwell assay

Three days prior to the co-exposure of target cells with CTLs, HCT116 or THP-1 was seeded in a 24 well plate at 0.25M/ml in McCoy5'a, supplemented with 10% v/v foetal calf serum (Sigma-Aldrich, UK), 2mM L-Glutamine and 1% v/v (500U/ml) penicillin streptomycin (Sigma-Aldrich, UK) at 37°C for 2-3 days to allow cancer cells to form a monolayer and to produce cytokines and chemokines. On the day of assay, 1M/ml CTLs were seeded on a 5μm pore size transwell insert (Corning) and rested in 37°C incubator for 30 minutes to let the cells to settle to the bottom of the insert. Afterwards, inserts were transferred to 24 well plates containing the target cells and further incubated at 37°C for 2 hours. Following this, the inserts were removed and cells in each well of the 24 well plate were harvested and quantified using flow cytometry. Migration was calculated as the total number of live CTLs present in the 24 well plate. For assessing the effect of blocking treatment, T cells were initially treated with 15μg/ml anti-CD103 or isotype control at 37°C for 20 minutes before co-culture with target cells. Imaging was performed using IncuCyte (Essence Bioscience) and quantified using ImageJ (NIH).

2.13 Mitochondrial and glycolytic analysis

CTLs were starved of IL-2 three days prior to the experiment. On the day of the assay, 7.5M/ml CTLs were seeded on a Seahorse 96 well microplate (Seahorse Biosciences) containing XF

complete media (for mito stress: DMEM plus 2mM L-glutamine, 10mM glucose and 1mM sodium pyruvate; for glycol stress: DMEM plus 2mM L-glutamine). For the mito stress assay, drugs were injected onto cells, initially with 1mM oligomycin, 1.5mM FCCP and finally with 100μM rotenone/ 1mM antimycin A at 20-minute intervals. For the glycolysis stress assay, drugs were injected onto cells, initially with 10mM glucose, 1μM oligomycin and finally with 50mM 2-deoxy-glucose (2-DG) at 20-minute intervals. Drug injection and analysis were performed by the Seahorse XF96 extracellular Flux analyser (Seahorse Biosciences), connected with the Seahorse Wave software (Agilent). The oxygen consumption rate (OCR) was recorded as pmol/min while the extracellular acidification rate (ECAR) was recorded as mpH/min.

2.14 Live cell imaging

Live cell imaging was performed and headed by Huw Colin-York (Fritzsche group, WIMM). Briefly, HCT116 or THP-1 was seeded at 0.05M/ml per well in μ-slide 8 well glass bottom (Ibidi; cat number:80841) in McCoy5'a, supplemented with 10% v/v foetal calf serum, 2mM L-Glutamine and 1% v/v (500U/ml) penicillin streptomycin and incubated at 37°C for 2 days to allow cells to attach to the glass, grow and produce cytokines and chemokines. On the day of the killing duration assay, 1μg/ml peptide was added 1 hour before imaging. The seeded target cell culture was also supplemented with 2mM calcium chloride and 5μl/well of Alexa-Fluor 647-Annexin V (Cat number: A23204; ThermoFisher, UK). The imaging chamber was then loaded onto a spinning disk confocal microscope equipped with a 10X air objective, enclosed in an incubator chamber at 37°C and 5% CO_2. CTLs were then added at 2M/ml and imaging was carried out of each individual well in parallel, using brightfield and 632nm excitation at 20% of maximum. Imaging was carried out for 12 hours at 1 frame per four minutes. Annexin V positive staining is illustrated in the figures as blue.

For the killing efficiency assay, target cells and CTLs were prepared as described above. On the day of assay, CTLs were labelled with 10μg/ml calcium sensitive probe Fluo4-AM (F14201, Sigma Aldrich, UK) and 2.5μM probenecid (Sigma Aldrich, UK) and incubated at 37°C for 5 minutes. CTLs were then washed twice in fresh medium containing probenecid. The imaging chamber was set up as described above. Flou4-AM-labelled CTLs were added to each well of the imaging slide before imaging was carried out using brightfield and 488nm excitation at 20% of maximum. Imaging was carried out for 2 hours at 4 frames per minute. Fluo4-AM positive staining is illustrated in the figures as red. All images were analysed using ImageJ (NIH, US).

2.15 Immunohistochemical analysis

Preparation of immunohistochemical slides is as previously described (Freedman et al., 2018; Pell et al., 2019). All immunohistochemistry staining was carried out by Molly Browne and Lucia Cerundolo (Verrill group, JR Hospital). Briefly, adjacent tissue sections of formalin-fixed, paraffin-embedded tumor tissue from five lung cancer patients were stained immunohistochemically for E-Cadherin (Dako, Denmark), CD103 (AbCAM, UK) and CD8 (Agilent Technologies). Automated staining was carried out using the Leica BOND-MAX autostainer (Leica Microsystems) following antigen retrieval method using Epitope Retrieval Solution 2 (Leica Microsystems). Immunohistochemistry computerized analysis was carried out by Nasullah Khalid Alham (Verrill Group, JR Hospital), using the Visiopharm Integrator System platform. This platform was made for analysing digitized serial slides, with protocol implemented as Analysis Protocol Packages (APP). Several APPs were designed to quantify slides stained individually with the antibodies following tissue section realignment. Realignment was performed at both large scale and finer detailed level, to get the best match between the three adjacent slides. Region of interest (ROI) was conducted and first auxiliary

APP runs using threshold classification that identifies the tissue regions. The second auxiliary APP runs done on the E-Cadherin slides used threshold classification identifying positive and margin regions. ROI was then superimposed on aligned CD8 and CD103 stained slides for subsequent analysis. HDAB-DAB colour deconvolution band was used to detect positively stained cells on CD103 and CD8 slides. To enhance the stained cells, while suppressing the background variation, several pre-processing steps were included, including the colour deconvolution bands were input to a threshold classifier. The thresholding classification method defines a threshold for a given feature and assigns one class to all pixels with a feature value above or equal to that value, and another class for the rest.

The classification rule is defined as:

$$Class\big(Feature(X,Y)\big) = \begin{cases} A, Feature(x,y) \geq T \\ B, \qquad\quad Otherwise \end{cases}$$

where T is the user-selected threshold (cut-off value), A and B are the labels/classes to which the pixel is assigned. As post-processing steps; a method for cell separation which is based on shape and size was used; cell areas that are too small are removed and finally applying unbiased counting frames to avoid the cells that are intersecting with neighbouring tile boundaries counted twice (or more).

2.16 mRNA expression analysis

Simultaneous IFNγ and TNFα protein and mRNA levels in antigen-specific CTLs were determined using the PrimeFlow^{TM} RNA assay kit (ThermoFisher Inc,), carried out according to manufacturer's instruction. Briefly, each T cell type was treated with 10µl/ml ImmunoCult^{TM} Human CD3/CD28 T cell Activator (StemCell Technologies) at 1-hour period (for up to 3 hours) before stained with LIVE/DEAD® Fixable Aqua Dead Cell Stain Kit (ThermoFisher,

UK) for 20 minutes at 4°C. Cells were then stained for PE/Dazzle594-CD8 (Biolegend, SK1, RRID:AB_2566515) for 20 minutes at 4°C. Cells were later fixed and permeabilised using PrimeFlow Fixation Buffer and PrimeFlow RNA Permeabilisation Buffer with RNAse Inhibitors. Cells were then stained for intracellular IFNγ and TNFα as described above. Following this, cells were treated with IFNγ and TNFα mRNA target probe sets and incubated for 30 minutes at 40°C. Hybridisation of the probes were performed using PrimeFlow RNA PreAmp Mix, followed with RNA Amp Mix, at 40°C incubation for 30 minutes for each step. Labelling of hybridised mRNA were performed using PrimeFlow RNA label probes, containing fluorophore Alexa Fluor 488, Alexa Fluor 647 and Alexa Fluor 750. Samples were then acquired on Attune Nxt flow cytometer (ThermoFisher Inc.).

2.17 Bisulphite treatment, PCR and methylation sequencing

Firstly, 2M CTLs were treated with protein precipitation solution (Qiagen) and isopropanol before cells were collected as pellet using microcentrifuge at 13000rpm for 5 minutes. Pellet were then resuspended using 70% ethanol to bind gDNA and later pelleted by microcentrifugation again before resuspending in nuclease-free water. The extracted gDNA was bisulfite-treated using EZ DNA methylation-Gold kit (Zymo Research), according to manufacturer's instruction. Briefly, gDNA was treated with CT Conversion Reagent solution before treated with M-binding buffer. The gDNA was then treated with M-Desulphonation buffer to remove salt from isolated gDNA and later eluted using nuclease-free water. gDNA concentration was measured using Nanodrop One spectrophotometer (ThermoFisher Inc.).

Sets of forward and reverse bisulfited primers were designed for each CpG site of the IFNγ promoter (GenBank accession no. J00219)**.** The list of bisulfited primers sets are as follows: for CpG site -295 (set sequences: 5'-

TGTTTTTAATTATAAGTAAATGATTAATGTGTTTTG-3’ and 5’-CATTATACCCACCTATACCATTCTAATAAAA-3’), for CpG site -186 (5’-GTGGGGAGGTATAAAAAAATTTTTAG-3’ and 5’-CATTTAAATATTATAATTAAAATTTCCTTTAAACTCC-3’), for CpG site -54 (5’-GGATTTAAGGAGTTTAAAGGAAATTTTAATTAT-3’ and 5’-CCTCCTCTAACTACTAATATTTATACCTAAT-3’) and for CpG sites +122 and +128 (5’-TAGTTAAGTTTTTTGGATTTGATTAGTTTGA-3’ and 5’-AATCCTAACAATAACAACCAAAAAAAC-3’). The PCR was performed using Advantage-HF 2 PCR kit (Takara Biotech), as per manufacturer’s instruction. Briefly, 100nM of PCR primers were used in mix with minimum 100ng of bisulfite-treatment gDNA, HF-PCR buffer solution, 0.2mM dNTPs and 1U Titanium *Taq* DNA Polymerase Mix. The cycling parameters were 94°C for 90 seconds (1 cycle), 94°C for 15 seconds, 54°C for 60 seconds, 68°C for 75 seconds (35 cycles) and 68°C for 180 seconds (1 cycle). The PCR product was confirmed using 1.2% agarose gel at 50V for 60 minutes. Once band presence was confirmed, the PCR product was cloned using TOPO TA cloning kit for sequencing (ThermoFisher Inc.). Briefly, the PCR product was cloned into PCR4-TOPO plasmid and transformed onto TOP10 *E.coli* competent bacteria and grown in LB agar plate with 100mM ampicillin. Grown colonies were selected and miniprep was performed to isolate plasmid using Plasmid Miniprep Kit (Qiagen). Plasmid was sequenced by Timothy Rostron and John Frankland (WIMM) using M13 forward and reverse primers with Big Dye Terminator v3 Chemistry (Applied Biosystems) as per manufacturer’s instruction and analysed on an AB-3730 capillary electrophoresis instrument. Data was then further analysed for methylation presence using SnapGene software (GSL Biotech LLC).

2.18 Statistical analysis

All graph generation and statistical analyses were conducted using GraphPad Prism v.7 software. Unless stated otherwise, data were summarized as median ± s.e.m. All statistical details of experiments and number of patients used for each analysis can be found in figure legends and results sections. All *in vitro* T cell experiments were performed three times for each type of experiments. Statistically significant differences between two groups were assessed using a two-tailed paired *t*-test, with Wilcoxon adjustments for non-parametrically distributed variable. For comparisons between more than two paired groups of tissues or treatments, one-way ANOVA with Tukey's multiple comparison test were performed. Comparisons between different blocking treatments on different T cell populations and of the difference in TILs populations across different TNM stages were carried out using two-way ANOVA with Tukey's multiple comparisons test. Correlation analysis was performed using non-parametric Spearman test. All tests were two-sided, and differences were considered statistically significant at *p*-value <0.05.

Chapter 3: Enriched HLA-E and CD94/NKG2a interaction limits antitumor $CD8^+$ tumor-infiltrating T lymphocytes responses

3.1 Introduction

Avoidance of immune destruction is a hallmark of cancer. Tumor employs diverse mechanisms to escape anti-tumor immunity such as by enhancing the immune checkpoint expression of PD-1 and CTLA-4 on TILs and by downregulating the MHC Class Ia surface expression on cancer cells (Ahmadzadeh et al., 2009; Koopman et al., 2000; Leone et al., 2013). The tumor microenvironmental changes can negatively affect the efficacy of tumor-localized T cell priming, leading to impaired anti-tumor immunity and increased tumor progression. Although past clinical studies of checkpoint blockade using anti-PD-1 or anti-CTLA-4 have shown improvement in some patients, these treatments failed to improve overall response rates in many treated cancer patients (Besser et al., 2013; Garon et al., 2015; Hodi et al., 2010; Muro et al., 2016).

Various studies have associated an enrichment of the non-classical MHC-Ib molecule, HLA-E, with poorer clinical outcome in cancer patients (Andre et al., 2018; Bossard et al., 2012; de Kruijf et al., 2010; Gooden et al., 2011; Levy et al., 2008; van Montfoort et al., 2018). For example, high numbers of head-and-neck cancer patients were found to have HLA-E-enriched carcinomas and lower survival rates. Importantly, lymphoma-transplanted Qa-1^b knockout mice (Qa-1^b is the murine HLA-E homologue) were demonstrated to have better tumor regression (Andre et al., 2018; van Montfoort et al., 2018). However, it still remains unclear whether theenrichment of HLA-E is specific to certain cells and tissue locations, as well as if this enrichment can negatively affect anti-tumor cancer-specific T cell responses in cancer patients.

The MHC Class Ia molecules help in the recognition of cancer cells, primarily through the TCR. In contrast, the HLA-E can be recognized by the inhibitory heterodimeric CD94/NKG2a receptor complex, known to be expressed by NK cells and a subset of T cells (Braud et al., 1998). The HLA-E and CD94/NKG2a interaction is well-established to inhibit spontaneous NK cell cytotoxic functions and prevents autoimmunity, but it is also known to be exploited by cytomegalovirus (CMV) to evade anti-viral immunity (Braud et al., 2003; Lazetic et al., 1996; Lee et al., 1998; Tomasec et al., 2000; Ulbrecht et al., 2000). In cancer, a phase II human clinical trial using anti-NKG2a in combination with anti-EGFR to treat head and neck cancer patients have demonstrated an improvement in the overall response rate in majority of the patients treated (Andre et al., 2018). However, it is still unknown in other human cancers whether the HLA-E and CD94/NKG2a inhibitory machinery could be exploited to specifically impair TIL priming capacity and inhibit anti-tumor T cell responses.

The efficacy of cytotoxic T-cell priming in cancer relies on the uptake and presentation of tumor antigen by antigen-presenting cells (APCs) via the MHC Class Ia molecules. For example, tumor-localized $CD141^{+}$ cDC can mediates prolonged tissue-localized cross-priming of T cell activation and maintenance (Bachem et al., 2010; Roberts et al., 2016). In contrast, tumor-infiltrating macrophages treated with anti-CD47 showed improved phagocytosis and antigen priming capacity in murine model (Tseng et al., 2013). However, studies using DC vaccines that solely targeted the recovery of MHC Class Ia surface expression on tumor APCs failed to improve the outcomes in mice and cancer patients (Iversen et al., 2014; Kavanagh et al., 2007; Slingluff et al., 2007). This is possibly due to the expression of inhibitory receptors such as PD-1 on tumor-localized APCs that can affect the efficacy of MHC Class Ia–T cell priming and likely further contribute towards tumor growth (Laoui et al., 2016; Ruffell et al.,

2014; Salmon et al., 2016). It is therefore likely that an enriched inhibitory HLA-E presence in tumor could interfere with efficient presentation of tumor neoantigens, by dampening and masking MHC Class Ia–T cell priming through the CD94/NKG2a interaction.

Therefore, in this chapter, we sought to address the main question on the association and contribution of HLA-E and CD94/NKG2a to anti-tumor cancer-specific CTLs responses. Specifically, we investigated the correlation between HLA-E and CD94/NKG2a expressions in tumor, and the *ex vivo* phenotype of CD94/NKG2a^{+} CTLs derived from paired tumor, paratumor and peripheral blood samples of cancer patients. Most importantly, we assessed the characteristics and possible inhibitory mechanisms of HLA-E and CD94/NKG2a interaction on cancer-specific CTLs functions.

3.2 Results

3.2.1 HLA-E expression is upregulated on specific cell populations in tumor

Previous studies have highlighted enrichment of HLA-E across cancer tissue sections (Andre et al., 2018; Bossard et al., 2012; Gooden et al., 2011; van Montfoort et al., 2018), but it remains uncertain on whether specific cell populations in cancer actually contributed towards the enrichment. We first evaluated if HLA-E upregulation could be exhibited by specific subpopulation of cancer cells, such as the epithelial cell adhesion molecule (EpCAM)-specific cancer cells. This is as past studies have demonstrated the commonality of EpCAM overexpression on a majority of epithelial-derived tumor cells of gastrointestinal origin (El-Sahwi et al., 2010; Kuiper et al., 2011; Lazetic et al., 1996; Osta et al., 2004). Following exclusion of immune cells from our flow cytometry analysis (**Figure 3.1**), we confirmed tumor carcinomas do have EpCAM^{high} cells which were absent in paired paratumor tissue and PBMC, indicating that EpCAM^{high} cells in tumor are specifically epithelial cancer cells (**Figure 3.2**).

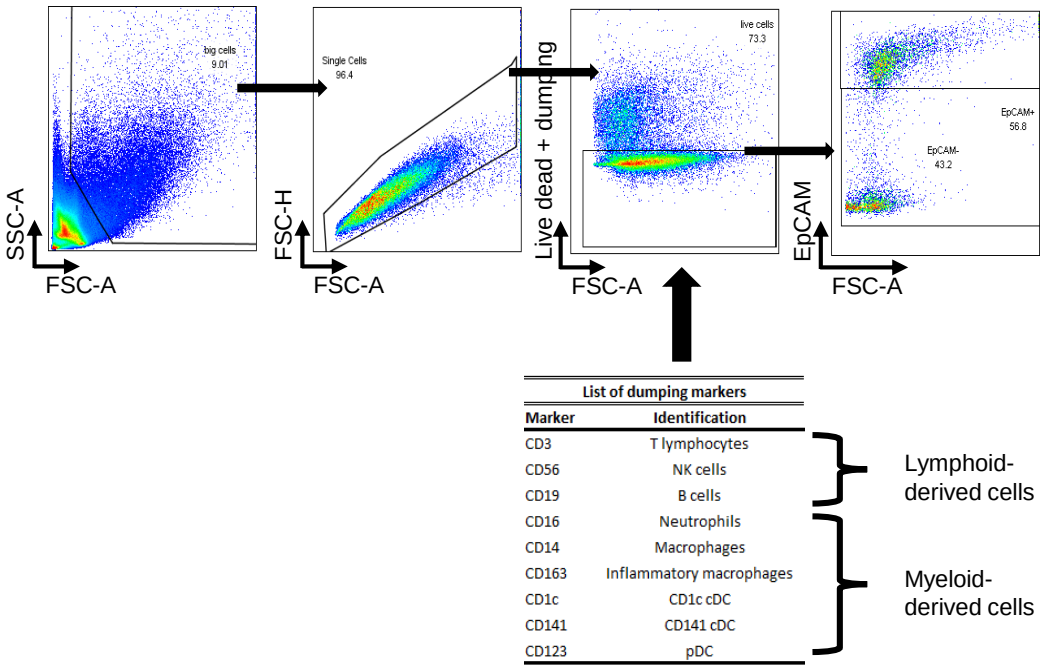


Figure 3.1 Gating strategy to identify EpCAM-specific cells. Identification of EpCAM-specific cells, by using dumping markers to exclude lymphoid-derived and myeloid-derived cells.

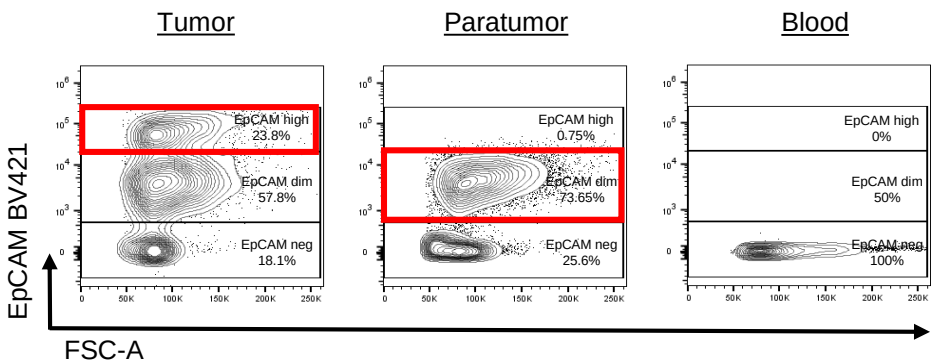


Figure 3.2. **EpCAM expression on cells derived from tumor, paratumor and peripheral blood of a esophageal patient.** Representative gating of contour plots on epithelial cell adhesion molecule (EpCAM) expression on cells isolated from paired tumor, paratumor and peripheral blood, with EpCAM-high-expressing cells observed only in tumor-derived tissue identified as cancer cells whereas $EpCAM^{dim}$ as possibly tumorigenic cells.

This is consistent with previous studies highlighting tumor epithelial cells exhibiting over-expression of EpCAM as a result of their tumorigenesis process (El-Sahwi et al., 2010; Kuiper et al., 2011; Lazetic et al., 1996; Osta et al., 2004). In addition, we showed that the proportion of $EpCAM^{dim}$ tumor-derived cells (average: 50.8%) are lower than the $EpCAM^{dim}$ paratumor-derived cells (average: 74.4%) **(Figure 3.2)**, indicating that $EpCAM^{dim}$ population as possibly becoming tumorigenic (not specifically cancer cells).

Upon evaluation of HLA-E on these populations, we observed higher frequency of $HLA\text{-}E^{+}$ $EpCAM^{high}$ epithelial cancer cells (average= 81%), compared to the $EpCAM^{dim}$ tumor-derived epithelial cells (average 41.3%) and the $EpCAM^{dim}$ paratumor-derived epithelial cells (average 21%) **(Figure 3.3A).** This is consistent with significantly higher HLA-E surface expression on the $EpCAM^{high}$ epithelial cancer cells ($p<0.01$) (**Figure 3.3B**). In contrast, the MHC Class Ia surface expression is downregulated on $EpCAM^{high}$ epithelial cancer cells (**Figure 3.3C**). We saw similar patterns of gradual HLA-E upregulation from $EpCAM^{dim}$ paratumor-derived cells to the $EpCAM^{high}$ epithelial cancer cells across different cancers of gastrointestinal origin, namely esophageal, gastric and colorectal cancers **(Figure 3.4).**

In addition to cancer cells, the immunosuppressive tumor microenvironment is well known to dysregulate the functionality of tumor-infiltrating immune cells (Laoui et al., 2016; Ruffell et al., 2014; Salmon et al., 2016). We thus decided to assess whether the HLA-E expression could also be upregulated on macrophages, cDC subsets and plasmacytoid DC (pDC) residing in solid tumors (gating strategy and identification of APC subpopulations as per **Figure 3.5A and B.**

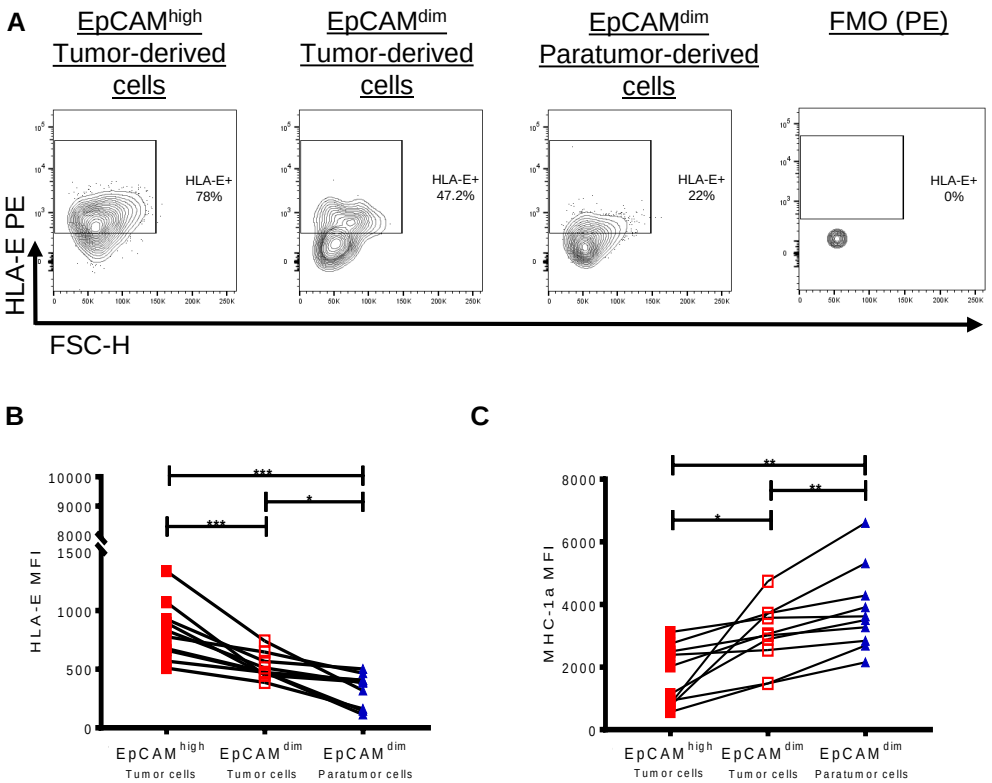


Figure 3.3. HLA-E and MHC Class Ia expression on EpCAM-expressing cells. (A) Representative gating of HLA-E^{+} population on tumor-derived EpCAM^{high} cancer cells *(left)*, tumor-derived EpCAM^{dim} tumorigenic cells *(middle-left)*, paratumor-derived EpCAM^{dim} epithelial cells *(middle-right)*, and FMO *(right)*. Gating was based initially on **Figure 3.1**. The HLA-E expression (B) and MHC-1a expression (C) by median fluorescence intensity (MFI) on three different populations of EpCAM-expressing populations, from patients with different cancer. N, number of patients=10 (esophageal cancer, n=3, gastric cancer, n=4, colorectal cancer, n=3). Analysis: one-way ANOVA with Tukey's post hoc analysis. Connecting lines represents samples from the same patients. * indicates p-value<0.05, ** p-values<0.01, *** p-values<0.001, ns, not significant. Data represent with median±s.e.m.

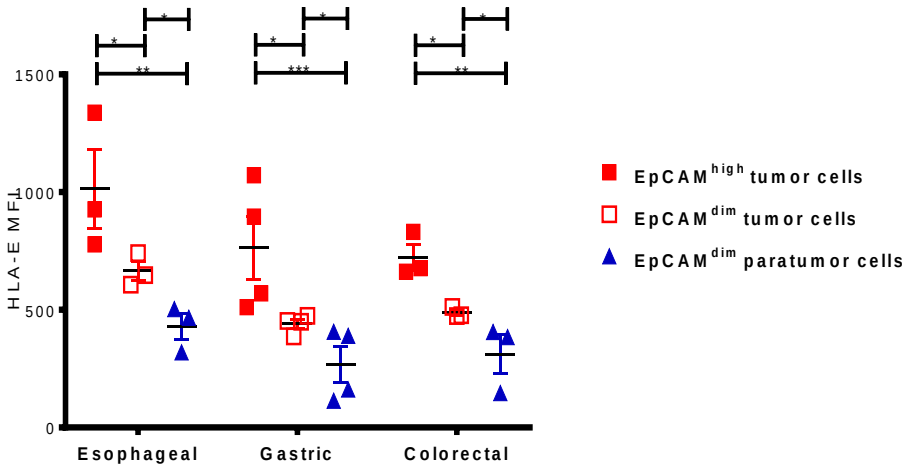


Figure 3.4. HLA-E expression on EpCAM-expressing cells in different cancer types. The HLA-E expression by median fluorescence intensity (MFI) on three different populations of EpCAM-expressing populations in esophageal cancer patients, gastric cancer patients and colorectal cancer patients respectively. N, number of patients: esophageal cancer, n=3, gastric cancer, n=4, colorectal cancer, n=3); Analysis: one-way ANOVA with Tukey's post hoc analysis. Horizontal line represents median; interval represent 95% confidence. * indicates p-value<0.05, ** p-values<0.01, *** p-values<0.001, ns, not significant. Data represent with median±s.e.m.

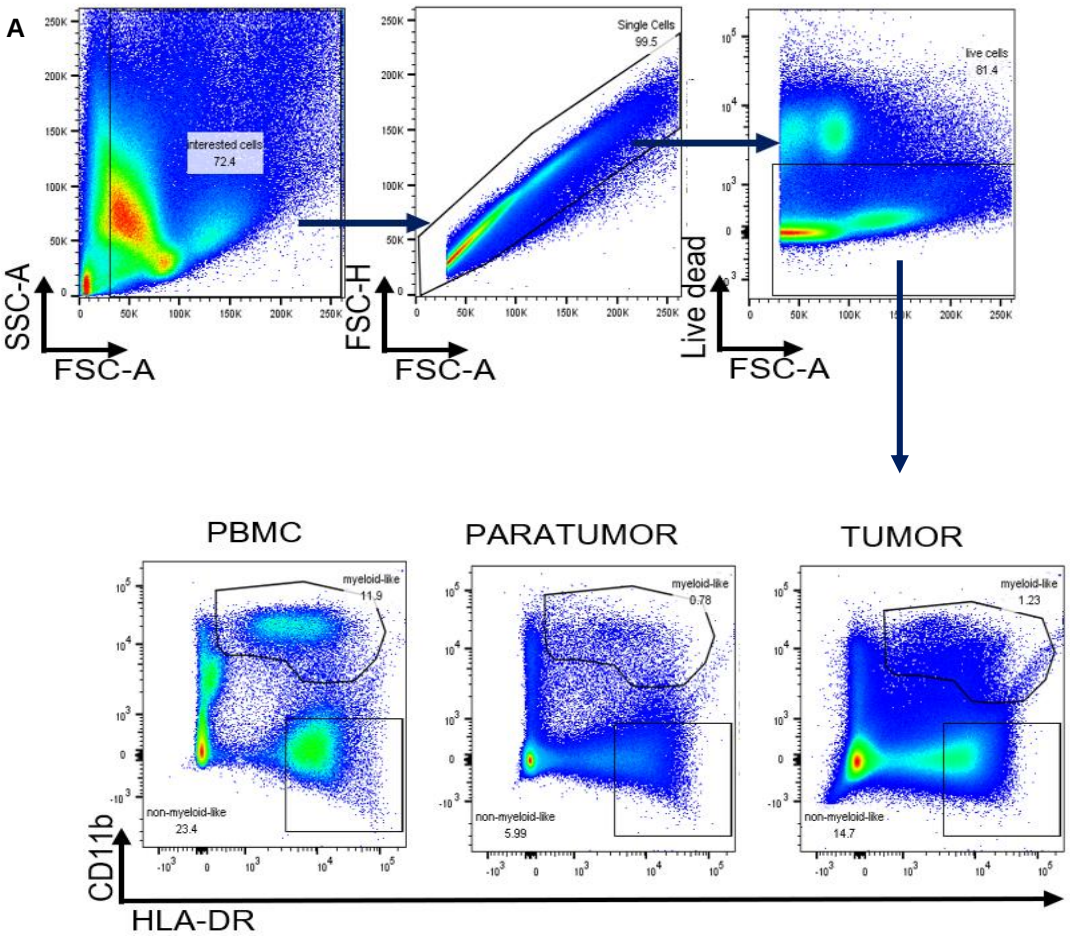


Figure 3.5 Gating strategy for APC subsets. (A) Initial gating strategy to identify myeloid and non-myeloid cells in peripheral blood, paratumor and tumor samples.

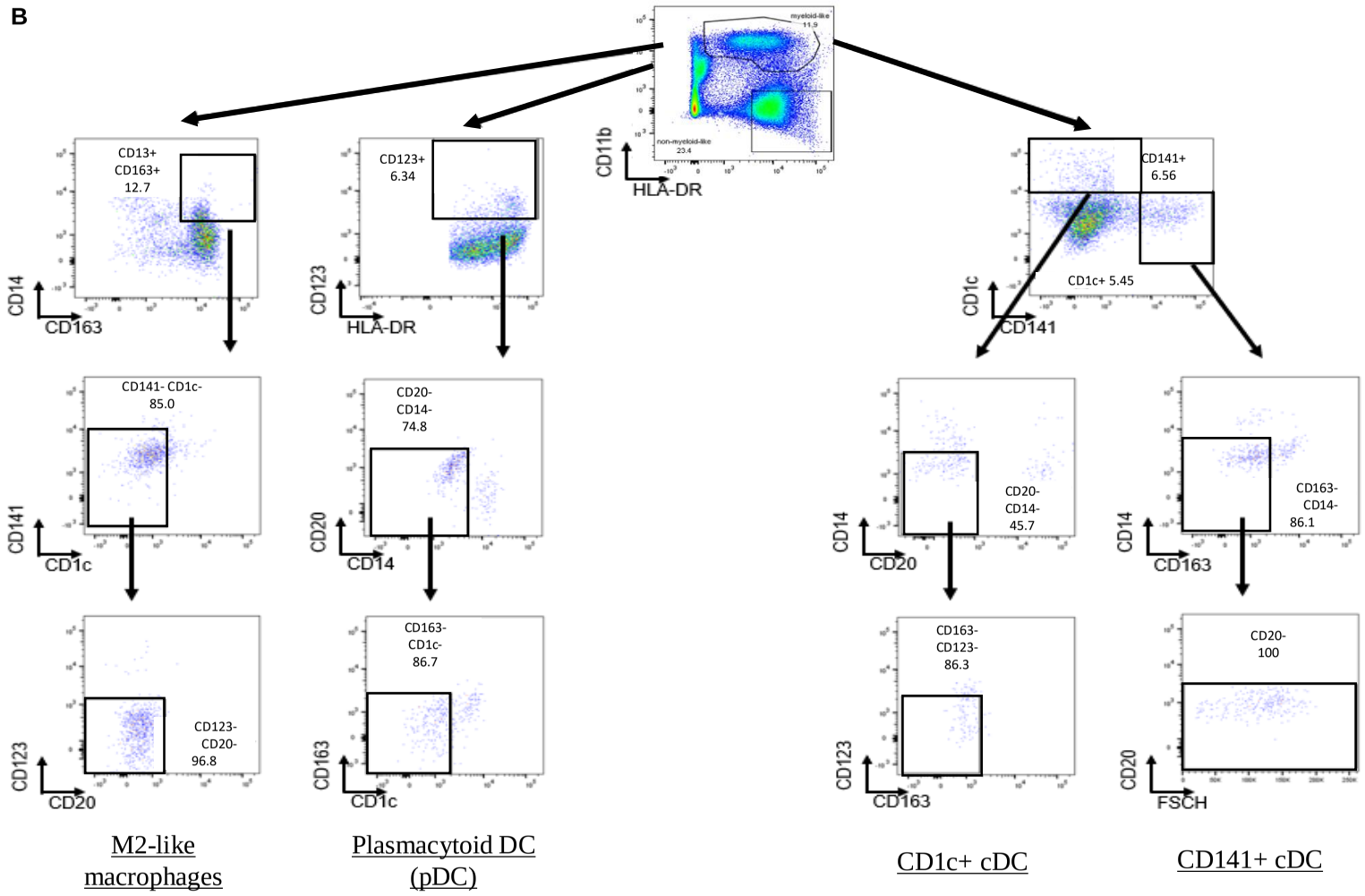


Figure 3.5 Gating strategy for APC subsets. (B) Further gating strategy to identify and confirm macrophages, pDC, CD1c cDC and CD141 cDC.

In particular, we found that tumor-localized CD141$^+$ cDC have significantly reduced MHC Class Ia expression (average of 2-fold to 4-fold) but increased HLA-E expression (average of 2-fold) compared to the same population derived from paired paratumor tissue and PBMC (**Figure 3.6A and B**). Other professional APC subsets in tumor, namely CD1c$^+$ cDC, pDC and inflammatory macrophages, were also found to have an increased HLA-E expression and decreased MHC-Ia expression **(Figure 3.6B)**. Non-professional APC such as B cells also demonstrated significant increase of its HLA-E and reduced MHC-Ia expressions in solid tumors (**Figure 3.7**). From the total myeloid-like cells, the higher frequency paratumor-derived and PBMC-derived APC subpopulations have significantly lower HLA-E expression **(Figure 3.8)**.

A similar pattern of HLA-E upregulation on tumor-derived DCs was observed across the three different cancers of gastrointestinal origin as well as in kidney cancer (**Figure 3.9**). This therefore suggests that HLA-E upregulation is not only enriched on cancer cells but also possibly on other tumor-residing cells such as on APCs, indicating a potential contributory role of HLA-E in evading anti–tumor cell responses in cancer.

3.2.2 Inhibitory CD94/NKG2a ligand is upregulated on CD8$^+$ TILs

Given the upregulation of HLA-E in the tumor microenvironment, we then investigated whether the inhibitory receptor of HLA-E, the heterodimeric CD94/NKG2a, displayed a similar pattern of enrichment in the same set of cancer patients from paired tumor, paratumor and peripheral blood samples.

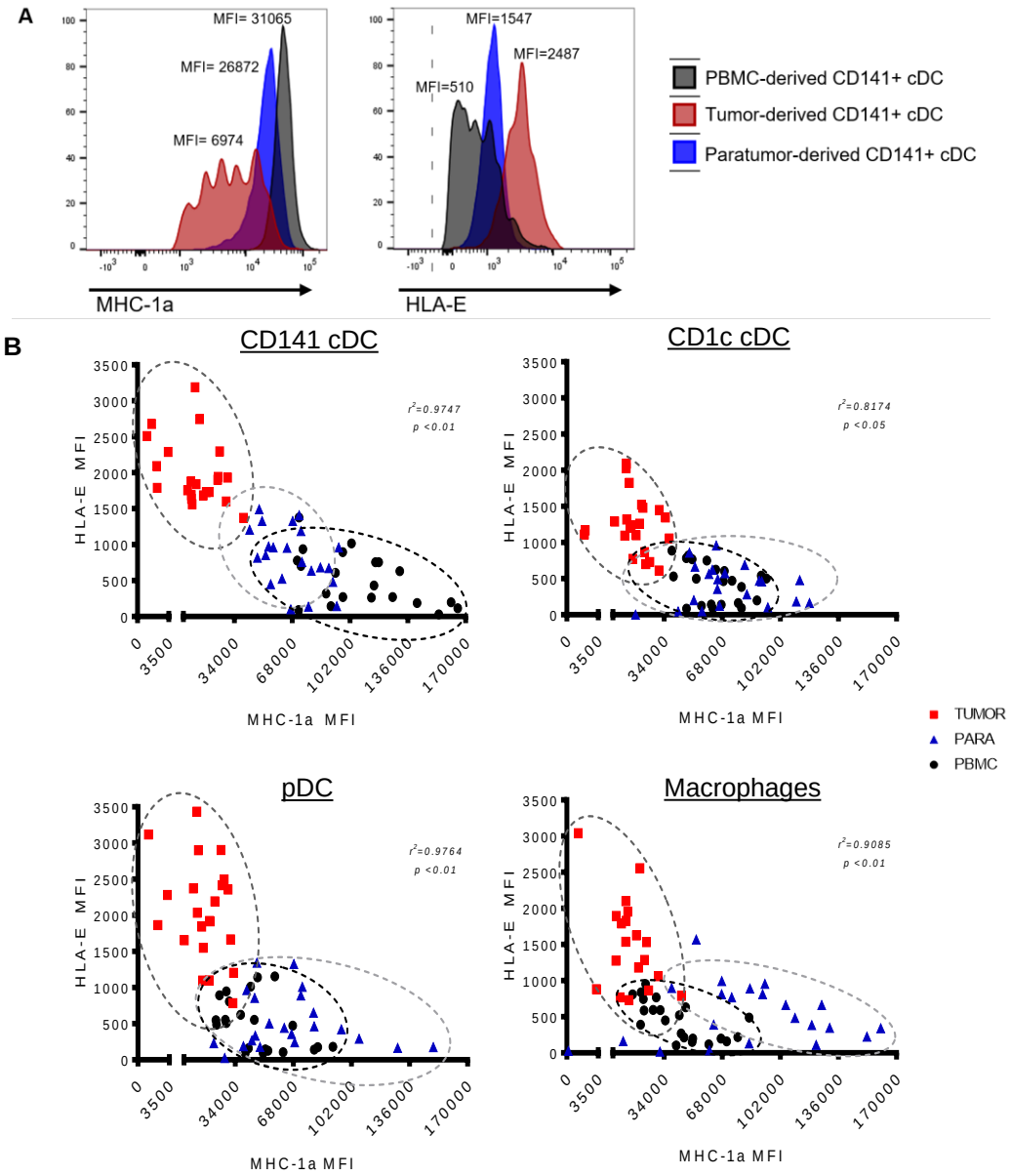


Figure 3.6 HLA-E and MHC Class Ia expression on different APC subsets. (A) An example of overlapping histogram plots illustrating MHC Class Ia and HLA-E expresssion on CD141 cDCs of three different but paired tissue sites (tumor, paratumor and peripheral blood). (B) Correlative expression of HLA-E and MHC-1a by MFI on $CD141^{+}$ cDC, $CD1c^{+}$ cDC, pDC and inflammatory macrophages derived from paired tumor, paratumor and PBMC. N, number of patients=22 Analysis: correlative analysis with Spearmen test. * indicates p-value<0.05, ** p-values<0.01, *** p-values<0.001, ns, not significant. Data represent with median±s.e.m.

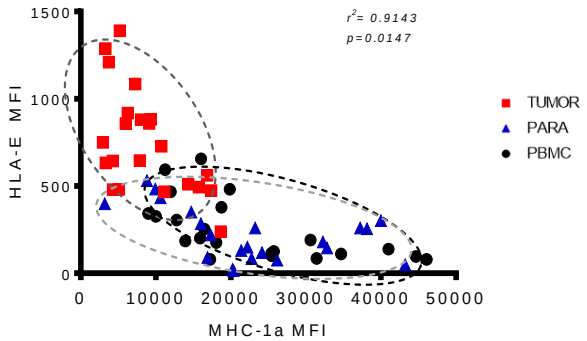


Figure 3.7 HLA-E and MHC Class Ia expression on non-professional APC, B cells. Correlative expression of HLA-E and MHC-1a by MFI on B cells derived from paired tumor, paratumor and PBMC. N, number of patients=22 Analysis: correlative analysis with Spearmen test. * indicates p-value<0.05, ** p-values<0.01, *** p-values<0.001, ns, not significant. Data represent with median±s.e.m.

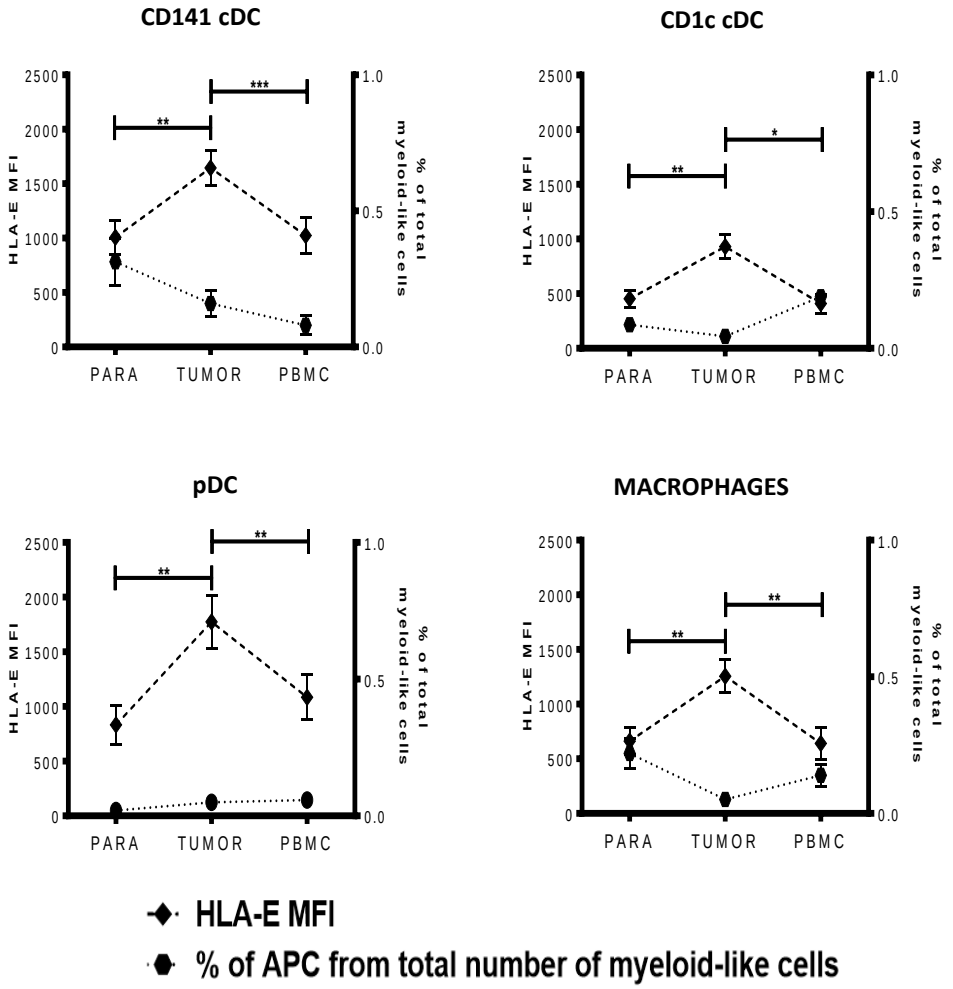


Figure 3.8 Correlative analysis between HLA-E expression and proportion of each APC subsets. The proportion of each APC subset was determined from the total number of myeloid-like cells (<1%). N, number of patients=22. Analysis: two-way ANOVA with Tukey's post hoc analysis. Horizontal line represents median; interval represent 95% confidence. Long dash line represent HLA-E expression and dot line represent frequency. * indicates p-value<0.05, ** p-values<0.01, *** p-values<0.001, ns, not significant. Data represent with median±s.e.m.

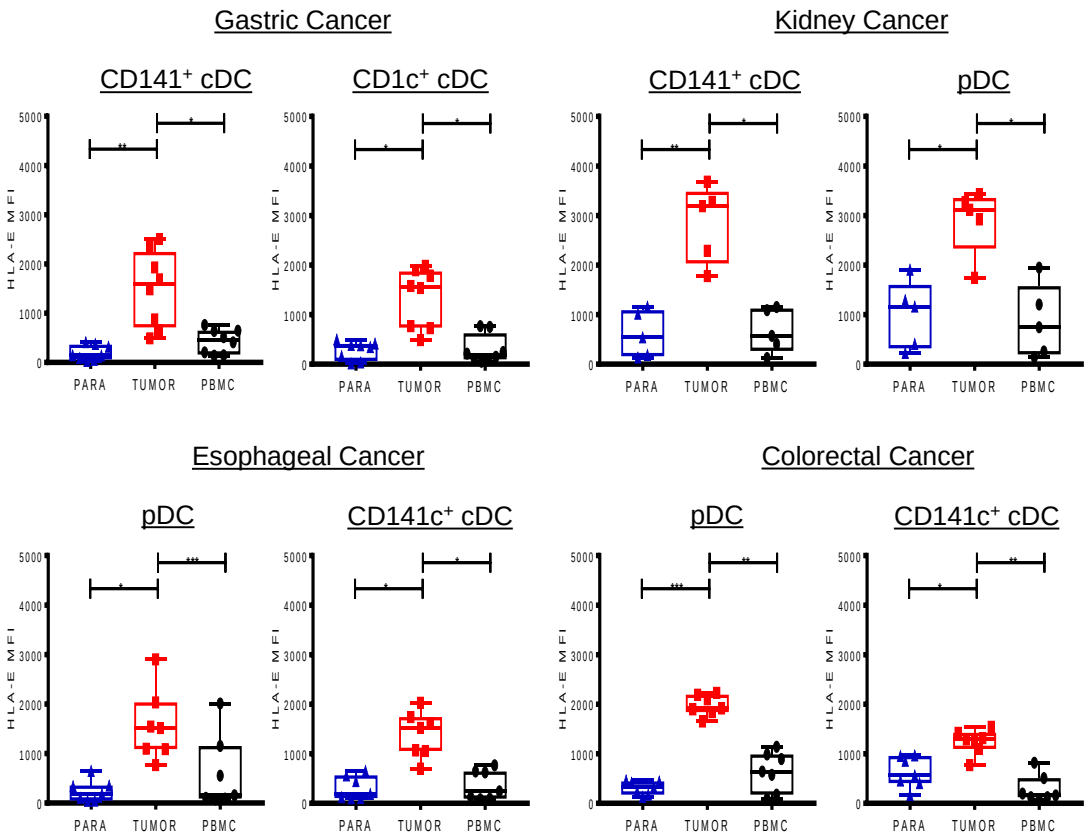


Figure 3.9 HLA-E expression on different APC subsets derived from paired tumor, paratumor and peripheral blood samples, in different cancer types HLA-E expression by MFI on DC subsets from paired tumor, paratumor and PBMC samples in four different cancer types. (N, number of esophageal cancer patients=7; gastric cancer n=8; colorectal cancer n=7; kidney cancer n=5). For analysis: one-way ANOVA with Tukey's post hoc analysis. Horizontal line represents median; interval represent 95% confidence. Connecting lines represents samples from the same patients. * indicates p-value<0.05, ** p-values<0.01, *** p-values<0.001, ns, not significant. Data represent with median±s.e.m.

We observed significant CD94 and NKG2a co-expression and heterodimeric CD94/NKG2a$^+$ T cell population in tumor, but minimal CD94/NKG2a population and co-expression on T cells derived from paratumor tissue and PBMC **(Figure 3.10A and B)**. In contrast, we did not observe any heterodimeric CD94/NKG2c$^+$ T cell population from either tumor, paratumor or PBMC **(Figure 3.11).** The enrichment of CD94/NKG2a$^+$ TILs population is directly correlated with the enrichment of HLA-E on both epithelial cancer cells and tumor-derived CD141$^+$ cDCs on the same cancer patients **(Fig. 3.12)**.

Effector-based immune cells such as CD8$^+$ T cells, NKT cells and NK cells were the ones that had significantly higher CD94/NKG2a$^+$ population in tumor whereas regulatory-based cells such as CD4$^+$ T cells lack CD94/NKG2a$^+$ population in each of the tissue sites evaluated (**Figure 3.13**). The enrichment of the CD94/NKG2a$^+$ CD8$^+$ T cell population in tumor was similarly observed across different types of gastrointestinal cancers, namely esophageal, gastric and colorectal tumors **(Figure 3.14).**

Interestingly, we observed that gastrointestinal cancer patients with later TNM stage of cancer size (indicative of tumor progression) have a significant, but gradual increment of CD94/NKG2a$^+$ CD8$^+$ TILs population (**Figure 3.15**). This likely suggests the preferential selection of CD94/NKG2a overexpression during tumor growth in human cancers.

In assessing the maturation phenotype of TILs in tumor, we found that CD94/NKG2a$^+$ CD8$^+$ TILs are primarily of late stage effector memory phenotype (CD27$^-$ CD45RA$^-$ CCR7$^-$), in contrast to the predominantly early stage effector phenotype of the CD94/NKG2a$^-$ population (CD27$^+$ CD45RA$^+$ CCR7$^-$) (**Figure 3.16**).

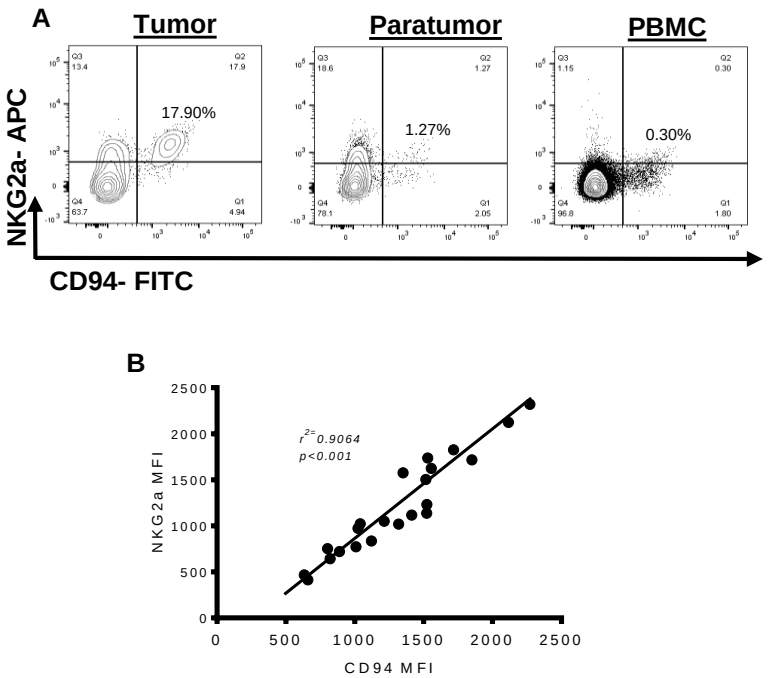


Figure 3.10 CD94/NKG2a expression on tumor-infiltrating T cells. (A) Representative contour plots on CD94 and NKG2a staining on $CD3^+$ T cells from paired tumor, paratumor and PBMC samples from one cancer patient (Proportion of CD94/$NKG2a^+$ T cells in tumor=17.9%; in paratumor=1.27%; in PBMC=0.3%). (B) Correlative analysis on NKG2a and CD94 expression by MFI on tumor-derived $CD3^+$ T cells. N, number of patients= 22 (esophageal cancer, n=7, gastric cancer, n=8, colorectal cancer, n=7). For analysis: correlative analysis of non-parametric Spearman test, * indicates p-value<0.05, ** p-values<0.01, *** p-values<0.001, ns, not significant. Data represent with median±s.e.m.

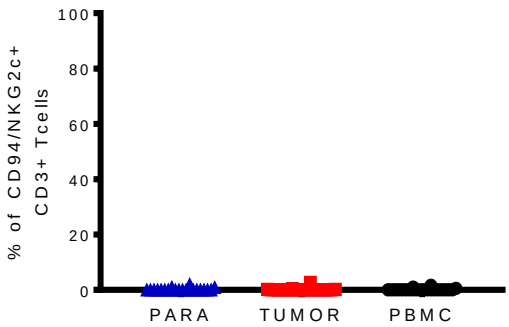


Figure 3.11 Activating CD94/NKG2c+ T cells in paired samples. The frequency of CD94/NKG2c^{+} T cells from paired tumor, paratumor and PBMC samples. N, number of patients=22 (esophageal cancer, n=7, gastric cancer, n=8, colorectal cancer, n=7).

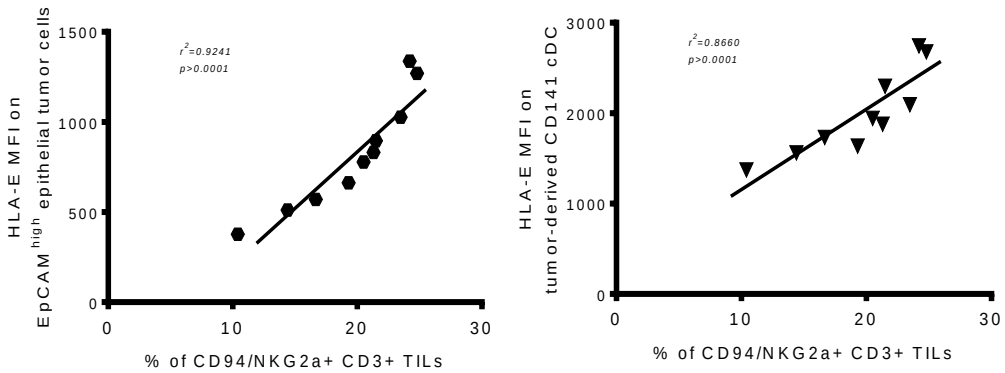


Figure 3.12 Correlation between HLA-E and CD94/NKG2a expression in tumor. Correlative analysis between the frequency of CD94/NKG2a^{+} CD3^{+} TILs with the HLA-E expression by MFI on EpCAM(high) epithelial tumor cells *(left)* and the HLA-E expression by MFI on tumor-derived CD141^{+} cDC *(right)*. N, number of patients= 10 (esophageal cancer, n=3, gastric cancer, n=4, colorectal cancer, n=3); correlative analysis of non-parametric Spearman test, * indicates p-value<0.05, ** p-values<0.01, *** p-values<0.001, ns, not significant. Data represent with median±s.e.m.

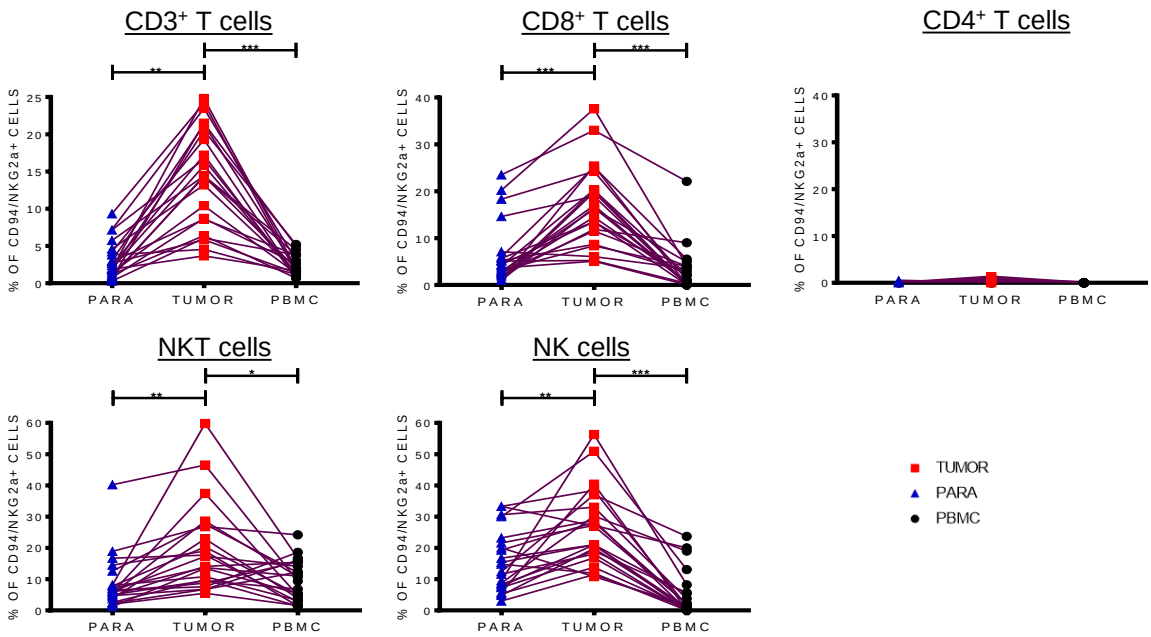


Figure 3.13 Frequency of CD94/NKG2a+ immune cells population in paired samples. The proportion of CD94/NKG2a^{+} populations of CD3^{+} T cells, CD8^{+} T cells, CD4+ T cells, NKT cells and NK cells from paired tumor, paratumor and PBMC. N, number of patients=22 (esophageal cancer, n=7, gastric cancer, n=8, colorectal cancer, n=7); one-way ANOVA with Tukey's post hoc analysis, * indicates p-value<0.05, ** p-values<0.01, *** p-values<0.001, ns, not significant. Data represent with median$\pm$s.e.m.

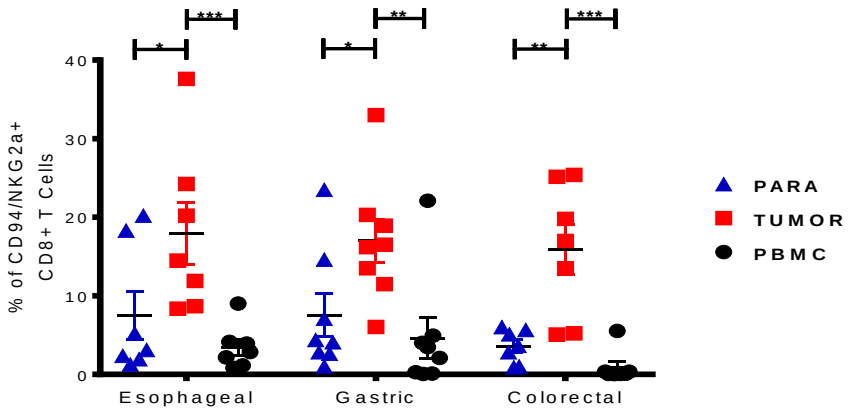


Figure 3.14 Frequency of CD94/NKG2a+ CD8+ T cell populations in paired samples of different cancer types. The proportion of CD94/NKG2a^{+} populations of CD8^{+} T cells from paired tumor, paratumor and PBMC. N, number of patients; esophageal cancer, n=7, gastric cancer, n=8, colorectal cancer, n=7. For analysis: one-way ANOVA with Tukey's post hoc analysis, * indicates p-value<0.05, ** p-values<0.01, *** p-values<0.001, ns, not significant. Data represent with median±s.e.m.

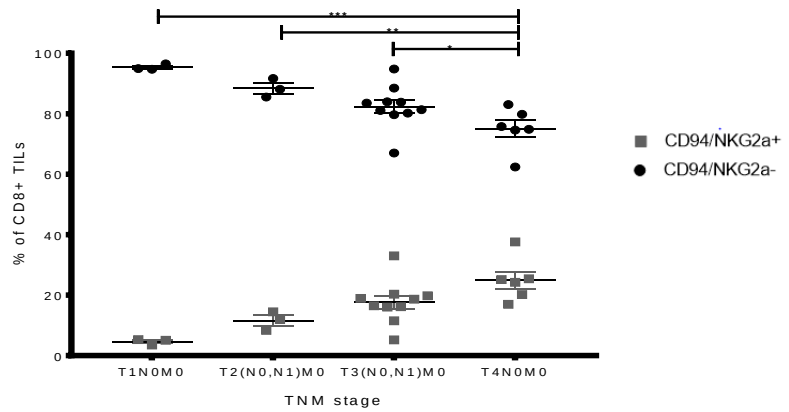


Figure 3.15 Frequency of CD94/NKG2a+ and CD94/NKG2a- CD8+ TILs according to TNM stages of cancer. The proportion of CD94/NKG2a^{+} and CD94/NKG2a^{-} populations of CD8^{+} TILs according to TNM stage of clinical prognosis. N, number of patients =22; (esophageal carcinoma, n=7, gastric carcinoma, n=8, colorectal carcinoma, n=7); two-way ANOVA with Tukey's post hoc analysis. * indicates p-value<0.05, ** p-values<0.01, *** p-values<0.001, ns, not significant. Data represent with median$\pm$s.e.m.

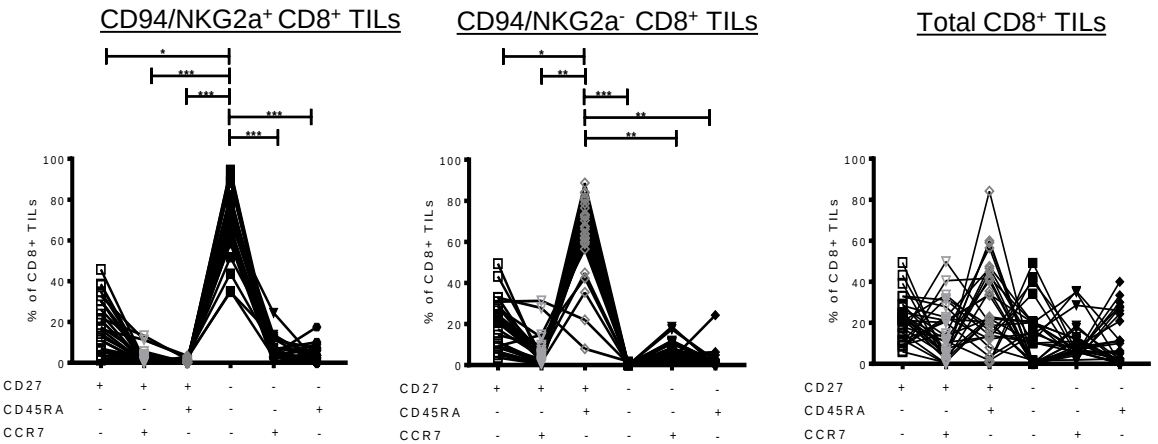


Figure 3.16 Differentiation phenotype of CD94/NKG2a+ and CD94/NKG2a- CD8+ TILs in tumor. The proportion of CD94/NKG2a^{+} CD8^{+} TILs *(left)*, CD94/NKG2a^{-} CD8^{+} TILs *(middle)* and total CD8 $^{+}$ TILs *(right)* according to maturation phenotype expression of CD27, CD45RA and CCR7 in carcinoma. (N, number of patients =22; (esophageal carcinoma, n=7, gastric carcinoma, n=8, colorectal carcinoma, n=7); one-way ANOVA with Tukey's post hoc analysis Horizontal line represents median; interval represent 95% confidence. Connecting lines represents samples from the same patients * indicates p-value<0.05, ** p-values<0.01, *** p-values<0.001, ns, not significant. Data represent with median±s.e.m.

This matured phenotype is characteristic of the tumor-derived CD94/NKG2a$^+$ population as the CD94/NKG2a$^+$ population from paratumor tissue is primarily early stage effector memory (CD27$^+$ CD45RA$^-$ CCR7$^-$) and the CD94/NKG2a$^+$ population from PBMC is mostly early stage central memory phenotype CD27$^+$ CD45RA$^-$ CCR7$^+$) **(Figure 3.17).** The highly matured phenotype of CD94/NKG2a$^+$ CD8$^+$ TILs population suggest that these TILs in tumor are antigen-experienced T cells that could be selected to upregulates inhibitory CD94/NKG2a expression in order to impair and exhaust anti-tumor TIL responses.

3.2.3 CD94/NKG2a and PD-1 are co-expressed on CD8$^+$ TILs

PD-1^{high} T cells are dysfunctional in solid tumors (Thommen et al., 2018) and thus we evaluated whether the CD94/NKG2a$^+$ CD8$^+$ TILs could also have high PD-1 and other inhibitory receptors expression. Gating strategy as described in **Figure 3.18**. We found that CD8$^+$ TILs are enriched for the PD-1^{high} NKG2a$^+$ population whereas the PD-1^{int} TILs have significantly reduced NKG2a co-expression (**Figure 3.19A and B**). Meanwhile, the PD-1$^-$ population lacks CD94/NKG2a expression. Specifically, the PD-1^{high} CD94/NKG2a$^+$ population is present in tumors at a greater frequency (average of 37% of total CD8$^+$ T cells), compared to paired paratumor tissue and PBMC (**Figure 3.19C**).

A similar pattern of PD-1 and CD94/NKG2a co-enrichment on TILs was found in patients with either colorectal or gastric cancers (**Figure 3.20A**). In contrast, BTLA and KLRG-1 was found not to be co-expressed on CD94/NKG2a$^+$ TILs (**Figure 3.20B**), thus suggesting the exclusive co-expression of CD94/NKG2a with PD-1 in carcinoma and this dual co-expression might contribute to the overall dysfunctionality of PD-1$^+$ TILs.

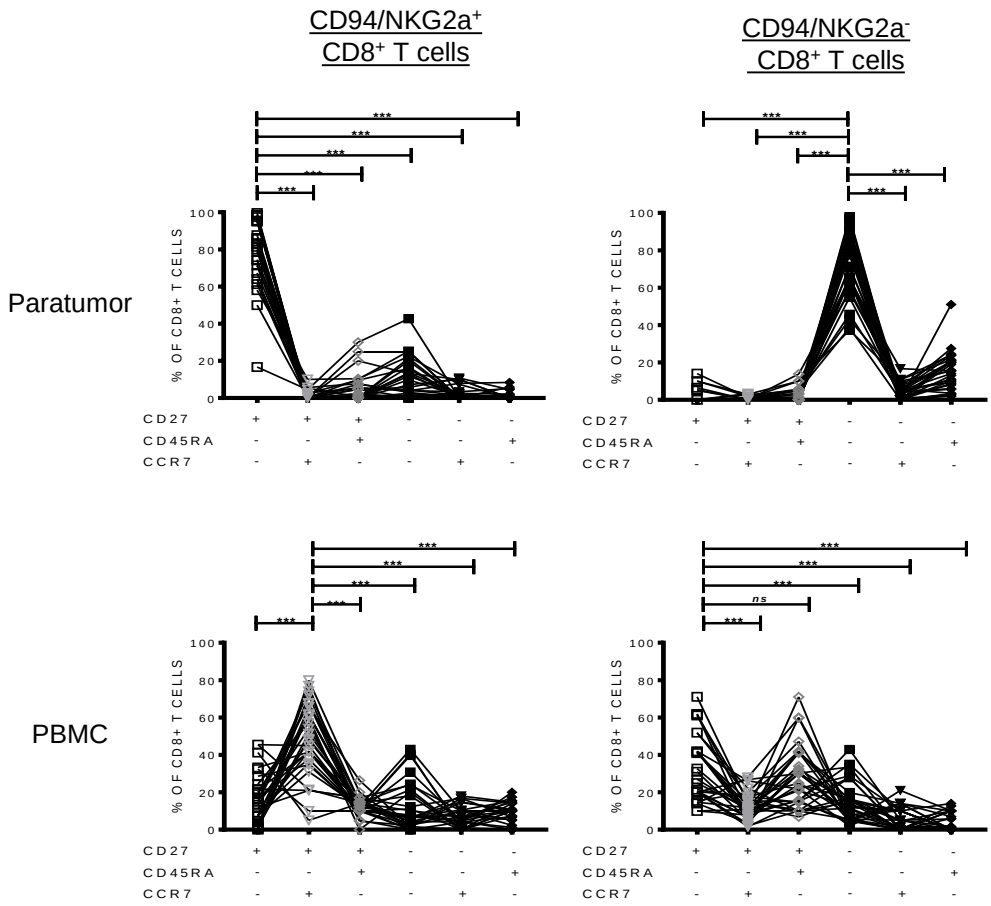


Figure 3.17 Differentiation phenotype of CD94/NKG2a+ and CD94/NKG2a- CD8+ TILs in paired paratumor and peripheral blood. The proportion of CD94/NKG2a^{+} CD8^{+} T cells *(left)* and CD94/NKG2a^{-} CD8^{+} T cells *(right)* according to maturation phenotype expression of CD27, CD45RA and CCR7 in paired paratumor and peripheral blood. (N, number of patients =22; (esophageal carcinoma, n=7, gastric carcinoma, n=8, colorectal carcinoma, n=7); one-way ANOVA with Tukey's post hoc analysis Horizontal line represents median; interval represent 95% confidence. Connecting lines represents samples from the same patients * indicates p-value<0.05, ** p-values<0.01, *** p-values<0.001, ns, not significant. Data represent with median±s.e.m.

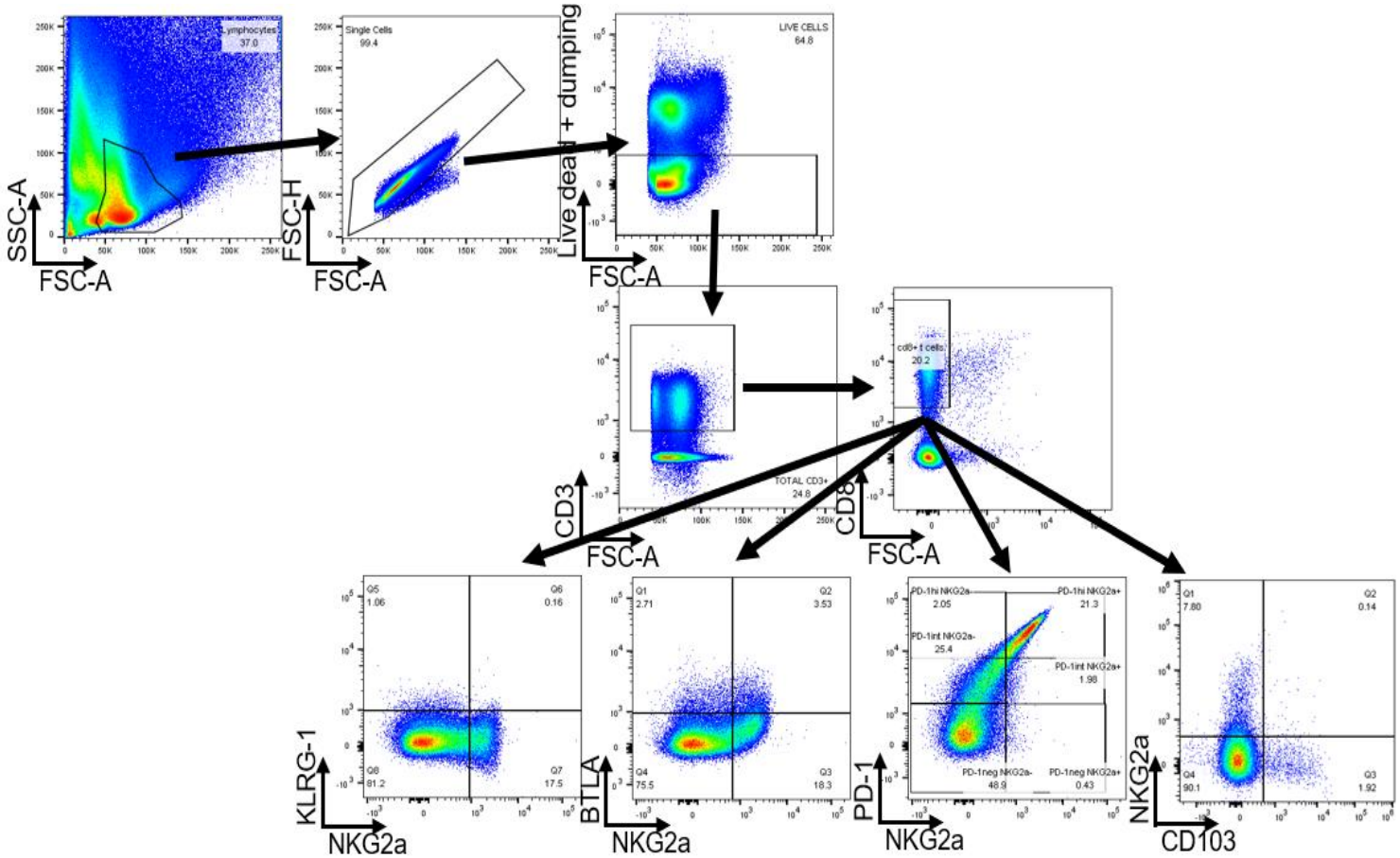


Figure 3.18 Gating strategy for inhibitory receptors and tissue-resident marker expression. Initial and subsequent gating on live CTLs that can express either KLRG-1, BTLA, PD-1 and CD103 on NKG2a+ CTLs.

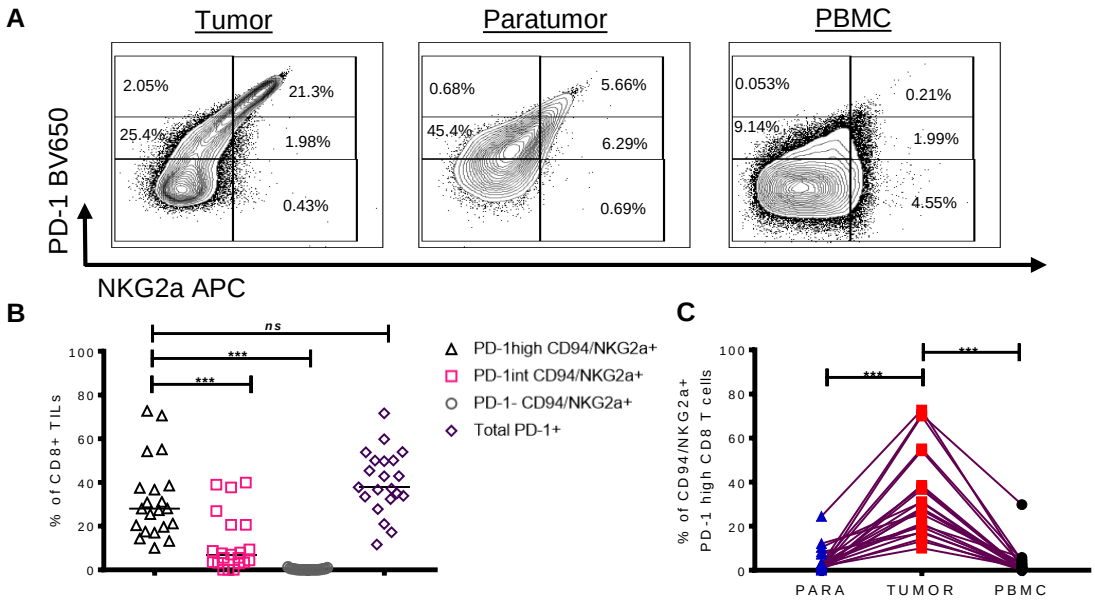


Figure 3.19 CD94/NKG2a$^+$ TIL co-expression of PD-1. (A) Representative contour plots of PD-1 and NKG2a expression on CD8$^+$ T cells derived from paired tumor, paratumor and PBMC, according to PD-1 high, intermediate or negative expression (B) The proportion of CD94/NKG2a$^+$ CD8$^+$ TILs expressing either PD-1^{high}, PD-1^{int} or PD-1$^-$. (C) Proportion of CD94/NKG2A$^+$ PD-1^{high} CD8$^+$ T cells from paired tumor, paratumor and PBMC. N, number of patients=22 (esophageal cancer, n=7, gastric cancer, n=8, colorectal cancer, n=7); one-way ANOVA with Tukey's post hoc analysis. Horizontal line represents median; interval represent 95% confidence. Connecting lines represents samples from the same patients * indicates p-value<0.05, ** p-values<0.01, *** p-values<0.001, ns, not significant. Data represent with median±s.e.m.

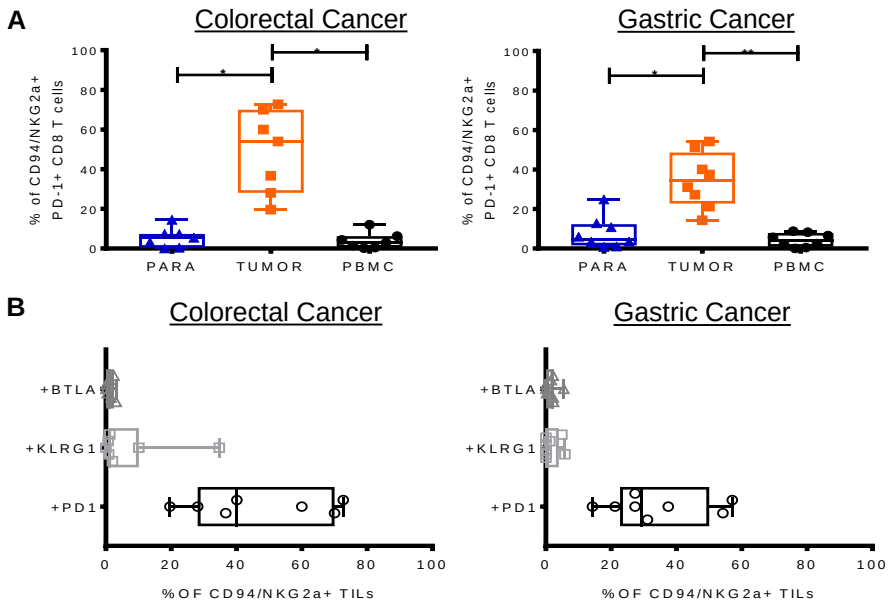


Figure 3.20 CD94/NKG2a^{+} TIL co-expression of different inhibitory receptors. (A) The proportion of CD94/NKG2a^{+} PD-1^{high} CD8^{+} T cells from paired tumor, paratumor and PBMC according to cancer types; colorectal cancer patients n=7 *(left)* and gastric cancer patients n=8 *(right);* one-way ANOVA with Tukey's post hoc analysis. (B) Proportion of CD94/NKG2a^{+} CD8^{+} TILs expressing either BTLA, KLRG-1 or PD-1 according to cancer types; colorectal cancer patients n=7 *(left)* and gastric cancer patients n=8 *(right)*. Horizontal line represents median; interval represent 95% confidence. * indicates p-value<0.05, ** p-values<0.01, *** p-values<0.001, ns, not significant. Data represent with median±s.e.m.

3.2.4 CD94/NKG2a$^+$ TILs lack intratumoral CD103 expression

We also found that NKG2a$^+$ T cells lack CD103 surface expression, such that only the CD94/NKG2a$^-$ TILs population are able to express CD103 in tumor (**Figure 3.21A and B**). This suggest diametrically opposed expression between both markers on TILs. Patients with later TNM stage of cancer size had gradually increased CD94/NKG2a$^+$ CD8$^+$ TIL populations but with steadily decreased CD103$^+$ CD8$^+$ TIL populations (**Figure 3.22A**). This is consistent with the higher CD103$^+$ T cell population but a reduced NKG2a$^+$ population in paratumor tissue compared to the paired carcinoma (**Figure 3.22B**). These observations therefore suggest differential functions of each receptor on T cell functions.

3.2.5 CD94/NKG2a$^+$ antigen-specific T cells have impaired proliferation capacity

To investigate the potential role of HLA-E and CD94/NKG2a interaction on T cell immune responses, we isolated CD94/NKG2a$^+$ and CD94/NKG2a$^-$ populations of HLA-A2-restricted tumor-associated antigen (TAA) (SSX-2)-specific CTLs from a cancer patient and co-cultured with peptide-stimulated HLA-A2-matched allogeneic HCT116 human cancer cell line. As shown in **Figure 3.23A,** we first confirmed that the HCT116 express high HLA-E, even at steady-state. Interestingly, we observed reduced proliferation of CD94/NKG2a$^+$ SSX-2-specific CTLs compared to the CD94/NKG2a$^-$ population (60% versus 7%, $p<0.001$) (**Figure 3.23B**). Upon anti-CD94/NKG2a-mediated blocking treatment, most cells of the CD94/NKG2a$^+$ CTLs have reduced CFSE expression, indicative of higher proliferation, compared to the isotype and no blocking treatments (**Figure 3.23C**).

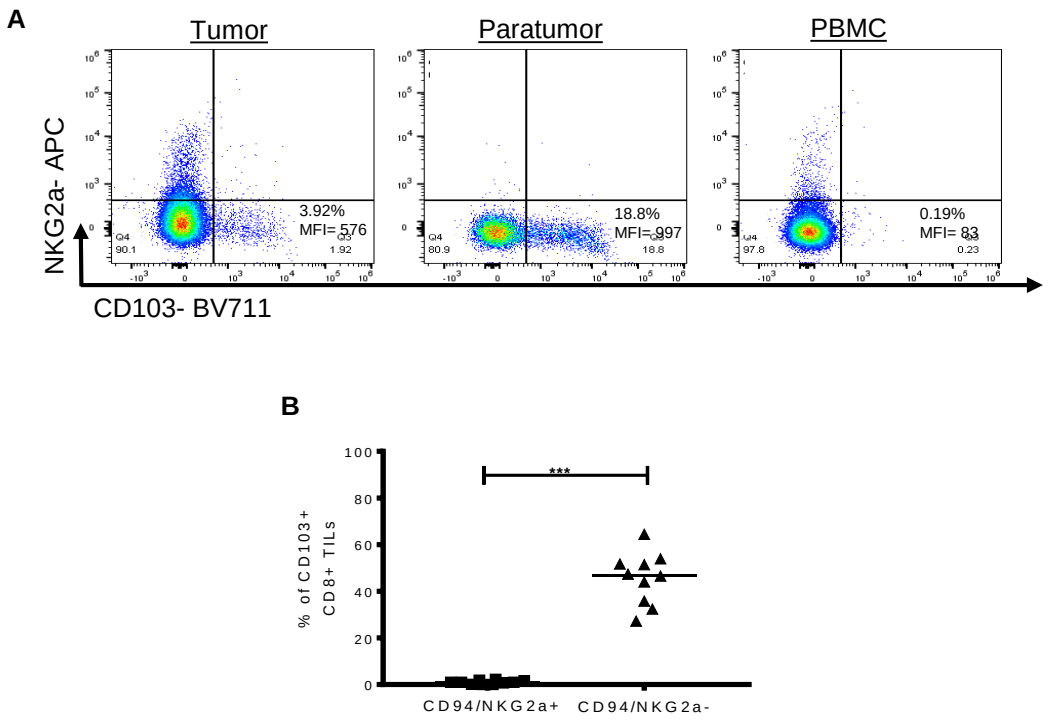


Figure 3.21 CD94/NKG2a^{+} TILs lack tissue resident CD103 marker. (A) Representative FACS plot on NKG2a and CD103 expression on CD8^{+} T cells derived from paired tumor, paratumor and PBMC, by MFI and proportion of CD103^{+} NKG2a^{-} population. (B) Proportion of CD103^{+} CD8^{+} TILs being either CD94/NKG2a^{+} or CD94/NKG2a^{-}. N, number of patients=10; (esophageal carcinoma, n=2, gastric carcinoma, n=2, colorectal carcinoma, n=3, lung carcinoma, n=3); paired student t-test with Wilcoxon adjustments. Horizontal line represents median; interval represent 95% confidence. * indicates p-value<0.05, ** p-values<0.01, *** p-values<0.001, ns, not significant. Data represent with median±s.e.m.

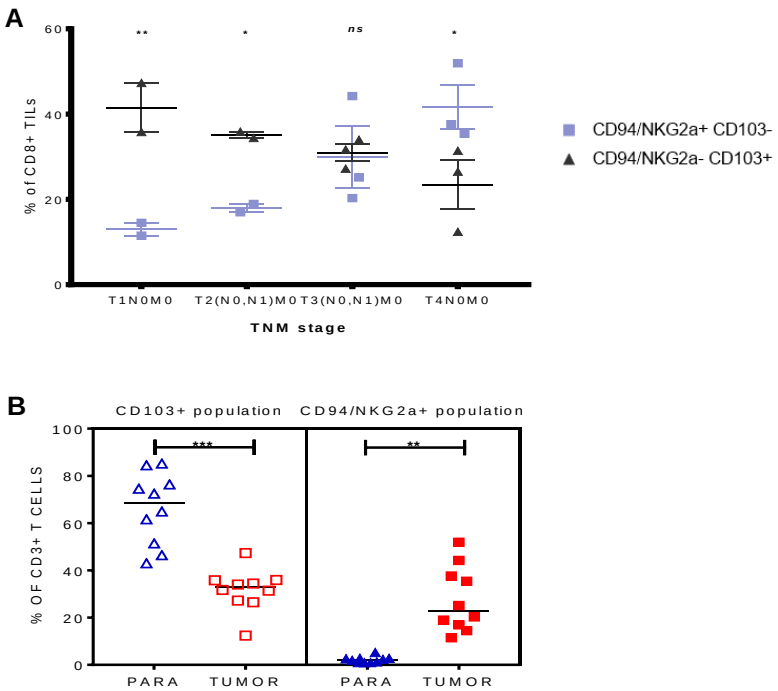


Figure 3.22 CD94/NKG2a^{+} TILs frequency increased as tumor progress while CD103+ TILs decreased. (A) The proportion of CD94/NKG2a^{+} CD103^{-} and CD94/NKG2a^{-} CD103^{+} populations on CD8^{+} TILs according to TNM stage of clinical prognosis. (B) The proportion of CD103^{+} and CD94/NKG2a^{+} populations of CD3^{+} T cells derived from paired tumor and paratumor tissue. N, number of patients=10; (esophageal carcinoma, n=2, gastric carcinoma, n=2, colorectal carcinoma, n=3, lung carcinoma, n=3). For analysis: either two-way NAOVA with Tukey's multiple comparison, or paired student t-test with Wilcoxon adjustments, Horizontal line represents median; interval represent 95% confidence. * indicates p-value<0.05, ** p-values<0.01, *** p-values<0.001, ns, not significant. Data represent with median±s.e.m.

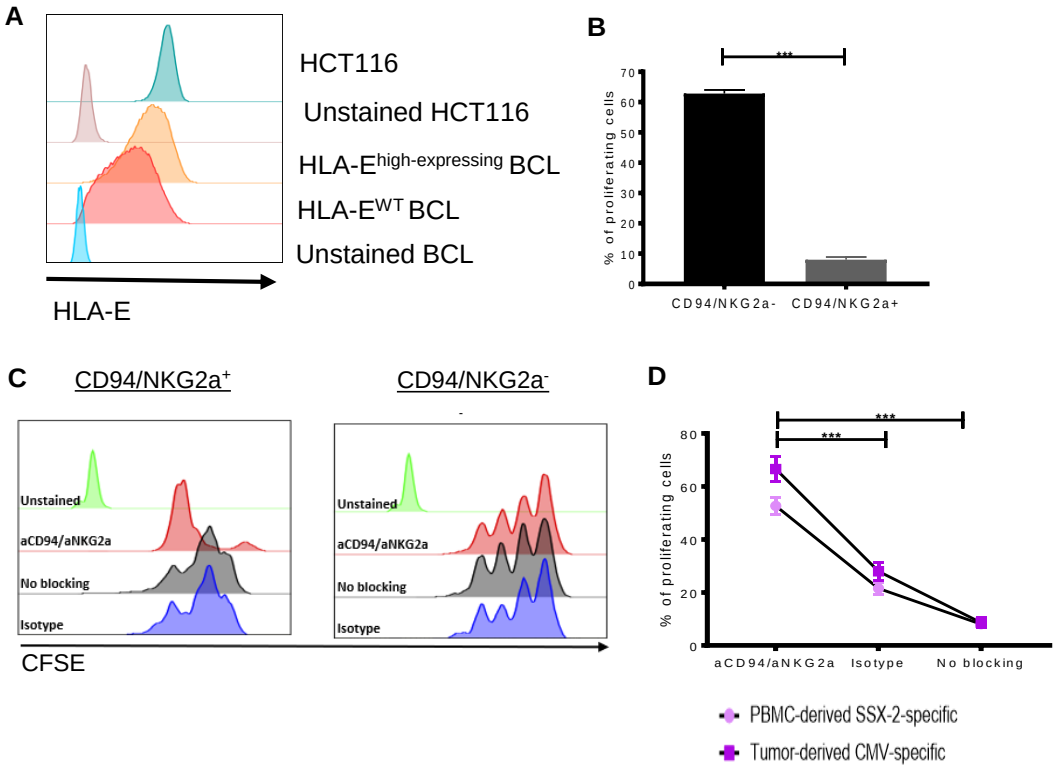


Figure 3.23 Proliferation of CD94/NKG2a$^+$ HLA-A2-restricted antigen-specific CTLs *in vitro*. (A) The HLA-e expression on HCT116, HLA-E high-expressing BCL generated in-house and HLA-Ewt BCL. (B) The proportion of proliferating cells of CD94/NKG2a$^+$ or CD94/NKG2a$^-$ SSX-2-specific T cells following co-cultured with HCT116. (C) Representative histogram plots of CFSE-based proliferating cells of CD94/NKG2a$^+$ *(left)* and CD94/NKG2a$^-$ *(right)* SSX-2-specific T cells following three different treatments, either (i) anti-CD94 and anti-NKG2a treatment, (ii) no antibody treatment, or (iii) isotype antibody treatment. (D) The proportion of proliferating cells on PBMC-derived SSX-2-specific T cells and tumor-derived CMV-specific T cells following three different treatments, either (i) anti-CD94 and anti-NKG2a treatment, (ii) no antibody treatment, or (iii) isotype antibody treatment. N, number of experimental repeats=3; one-way ANOVA with Tukey's post hoc analysis. P value represent 95% confidence. * indicates p-value<0.05, ** p-values<0.01, *** p-values<0.001, ns, not significant. Data represent with median±s.e.m.

To validate that no external influence of HCT116 are acting on the proliferation capacity of CD94/NKG2a^{+} CTLs, we co-cultured either CD94/NKG2a^{+} SSX-2-specific CTLs or the tumor-derived CD94/NKG2a^{+} CMV-specific CTLs with HLA-E^{high} BCL (to provide a more cleaner system of co-culture). Consistently, we observed similar improvement of proliferation on both CTLs type following anti-CD94/NKG2a blocking treatment **(Figure 3.23D)**.

The improvement in T cell proliferation was contributed by the increase in IL-2 receptor (CD25) expression on CD94/NKG2a^{+} SSX-2-specific CTLs following the antibody blocking treatment, reaching a similarly high IL-2-receptor expression as of the CD94/NKG2a^{-} population **(Figure 3.24A).** This is again observed on the CD94/NKG2a^{+} SSX-2-specific CTLs or the tumor-derived CD94/NKG2a^{+} CMV-specific CTLs with HLA-E^{high} BCL, following antibody treatment **(Figure 3.24B)**.

As expected, the upregulation of CD25 on the antibody-treated CD94/NKG2a^{+} CTLs corresponded to the increment in IL-2 cytokine production and the proportion of IL-2-producing cells **(Figure 3.25A and B).** The recovery of IL-2 receptor-dependent proliferation following antibody-mediated treatment suggested that enriched HLA-E and CD94/NKG2a interaction on tumor-specific T cells can impair the proliferation capacity, which might subsequently affect its anti-tumor T cell responses.

3.2.6 Impaired effector and cytotoxic responses recovered after CD94/NKG2a antibody blockade *in vitro*

We next investigated whether the reduced proliferation of CD94/NKG2a^{+} T cells can affect its anti-tumor killing ability. We found that CD94/NKG2a^{+} population of SSX-2-specific CTLs have poor killing ability when co-cultured with HCT116 cancer cell line compared to the CD94/NKG2a^{-} population **(Figure 3.26A)**. The poor killing ability is evident from the

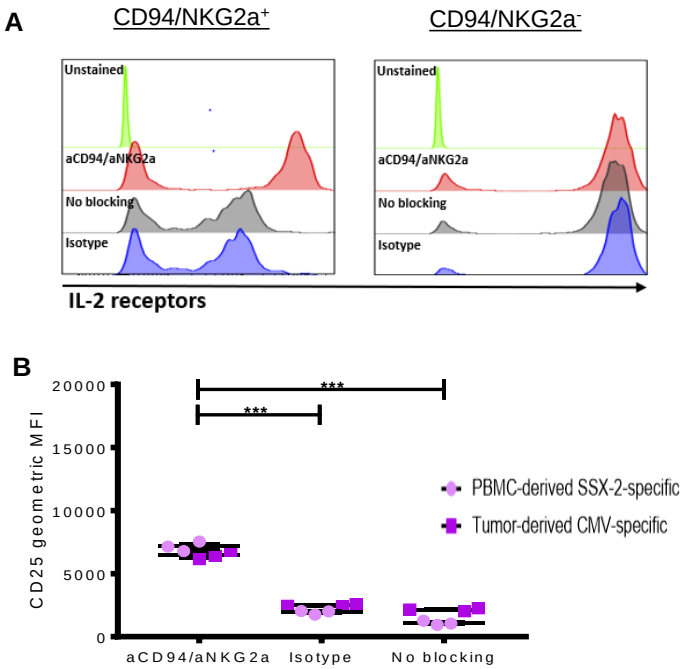


Figure 3.24 IL-2 receptor alpha (CD25) expression on CD94/NKG2a$^+$ HLA-A2-restricted antigen-specific CTLs following antibody-mediated blocking treatment *in vitro*. (A) Representative histogram plots of IL2 receptor (CD25) expression by MFI on CD94/NKG2a$^+$ *(left)* and CD94/NKG2a$^-$ *(right)* SSX-2-specific T cells following three different treatments. (B) IL2 receptor (CD25) expression by MFI on PBMC-derived SSX-2-specific T cells and tumor-derived CMV-specific T cells following three different treatments. N, number of experimental repeats=3; one-way ANOVA with Tukey's post hoc analysis.. P value represent 95% confidence. * indicates p-value<0.05, ** p-values<0.01, *** p-values<0.001, ns, not significant. Data represent with median$\pm$s.e.m.

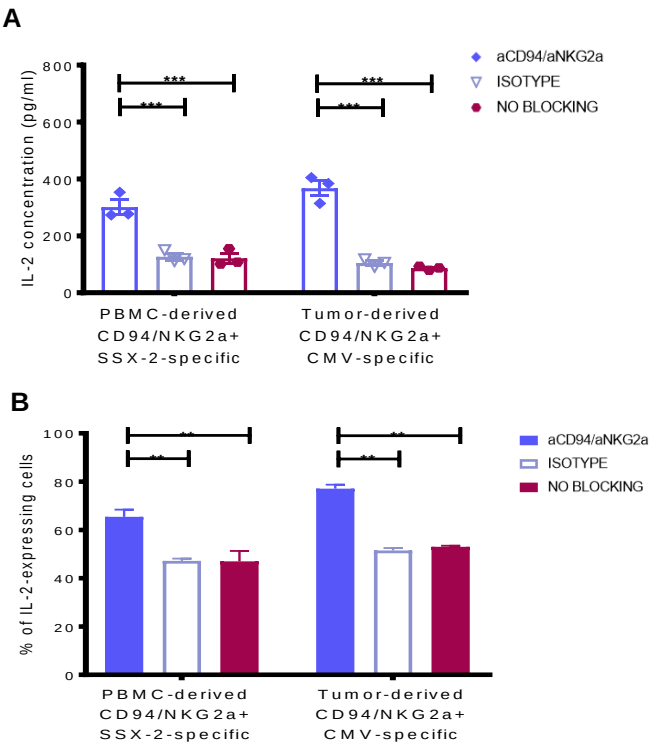


Figure 3.25 IL-2 production and expression on CD94/NKG2a$^+$ HLA-A2-restricted antigen-specific CTLs following antibody-mediated blocking treatment *in vitro*. The IL2 production (A) and IL2$^+$ cells proportion (B) on PBMC-derived SSX-2-specific T cells and tumor-derived CMV-specific T cells following three different treatments. N, number of experimental repeats=3; one-way ANOVA with Tukey's post hoc analysis.. P value represent 95% confidence. * indicates p-value<0.05, ** p-values<0.01, *** p-values<0.001, ns, not significant. Data represent with median$\pm$s.e.m.

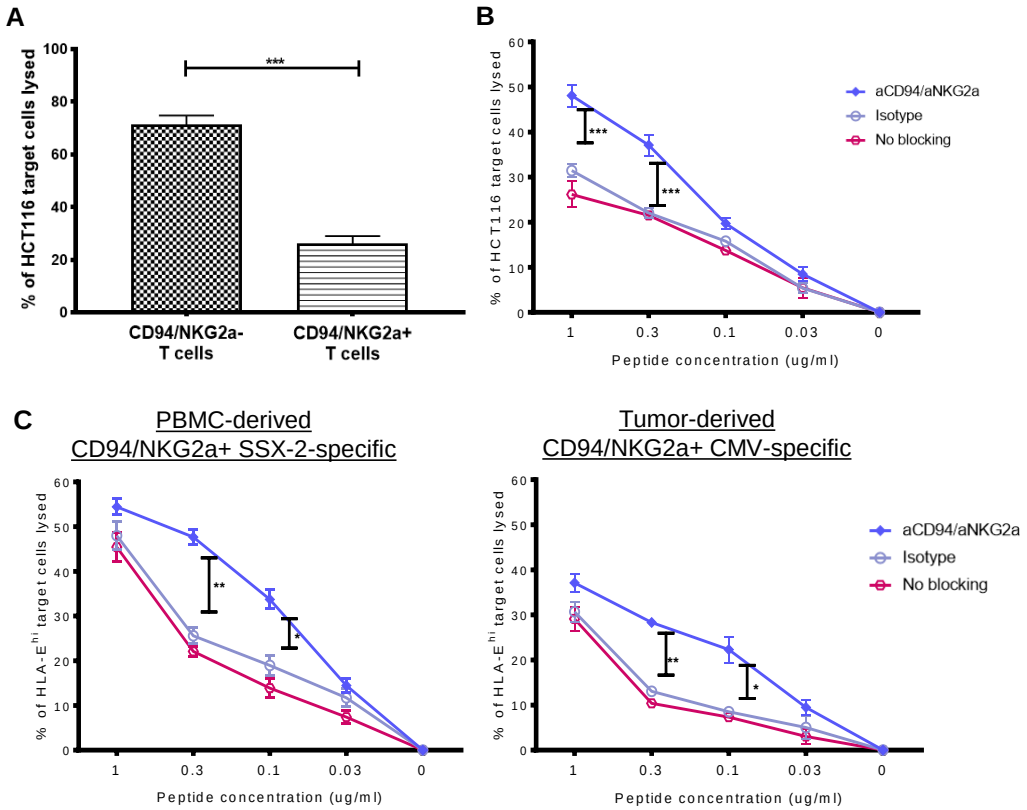


Figure 3.26 Cytotoxicity by CD94/NKG2a^{+} HLA-A2-restricted antigen-specific CTLs *in vitro*. (A) The proportion of lysed cancer cells following CD94/NKG2a^{+} or CD94/NKG2a^{-} SSX-2-specific T cells co-cultured with HCT116. (B) The proportion of lysed cancer cells following CD94/NKG2a^{+} SSX-2-specific T cell population co-culture with HCT116, following either CD94/NKG2a antibody blockade, isotype or no blocking treatments at five different concentration of antigen stimulation. (C) The proportion of lysed cancer cells following co-culture of CD94/NKG2a^{+} population of PBMC-derived SSX-2-specific T cells *(left)* and tumor-derived CMV-specific T cells *(right)* with HLA-E^{high} BCL. N, number of experimental repeats, n=3; For analysis: two-tailed t-test or two-way ANOVA with Tukey's post hoc analysis* indicates p-value<0.05, ** p-values<0.01, *** p-values<0.001, ns, not significant. Data represent with median±s.e.m.

significant improvement of cytotoxicity observed on CD94/NKG2a^{+} SSX-2-specific CTLs and tumor-derived CD94/NKG2a^{+} CMV-specific CTLs, when treated with the anti-CD94/NKG2a blocking antibody and is sensitive up to 0.3μM antigen stimulation of HCT116 and up to 0.1μM antigen stimulation of HLA-E^{high} BCL **(Figure 3.26B and C).**

In addition, the CD94/NKG2a^{+} SSX-2-specific T cell population has significantly impaired IFNγ production compared to the CD94/NKG2a^{-} population **(Figure 3.27A)**. This corresponded to the significantly reduced number of IFNγ-expressing cells of the CD94/NKG2a^{+} population, when co-cultured with either HCT116 or HLA-E^{high} BCL, even at high antigen stimulation of 1 μg/ml **(Figure 3.27B)**. Similar to the recovery in proliferation and cytotoxicity, IFNγ production and expression recovered following antibody blockade treatment **(Figure 3.27C and D)**.

However, no differences were observed in TNFα and MIP-1β responses following the antibody treatment. Only the chemotactic CCL5 was significantly elevated 48 hours later (**Figure 3.28**). Taken altogether, these *in vitro* data suggest that enriched HLA-E and CD94/NKG2a interaction, particularly on cancer-specific T cells, could affect the survivability and responses of T cells through their proliferation capacity, anti-tumor cytotoxicity and cytokine responses.

3.2.7 Recovery of T cell functions after CD94/NKG2a antibody blockade *ex vivo*

To corroborate the *in vitro* observations, we then set up an *ex vivo* study by isolating cell mixtures from tumors of four gastric cancer patients with confirmed presence of at least 5% of CD94/NKG2a^{+} TILs and stimulated with SEB before being treated with anti-CD94/NKG2a blocking antibody.

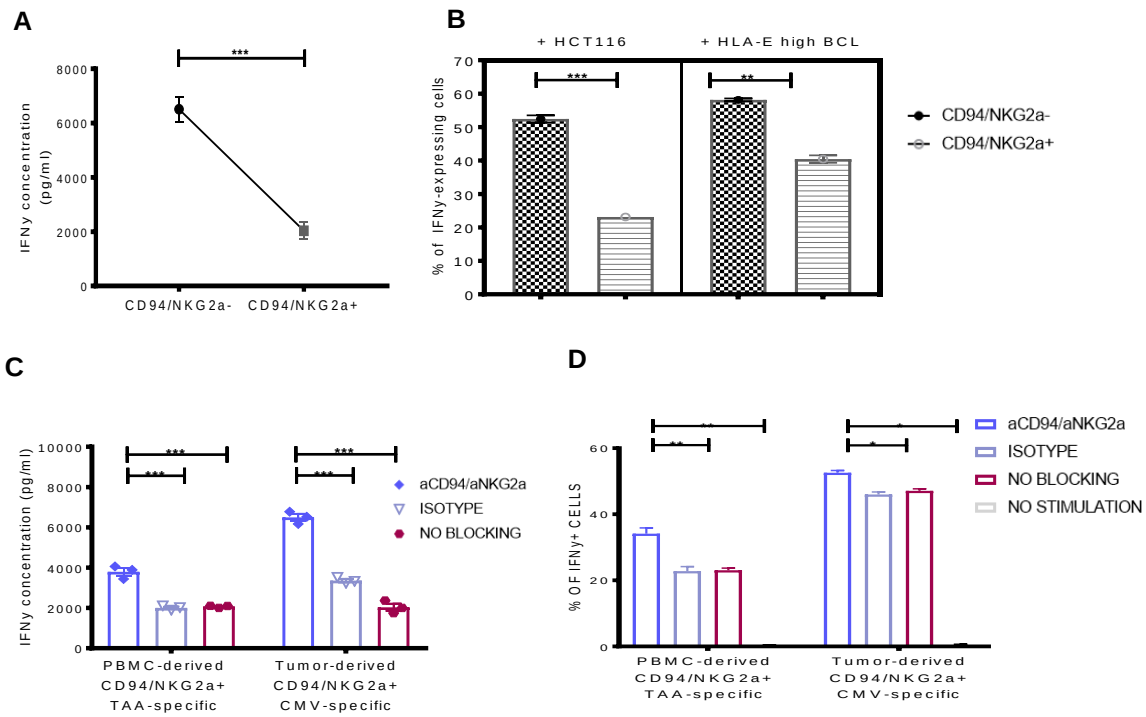


Figure 3.27 IFNγ response by CD94/NKG2a$^+$ HLA-A2-restricted antigen-specific CTLs *in vitro*. (A) The IFNγ production of CD94/NKG2a$^+$ or CD94/NKG2a$^-$ SSX-2-specific T cells following co-cultured with HLA-A2-matched HLA-E^{high} BCL. (B) The proportion of IFNγ$^+$ cells of CD94/NKG2a$^+$ or CD94/NKG2a$^-$ SSX-2-specific T cells following co-culture with either HCT116 or HLA-E^{high} BCL The proportion of IFNγ$^+$ cells (C) and IFNγ production (D) of CD94/NKG2a$^+$ population of PBMC-derived SSX-2-specific T cells and tumor-derived CMV-specific T cells following either CD94/NKG2a antibody blockade, isotype or no blocking treatments. N, number of experimental repeats, n=3; CD94/NKG2a$^+$ or CD94/NKG2a$^-$ SSX-2-specific T cells were isolated from a gastric cancer patient, whereas CD94/NKG2a$^+$ CMV-specific T cells were isolated from a colorectal cancer patient. For analysis: one-way ANOVA with Tukey's post hoc analysis. P value represent 95% confidence. * indicates p-value<0.05, ** p-values<0.01, *** p-values<0.001, ns, not significant. Data represent with median±s.e.m.

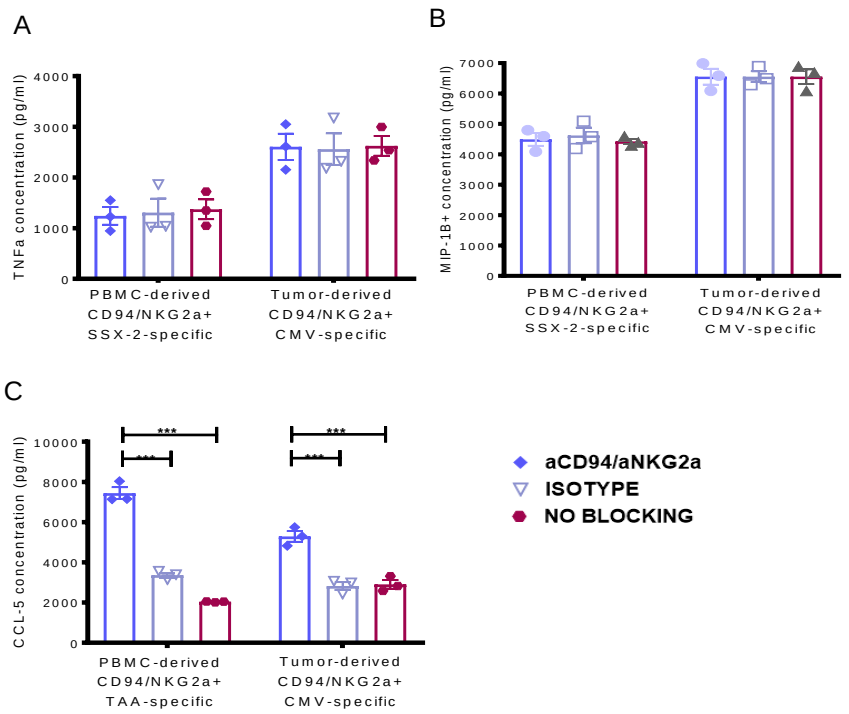


Figure 3.28 Cytokines by CD94/NKG2a^{+} HLA-A2-restricted antigen-specific T cells which recovers following antibody-mediated blocking treatment *in vitro*.

The production of TNFα (A), MIP-1β (B) and CCl-5 (C) following either CD94/NKG2a antibody blockade, isotype or no blocking treatments. N, number of experimental repeats, n=3; one-way ANOVA with Tukey's post hoc analysis. P value represent 95% confidence. * indicates p-value<0.05, ** p-values<0.01, *** p-values<0.001, ns, not significant. Data represent with median±s.e.m.

Consistent with our *in vitro* findings, we confirmed that the frequency of IFNγ-expressing cells and the amount of IFNγ produced were significantly improved following antibody-mediated treatment compared to the isotype and no blocking treatments (**Figure 3.29A and B**). Furthermore, more stages of cell proliferation were observed after the anti-CD94/NKG2a blocking treatment (**Figure 3.30A**), corresponding to significantly elevated IL-2 receptor (CD25) expression on $CD8^+$ TILs 48 hours later (**Figure 3.30B**). The IL-2 receptor-dependent proliferation was vital in the recovery of $CD8^+$ TILs *ex vivo* after antibody treatment, as the IL-2 expression and production were also found to be significantly elevated on $CD8^+$ TILs (**Figure 3.30C and D**).

Altogether, both *in vitro* and *ex vivo* observations highlighted the enriched presence and interaction between HLA-E and CD94/NKG2A, particularly on cancer-specific T cells, can negatively affect anti-tumor T cell immune responses and contribute to a dysfunctional TILs.

3.3 Discussion

Using comparison between paired tumor, paratumor and peripheral blood from mainly gastrointestinal cancer patients, we reported on enrichment of HLA-E in carcinoma that is contributed not only by the epithelial cancer cells but also by tumor dendritic cells and macrophages. The HLA-E enrichment paralleled the increment to the inhibitory CD94/$NKG2a^+$ $CD8^+$ TIL population that is exclusively associated with PD-1^{high} expression in solid tumors, but minimally present in paired paratumor tissue and absent in peripheral blood of cancer patients.

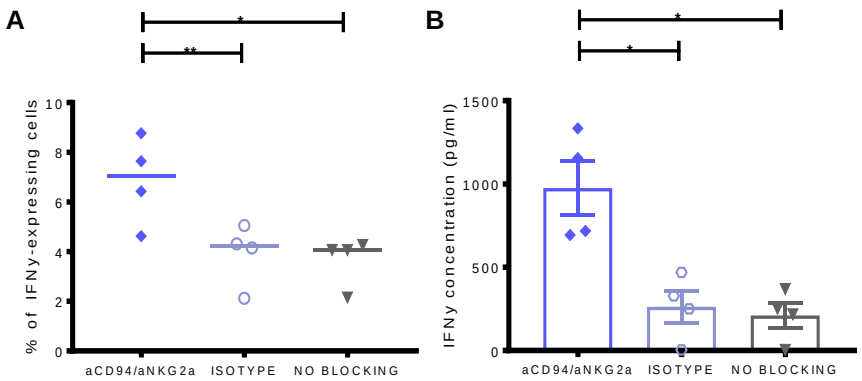


Figure 3.29 Recovery of CD8⁺ TILs IFNγ following anti-CD94/NKG2a-mediated blocking treatment *ex vivo*. The proportion of IFNγ⁺ cells (A) and IFNγ production (B) of CD8⁺ TILs stimulated with 0.1μM SEB stimulation following either antibody blockade, isotype or no blocking treatment. N, number of gastric cancer patients, n=4; one-way ANOVA with Tukey's post hoc analysis* indicates p-value<0.05, ** p-values<0.01, *** p-values<0.001, ns, not significant. Data represent with median±s.e.m.

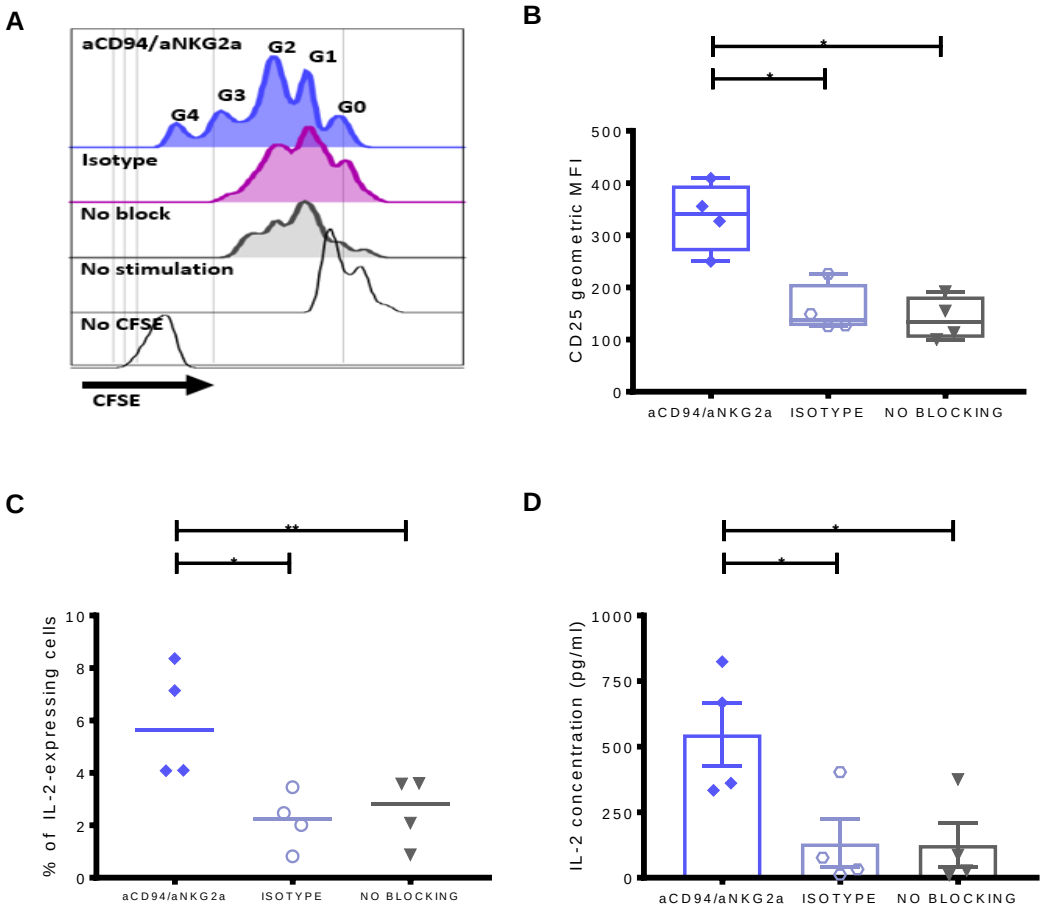


Figure 3.30 Recovery of CD8$^+$ TILs IL-2-dependent proliferation following anti-CD94/NKG2a-mediated blocking treatment *ex vivo*. (A) Representative histogram plot of CFSE-based proliferating cells of CD8$^+$ TILs following different treatments. The IL2 receptor (CD25) geometric MFI expression (B), proportion of IL2$^+$ cells (C) and IL2 production (D) on CD8$^+$ TILs following different treatments. N, number of gastric cancer patients, n=4; one-way ANOVA with Tukey's post hoc analysis. P value represent 95% confidence. * indicates p-value<0.05, ** p-values<0.01, *** p-values<0.001, ns, not significant. Data represent with median±s.e.m.

Previous studies by Andre and colleagues as well as by van Manfoort and colleagues in 2018 highlighted the improvement in survival rates and tumor control in anti-NKG2a-treated murine cancer models and the increased disease stability of combinatory anti-NKG2a and anti-EGFR-treated head-and-neck cancer patients of a phase II clinical trial (Andre et al., 2018; van Montfoort et al., 2018). Our current study revealed the means by which enriched presence and interaction of HLA-E with CD94/NKG2a could impair T cell responses in human cancer **(Figure 3.31)**. The improvement of IL-2/IL-2 receptor-dependent proliferation and anti-tumor killing by cancer-specific CTLs treated with anti-CD94/NKG2a revealed the inhibitory effect of enriched CD94/NKG2a presence on human TILs, which could contribute to worsen clinical outcomes in patients as tumor progresses.

In addition, previous studies indicating abundance of HLA-E in cross-sectional cancer tissue analysis lack corresponding comparison with paired paratumor tissue and peripheral blood of the patients and did not further examine the types of cells that contribute to this abundance. Here, we showed that HLA-E enrichment occurred on epithelial cancer cells and on tumor-residing APCs. Tumor-residing APCs is known to help in tissue-localized antigen presentation and maintenance of antitumor T cell responses (Bachem et al., 2010; Roberts et al., 2016; Tseng et al., 2013). However, other murine studies have also shown that tumor APCs can be dysregulated to become tolerogenic, a process driven by immunosuppressive factors such as IL-10 and β-catenin (Laoui et al., 2016; Ruffell et al., 2014; Scarlett et al., 2012; Spranger et al., 2015). Furthermore, the inhibitory PD-1/PD-L-1 axis is upregulated on murine tumor APCs and contributed to progressively growing tumor (Hildner et al., 2008; Okazaki et al., 2013; Salmon et al., 2016).

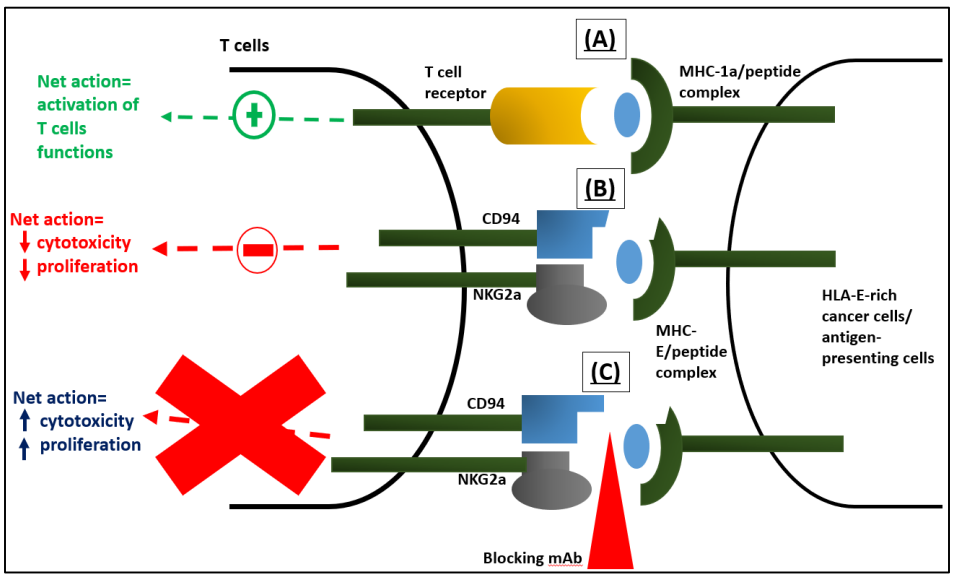


Figure 3.31 Effects of CD94/NKG2a on T cell functions. (A) TCR recognition of cancer cells leads to net activation and killing of cancer cells. (B) In the presence of NKG2a, NKG2a+ cancer-specific CTLs have net inhibitory effects on T cell functions, including impaired anti-tumor cytotoxicity and reduced IL-2-dependent proliferation. (C) Blocking of HLA-E and CD94/NKG2a interaction can recover the anti-tumor cytotoxicity and proliferation of cancer-specific CTLs.

We further demonstrated that not only can HLA-E be upregulated on tumor-residing APCs, but its inhibitory CD94/NKG2a ligand on TILs is also upregulated in larger tumors. This observation could elucidate the reasons that past DC-based vaccines that solely targeted recovery of tumor neoantigen presentation on MHC Class Ia of tumor DCs were not successful at improving recovery in murine cancer models and cancer patients (Iversen et al., 2014; Kavanagh et al., 2007; Slingluff et al., 2007). The enriched HLA-E and CD94/NKG2a presence and interaction between tumor-APCs and $CD8^+$ TILs could overpower and dampen the activating MHC Class Ia-T cell receptor signaling, causing ineffective anti-tumor priming and anergic T cell activation.

The corresponding increment of CD94/NKG2a on TILs in gastrointestinal cancer patients is diametrically opposed to the downregulation of the intratumoral CD103 expression. $CD103^+$ T cells are T cell mediators of long-lived protection against viral infections in peripheral tissues such as intestines and lung (Gebhardt et al., 2009; Masopust et al., 2010). In the cancer setting, the presence of CD103 aids T cell infiltration into intraepithelial murine tumors whereas the accumulation of CD103 contributed to extensive granzyme B degranulation in the immunological synapse, leading to better killing of cancer cells *in vitro* (Djenidi et al., 2015; Le Floc'h et al., 2007). The observation of gradual loss of CD103 in progressively growing gastrointestinal tumors suggests that CD103 absence is detrimental towards cancer survival and that cancer preferentially upregulates inhibitory markers such as CD94/NKG2a and PD-1 expression as a mechanism to avoid anti-tumor immunity. Our observation of diametrically opposite expression is contradictory to the co-expression of NKG2a with CD103 on TILs observed by van Manfoort and colleagues on human papilloma virus (HPV)-positive cervical carcinoma patients (van Montfoort et al., 2018).

A previous study has demonstrated that patients with PD-1^{high} T cells is a good target for anti-PD-1 treatment due to their impaired functionality and characteristics (Thommen et al., 2018). Although anti-PD-1 treatment in various clinical studies has supported recovery towards prolonged survival in cancer patients, there is still a sizeable portion of patients that lacked major improvement (Garon et al., 2015; Muro et al., 2016). Interestingly, in our current study, we demonstrated that PD-1^{high} TILs in gastrointestinal cancer patients have enriched CD94/NKG2a expression. This is consistent with findings in recent studies in head-and-neck cancer patients (Andre et al., 2018; van Montfoort et al., 2018). As we further show that the enriched CD94/NKG2a^{+} cancer-specific T cells lack efficient proliferation capacity, this can therefore lead to detrimental outcome on the long-term survivability of anti-tumor T cells. Subsequently, the reduced proliferation of TILs could eventually contribute to the impaired anti-tumor cytotoxicity and responses against cancer, albeit even after being treated with anti-PD-1 treatment. The commonality of HLA-E and CD94/NKG2a enrichment across different cancer types, together with the exclusivity of PD-1^{high} expression highlight the key role of CD94/NKG2a as a compensatory exhaustive marker of TILs that limits the effectiveness of anti-tumor TILs.

Considering cancer immunotherapy, targeting the inhibitory CD94/NKG2a signaling pathways on TILs and their interaction with HLA-E in tumors could prove beneficial to patients with HLA-E and PD-1 co-enriched tumors. Targeting CD94/NKG2a could improve the long-term survivability of effector cells such as CTLs with better cytotoxic functions following combinatory anti-PD-1 treatment.

Chapter 4: Self-maintaining $CD103^+$ cancer-specific CTLs are highly energetic, with rapid cytotoxic and effector responses

4.1 Introduction

CD103 (integrin α_E) is primarily expressed on tissue-resident memory T cells (Trm) and is widely recognised as a key player in viral tissue-localised immunity, including in the clearance of murine herpes simplex virus (HSV) skin infection and murine lung influenza infection (Mackay et al., 2013; Piet et al., 2011). In recent years, there has been increasing interest in its potential in human cancer control and eradication. The enrichment of $CD103^+$ TILs is associated with improved outcomes in cancer patients either with melanoma, colorectal, urothelial or early stage lung cancers (Djenidi et al., 2015; Ganesan et al., 2017; Malik et al., 2017; Quinn et al., 2003; Wang et al., 2015).

The induction and development of CD103 on developing T cells require initial antigenic contact and the presence of microenvironmental TGF-β1 cues, presumably produced by murine Batf3-dependent dendritic cells (DC), human $CD1c^+$ conventional DC (cDC) and regulatory T cells (Treg) (Enamorado et al., 2017; Graham et al., 2014; Yu et al., 2013). Impaired $CD103^+$ Trm populations in tissues occurred when there is an absence of TGF-β1 as well as the inactivation of its receptor on T cells (Nizard et al., 2017). However, as DCs in the tumor microenvironment are known to be highly dysfunctional (Cubillos-Ruiz et al., 2015; Herber et al., 2010; Karyampudi et al., 2016), it remains unclear how continuous CD103 expression on matured cancer-specific TILs is maintained, especially during prolonged cancer exposure.

Human cancer testis antigens (CTAs), such as synovial sarcoma X-2 (SSX-2) and New York-esophageal squamous cell carcinoma-1 (NY-ESO-1) proteins are a class of antigens that

are not expressed on healthy tissue but are highly upregulated on cancer cells. While CTA-specific CTLs are promising targets for immunotherapy, they have low affinity TCRs and low sensitivity to tumor antigen/MHC complex (Aleksic et al., 2012; Thomas et al., 2011). This can result in an overall impaired efficacy of anti-tumor T cells responses and thus poor tumor control. Interestingly, CD103 molecules were found to accumulate in the immunological synapse following T cell interaction with autologous cancer cells (Le Floc'h et al., 2011; Le Floc'h et al., 2007). It is, therefore, possible that CD103 could help in TCR-mediated anti-tumor CTLs immune responses.

A recent study by Duhen and colleagues in 2018 highlighted tumor-reactive TILs with a CD103 and CD39 co-expression signature, with an increased inhibitory receptors expression that may contribute to T cell dysfunction (Duhen et al., 2018). However, as enrichment of $CD103^+$ TILs is known to improve clinical outcomes in patients, its possible dysfunctional immunophenotype raises uncertainty about its relevance as the primary target for immunotherapy and its significance to the overall anti-tumor immune activities. Therefore, a comprehensive understanding of the properties of human $CD103^+$ cancer-specific CTLs and the specific contribution of CD103 towards anti-tumor T cell effector and cytotoxic responses is urgently required.

In this chapter, we sought to address the CD103-mediated characteristics and immune mechanisms of human $CD103^+$ cancer-specific CTLs. Specifically, we investigated *in vitro*, the CD103 maintenance capacity of matured cancer-specific CTLs as well as the metabolism, mobility and cancer cells recognition capacity of $CD103^+$ cancer-specific CTLs. We further evaluated *ex vivo*, the inhibitory receptors co-expression on various $CD103^+$ $CD39^+$ TILs subpopulations and assessed the possible effects of this on $CD103^+$ T cell survival.

4.2 Results

4.2.1 Cancer-specific CTLs self-regulate CD103 expression by producing activated TGF-β1

Following initial antigen contact, naïve T cells develop and acquire CD103 expression in the presence of TGF-β1, known to be produced by DCs and Tregs (Enamorado et al., 2017; Graham et al., 2014; Yu et al., 2013). However, in cancer patients, cancer DCs are known to be highly dysfunctional (Cubillos-Ruiz et al., 2015; Herber et al., 2010; Karyampudi et al., 2016). Thus, it remains unclear how CD103 expression can be maintained on matured differentiated cancer-specific CTLs.

To assess the effect of CD103 and to reduce the influence of other confounding factors, we selected CTL pairs that have highest similarities between the T cells. Two pairs of $CD103^+$ and $CD103^-$ cancer-specific CTLs were sorted and clonally expanded (SSX-2-specific CTLs; NY-ESO-1-specific CTLs). Both paired $CD103^+$ and $CD103^-$ cancer-specific CTLs have predominantly late stage effector memory phenotype($CD28^-CD27^-CD45RO^+CD45RA^-CCR7^-$) (**Figure 4.1A).** As found by Dr. Yanchun Peng, each pair of CTLs has the same TCR usage and surface density, indicative of each CTLs having the same basal affinity **(Figure 4.1B and Table 4.1)**. Specifically, the paired $CD103^+$ and $CD103^-$ SSX-2-specific CTL clones used TRAV 8-6 TRAJ 30 and TRBV 6-1 TRBJ 2-7, while the paired $CD103^+$ and $CD103^-$ NY-ESO-1-specific CTLs clones used TRAV 12-2 TRAJ 31 and TRBV 12-4 TRBJ 1-2. The TCR and phenotype standardization helps (i) to eliminate other confounding factors that could impact CTLs functions, such as different TCR affinity and recognition strength, and most importantly (ii) to ensure any observational changes to the CTLs functions is contributed by the action of CD103 on T cells.

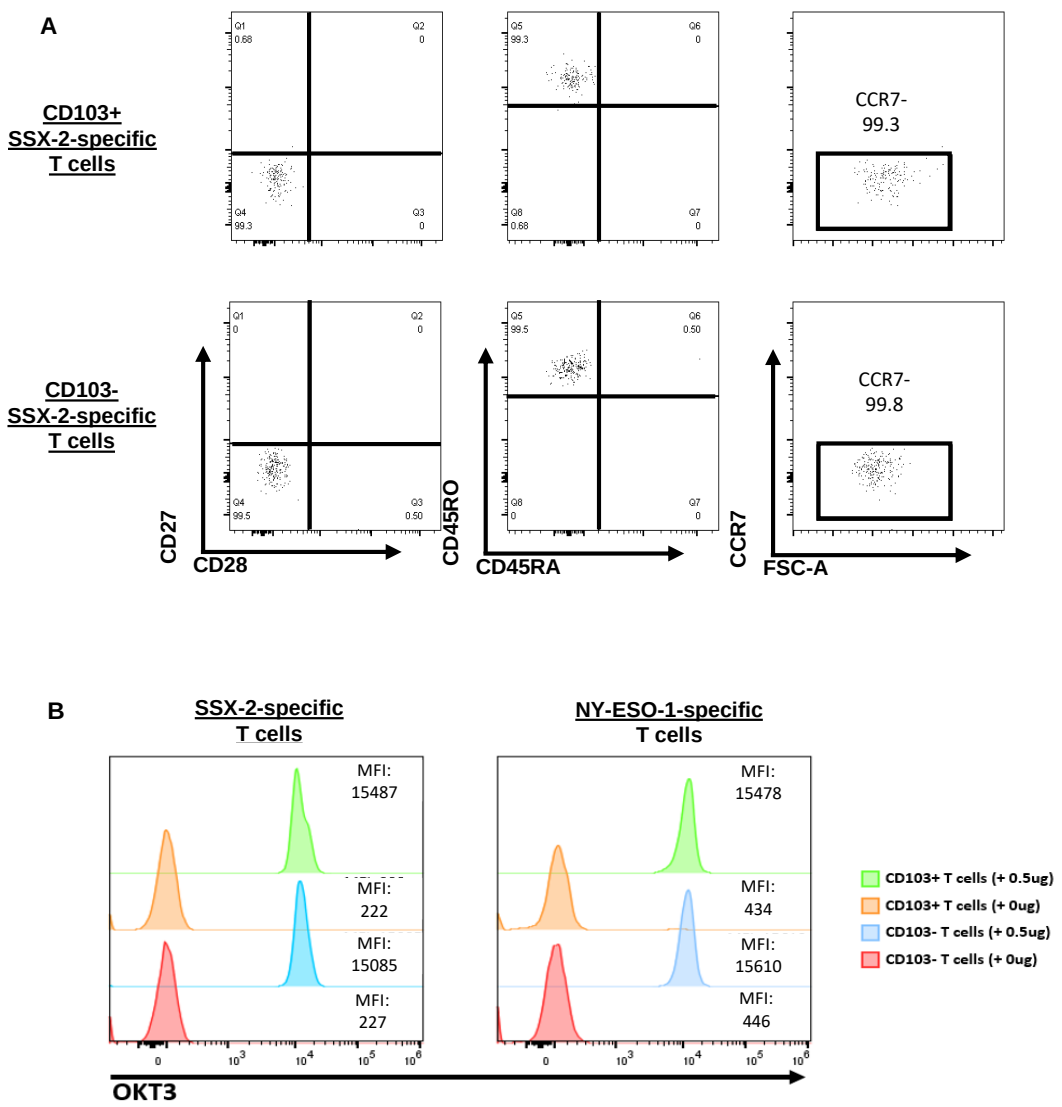


Figure 4.1 Phenotype of paired CD103^{+} and CD103^{-} cancer-specific T cells. **(**A) Representative of FACS dot plots of the differentiation stage of CD103+ and CD103- cancer-specific T cells (SSX-2-specific). (B). T cell receptor densities (by OKT3 staining MFI) of either CD103^{+} or CD103^{-} T cells of SSX-2-specific T cells *(left)* or NY-ESO-1-specific T cells *(right)* following OKT3 binding staining of 0.5μg.

Table 4.1 The TCR alpha and beta chain of each CTL pairs

SSX-2-specific T cells

Clone type	TCRα	TCRβ
CD103+ T cells	TRAV 8-6 TRAJ 30	TRBV 6-1 TRBJ 2-7
CD103- T cells	TRAV 8-6 TRAJ 30	TRBV 6-1 TRBJ 2-7

NY-ESO-1-specific T cells

Clone type	TCRα	TCRβ
CD103+ T cells	TRAV 12-2 TRAJ 31	TRBV 12-4 TRBJ 1-2
CD103- T cells	TRAV 12-2 TRAJ 31	TRBV 12-4 TRBJ 1-2

As TGF-β1 is known to induce CD103 expression on CTLs, we firstassessed the TGF-β1 level on $CD103^+$ cancer-specific CTLs. Interestingly, significantly high levels of TGF-β1 were produced by $CD103^+$ cancer-specific CTLs but not by the $CD103^-$ cancer-specific CTLs, following co-culture with peptide-loaded target cells HCT116 **(Figure 4.2).** There was still significant production of TGF-β1 by $CD103^+$ CTLs even after taking into consideration the cytokine production by HCT116 itself **(Figure 4.2).**

Previous studies have shown that HCT116 do not express NY-ESO-1 and SSX-2 proteins (Gjerstorff et al., 2014; Greve et al., 2014; Purbhoo et al., 2006; Saias et al., 2015). In our current study, we validated that cancer-specific CTLs do not induced any immune responses (by IFNγ and TNFα) in a co-cultured with HCT116 in the absence of external peptide loading **(Figure 4.3).** Therefore, this confirmed that HCT116 on its own does not induce SSX-2-specific and NY-ESO-1-specific T cell responses, due to lack of SSX-2 and NY-ESO-1.

As the presence of CD103 on cancer-specific CTLs may contribute to self- TGF-β1 production, we next evaluated whether interfering with the CD103 and its ligand E-Cadherin interaction on HCT116 can affect the TGF-β1 production. Following anti-CD103 antibody treatment, we found that the TGF-β1 production still remained high even after the treatment **(Figure 4.4)**. The TGF-β1 self-producing capacity by $CD103^+$ CTLs was further validated using intracellular cytokine staining analysis. As shown in **Figure 4.5A and B,** we found that the majority of $CD103^+$ CTLs expressed intracellular TGF-β1 but not the $CD103^-$ CTLs. The TGF-β1 expression can also be produced by $CD103^+$ CTLs even after treatment with anti-CD3/CD28, in the absence of target cells **(Figure 4.5B)**. These observations therefore suggest that the $CD103^+$ CTLs are possibly self-independent to express and produce TGF-β1, and likely responsible for sustaining its own CD103 expression.

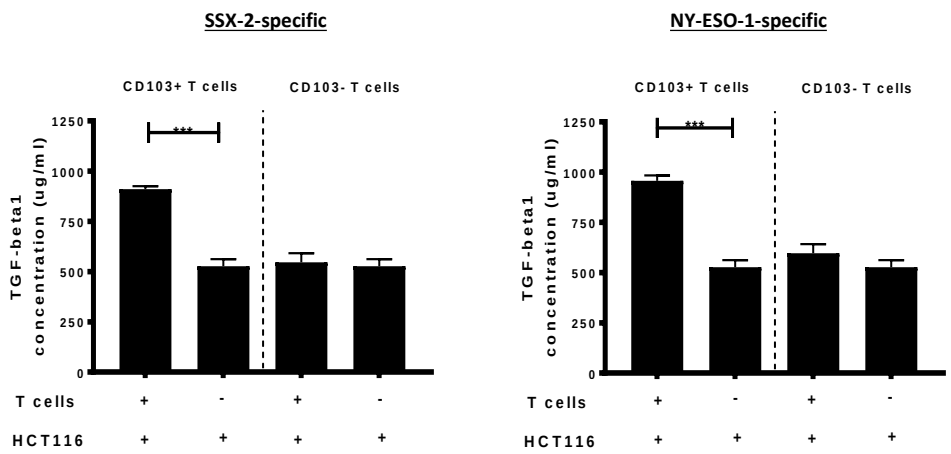


Figure 4.2 TGF-β1 production by CD103$^+$ cancer-specific T cells. TGF-β1 production by either CD103$^+$ or CD103$^-$ T cells following co-culture with HCT116 at 1μM antigen stimulation, with TGF-β1 production by HCt116 itself (as control). (N, number of repeats=3) Data represented as median ± s.e.m. * indicates p-value<0.05, ** p-values<0.01, *** p-values<0.001, ns, not significant. p-values were calculated using either one-way ANOVA with Tukey post hoc analysis or paired student t-test with Wilcoxon adjustments.

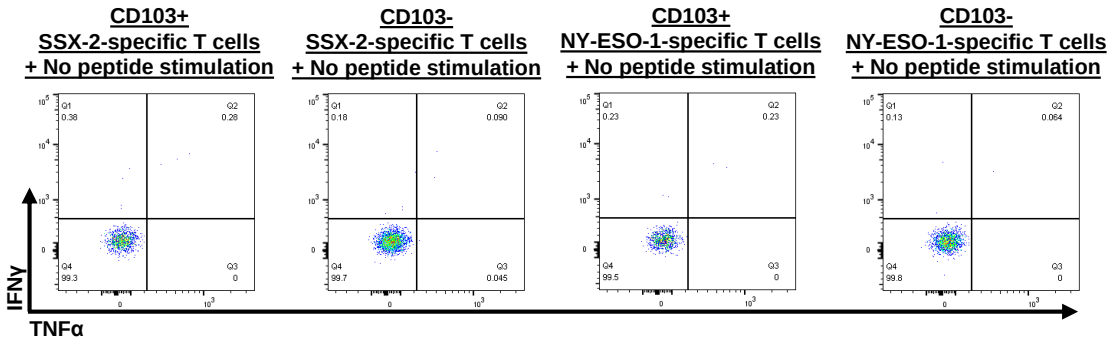


Figure 4.3 T cell-mediated response of cancer-specific T cells without external antigen stimulation. Flow cytometry plots of IFNγ and TNFα responses by CD103+ of CD103- SSX-2-specific or NY-ESO-1-specific T cells following co-culture with HCT116 cancer cell line without external tumor antigen peptide stimulation.

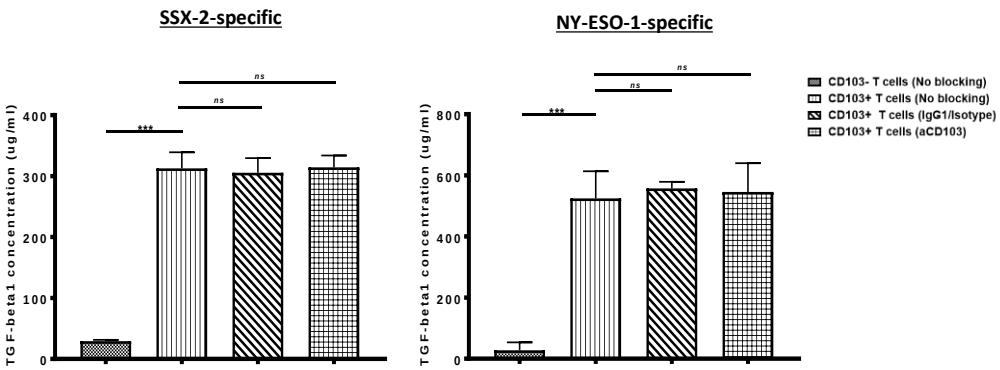


Figure 4.4 TGF-β1 production by CD103$^+$ cancer-specific T cells following interference of CD103. TGF-β1 production by either CD103$^+$ or CD103$^-$ T cells following co-culture with HCT116 with either no treatment, isotype treatment or anti-CD103 antibody treatment. SSX-2-specific T cell clones shown on the *left* and NY-ESO-1-specific T clones shown on the *right.* (N, number of repeats=3) Data represented as median $\pm$ s.e.m. * indicates p-value<0.05, ** p-values<0.01, *** p-values<0.001, ns, not significant. p-values were calculated using either one-way ANOVA with Tukey post hoc analysis or paired student t-test with Wilcoxon adjustments.

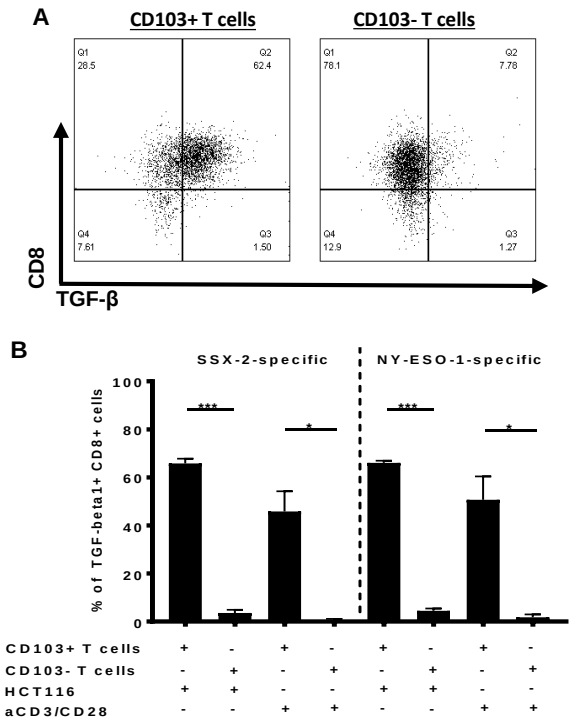


Figure 4.5 TGF-β1 intracellular expression by CD103$^+$ cancer-specific T cells. (A) Representative flow cytometry dot plots of TGF-β1-expressing CD8$^+$ cells either by CD103$^+$ or CD103$^-$ SSX-2-specific T cells following co-culture with HCT116 at 1μM antigen stimulation. (B) Proportion of TGF-β1$^+$ cells of either CD103$^+$ or CD103$^-$ T cells following co-culture with HCT116 at 1μM antigen stimulation or treated with CD3/CD28 antibody. (N, number of repeats=3) Data represented as median±s.e.m. * indicates p-value<0.05, ** p-values<0.01, *** p-values<0.001, ns, not significant. p-values were calculated using either one-way ANOVA with Tukey post hoc analysis or paired student t-test with Wilcoxon adjustments.

As the active form of TGF-β1 is an essential component for CD103 induction, we then assessed whether the integrin β8 (known to cleave the inactive form of TGF-β1) could be upregulated on TGF-β1$^+$ CD103$^+$ CTLs. Interestingly, the TGF-β1$^+$ CD103$^+$ CTLs have significant upregulation of the membranous β8 expression compared to the CD103$^-$ CTLs, following peptide-loaded target cells HCT116 exposure for 12 hours **(Figure 4.6A and B)**. The upregulation of integrin β8 on CD103$^+$ CTLs cell surface likely suggest that integrin β8 contributed to CD103 expression maintenance on the T cells by aiding synthesis of TGF-β1 active form.

4.2.2 CD103 helps to improve TCR-mediated tumor antigen sensitivity of CTLs

It is well-established that human CTA-specific T cells have low affinity TCRs (Aleksic et al., 2012; Thomas et al., 2011). Thus, we next assessed whether CD103 presence on T cells could assist in improving tumor antigen sensitivity and strengthen the TCR-mediated effector responses. Following co-culture of CTLs with HCT116, we found that the CD103$^+$ CTLs demonstrated significantly elevated IFNγ responses compared to the CD103$^-$ CTLs and was sensitive up to 0.4μg/ml antigen stimulation **(Figure 4.7A and B).** The IFNγ production by CD103$^+$ CTLs was reduced following treatment with anti-CD103 **(Figure 4.7A and B)** clearly indicates that CD103$^+$ CTLs display superior functional activity, particularly of IFNγ responses.

The CD107a marker is a good indicator of the degranulation activities and potential granules-mediated cytotoxic responses of T cells. Therefore, we evaluated whether the enhanced TCR tumor antigen sensitivity could affect the degranulation action by CD103$^+$ CTLs. The CD107a response was also significantly elevated on CD103$^+$ CTLs and was sensitive up to 0.4μg/ml antigen stimulation **(Figure 4.7A and C).** The CD107a response was impaired after anti-CD103 treatment of CD103$^+$ CTLs **(Figure 4.7A and C)**.

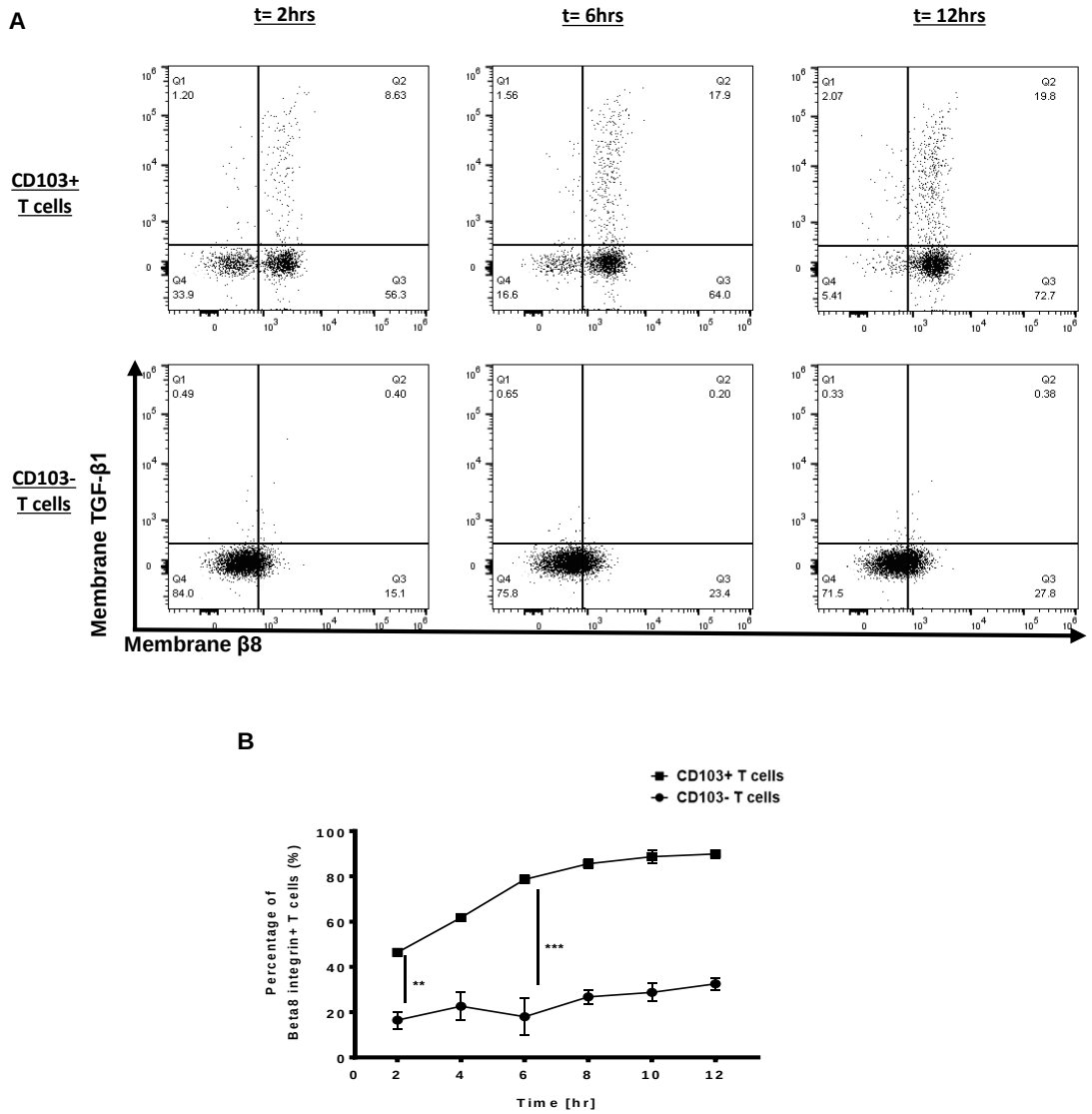


Figure 4.6 Membrane β8 surface expression by CD103^{+} cancer-specific T cells. (A) Flow cytometry plots of membranous TGF-β1 and membranous β8 expression on either CD103+ or CD103- T cells, at t=2,6 and 12 hours post co-culture with 1μM antigen stimulation HCT116. (B) Frequency of either CD103+ or CD103- T cells being β8+ across 12 hours' period (N, number of repeats n=3). Data information: data represented as median ± s.e.m. * indicates p-value<0.05, ** p-values<0.01, *** p-values<0.001, ns, not significant. p-values were calculated using either one-way ANOVA with Tukey post hoc analysis or paired student t-test with Wilcoxon adjustments.

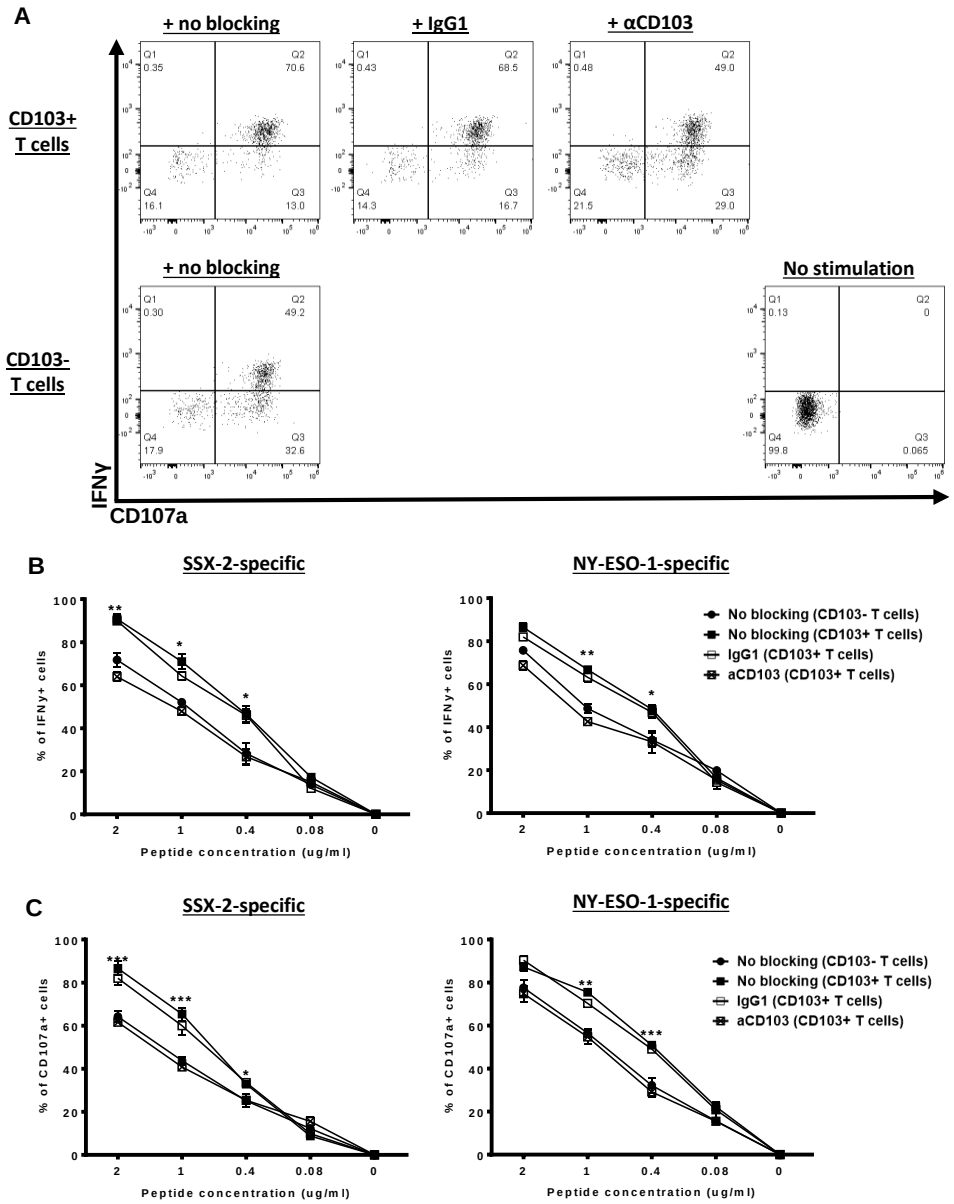


Figure 4.7 TCR antigen sensitivity by evaluating IFNγ and degranulation CD107a on CD103$^+$ cancer-specific T cells. (A) Representative flow cytometry plots of IFNγ and CD107a expression following T cells co-culture with/without antigen-stimulated HCT116, with either anti-CD103 blocking treatment, isotype control treatment or no treatment. Proportion of IFNγ$^+$ cells (B) and CD107a$^+$ cells (C) of CD103$^+$ T cells with either anti-CD103 blocking treatment, isotype control treatment or no treatment, as well as of CD103$^-$ T cells with no treatment, following co-culture with HCT116 at five different concentrations of tumor-associated antigen stimulation, SSX-2 *(left)* and NY-ESO-1 *(right).* (N, number of repeats=3) Data represented as median±s.e.m. * indicates p-value<0.05, ** p-values<0.01, *** p-values<0.001, ns, not significant. p-values were calculated using two-way ANOVA with Tukey post hoc analysis.

We then assessed whether the enhanced degranulation capacity can improve the $CD103^+$ CTLs anti-tumor cytotoxicity. As expected, significantly higher numbers of target cells HCT116 were killed by $CD103^+$ cancer-specific CTLs as compared to the $CD103^-$ cancer-specific CTLs, up to 0.4μg/ml antigen stimulation **(Figure 4.8)**.

As E-Cadherin is a known ligand of CD103, we next considered whether the requirement of CD103 and E-Cadherin interaction is necessary to improve the tumor antigen sensitivity. To do this, we co-cultured $CD103^+$ CTLs with the E-Cadherin-negative THP-1 cancer cell line. As shown in **Figure 4.9A,** the $CD103^+$ CTLs have significantly reduced degranulation activity in response to co-culturing with E-Cadherin-negative THP-1, as compared to the E-Cadherin-positive HCT116. We further found that in the absence of E-Cadherin, the $CD103^+$ CTLs showed significant reduction in the target cell THP-1 killing **(Figure 4.9B)**. These observations suggest that CD103 and its interaction with E-Cadherin on target cells contributes to enhanced TCR recognition and tumor antigen sensitivity, thus resulting in enhanced granules-mediated cytotoxicity and IFNγ response.

4.2.3 Rapid and accumulating cytotoxicity by $CD103^+$ CTLs

We next assessed whether the tumor antigen-sensitive $CD103^+$ CTLs could enable more efficient individual cancer cell killing, by using live cell imaging (with the assistance from Huw Colin-York, Friztsche Group, WIMM). Using this technique, we measured the timing of individual cytotoxic events following CTLs exposure with peptide-loaded HCT116. Interestingly, the $CD103^+$ CTLs initiated significantly faster target cell killing compared to the $CD103^-$ CTLs, which required a longer period to initiate killing **(Figure 4.10A and B).** In addition, higher numbers of $CD103^-$ CTLs are required to initiate the killing of individual target cell **(Figure 4.10A).**

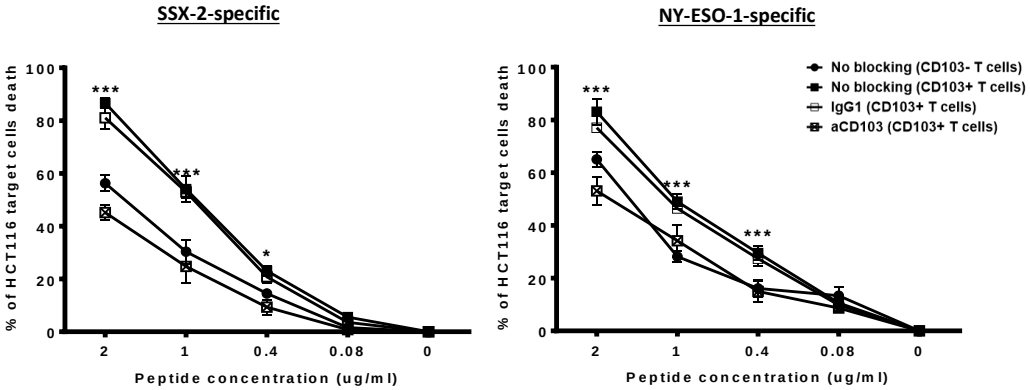


Figure 4.8 TCR tumor antigen sensitivity measured by cytotoxicity on CD103$^+$ cancer-specific T cells. Proportion of HCT116 cancer cells death following co-culture with either CD103$^+$ T cells with either anti-CD103 blocking treatment, isotype treatment or no treatment, as well as of CD103$^-$ T cells with no treatment, at five different antigen concentrations. (N, number of repeats=3). Data represented as median$\pm$s.e.m. * indicates p-value<0.05, ** p-values<0.01, *** p-values<0.001, ns, not significant. p-values were calculated using two-way ANOVA with Tukey post hoc analysis.

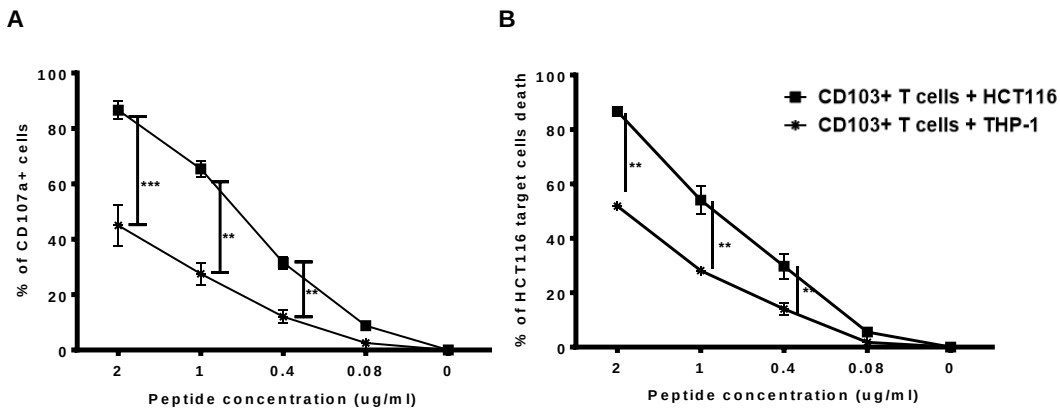


Figure 4.9 TCR antigen sensitivity by evaluating the need of CD103 and E-Cadherin interaction by CD103$^+$ cancer-specific T cells. (A) Proportion of CD107a$^+$ cells of CD103$^+$ SSX-2-specific T cells following either co-culture with E-Cadherin+ HCT116 or E-Cadherin- THP-1, at five different concentrations of tumor-associated antigen stimulation (B) Proportion of cancer cell deaths following either co-culture with E-Cadherin+ HCT116 or E-Cadherin- THP-1, at five different concentrations of tumor-associated antigen stimulation, Data represented as median$\pm$s.e.m. * indicates p-value<0.05, ** p-values<0.01, *** p-values<0.001, ns, not significant. p-values were calculated using two-way ANOVA with Tukey post hoc analysis.

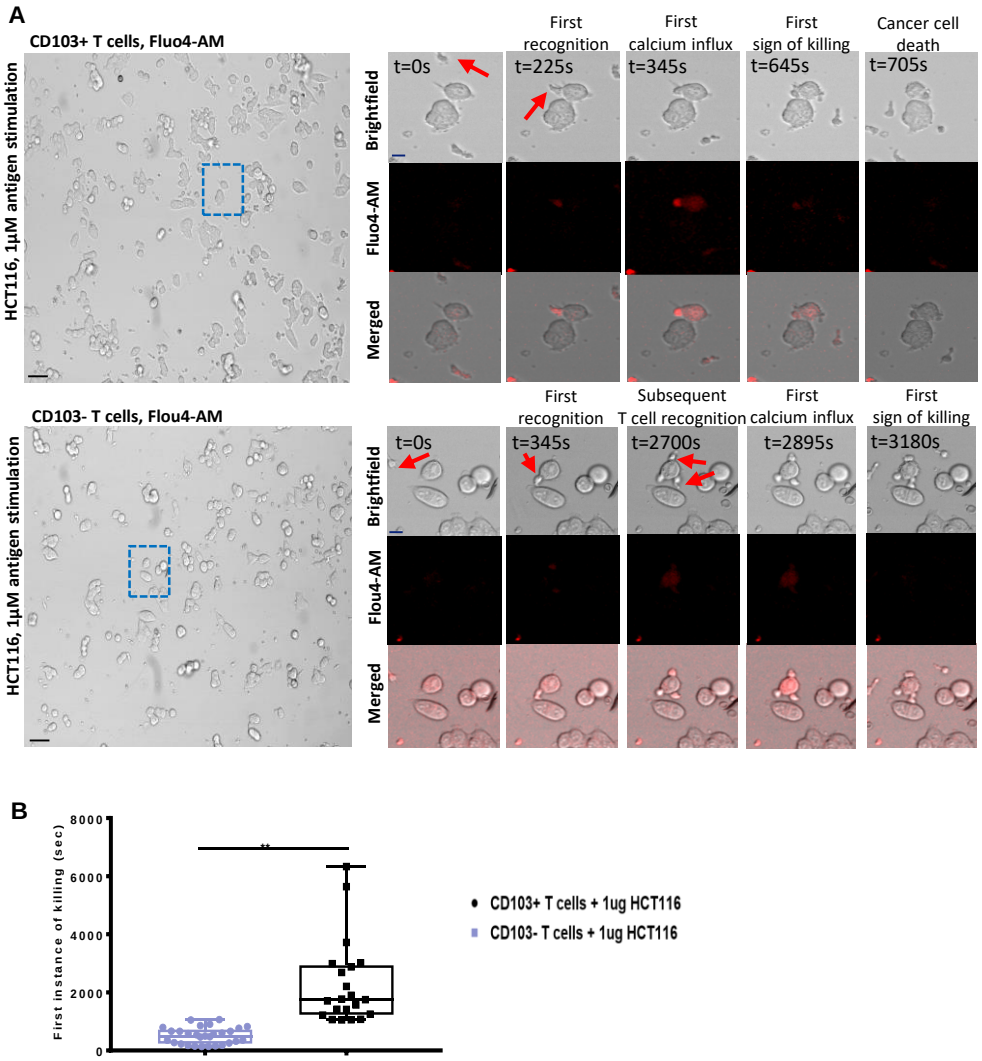


Figure 4.10 The timing of CD103$^+$ cancer-specific T cells cytotoxicity. (A). Confocal imaging time-lapse of HCT116 cancer cells with co-cultured either CD103$^+$ *(top)* or CD103$^-$ *(bottom)* SSX-2-specific T cells and labelled with flou4-AM calcium staining. Close-up images showing brightfield *(top)*, flou4-AM stain *(middle)* and merged *(bottom)*. Flou4-AM calcium staining shown in red. Cancer cell death is indicated by the disruption/bubbling of the cell membrane. (B). Amount of time (in seconds) required for first instance of cancer cell killing by either CD103$^+$ or CD103$^-$ SSX-2-specific T cells. N_1, number of events collected for CD103$^+$ T cells: 29; N_2, number of events collected for CD103$^-$ T cells: 29. (N, number of repeats=3) Data represented as median$\pm$s.e.m.* indicates p-value<0.05, ** p-values<0.01, *** p-values<0.001, ns, not significant. p-values were calculated using either paired student t-test with Wilcoxon adjustments, one-way or two-way ANOVA with Tukey post hoc analysis.

These observations strongly suggest that the presence of CD103 could potentially help to mediate a quicker cytotoxic activity of T cells. Indeed, the efficient individual target cell killing by $CD103^+$ cancer-specific CTLs become more apparent as early as 4 hours after target cell exposure **(Figure 4.11A and B).** The cytotoxic activities of $CD103^+$ CTLs had resulted in significantly higher accumulation of HCT116 cell deaths over a 12-hour time period compared to the $CD103^-$ CTLs **(Figure 4.12 and 4.13)**.

To confirm that CD103 and E-Cadherin interaction is vital in contributing to the enhanced cancer-specific CTLs cytotoxicity, we also co-cultured $CD103^+$ CTLs with peptide-loaded E-Cadherin-negative THP-1. There was no difference in the numbers of THP-1 cell deaths following co-culture with either $CD103^+$ CTLs or $CD103^-$ CTLs across a 12-hour time period, as shown in **Figure 4.14**. Taken together, these observations clearly highlight the importance of the CD103, and its interaction with E-Cadherin in elevating CTLs anti-tumor cytotoxic responses.

4.2.4 $CD103^+$ cancer-specific CTLs have high energetic potential

Previous studies have highlighted the importance of aerobic glycolysis (glucose oxidation), not only as the major energy source for activated T cell functions but also as a regulator of cytokine production (Chang et al., 2013; Menk et al., 2018). Thus, we next assessed the metabolic capacity of $CD103^+$ cancer-specific CTLs by evaluating their glycolytic activity.

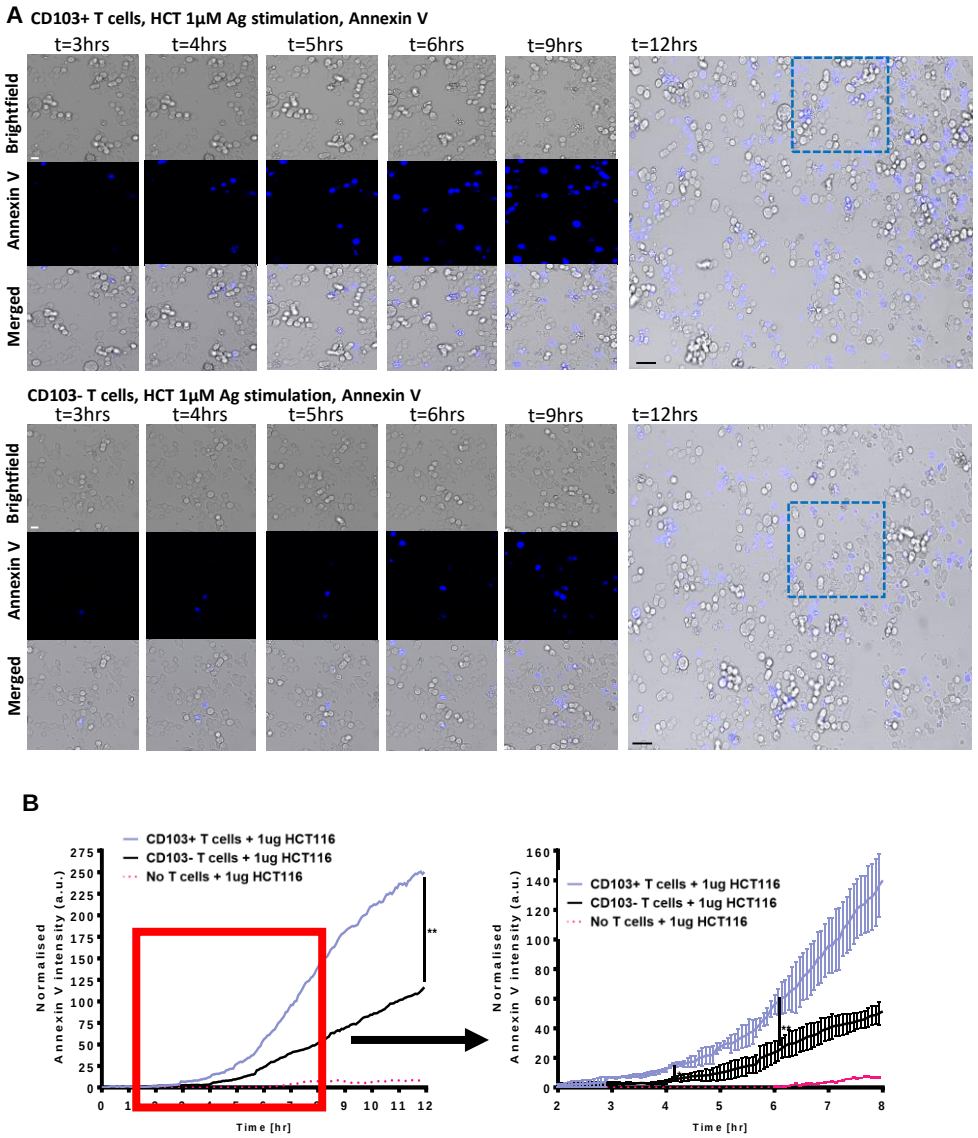


Figure 4.11 The CD103^{+} cancer-specific T cells cytotoxicity across 12-hours period. (C) Confocal imaging time-lapse of HCT116 cancer cells with co-cultured either CD103^{+} *(top)* or CD103^{-} *(bottom)* SSX-2-specific T cells and labelled with Annexin V. Close-up images showing brightfield *(top),* Annexin V *(bottom)* and merged *(bottom)* at 3,4,5,6,9,12 hours after co-culture. Annexin V staining shown in blue. (D). Normalised annexin V intensity representing HCT116 cell death across a 12-hour time period following co-culture with no T cell control, with a close-up detailing 2 to 8 hours co-culture. (N, number of repeats=3) Data represented as median±s.e.m.* indicates p-value<0.05, ** p-values<0.01, *** p-values<0.001, ns, not significant. p-values were calculated using either paired student t-test with Wilcoxon adjustments, one-way or two-way ANOVA with Tukey post hoc analysis.

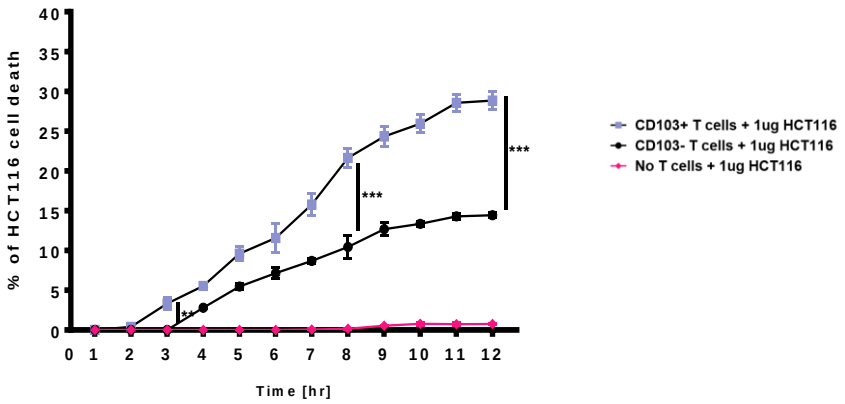


Figure 4.12 The target cells death over time by CD103^{+} cancer-specific T cells cytotoxicity. Percentage of HCT116 cell death across a 12-hour time period following co-culture with no T cells as control. (N, number of repeats=3). Data represented as median±s.e.m.* indicates p-value<0.05, ** p-values<0.01, *** p-values<0.001, ns, not significant. p-values were calculated using either paired student t-test with Wilcoxon adjustments, one-way or two-way ANOVA with Tukey post hoc analysis.

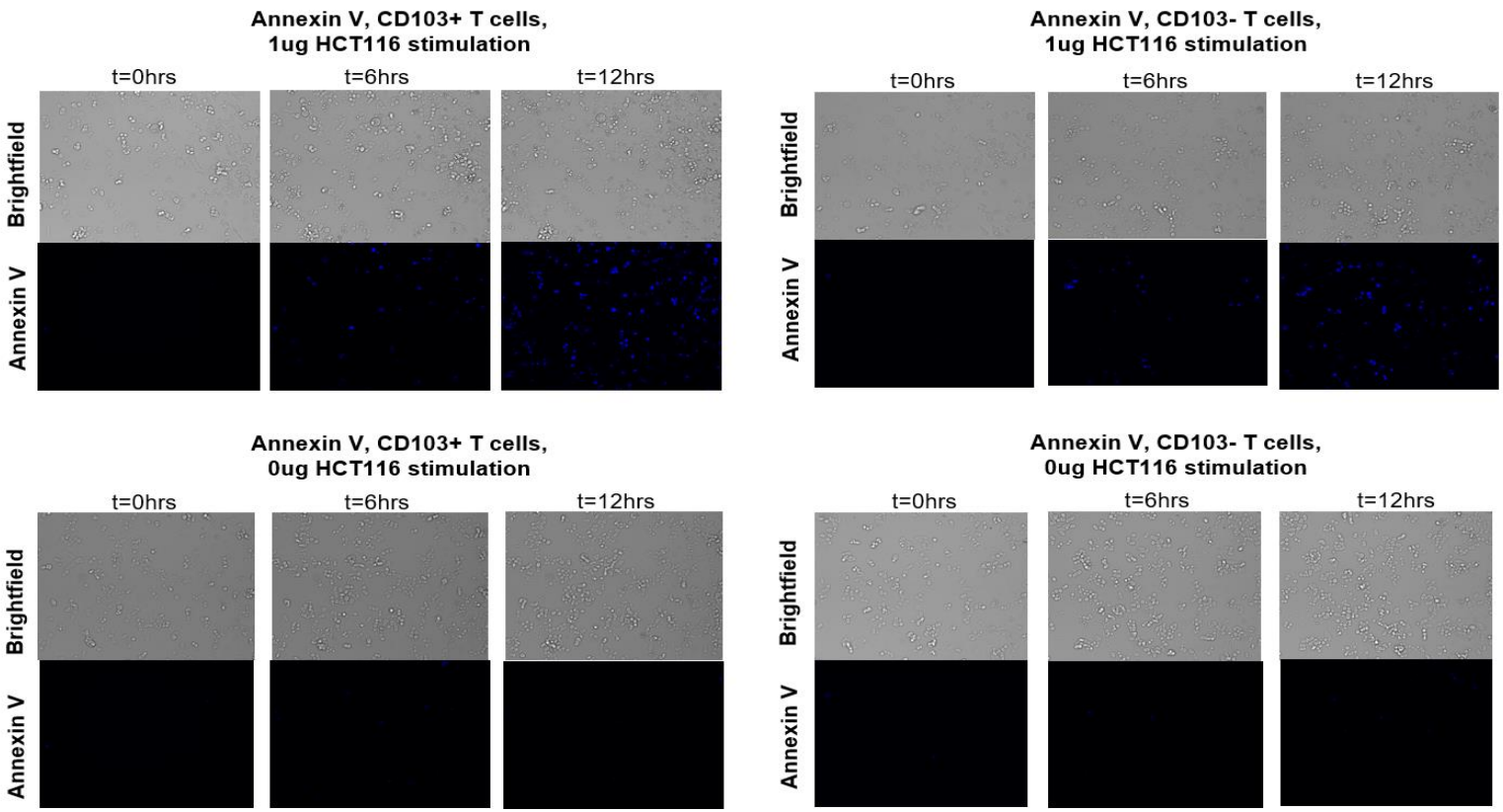


Figure 4.13 T cell cytotoxic events. Brightfield and Annexin V images of antigen stimulated HCT116 cell death following co-exposure with either $CD103^+$ *(left)* or $CD103^-$ *(right)* SSX-specific T cells at 0,6 and 12 hours, with 0μM-stimulated HCT116 co-culture as controls. Annexin V excited at 632nm excitation and illustrated in blue.

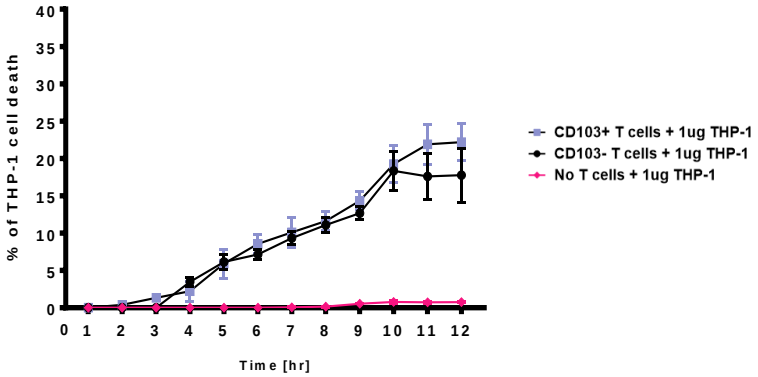


Figure 4.14 Anti-tumor T cells cytotoxicity E-Cadherin-negative THP-1. Percentage of THP-1 cell death across a 12-hour time period following co-culture with no T cells as controls. (N, number of repeats=3). Data represented as median±s.e.m.

Interestingly, the $CD103^+$ CTLs have significantly higher basal glycolytic rates compared to the $CD103^-$ CTLs **(Figure 4.15A and B)**. More notably, the $CD103^+$ CTLs showed significantly elevated maximal glycolytic capacity **(Figure 4.15A and C)**. This suggests that $CD103^+$ CTLs can utilise and convert high levels of glucose at a faster rate compared to the $CD103^-$ CTLs, which could potentially be used to induce more efficient, rapid and effective immune responses.

However, in the tumor microenvironment, enhanced glucose consumption by cancer cells is known to deprive TILs of the much-needed glucose for their cellular functions (Chang et al., 2015). It is, therefore, vital for $CD103^+$ cancer-specific CTLs to be able to efficiently catalyse multiple metabolites, especially during conditions of stress. Therefore, we evaluated the total metabolite consumption capacity of activated $CD103^+$ CTLs by assessing the total oxygen consumption rate (OCR), as a measure of the overall T cell mitochondrial activity. We found that the $CD103^+$ CTLs have a significantly higher basal metabolic activity compared to the $CD103^-$ CTLs (**Figure 4.16A and B).** More importantly, the $CD103^+$ CTLs have a substantially larger spare mitochondrial capacity **(Figure 4.16A and C)**, suggesting their potential in utilising various metabolites at a higher level compared to the $CD103^-$ CTLs in order to meet its energy requirements.

4.2.5 $CD103^+$ CTLs have better homing capacity and localise on E-Cadherin rich tumor cells

Activation of CD103 and its cytoplasmic tail domain on T cells is known to enhance T cell retention in tissue (Boutet et al., 2016; Gauthier et al., 2017; Sathaliyawala et al., 2013). We therefore assessed whether CD103 could mediate better recognition, homing and retention of T cells to cancer cells.

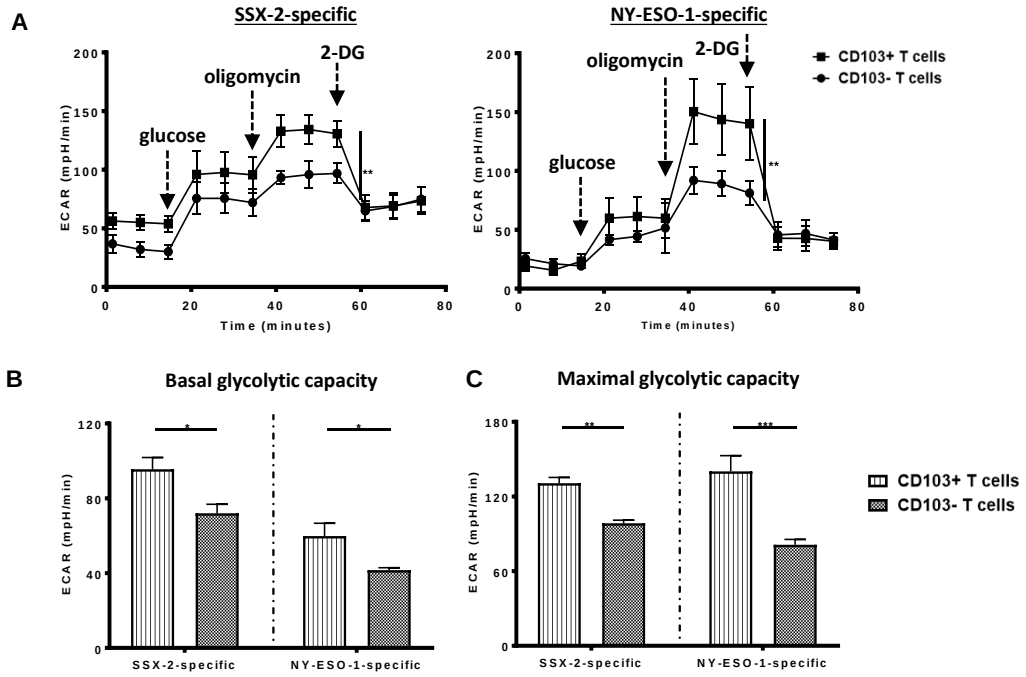


Figure 4.15 Glycolytic activities of CD103$^+$ cancer-specific T cells. A. The extracellular acidification rates (ECAR) of CD103$^+$ or CD103$^-$ T cells across 80 minutes period. SSX-2 *(left)* and NY-ESO-1 *(right).* (N, number of repeats=3). The ECAR of basal glycolytic capacity (B) and the maximal glycolytic capacity (C) of CD103$^+$ or CD103$^-$ T cells. (N, number of repeats=3) Data represented as median$\pm$s.e.m.* indicates p-value<0.05, ** p-values<0.01, *** p-values<0.001, ns, not significant. p-values were calculated using either paired student t-test with Wilcoxon adjustments, one-way or two-way ANOVA with Tukey post hoc analysis.

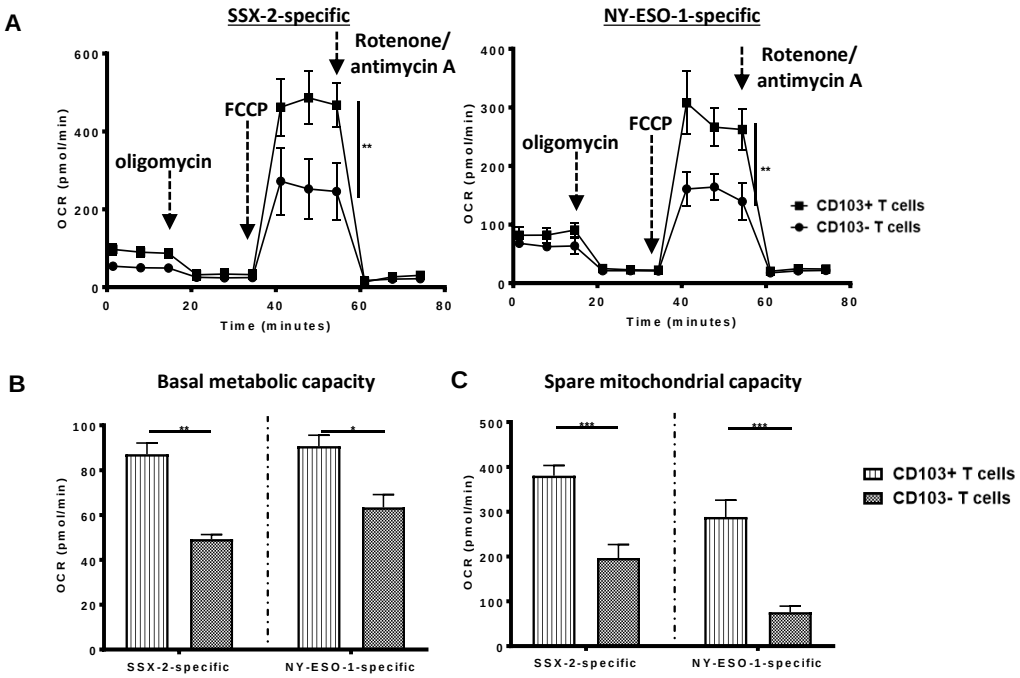


Figure 4.16 Mitochondrial activities of CD103$^+$ cancer-specific T cells. (A) The oxygen consumption rates (OCR) of CD103$^+$ or CD103$^-$ T cells across 80 minutes period. SSX-2 *(left)* and NY-ESO-1 *(right)*. (N, number of repeats=3). The OCR at basal respiration stage (B) and the spare respiratory capacity (C) of CD103$^+$ or CD103$^-$ T cells. (N, number of repeats=3). Data represented as median $\pm$ s.e.m.* indicates p-value<0.05, ** p-values<0.01, *** p-values<0.001, ns, not significant. p-values were calculated using either paired student t-test with Wilcoxon adjustments, one-way or two-way ANOVA with Tukey post hoc analysis.

To do this, we initially placed either the $CD103^+$ or $CD103^-$ cancer-specific CTLs across a transwell barrier, away from HCT116, and allowed any movement to occur within 2 hours period. Within the first hour, the $CD103^+$ cancer-specific CTLs had already migrated in significantly larger numbers across the barrier towards HCT116 **(Figure 4.17A).** Treatment of the $CD103^+$ CTLs with anti-CD103 significantly reduced the number of T cells migrating to the target cells, to a level similar to that of the $CD103^-$ CTLs **(Figure 4.17B)**.

To further validate the necessity of CD103 in T cell mobility and homing, we exposed $CD103^+$ CTLs with E-Cadherin-negative THP-1. As shown in **Figure 4.18,** no significant difference in the numbers of $CD103^+$ CTLs and $CD103^-$ CTLs migrating towards THP-1 was found. These *in vitro* data indicate the importance of CD103 in the movement and migration of CTLs towards E-Cadherin-positive cancer cells such as HCT116.

In support of our *in vitro* observations, we also carried out *ex vivo* immunohistochemistry analysis on cross-sectional tumor tissues from five lung cancer patients. Immunohistochemistry staining was performed by Lucia Cerundolo and Molly Browne, and digital imaging gating and analysed was carried out by Nasullah Khalid-Alham. It was found that $CD103^+$ $CD8^+$ TILs clearly localised at the E-cadherin rich tumor islets, while the $CD103^-$ $CD8^+$ TILs were mainly in the E-Cadherin-absent tumor regions. The $CD103^+$ $CD8^+$ TILs significantly clustered around, as well as within, the E-cadherin rich tumor islets, at a significantly higher frequency and density **(Figure 4.19A and B)**. In contrast, the $CD103^-$ $CD8^+$ TILs are much denser distal from the E-$Cadherin^+$ tumor islets **(Figure 4.19A and B)**. Altogether, these observations highlighted the feature of $CD103^+$ CTLs, having better homing and clustering capacity to cancer cells expressing E-Cadherin.

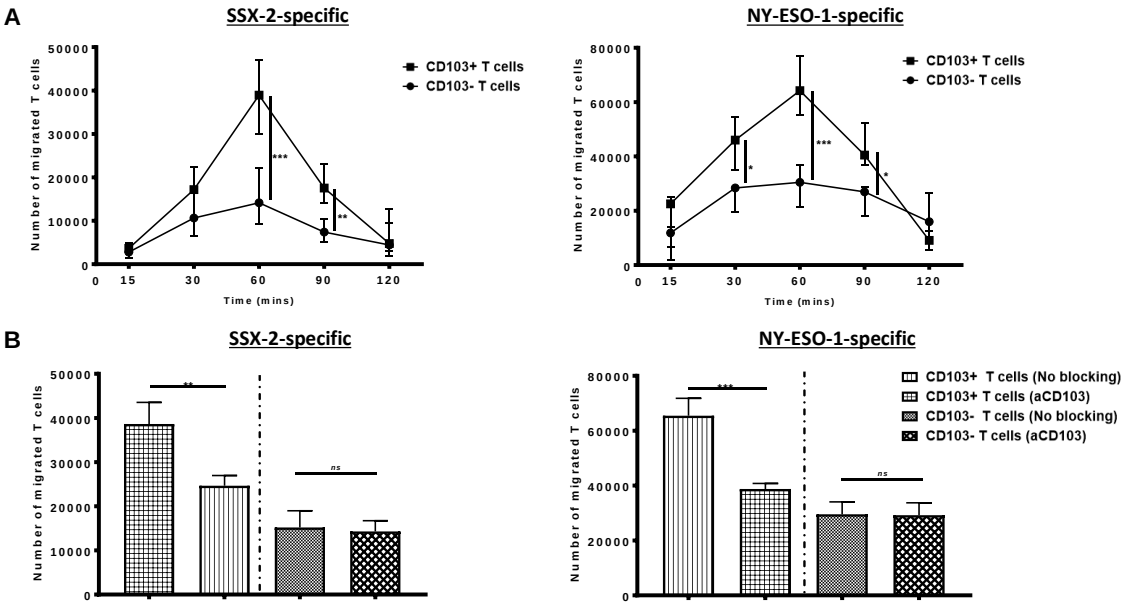


Figure 4.17 CD103 expression on T cells enables faster migration *in vitro*. **(**A). The number of T cells (either $CD103^+$ or $CD103^-$ T cells) that migrated across a transwell membrane over a time period of 2 hours. SSX-2-specific T cell clones shown on the *left* and NY-ESO-1-specific T clones shown on the *right.* (N, number of repeats=3) (B). The number of T cells (either $CD103^+$ or $CD103^-$ T cells) migrated across a transwell membrane at 60 minutes, with or without anti-CD103 blocking treatment. SSX-2-specific T cell clones shown on the *left* and NY-ESO-1-specific T clones shown on the *right.* (N, number of repeats=3) In (A and B), data represented as median$\pm$s.e.m.* indicates p-value<0.05, ** p-values<0.01, *** p-values<0.001, ns, not significant. p-values were calculated using either one-way or two-way ANOVA with Tukey post hoc analysis.

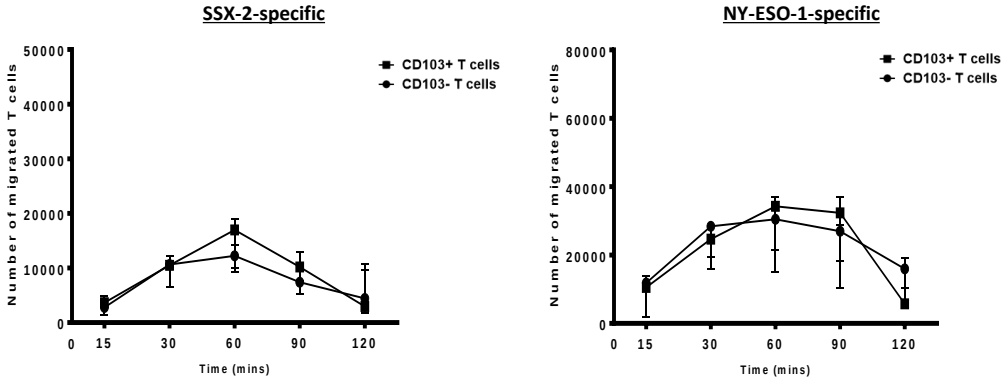


Figure 4.18 CD103+ or CD103- cancer-specific T cells migration towards E-Cadherin-negative THP-1. The number of T cells (either $CD103^+$ or $CD103^-$ T cells) that migrated across a transwell membrane over a time period of 2 hours. SSX-2-specific T cell clones shown on the *left* and NY-ESO-1-specific T clones shown on the *right.* (N, number of repeats=3).

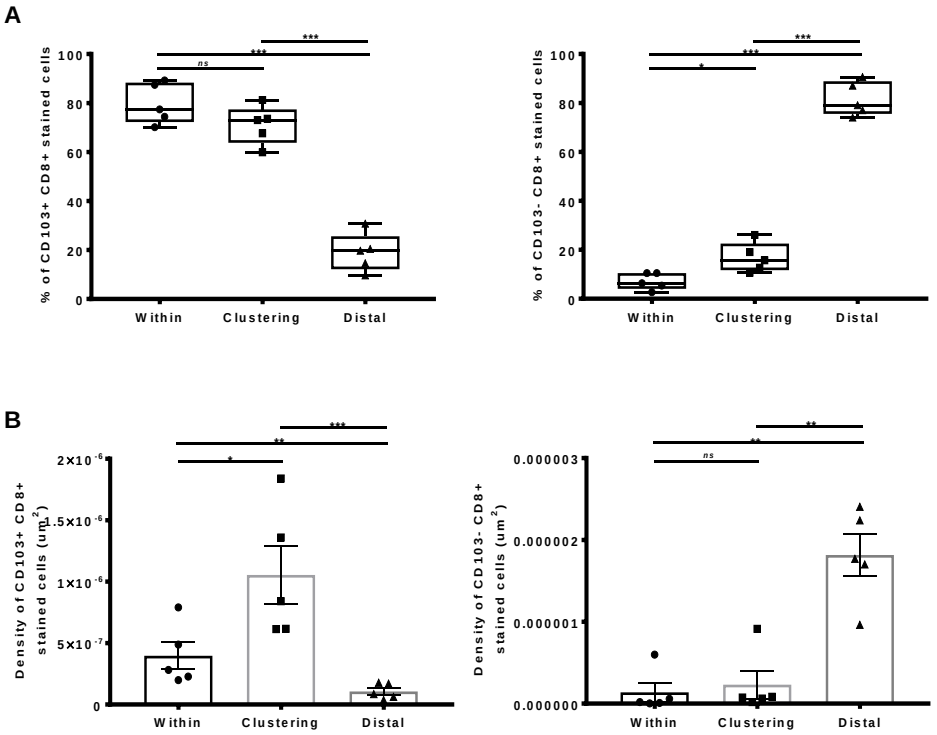


Figure 4.19 CD103$^+$ CD8$^+$ TILs localisation in tumors. (A) Proportion of CD103$^+$ CD8$^+$ stained cells *(left)* or CD103$^-$ CD8$^+$ stained cells *(right)* present either within, clustering around or distal of E-cadherin$^+$ stained cells. (B) Density (by μm^2) of CD103$^+$ CD8$^+$ stained cells *(left)* or CD103$^+$ CD8$^+$ stained cells *(right)* present either within, clustering around or distal of E-cadherin$^+$ staining cells. (N, number of patients=5). In (B and C), data represented as median±s.e.m.* indicates p-value<0.05, ** p-values<0.01, *** p-values<0.001, ns, not significant. p-values were calculated using one-way ANOVA with Tukey post hoc analysis.

4.2.6 Prolonged exposure of CD103$^+$ T cells to cancer contributes to T cell death

It was previously shown that TILs co-expressing CD103 and CD39 are 'tumor-reactive' TILs, with increased inhibitory receptors expression (Duhen et al., 2018). However, it remains unclear whether CD103$^+$ TILs have different subpopulations with distinctive exhaustion immunophenotypes. We first categorised *ex vivo* TILs derived from paired tumor and paratumor tissue from five lung cancer patients according to their CD103 and CD39 expression. Interestingly, only the CD103$^+$ TILs derived from the tumor expressed high levels of CD39 (CD39^{high}) but not the CD103$^+$ T cells derived from the paratumor tissue **(Figure 4.20A and B)**. In contrast, the CD103$^+$ CD39^{lo} T cell subpopulation can be found in both paired tissue samples **(Figure 4.20A)**. This therefore indicates the presence of multiple CD103$^+$ TIL subpopulations in tumor and suggests potential differences in their immunophenotypes.

Notably, only the CD103$^+$ CD39^{high} TILs subpopulation has higher expression of PD-1, Tim3 and TIGIT **(Figure 4.21).** This subpopulation has a significantly higher frequency of PD-1$^+$ Tim3$^+$ TIGIT$^+$ co-expressed cells **(Figure 4.22A).** In contrast, the CD103$^+$ CD39^{low} TILs subpopulation lack Tim3 and NKG2a expression, with only 40% of PD-1$^+$ TIGIT$^+$ co-expressed cells **(Figure 4.22B)**. These observations suggest that only some CD103$^+$ TILs acquire Tim3 expression and express high levels of different inhibitory receptor co-expression.

Upregulation of inhibitory receptors on TILs is one of the marks of T cell activation as well as exhaustion. To further assess whether prolonged antigen exposure of CD103$^+$ CTLs in cancer can impair activated T cell survival, we co-cultured CD103$^+$ cancer-specific CTLs with target cells HCT116 for a 12-hour period *in vitro*.

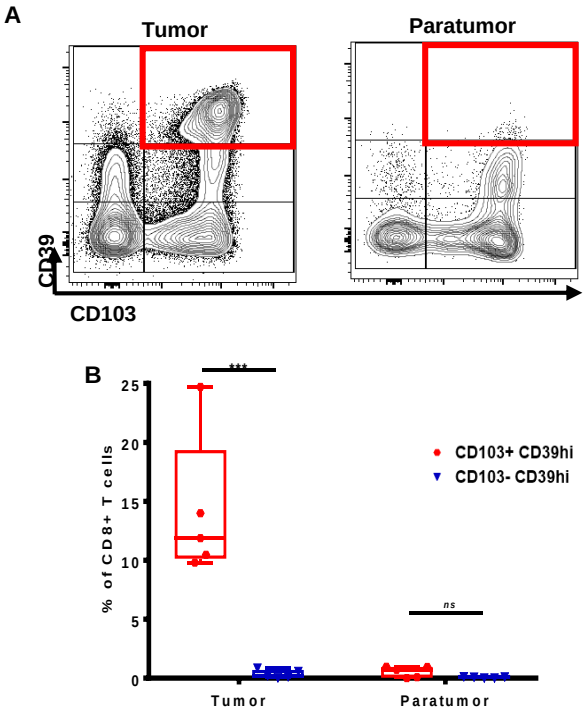


Figure 4.20 *Ex vivo* CD103^{+} TILs subpopulations analysis. Representative flow cytometry contour plots of CD39 and CD103 expression on total CD8^{+} TILs derived from either tumor or paratumor tissue (A), with graph showing frequency of CD8^{+} TILs coexpressing CD39 and CD103 across five different lung cancer patients (B). Data represented as median$\pm$s.e.m. * indicates p-value<0.05, ** p-values<0.01, *** p-values<0.001, ns, not significant. p-values were calculated using either one-way or two-way ANOVA with Tukey post hoc analysis.

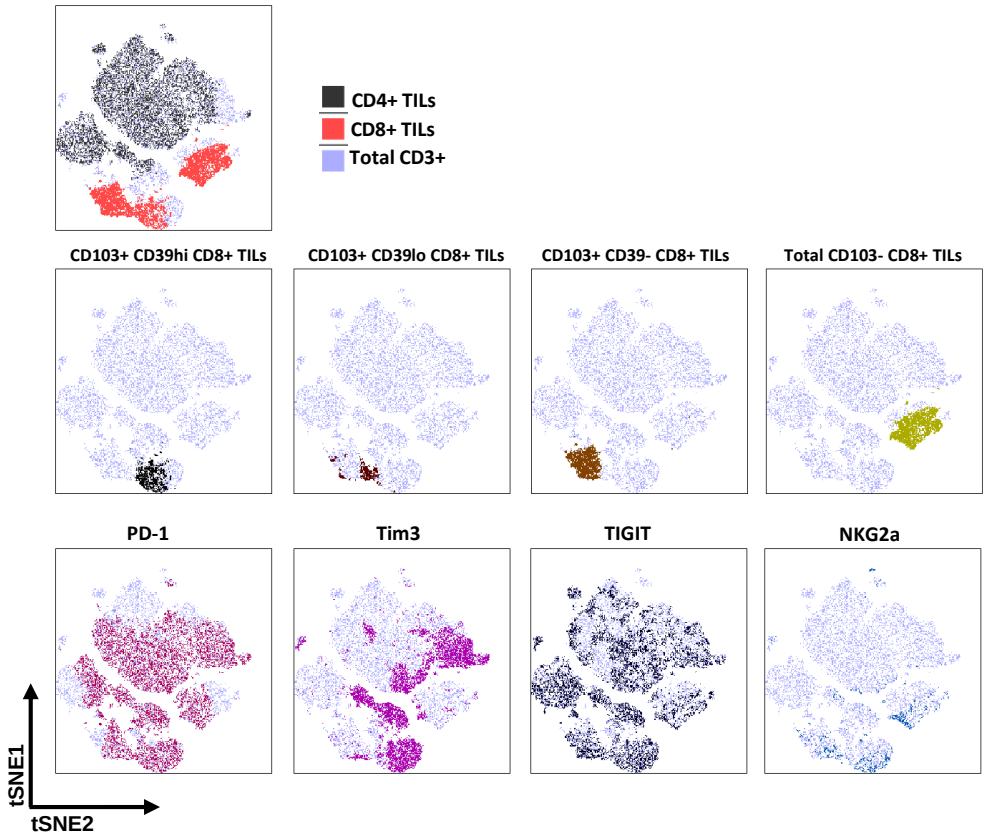


Figure 4.21 *Ex vivo* CD103^{+} TILs inhibitory receptors expression. tSNE plots identifying CD8^{+} and CD4^{+} TILs populations *(top)*, the CD103^{+} CD39^{high}, CD103^{+} CD39^{low}, CD103^{+} CD39^{-} and total CD103^{-} TILs of CD8^{+} populations *(middle)* and the PD-1, Tim3, TIGIT and NKG2a expressing TILs populations.

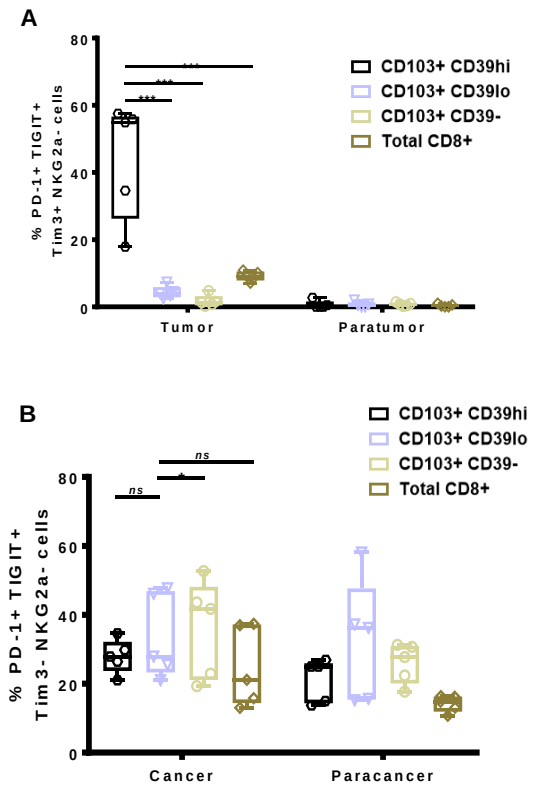


Figure 4.22 *Ex vivo* CD103^{+} TILs inhibitor receptors co-expression phenotype. (A) Proportion of PD1^{+} TIGIT^{+} Tim3^{+} NKG2a^{-} cells of either CD103^{+} CD39^{high}, CD103^{+} CD39^{low}, CD103^{+} CD39^{-} or total CD8^{+} TILs derived from paired tumor and paratumor. (B). Proportion of PD1^{+} TIGIT^{+} Tim3^{-} NKG2a^{-} cells of either CD103^{+} CD39^{high}, CD103^{+} CD39^{low}, CD103^{+} CD39^{-} or total CD8^{+} TILs derived from paired tumor and paratumor. (N, number of patients=5). Data represented as median$\pm$s.e.m. * indicates p-value<0.05, ** p-values<0.01, *** p-values<0.001, ns, not significant. p-values were calculated using either one-way or two-way ANOVA with Tukey post hoc analysis.

Interestingly, we found that prolonged cancer exposure resulted in significantly increased $CD103^+$ CTLs expressing activated caspase-3 when compared to the $CD103^-$ CTLs **(Figure 4.23A).** As activated caspase-3 presence is known to be an indicator of cellular apoptosis, we next evaluated $CD103^+$ CTLs cell death after prolonged cancer exposure. As expected, significantly higher number of $CD103^+$ T cell deaths were observed following prolonged cancer exposure, compared to $CD103^-$ T cell deaths **(Figure 4.23B)**. These observations taken altogether therefore suggest that $CD103^+$ CTLs are more prone to apoptosis in nature, in the event of prolonged cancer exposure.

4.3 Discussion

The association of $CD103^+$ TILs enrichment with good clinical outcomes in cancer patients (Djenidi et al., 2015; Ganesan et al., 2017) highlights the need to have a clear and comprehensive understanding of the characteristics of $CD103^+$ cancer-specific CTLs and their implications for future immunotherapies. We have demonstrated that matured differentiated $CD103^+$ cancer-specific CTLs can self-regulate their CD103 expression by producing activated TGF-β1, without needing to rely on external cues from other TGF-β1-producing cells. We further showed that the presence of CD103 could help to improve TCR antigen sensitivity, enabled faster cancer recognition and more rapid and efficient cancer cell killing. Moreover, $CD103^+$ CTLs were also found to have an elevated energy potential and faster migration capacity **(Figure 4.24)**. However, our data also demonstrated that $CD103^+$ cancer-specific CTLs are more susceptible to apoptosis following prolonged cancer exposure.

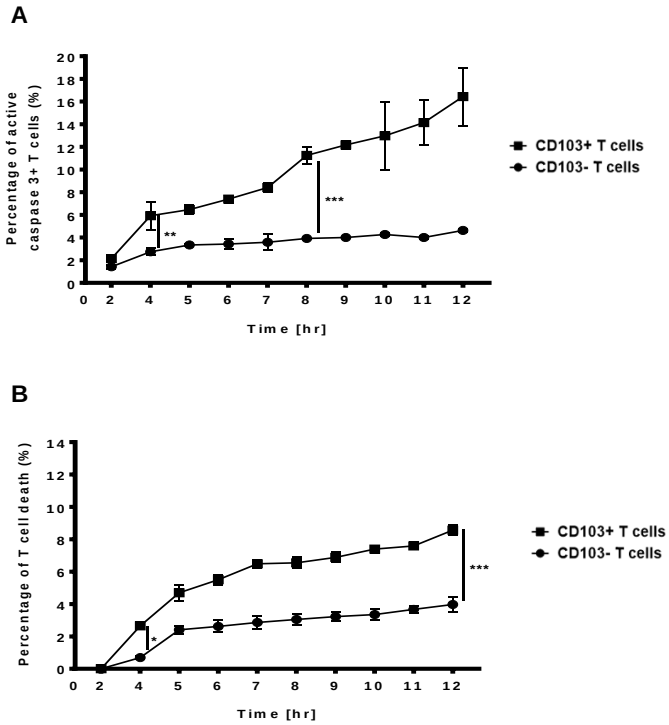


Figure 4.23 *In vitro* analysis of caspase-mediated T cell death during prolonged cancer exposure. The proportion of activated caspase-3+ T cells (E) and T cell death (F) following co-culture with HCT116 at 1μM antigen stimulation across a time period of 12 hours. (N, number of repeats=3). Data represented as median±s.e.m. * indicates p-value<0.05, ** p-values<0.01, *** p-values<0.001, ns, not significant. p-values were calculated using either one-way or two-way ANOVA with Tukey post hoc analysis.

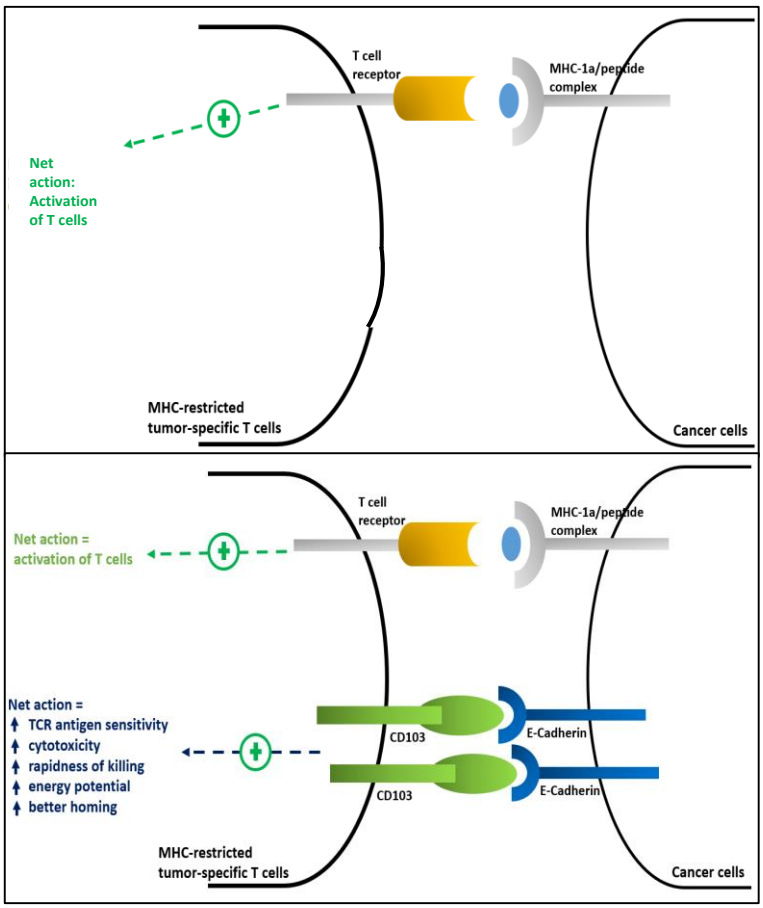


Figure 4.24 Effects of CD103 on CTLs functions. TCR interaction with MHC/peptide complex enables net activation of classical MHC-restricted tumor-specific T cells. However, it remains unclear whether the presence of CD103 on classical MHC-restricted tumor-specific T cells will have any effects on T cells activation, functions and activities.

It is well established that DCs, and most likely Tregs, are the main players in producing TGF-β1 for inducing CD103 expression on developing CTLs (Enamorado et al., 2017; Graham et al., 2014; Yu et al., 2013). Both TGF-β1 and an initial antigen exposure are required to induce a CD103 tissue residential T cell signature (Ling et al., 2007; Pallett et al., 2017). Surprisingly, we found that matured $CD103^+$ cancer-specific CTLs, but not $CD103^-$ CTLs, can self-produce activated TGF-β1 to continually sustain prolonged CD103 expression, without needing to rely on other external TGF-β1-producing cells. The self- maintenance of CD103 indicates a possibly unique subset of cancer-specific T cells that could be present in the tumor microenvironment with unique and effective anti-tumor immune properties. However, the frequency of this CD103/TGF-β1 self-regulatory cytotoxic T cell population and its importance, especially during cancer growth, merits further investigation.

Our *in vitro* data showed that $CD103^+$ cancer-specific CTLs have higher energy potential compared to the $CD103^-$ CTLs. However, in the tumor microenvironment, enhanced glucose consumption by cancer cells can deprive TILs of the glucose needed for proper $CD103^+$ CTL functions (Chang et al., 2015). This suggests that $CD103^+$ CTLs need to be able to utilise different metabolites to meet its high energy demand. Previous work by Kupper and colleagues in 2017 has highlighted the capacity of virus-specific Trm cells to take up exogenous free fatty acids (FFA) and this accounts for the long-term survival of T cells, and further help in mediating protective immunity in virus-infected tissues (Pan et al., 2017). Considering this, it merits further investigation whether $CD103^+$ cancer-specific CTLs could metabolise non-glucose metabolites to supply is energy demand. It is also worth to assess how the multiplicity in Trm cells metabolism capacity could impact their anti-tumor effector functions and survival, especially in the glucose-deprived tumor microenvironment.

It is well-established that human cancer-specific T cells have low affinity TCRs and, therefore, have less efficient TCR-mediated activating signaling (Thomas et al., 2011). As CD103 is known to accumulate in the immunological synapse (Le Floc'h et al., 2011), it is likely that the increasing CD103 and E-Cadherin interaction could strengthen the affinity of TCR binding and, therefore, increasing the sensitive engagement with the tumor antigen/MHC complex on cancer cells. We demonstrated that in the presence of the CD103 and E-Cadherin interaction, the $CD103^+$ CTLs have improved and efficient TCR-mediated effector responses and cytotoxicity. In addition to improving TCR sensitivity, it is also likely that CD103 could assist in improving TCR-mediated signaling. Previous work has highlighted that CD103 could enhance the phosphorylation of two key downstream proteins of TCR signaling, particularly ERK1/2 and PLCγ1 (Le Floc'h et al., 2011). Therefore, the specific mechanisms of CD103 molecule in mediating TCR downstream signaling necessitates further investigation.

Coexpression of CD103 and CD39 has been demonstrated to mark 'tumor-reactive' TILs (Duhen et al., 2018). A recent study also indicated that immune functionality of TILs in tumor tissue could be regulated by a competition between anti-tumoral CD103-mediated Trm activity and the pro-tumoral exhaustion activity (O'Brien et al., 2019). Here, we demonstrated varying subpopulations of $CD103^+$ TILs that are present in the tumor microenvironment. More importantly, only the $CD39^{high}$ $CD103^+$ TILs subpopulation co-expressed multiple inhibitory receptors. In addition, our data also showed that prolonged exposure of $CD103^+$ CTLs to cancer can result in more T cell apoptosis. It is, therefore, not surprising that the overall frequency of $CD103^+$ TILs population diminishes as tumor size progresses, as shown in **Chapter 3**. As the $CD103^+$ $CD39^{high}$ TILs are likely more dysfunctional and exhausted, the $CD103^+$ $CD39^{low}$ TILs

subpopulation as an alternative tumor-reactive subpopulation could be a critical Trm population that can be improved and targeted using novel tissue-localised immunotherapy strategies.

In summary, our data shed the light on the working and characteristics of $CD103^+$ cancer-specific CTLs, which could provide significant insights for future design of novel tissue-localised anti-tumor T cell immunotherapies.

Chapter 5: Defective IFNγ production by cancer-specific CTLs is contributed by CpG hypermethylation of the IFNγ promoter

5.1 Introduction

Antigen-specific immunity drives the production of IFNγ (a type II interferon) by CTLs and help to control virus infection and cancer (Gordon-Alonso et al., 2017; Trilling et al., 2009). IFNγ expression is commonly used as a functional surrogate for CTLs. The current common methods to detect human antigen-specific T cells are often based on IFNγ production upon antigen stimulation, such as enzyme-linked immunosorbent assay (ELISpot) and intracellular cytokine assay (ICS) (Feske et al., 2008; Sargentini et al., 2009; Shen et al., 2017).

IFNγ expression in T cells is driven by T cell receptor (TCR)-mediated downstream signaling, particularly the NF-κB pathway (Corn et al., 2003). NF-κB signaling phosphorylates and activates several transcription factors, including cAMP response element binding protein (CREB), activating transcription factor (ATF) and activator protein-1 (AP-1). These transcription factors translocate into the nucleus upon activation and bind upstream of the IFNγ promoter to initiate mRNA transcription (Samten et al., 2008; White et al., 2002).

Cytosine methylation at position 5 of its pyrimidine ring (5'methylcytosine) is the most abundant DNA modification in the genome. CpG methylation at gene promoters can stably silence the genes by preventing transcription factor accessibility and protein biosynthesis (Moore et al., 2013). Many important genes involved in immunity are regulated by CpG methylation. For instance, the IFNγ promoter is demethylated and expressed in Th1-differentiated $CD4^+$ T cells but not in naïve $CD4^+$ T cells and Th2-differentiated T cells. It is

also likely that methylation can potentially influence the memory $CD8^+$ T cells epigenetics (Komori et al., 2015; Northrop et al., 2006).

Cancer can employ diverse mechanisms to induce T cell exhaustion and escape anti-tumor T cell immunity, including by downregulating the MHC Class Ia surface expression on cancer cells and by dysregulating inhibitory receptors expression, such as PD-1 on TILs (Ahmadzadeh et al., 2009; Koopman et al., 2000; Leone et al., 2013). In addition, epigenetic mechanisms that dysregulate cytokine expression have been suggested to be another manifestation of T cell exhaustion (Pauken et al., 2016; Qiu et al., 2019; Youngblood et al., 2017). Previous studies have shown that fewer memory and effector $CD4^+$ and $CD8^+$ T cells from peripheral blood of cancer patients can produce IFNγ in contrast to healthy individuals. Whereas, IFNγ-deficient mice has demonstrated reduced migration of activated T cells to tumor sites and enhanced tumor progression compared to wild-type mice (Nakajima et al., 2001; Sheng et al., 2017). These observations therefore highlight the importance of IFNγ in mediating anti-tumor T cell responses. However, it still remains unclear if matured cancer-specific CTLs can have deficient IFNγ responses and what actually contributed to the deficiency.

In this chapter, we addressed the IFNγ-mediated responses of cancer-specific CTLs. Specifically, we investigated the possibility of IFNγ deficiency in cancer-specific CTLs, the cause of the deficiency and how it might affect the transcription, protein production and T cell cytotoxicity.

5.2 Results

5.2.1 Several cancer-specific CTL clones have reduced IFNγ expression and impaired cytotoxicity

To evaluate IFNγ expression in tumor-specific CTLs, we initially sorted and clonally expanded HLA-A2-restricted SSX-2-specific CTL clones from a gastric cancer patient. Upon co-culture with peptide-loaded HLA-A2-matched B cell lymphoblastoid (BCL), we observed reduced IFNγ expression on four out of six clones ($IFN\gamma^-$ clones: Clone 6, 14, 22 and 41), whereas the other two displayed high IFNγ expression ($IFN\gamma^+$ clones: Clone 17 and 29) **(Figure 5.1A and B).** However, the $IFN\gamma^-$ and $IFN\gamma^+$ clones maintained similarly high expression of TNFα **(Figure 5.1A and B).** We further confirmed that the $IFN\gamma^-$ T cell clones can secrete TNFα but not IFNγ, even upon activation with very strong antigen stimulation of 10μg/ml **(Figure 5.1C).**

We hypothesized that the $IFN\gamma^-$ T cell clones have altered cytotoxic activity. Indeed, we observed a significantly reduced frequency of BCL death following co-culture with the $IFN\gamma^-$ T cell clones compared to the $IFN\gamma^+$ T cell clones **(Figure 5.2)**. This therefore indicates that the $IFN\gamma^-$ T cell clones have reduced cytotoxic responses. As each T cell clone has the same T cell receptor (TCR) and the same late stage effector memory differentiation phenotype *in vitro* **(Table 5.1 and Figure 5.3),** these data therefore suggest that the reduced cytotoxic responses of $IFN\gamma^-$ T cell clones are not due to confounding factors such as different T cell receptor (TCR) affinity. We infer that the defective IFNγ-mediated T cell responses of $IFN\gamma^-$ T cell clones underlie their reduced cytotoxic response.

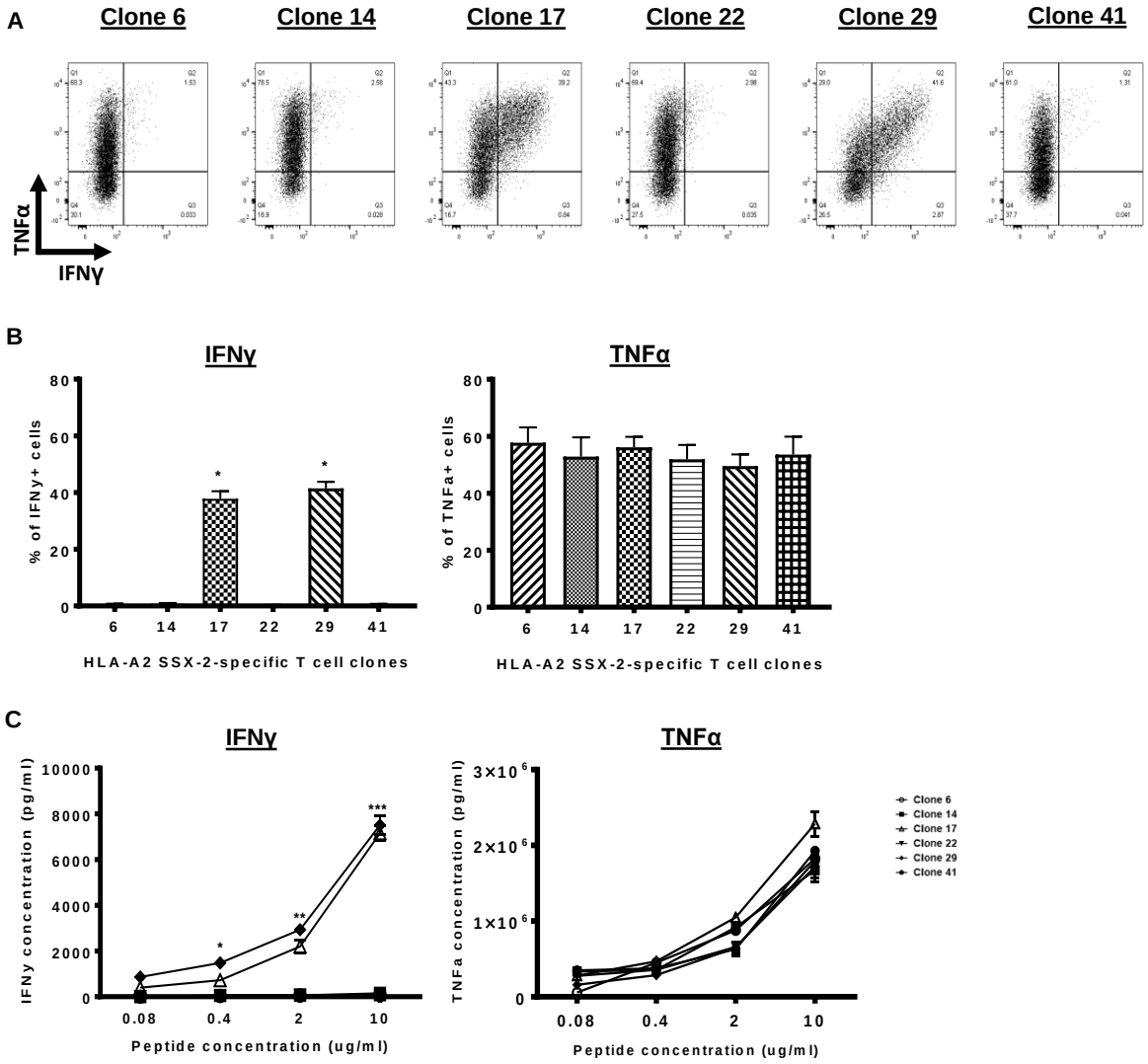


Figure 5.1 A high frequency of tumor-specific CD8$^+$ T cell clones do not express or secrete IFNγ. (A) Flow cytometry dot plots of six SSX-2-specific T cell clones. IFNγ is not expressed in 4 clones (IFNγ$^-$ clones: Clone 6, 14, 22, 41) and is expressed in 2 clones (IFNγ$^+$ clones: Clone 17, 29). All six clones express TNFα. (B) Proportion of IFNγ$^+$ cells *(left)* or TNFα$^+$ cells *(right)* for each T cell clone, after co-culture with peptide-stimulated BCL. (C) Level of IFNγ production *(left)* or TNFα production *(right)* by each T cell clone, after co-culture with peptide-stimulated BCL. (N, number of experimental repeats= 3. * represents P-value < than 0.05, ** represents P-value < than 0.01, *** represents P-value < than 0.001, analysis performed with one-way ANOVA with Tukey's multiple comparison test.

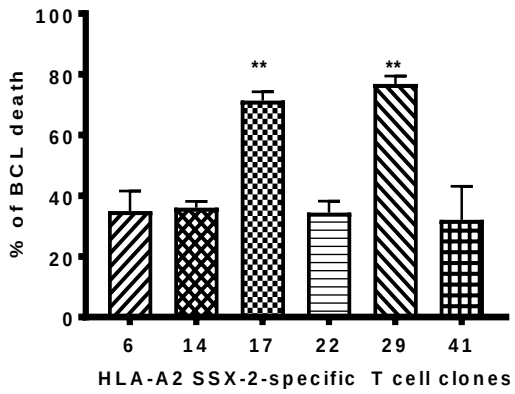


Figure 5.2 The IFNγ-negative T cell clones have reduced cytotoxicity. Proportion of BCL cell death following antigen stimulation at 1μg/ml and co-culture with each T cell clone. N, number of experimental repeats= 3. * represents P-value < than 0.05, ** represents P-value < than 0.01, *** represents P-value < than 0.001, analysis performed with one-way ANOVA with Tukey's multiple comparison test.

Table 5.1. The T cell receptor sequence of SSX-2-specific T cell clones.

SSX-2-specific clone ID	TCRα	TCRβ
Clone 6	TRAV-8-6 TRAJ 30	TRBV 6-1 TRBJ2-7
Clone 14	TRAV 8-6 TRAJ 30	TRBV 6-1 TRBJ 2-7
Clone 17	TRAV 8-6 TRAJ 30	TRBV 6-1 TRBJ 2-7
Clone 22	TRAV 8-6 TRAJ 30	TRBV 6-1 TRBJ 2-7
Clone 29	TRAV 8-6 TRAJ 30	TRBV 6-1 TRBJ 2-7
Clone 41	TRAV 8-6 TRAJ 30	TRBV 6-1 TRBJ 2-7

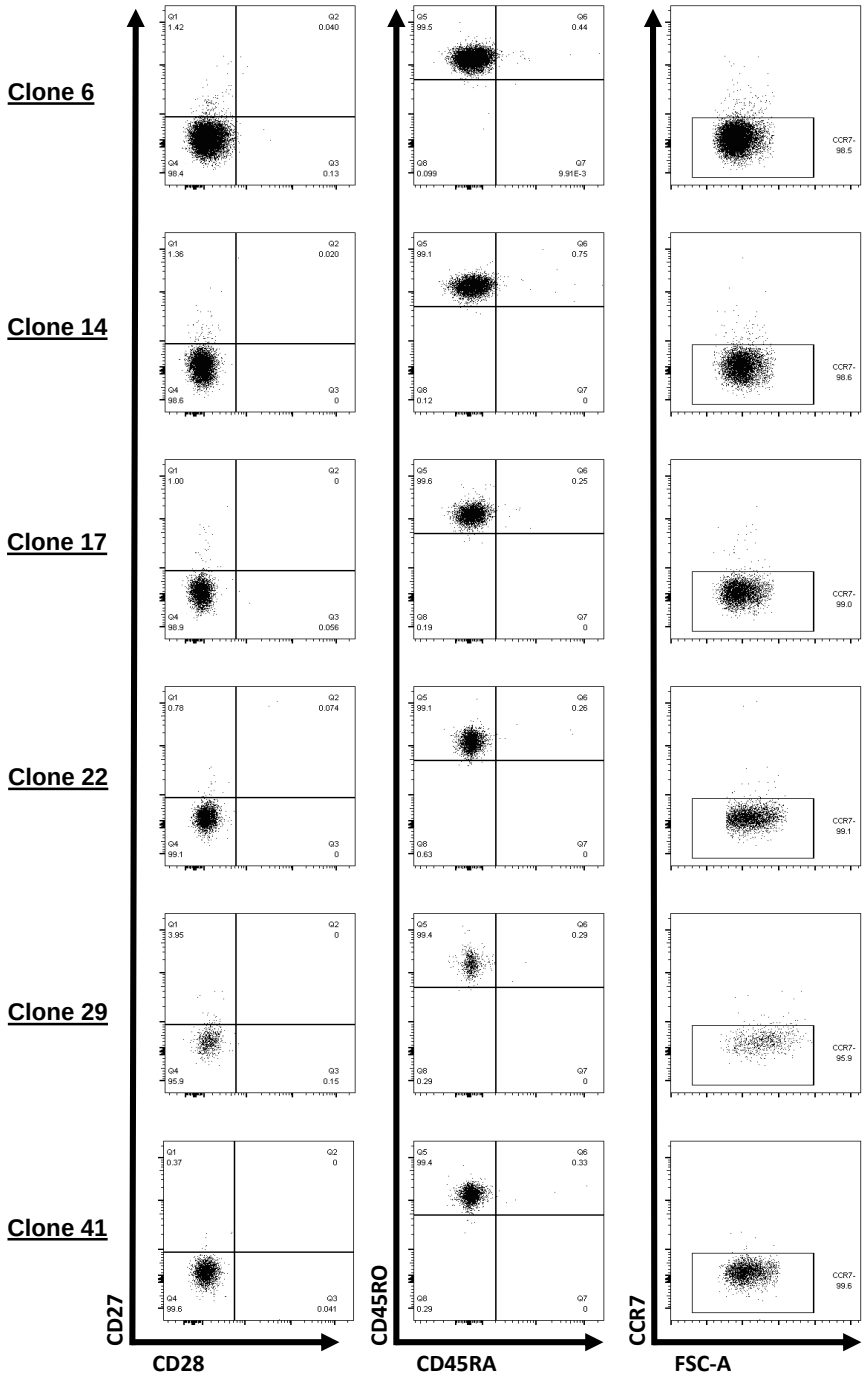


Figure 5.3 Differentiation immune expression of SSX-2-specific T cell clones. Representative dot plots showing that all six T cell clones have surface expression of CD45RO, but lack CD45RA, CCR7, CD27 and CD28 expression i*n vitro*.

5.2.2 CpG hypermethylation of the IFNγ promoter contributes to the IFNγ defect

The CpG at positions -186 and -54 within the IFNγ promoter, mapped to the transcription factor binding sites, are vital for IFNγ transcription (Samten et al., 2008; White et al., 2002). We thus assessed if the lack of IFNγ expression in IFNγ$^-$ T cell clones correlate with the methylation of CpGs at these specific sites and adjacent CpGs within the promoter **(Table 5.2)**.

To this end, we analysed the IFNγ promoter from the genomic DNA (gDNA) of each T cell clone, using bisulphite sequencing. The running of sequencing on AB-3730 capillary electrophoresis instrument was carried out by Timothy Rostron and John Frankland.

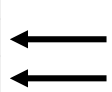
It was found that all the IFNγ$^-$ T cell clones were heavily methylated at positions -54 and -186, whereas the IFNγ$^+$ T cell clones were unmethylated at these positions **(Figure 5.4A)**. Adjacent CpGs were also methylated in the IFNγ$^-$ clones, including at position -295 (IFNγ$^-$ clones: 14, 22 and 41), position +122 (IFNγ$^-$ clones: 6, 22 and 41) and position +128 (IFNγ$^-$ clones: 22 and 41), whereas all three of these positions are unmethylated in the IFNγ$^+$ clones **(Figure 5.4B)**. The number of methylated CpGs were inversely correlated with the frequency of IFNγ$^+$ cells **(Figure 5.5)**. These data suggest that CpG hypermethylation within the IFNγ promoter can repress the IFNγ expression in cancer-specific CTLs.

5.2.3 The IFNγ defect is unique to cancer-specific CTLs

We extended and confirmed these findings in *ex vivo* isolated, short-term bulk expanded, HLA-A2-restricted SSX-2-specific or NY-ESO-1-specific CTLs, as well as HLA-A2-restricted CMV-specific and Influenza-specific CTLs, derived from seven different cancer patients.

Table 5.2 CpG locations within IFNγ promoter sequence

CpG position	Location	Gene sequence
1	-295	GGC**CG**AAG
2	-186	CAT**CG**TCA
3	-54	ATA**CG**TAA
4	+122	TCT**CG**GAA
5	+128	AAA**CG**ATG
6	+171	CAT**CG**TTT



Reside in transcription factor binding site

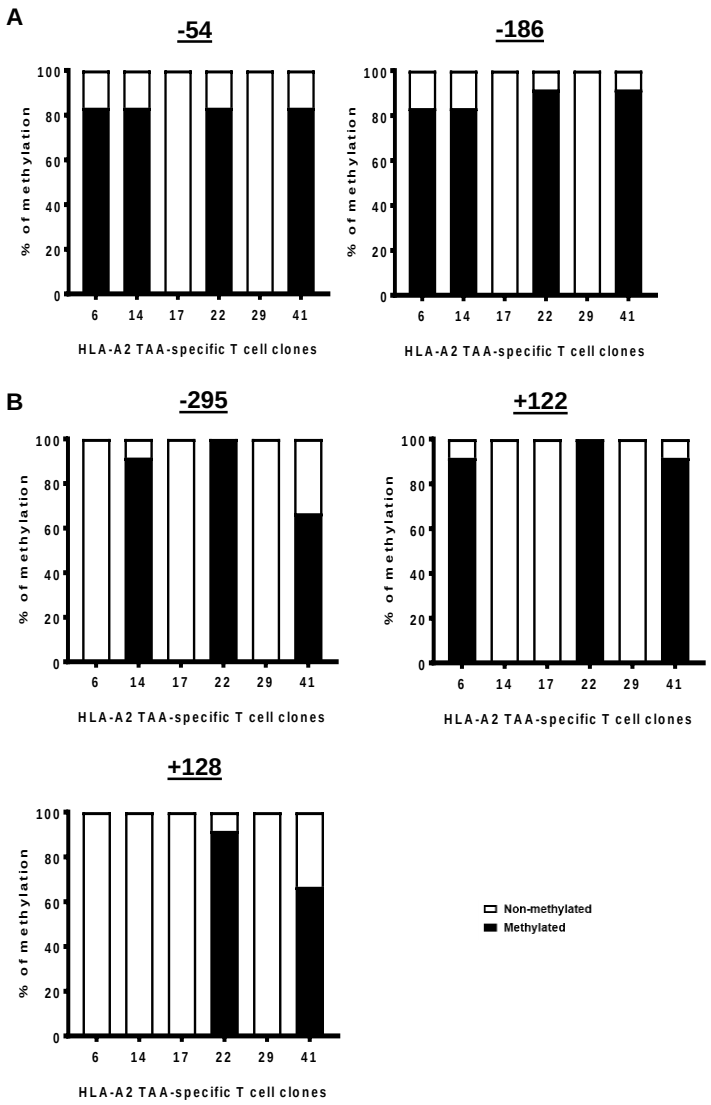


Figure 5.4 IFNγ⁻ T cell clones have CpG methylation in the IFNγ promoter. Proportion of DNA sequences that have CpG methylation, at position -51 and -186 (A) as well as at position -295, +122 and +128 (B).

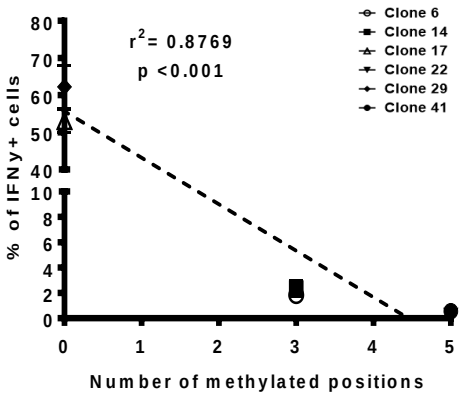


Figure 5.5 Correlation of IFNγ expression by different T cell clones with CpG methylation in the IFNγ promoter. The number of methylated sites within the IFNγ promoter correlates with the proportion of IFNγ$^-$ cells for each T cell clone. N, number of experimental repeats= 3, * represents P-value < than 0.05, ** represents P-value < than 0.01, *** represents P-value < than 0.001, analysis performed with non-parametric Spearman correlation test.

Intriguingly, 10-40% of the cancer-specific CTLs (both SSX-2-specific and NY-ESO-1-specific) displayed CpG methylation at positions -186 and -54 within their IFNγ promoter **(Figure 5.6)**. We further performed the same analysis with virus-specific CTLs and found that the CpGs at positions -186 and -54 were completely unmethylated in influenza-specific and CMV-specific CTLs **(Figure 5.6)**. Taken altogether, these observations suggest that cancer-specific CTLs can acquire CpG hypermethylation on its IFNγ promoter. The frequency of IFNγ promoter-methylated CTLs was inversely correlated with the activation-induced IFNγ expression (**Figure 5.7A**) and production (**Figure 5.7B**). Most importantly, the cytotoxic killing following co-culture with peptide-stimulated HCT116 were also negatively affected **(Figure 6.7C)**. Altogether, these observations suggest that CpG hypermethylation coincident with the lack of IFNγ synthesis.

5.2.4 CpG hypermethylation is associated with reduced IFNγ transcription

Transcription factor accessibility to the binding sites within the IFNγ promoter is vital for IFNγ transcription (Samten et al., 2008; White et al., 2002). To assess the kinetics of IFNγ transcript and protein accumulation in response to T cells activation, we performed a PrimeFlow RNA assay followed by flow cytometry analysis on the SSX-2-specific T cell clones. $IFN\gamma^+$ clones, such as Clone 29 showed a transient increase in IFNγ mRNA levels that peaked at 1-hour post-activation that then declined **(Figure 5.8A and B).** The IFNγ protein levels simultaneously peaked and stabilised 2 hours post-activation for the $IFN\gamma^+$ T cell clones **(Figure 5.8A and C)**. In contrast, the $IFN\gamma^-$ clones, such as Clone 22, lacked any IFNγ transcript or protein expression, even at three hours post-activation **(Figure 5.8A to C).**

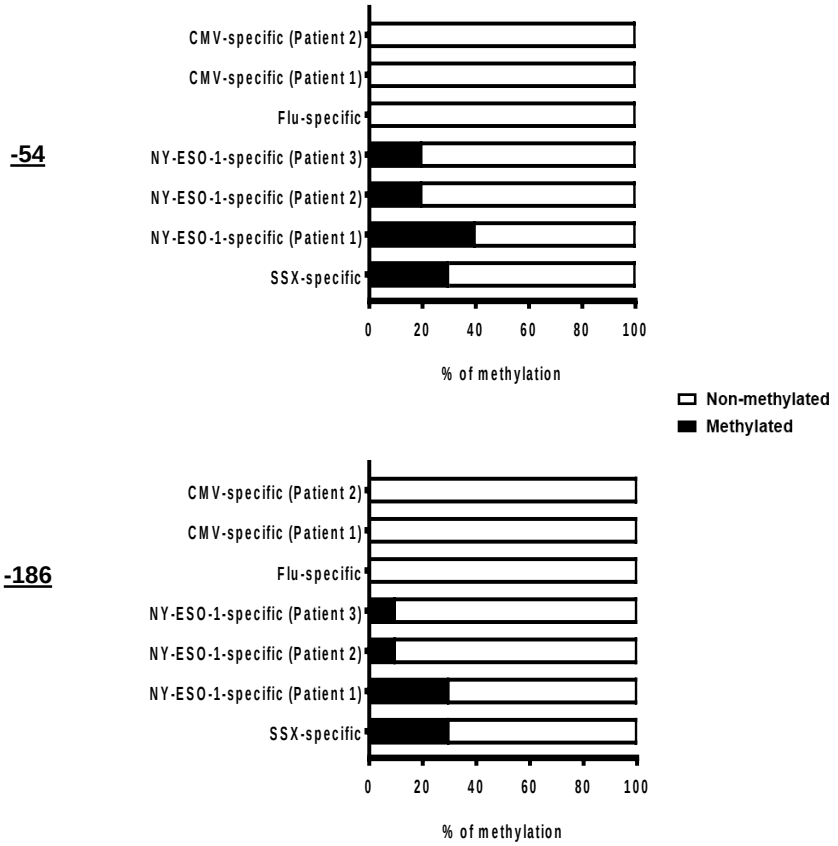


Figure 5.6 IFNγ methylation, in short-term expanded bulk antigen-specific CTLs. Proportion of cells with methylation at position -186 and -54 for each group of antigen-specific T cells (Influenza-specific T cells, CMV-specific T cells, SSX-2-specific T cells and NY-ESO-1-specific T cells derived from different patients).

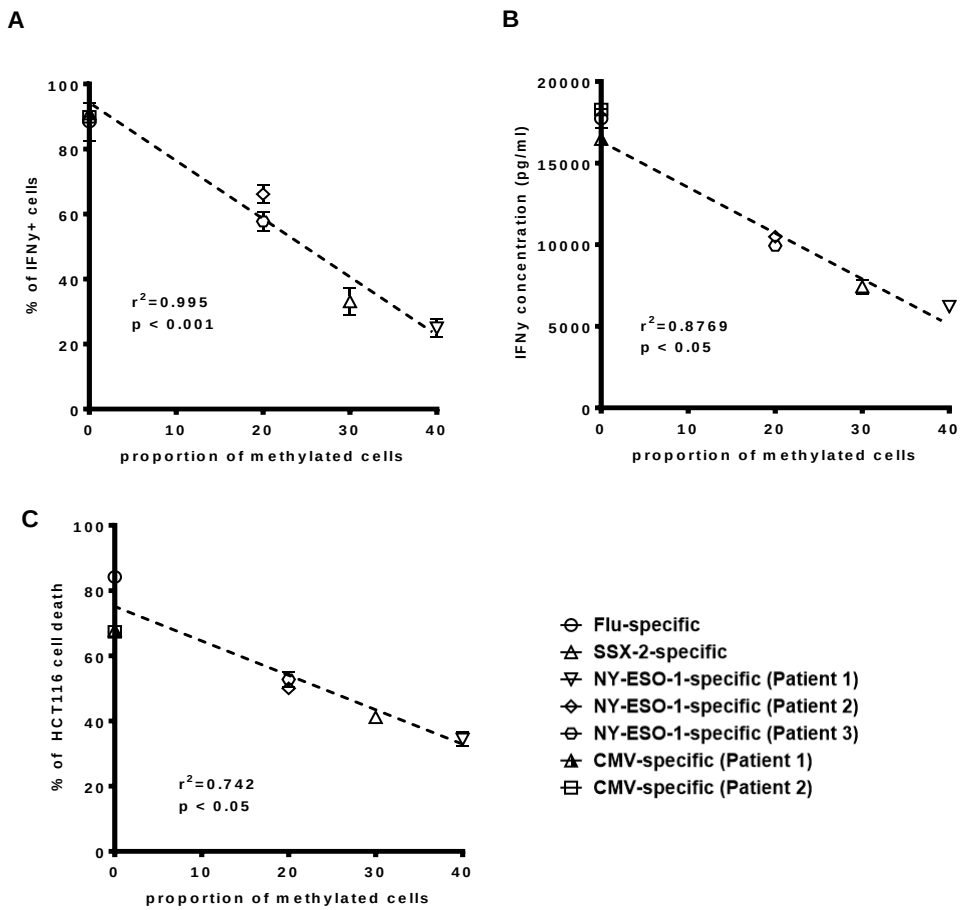


Figure 5.7 IFNγ methylation, and correlation to IFNγ production and T cell cytotoxicity of short-term expanded bulk antigen-specific CTLs. The proportion of cells with a hypermethylated IFNγ promoter inversely correlates with the proportion of IFNγ mRNA^{+} cells (A) and IFNγ protein production (B) expressed for each antigen-specific T cells type. (C) The proportion of cells with a hypermethylated IFNγ promoter inversely correlates with HCT116 cancer cell death induced by antigen-specific T cells at 1μg/ml antigen stimulation. N, number of experimental repeats= 3, * represents P-value < than 0.05, ** represents P-value < than 0.01, *** represents P-value < than 0.001, analysis performed with non-parametric Spearman correlation test.

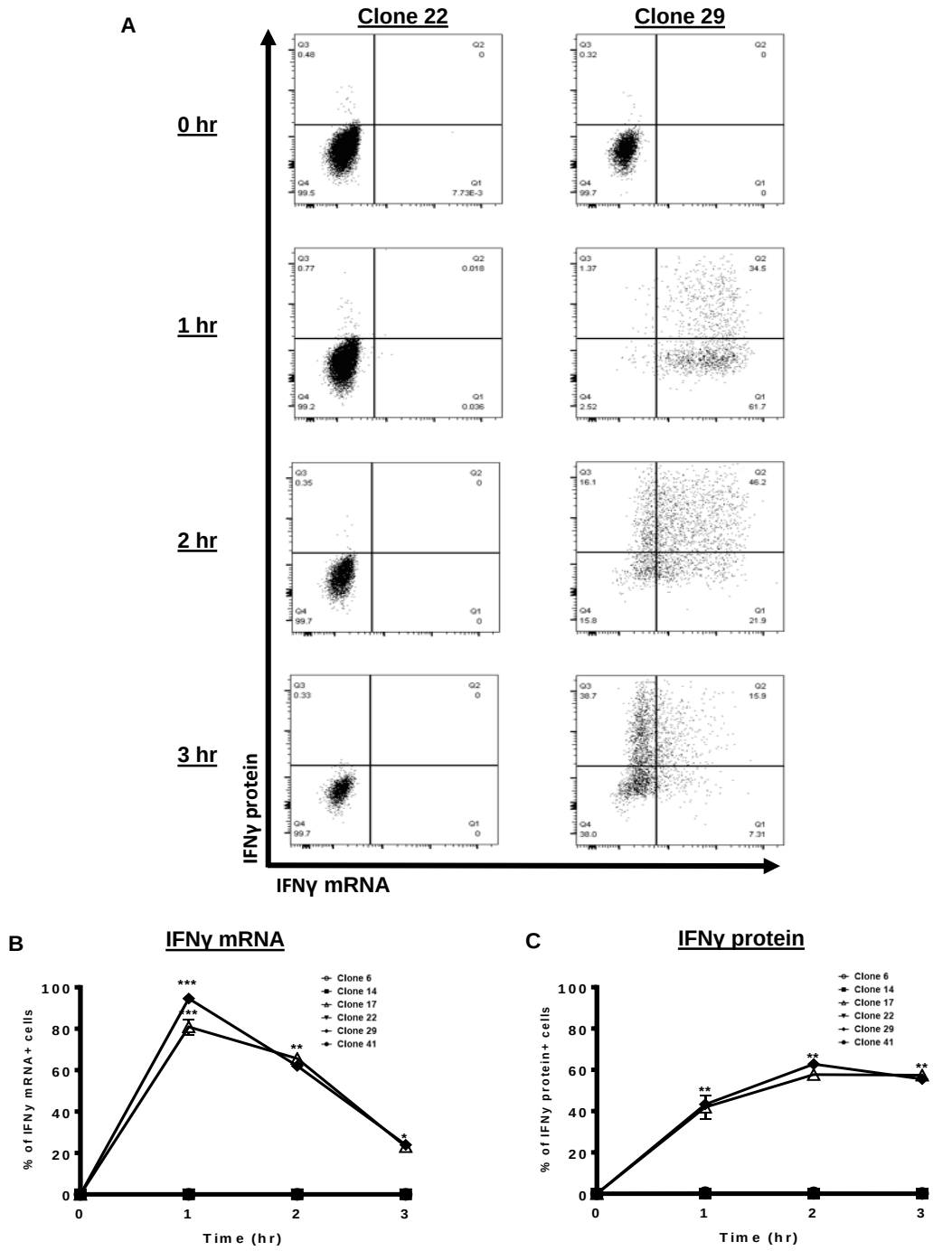


Figure 5.8 IFNγ kinetics of SSX-2-specific T cell clones. (A) Flow cytometry dot plots of IFNγ mRNA and protein levels following co-culture with CD3/CD28 activator antibody at the indicated time points. Proportion of cells with IFNγ mRNA (B) and protein (C) following co-culture with CD3/CD28 activator antibody at the indicated time points. N, number of experimental repeats= 3, * represents P-value < than 0.05, ** represents P-value < than 0.01, *** represents P-value < than 0.001, analysis performed with two-way ANOVA with Tukey's multiple comparison.

To validate that the deficiency in IFNγ synthesis is driven largely by the CpG hypermethylation of the IFNγ promoter and not a general T cell defect, we used the same approach to assess the TNFα kinetics for each T cell clone. All the $IFN\gamma^+$ and $IFN\gamma^-$ T cell clones showed strong and simultaneous induction of TNFα mRNA and protein, starting at 1-hour post-activation **(Figure 5.9A to C)**. Importantly, all T cell clones maintained high levels of TNFα protein at three hours post-activation. Therefore, the $IFN\gamma^-$ T cell clones likely have intact processing of TNFα, suggesting that the IFNγ defect is specific for IFNγ regulation.

To further confirm that the IFNγ defect is unique to cancer-specific CTLs, we thus assessed and compare the IFNγ transcription kinetics in the *ex vivo* isolated short-term expanded cancer-specific and virus-specific CTLs. Compared to the influenza-specific and CMV-specific CTLs, the cancer-specific CTLs showed significantly reduced IFNγ mRNA expression throughout the time course **(Figure 5.10)**. The IFNγ transcript peaked at 1-hour post-activation and then declined for all of the CTLs **(Figure 5.10)**, therefore indicating that the mRNA expression of IFNγ is diminished in cancer-specific CTLs, not delayed.

5.3 Discussion

This chapter showed that a substantial fraction of cancer-specific CTLs have a compromised IFNγ response and a hypermethylated IFNγ promoter, especially at the CpG positions within the transcription factor binding sites. Importantly, the frequency of cells with a hypermethylated IFNγ promoter correlates with the impaired IFNγ transcript, IFNγ production and CTL cytotoxic responses upon T cell activation. This would be predicted to compromise the overall anti-tumor effect of cancer-specific CTLs.

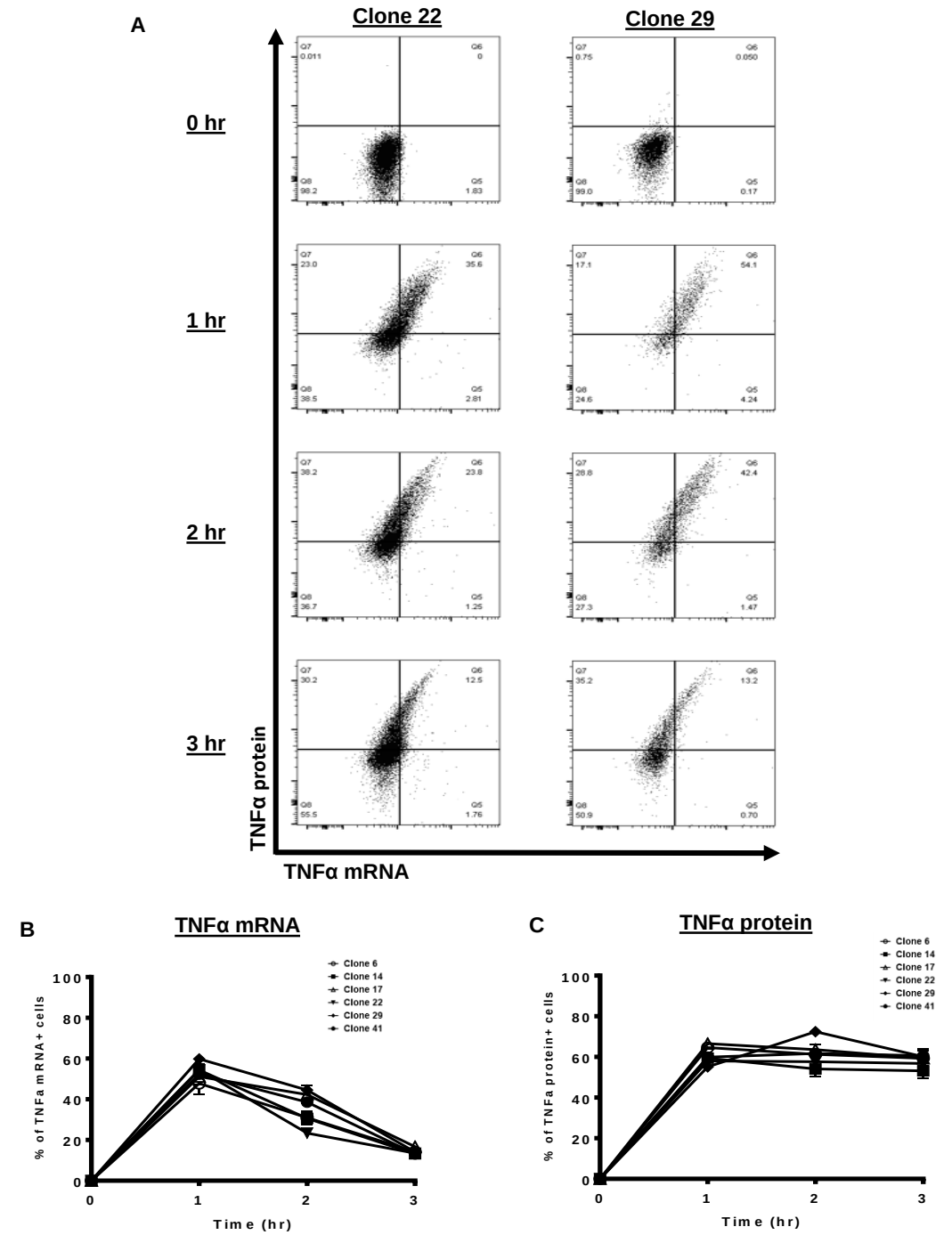


Figure 5.9 TNFα kinetics of SSX-2-specific T cell clones. (A) Histogram plots of TNFα mRNA and protein levels following co-culture with CD3/CD28 activator antibody at the indicated time points. Proportion of cells with TNFα mRNA (B) and protein (C) following co-culture with CD3/CD28 activator antibody at the indicated time points N, number of experimental repeats= 3, * represents P-value < than 0.05, ** represents P-value < than 0.01, *** represents P-value < than 0.001, analysis performed with two-way ANOVA with Tukey's multiple comparison.

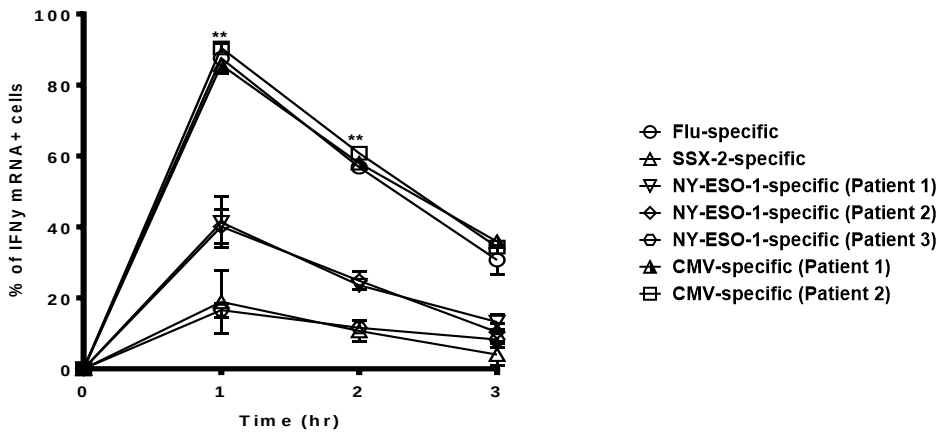


Figure 5.10 IFNγ kinetics comparison between short-term expanded bulk antigen-specific CTLs. IFNγ mRNA level of each antigen-specific T cell type (Influenza-specific T cells, CMV-specific T cells, SSX-2-specific T cells and NY-ESO-1-specific T cells derived from different patients) following treatment with CD3/CD28 activator antibody for 0,1,2 and 3 hours. N, number of experimental repeats= 3, * represents P-value < than 0.05, ** represents P-value < than 0.01, *** represents P-value < than 0.001, analysis performed with two-way ANOVA with Tukey's multiple comparison.

DNA methylation is a key epigenetic regulator of cellular functions. Although cancer cells themselves are known to hyper-methylate their own IFNγ promoter and thus promote tumorigenesis (Ma et al., 2014), it was not known whether this gene is dysregulated in cancer-specific CTLs. We showed that a sizeable portion of human cancer-specific CTLs is dysregulated by CpG hypermethylation of the IFNγ promoter. This can compromise mRNA transcription and in turn, the protein synthesis of IFNγ. Hypermethylation might be driven by the methyl-CpG binding proteins, such as DNA methyltransferases and enhancer of zester homolog 2 (EZH2), known to be upregulated in TILs as well as in cancer cells themselves (Balkhi et al., 2018; Feinberg et al., 2016). How a large fraction of cancer-specific CTLs acquired this CpG hypermethylation of their IFNγ promoter merits further investigation.

Currently, methods to detect and identify human antigen-specific CTLs primarily rely on IFNγ expression and production following stimulation, such as by using ELISpot and ICS (Feske et al., 2008; Sargentini et al., 2009; Shen et al., 2017). This demonstrates that a significant fraction of cancer-specific CTLs have CpG hypermethylation at the IFNγ promoter and are indeed IFNγ-deficient. Thus, identifying cancer-specific CTLs solely using IFNγ-based techniques might overlook a large fraction of antigen-specific T cells and could generate unexpected biases in analyses, especially during *ex vivo* evaluation of anti-tumor responses from TILs. Methods to detect multiple cytokines, such as TNFα, should be considered when assessing the presence of cancer-specific TILs and their response in cancer patients. As these observations clearly provide evidence of IFNγ defects in cancer-specific CTLs and its negative influence on the cytotoxic and effector responses, further studies should be conducted with larger sample sizes and in different cancer types to decipher the prevalence of IFNγ-deficient cancer-specific CTLs and their relevance to tumor progression and treatment outcome.

Chapter 6: Summary and Future Directions

One of the most significant discoveries in the field of cancer immunotherapy is the upregulation of inhibitory receptors such as CTLA-4 and PD-1 on TILs. Existing checkpoint blockade monotherapies such as anti-PD-1 (pembrolizumab) have shown significant improvement in tumor control and patients' survival (Hamid et al., 2013; Powles et al., 2014; Topalian et al., 2012; Tumeh et al., 2014). However, current immunotherapies have been unable to promote recovery in some patients and cancer types. The variability in response to present immunotherapy treatments is likely due to the heterogeneity of the tumor immune composition and their overall complex immunophenotype. Furthermore, the immunosuppressive tumor microenvironment plays a significant role in mediating cancer immune evasion by dysregulating the T cell properties. Therefore, it is important to have an in-depth characterisation of the anti-tumor features and mechanisms of TILs, especially cancer-specific CTLs, in order to help develop more effective T cell immunotherapies.

Current monotherapies of checkpoint blockade have improved the responses in a majority of cancer patients. However, there is still a sizeable portion of patients who do not respond well to the monotreatment. This is possibly due to the multiple co-expression of inhibitory receptors on TILs such as PD-1 and Tim3, as shown in previous studies including a study conducted by our group (10,11, Li et al, under revision). Our current study further highlighted that all NKG2a^{+} TILs are PD-1 positive. It is therefore likely that combinatory checkpoint blockade treatment can induce better anti-tumor T cell responses and tumor control.

The use of combinatory checkpoint blockade may eliminate the overlapping inhibitory effects of different inhibitory receptors on TIL functions. Previous studies have shown that PD-1 over-expression on TILs can impair the cytokine responses, cancer cell killing and T cell proliferation, whereas Tim3 upregulation attenuates the cytokines production by TILs (Fourcade et al., 2010; Gao et al., 2012; Patsoukis et al., 2015). Our current study further demonstrated an enrichment of CD94/NKG2a on TILs, in which the presence of NKG2a on cancer-specific CTLs also contributed towards impaired anti-tumor T cell effector responses, cytotoxicity and IL-2-dependent proliferation. These overlapping roles by different inhibitory receptors suggest that the co-presence of other inhibitory receptors such as NKG2a and Tim3 could compensate for the loss of PD-1 inhibitory signaling by anti-PD-1 monotreatment. Anti-PD-1 targeting alone would thus might not able to completely overcome the inhibition of TIL anti-tumor functions. In considering combinatory checkpoint blockade treatment, it merits further investigation into the specific inhibitory receptor combinations that could prove more effective for the immunotherapy targets.

In our current study, we highlighted the antagonistic expression between the inhibitory NKG2a receptor and the CD103 expression on TILs. It is possible that the presence of CD103 can help to improve anti-tumor T cell effector functions. In our current study, we indeed demonstrated that $CD103^+$ cancer-specific CTLs have enhanced TCR tumor antigen sensitivity and faster cancer cell recognition and efficient killing. This may be contributed by CD103 aiding the TCR-mediated responses, as previous studies have demonstrated that CD103 is highly clustered in the immunological synapse (Le Floc'h et al., 2011; Le Floc'h et al., 2007). Furthermore, the CD103 and its ligand E-Cadherin engagement was shown to contribute to the phosphorylation of PLCγ1 and ERK downstream of the TCR (Le Floc'h et al., 2011). These

observations therefore suggest that CD103 could elevate TCR-mediated downstream signaling, which warrants future investigation into the molecular functions of CD103.

In our current study, we demonstrated that the $CD103^+$ cancer-specific CTLs can self-produce TGF-β1, which is essential for their CD103 self-maintenance capacity. TGF-β is also known to be critical for anti-tumor control especially during the early stage of cancer. TGF-β is well-established to help suppress stroma-derived tumor mitogens, and to drive the cytostasis of early stage tumors (Guasch et al., 2007; Massague, 2008; Siegel and Massague, 2003; Sun et al., 1994). It is likely that the TGF-β-producing $CD103^+$ TILs could also contribute towards the TGF-β-mediated anti-tumor suppression capacity in early stage cancer. It therefore warrants further investigation into the direct effect of TGF-β production by TGF-β^+ $CD103^+$ TILs towards anti-tumor control and possible eradication.

In addition to TGF-β, a high presence of E-Cadherin in the early stage of cancer has been defined as a tumor suppressor marker, with its loss during epithelial-to-mesenchymal transition (EMT) contributing to tumor progression and metastasis (Birchmeier and Behrens, 1994; Bruner and Derksen, 2018; Tomita et al., 2000). As CD103 and E-Cadherin interaction was found to elevate the anti-tumor functions of cancer-specific CTLs, the E-Cadherin engagement by enriched $CD103^+$ TILs present in early stage cancer could result in a more effective tumor control. In addition to normal cancer cells, certain cancer stem cells isolated from several patients exhibited and still maintained moderate levels of E-Cadherin expression (preliminary finding in collaboration with Kanellakis and Rahman). As cancer stem cells are more resistant to radiotherapy and chemotherapy (Beck and Blanpain, 2013; Biddle et al., 2016; Diehn et al., 2009; Li et al., 2008), utilising T cell cancer immunotherapies targeting $CD103^+$ TILs against E-$Cadherin^+$ cancer stem cells (in combination with conventional therapy such as

radiotherapy) might provide a new strategy towards a more effective anti-tumor T cell response and cancer eradication, especially in early stage cancer patients.

Trm cell metabolism for energy production is known to be critical for Trm effector functions and survival in tissue-localised virus infection (Pan et al., 2017). In our current study, we demonstrated that the $CD103^+$ cancer-specific CTLs have elevated energy potential *in vitro,* by utilising elevated glucose at a faster rate. However, in the tumor microenvironment, enriched glucose uptake by cancer cells is known to lead to a glucose-deprived microenvironment that can negatively affect T cell function (Chang et al., 2015). It is therefore vital for $CD103^+$ cancer-specific CTLs to be able to use other metabolites such as ketones and lipids to meet their energy demand. The capacity to metabolise lipids has previously been demonstrated in Trm cells during virus infection (Pan et al., 2017). As our current study also demonstrated that $CD103^+$ cancer-specific CTLs have greater mitochondrial capacity, it is highly likely that they could also utilise non-glucose metabolites in the tumor microenvironment. This in turn might contribute to the enhanced anti-tumor responses by $CD103^+$ cancer-specific CTLs. It therefore merits further investigation into (i) the capacity of $CD103^+$ cancer-specific CTLs to utilise a variety of metabolites, and (ii) the contribution of metabolism and high energy usage by $CD103^+$ CTLs towards elevating anti-tumor immune responses.

While the $CD103^+$ cancer-specific CTLs demonstrated elevated anti-tumor responses, they are also more susceptible to caspase-3-mediated apoptosis following prolonged cancer exposure. It is therefore not surprising to also observe that the frequency of $CD103^+$ TILs diminishes as tumor size progresses. The T cell death could be contributed, at least in part, by the enriched co-expression of multiple inhibitory receptors on $CD103^+$ TILs. Specifically, only the $CD103^+$ $CD39^{high}$ TIL subpopulation exhibited co-expression of PD-1 and Tim3. In contrast,

we found that the $CD103^+$ $CD39^{low}$ TIL subpopulation are also present in the tumor but exhibited less inhibitory receptor co-expression. As Duhen and colleagues study in 2018 has highlighted the $CD103^+$ $CD39^+$ TILs as 'tumor-reactive' (Duhen et al., 2018), it is therefore likely that the $CD103^+$ $CD39^{low}$ TILs could be a critical tumor-reactive TIL subpopulation that could be targeted for cancer immunotherapy, especially in early stage cancer patients.

Importantly, as noted in **Chapter 3,** patients with later stage of cancer and larger tumor sizes have increased frequency of $NKG2a^+$ TILs, with a decreased number of $CD103^+$ TILs. This in turn may contribute to reduced effectiveness of anti-tumor T cell responses, thus possibly leading to weakened tumor control and decreased chance of patient's survival **(Figure 6.1).**

In addition to previous studies, our current observations throughout this study on CD103, NKG2a, PD-1 and Tim3 therefore suggest that using the specific 'tumor-reactive' $CD103^+$ $CD39^+$ TIL subpopulation, in possible combination with (i) combinatory immune checkpoint blockade, and (ii) conventional cancer therapies such as radiotherapy, may provide a more comprehensive and novel strategy to boost anti-tumor T cell responses and early stage cancer eradication.

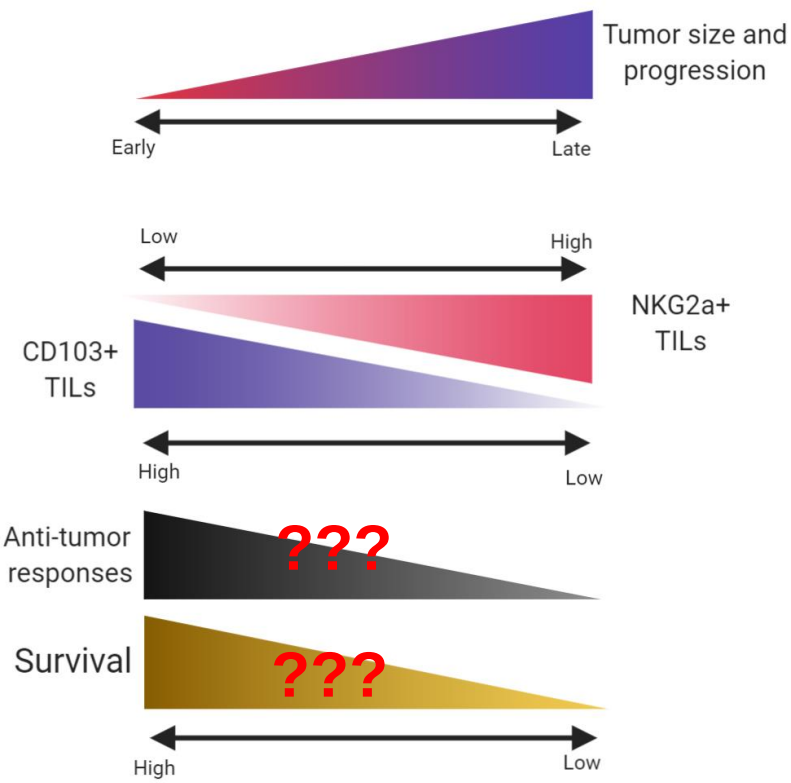


Figure 6.1 As tumor progresses, the frequency of NNKG2a+ TILs increased while the CD103+ TILs decreased. The reduced in highly efficient 'tumor-reactive' CD103+ TILs and elevated inhibitory receptors-rich TILs could contribute to the overall reduced anti-tumor responses. The lack of tumor control would subsequently result n decreased chance of patients survival.

Cancer immune evasion is now well-established to be associated with the downregulation of MHC Class Ia surface expression and the upregulation of inhibitory receptors on TILs. However, another evasive mechanism that has begun to be more explored but is still less highlighted is the epigenetic dysregulation of TILs. While previous studies have shown that cancer cells themselves can methylate their IFNγ gene transcription to enhance their tumorigenesis (Cui et al., 2018; Qu et al., 2010), it was unclear whether effector responses of cancer-specific CTLs in cancer patients could also be dysregulated through a similar mechanism. In our current study, we demonstrated a sizeable portion of cancer-specific CTLs in different cancer patients having enriched CpG hypermethylation, specifically on the IFNγ gene promoter sequence. This hypermethylation contributed to an impaired IFNγ transcription and production by the cancer-specific CTLs.

In healthy condition, the presence of methyl-CpG binding proteins such as DNA methyltransferases 3a (DNMT3a) is well-established to regulate the methylation level of both IL-4 and IFNγ loci in murine T cells (Gamper et al., 2009). However, the high presence of cancer-specific CTLs with hypermethylated IFNγ promoter suggests that the methylation process in cancer-specific T cells could be dysregulated. In melanoma cancer patients, the enhancer of zeste homolog 2 (EZH2) histone methyltransferase was found to be highly upregulated on overall TILs, in parallel to the PD-1 overexpression (Balkhi et al., 2018). It therefore merits further investigation on whether the methyltransferases are dysregulated in cancer-specific CTLs, and the possible contribution of inhibitory receptor signaling and overexpression on the dysregulation of methyl-CpG binding proteins.

The accessibility to the gene's promoter is vital for the ability of T cells to induce effective anti-tumor effector responses. Particularly in cancer, there could be other epigenetic

mechanisms that could be dysregulated and contributing to the inhibition of IFNγ responses, such as histone modification. In certain cancers, the whole IFNγ gene was demonstrated to be deacetylated, which prevented transcription factors accessibility to the gene promoter (Martini et al., 2010; Podlaha et al., 2014). It has also been highlighted that the tumor microenvironment can promote this histone modification to prevent different anti-tumor genes from being activated (Weissmann et al., 2018). However, it remains unclear if impaired IFNγ responses by cancer-specific CTLs also be contributed by histone modification dysregulation.

In conclusion, our whole study provided some insights into the factors that can negatively or positively affect anti-tumor T cell responses. This includes the (i) role of inhibitory NKG2a, and (ii) stimulatory CD103 on cancer-specific T cell functions, as well as, (iii) the contribution of epigenetic dysregulation on the functionality of cancer-specific CTLs **(Figure 6.2)**. These findings provide a fundamental foundation from which future research could and need to be undertaken to have a complete understanding of the anti-tumor T cell immunity. This may provide meaningful insights into designing more effective T cell-mediated cancer immunotherapy strategies.

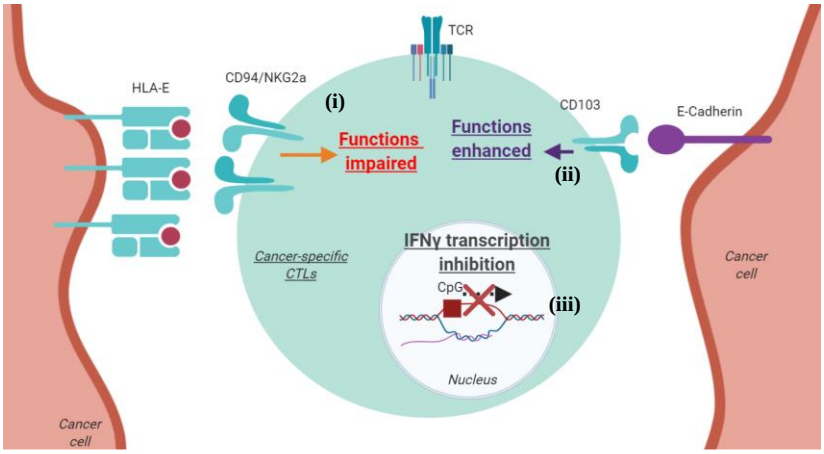


Figure 6.2 General summary of the study. (i) Enriched HLA-E and CD94/NKG2a interaction leads to impaired functions of cancer-specific CTLs. **(ii)** Presence of CD103 and its interaction with E-Cadherin boost anti-tumor responses of cancer-specific CTLs. **(iii)** The presence of CpG hypermethylation in the IFNγ promoter sequence impairs IFNγ responses.

References

Acuto, O., S.C. Meuer, J.C. Hodgdon, S.F. Schlossman, and E.L. Reinherz. 1983. Peptide variability exists within alpha and beta subunits of the T cell receptor for antigen. *J Exp Med* 158:1368-1373.

Adams, O., K. Besken, C. Oberdorfer, C.R. MacKenzie, D. Russing, and W. Daubener. 2004. Inhibition of human herpes simplex virus type 2 by interferon gamma and tumor necrosis factor alpha is mediated by indoleamine 2,3-dioxygenase. *Microbes Infect* 6:806-812.

Agata, Y., A. Kawasaki, H. Nishimura, Y. Ishida, T. Tsubata, H. Yagita, and T. Honjo. 1996. Expression of the PD-1 antigen on the surface of stimulated mouse T and B lymphocytes. *Int Immunol* 8:765-772.

Ahmadzadeh, M., L.A. Johnson, B. Heemskerk, J.R. Wunderlich, M.E. Dudley, D.E. White, and S.A. Rosenberg. 2009. Tumor antigen-specific CD8 T cells infiltrating the tumor express high levels of PD-1 and are functionally impaired. *Blood* 114:1537-1544.

Albert, M.L., B. Sauter, and N. Bhardwaj. 1998. Dendritic cells acquire antigen from apoptotic cells and induce class I-restricted CTLs. *Nature* 392:86-89.

Aleksic, M., N. Liddy, P.E. Molloy, N. Pumphrey, A. Vuidepot, K.M. Chang, and B.K. Jakobsen. 2012. Different affinity windows for virus and cancer-specific T-cell receptors: implications for therapeutic strategies. *Eur J Immunol* 42:3174-3179.

Allan, R.S., J. Waithman, S. Bedoui, C.M. Jones, J.A. Villadangos, Y. Zhan, A.M. Lew, K. Shortman, W.R. Heath, and F.R. Carbone. 2006. Migratory dendritic cells transfer antigen to a lymph node-resident dendritic cell population for efficient CTL priming. *Immunity* 25:153-162.

Altan-Bonnet, G., and R.N. Germain. 2005. Modeling T cell antigen discrimination based on feedback control of digital ERK responses. *PLoS Biol* 3:e356.

Andre, P., C. Denis, C. Soulas, C. Bourbon-Caillet, J. Lopez, T. Arnoux, M. Blery, C. Bonnafous, L. Gauthier, A. Morel, B. Rossi, R. Remark, V. Breso, E. Bonnet, G. Habif, S. Guia, A.I. Lalanne, C. Hoffmann, O. Lantz, J. Fayette, A. Boyer-Chammard, R. Zerbib, P. Dodion, H. Ghadially, M. Jure-Kunkel, Y. Morel, R. Herbst, E. Narni-Mancinelli, R.B. Cohen, and E. Vivier. 2018. Anti-NKG2A mAb Is a Checkpoint Inhibitor that Promotes Anti-tumor Immunity by Unleashing Both T and NK Cells. *Cell* 175:1731-1743 e1713.

Azimi, F., R.A. Scolyer, P. Rumcheva, M. Moncrieff, R. Murali, S.W. McCarthy, R.P. Saw, and J.F. Thompson. 2012. Tumor-infiltrating lymphocyte grade is an independent predictor of sentinel lymph node status and survival in patients with cutaneous melanoma. *J Clin Oncol* 30:2678-2683.

Bachem, A., S. Guttler, E. Hartung, F. Ebstein, M. Schaefer, A. Tannert, A. Salama, K. Movassaghi, C. Opitz, H.W. Mages, V. Henn, P.M. Kloetzel, S. Gurka, and R.A. Kroczek. 2010. Superior antigen cross-presentation and XCR1 expression define human CD11c+CD141+ cells as homologues of mouse CD8+ dendritic cells. *J Exp Med* 207:1273-1281.

Balkhi, M.Y., G. Wittmann, F. Xiong, and R.P. Junghans. 2018. YY1 Upregulates Checkpoint Receptors and Downregulates Type I Cytokines in Exhausted, Chronically Stimulated Human T Cells. *iScience* 2:105-122.

Barber, D.L., E.J. Wherry, D. Masopust, B. Zhu, J.P. Allison, A.H. Sharpe, G.J. Freeman, and R. Ahmed. 2006. Restoring function in exhausted CD8 T cells during chronic viral infection. *Nature* 439:682-687.

Beck, B., and C. Blanpain. 2013. Unravelling cancer stem cell potential. *Nat Rev Cancer* 13:727-738.

Bellone, M., G. Iezzi, P. Rovere, G. Galati, A. Ronchetti, M.P. Protti, J. Davoust, C. Rugarli, and A.A. Manfredi. 1997. Processing of engulfed apoptotic bodies yields T cell epitopes. *J Immunol* 159:5391-5399.

Benacerraf, B., and H.O. McDevitt. 1972. Histocompatibility-linked immune response genes. *Science* 175:273-279.

Berger, C.T., N. Frahm, D.A. Price, B. Mothe, M. Ghebremichael, K.L. Hartman, L.M. Henry, J.M. Brenchley, L.E. Ruff, V. Venturi, F. Pereyra, J. Sidney, A. Sette, D.C. Douek, B.D. Walker, D.E. Kaufmann, and C. Brander. 2011. High-functional-avidity cytotoxic T lymphocyte responses to HLA-B-restricted Gag-derived epitopes associated with relative HIV control. *J Virol* 85:9334-9345.

Besser, M.J., R. Shapira-Frommer, O. Itzhaki, A.J. Treves, D.B. Zippel, D. Levy, A. Kubi, N. Shoshani, D. Zikich, Y. Ohayon, D. Ohayon, B. Shalmon, G. Markel, R. Yerushalmi, S. Apter, A. Ben-Nun, E. Ben-Ami, A. Shimoni, A. Nagler, and J. Schachter. 2013. Adoptive transfer of tumor-infiltrating lymphocytes in patients with metastatic melanoma: intent-to-treat analysis and efficacy after failure to prior immunotherapies. *Clin Cancer Res* 19:4792-4800.

Bevan, M.J. 1976. Minor H antigens introduced on H-2 different stimulating cells cross-react at the cytotoxic T cell level during in vivo priming. *J Immunol* 117:2233-2238.

Biddle, A., L. Gammon, X. Liang, D.E. Costea, and I.C. Mackenzie. 2016. Phenotypic Plasticity Determines Cancer Stem Cell Therapeutic Resistance in Oral Squamous Cell Carcinoma. *EBioMedicine* 4:138-145.

Birchmeier, W., and J. Behrens. 1994. Cadherin expression in carcinomas: role in the formation of cell junctions and the prevention of invasiveness. *Biochim Biophys Acta* 1198:11-26.

Bjorkman, P.J., M.A. Saper, B. Samraoui, W.S. Bennett, J.L. Strominger, and D.C. Wiley. 1987a. The foreign antigen binding site and T cell recognition regions of class I histocompatibility antigens. *Nature* 329:512-518.

Bjorkman, P.J., M.A. Saper, B. Samraoui, W.S. Bennett, J.L. Strominger, and D.C. Wiley. 1987b. Structure of the human class I histocompatibility antigen, HLA-A2. *Nature* 329:506-512.

Boise, L.H., A.J. Minn, P.J. Noel, C.H. June, M.A. Accavitti, T. Lindsten, and C.B. Thompson. 1995. CD28 costimulation can promote T cell survival by enhancing the expression of Bcl-XL. *Immunity* 3:87-98.

Boni, A., P. Muranski, L. Cassard, C. Wrzesinski, C.M. Paulos, D.C. Palmer, L. Gattinoni, C.S. Hinrichs, C.C. Chan, S.A. Rosenberg, and N.P. Restifo. 2008. Adoptive transfer of allogeneic tumor-specific T cells mediates effective regression of large tumors across major histocompatibility barriers. *Blood* 112:4746-4754.

Bossard, C., S. Bezieau, T. Matysiak-Budnik, C. Volteau, C.L. Laboisse, F. Jotereau, and J.F. Mosnier. 2012. HLA-E/beta2 microglobulin overexpression in colorectal cancer is associated with recruitment of inhibitory immune cells and tumor progression. *Int J Cancer* 131:855-863.

Boutet, M., L. Gauthier, M. Leclerc, G. Gros, V. de Montpreville, N. Theret, E. Donnadieu, and F. Mami-Chouaib. 2016. TGFbeta Signaling Intersects with CD103 Integrin Signaling to Promote T-Lymphocyte Accumulation and Antitumor Activity in the Lung Tumor Microenvironment. *Cancer Res* 76:1757-1769.

Braud, V.M., H. Aldemir, B. Breart, and W.G. Ferlin. 2003. Expression of CD94-NKG2A inhibitory receptor is restricted to a subset of CD8+ T cells. *Trends Immunol* 24:162-164.

Braud, V.M., D.S. Allan, C.A. O'Callaghan, K. Soderstrom, A. D'Andrea, G.S. Ogg, S. Lazetic, N.T. Young, J.I. Bell, J.H. Phillips, L.L. Lanier, and A.J. McMichael. 1998. HLA-E binds to natural killer cell receptors CD94/NKG2A, B and C. *Nature* 391:795-799.

Bray, F., J. Ferlay, I. Soerjomataram, R.L. Siegel, L.A. Torre, and A. Jemal. 2018. Global cancer statistics 2018: GLOBOCAN estimates of incidence and mortality worldwide for 36 cancers in 185 countries. *CA Cancer J Clin* 68:394-424.

Bruner, H.C., and P.W.B. Derksen. 2018. Loss of E-Cadherin-Dependent Cell-Cell Adhesion and the Development and Progression of Cancer. *Cold Spring Harb Perspect Biol* 10:

Bubeck Wardenburg, J., C. Fu, J.K. Jackman, H. Flotow, S.E. Wilkinson, D.H. Williams, R. Johnson, G. Kong, A.C. Chan, and P.R. Findell. 1996. Phosphorylation of SLP-76 by the ZAP-70 protein-tyrosine kinase is required for T-cell receptor function. *J Biol Chem* 271:19641-19644.

Burton, A.L., B.A. Roach, M.P. Mays, A.F. Chen, B.A. Ginter, A.M. Vierling, C.R. Scoggins, R.C. Martin, A.J. Stromberg, L. Hagendoorn, and K.M. McMasters. 2011. Prognostic significance of tumor infiltrating lymphocytes in melanoma. *Am Surg* 77:188-192.

Busse, D., M. de la Rosa, K. Hobiger, K. Thurley, M. Flossdorf, A. Scheffold, and T. Hofer. 2010. Competing feedback loops shape IL-2 signaling between helper and regulatory T lymphocytes in cellular microenvironments. *Proc Natl Acad Sci U S A* 107:3058-3063.

Caccamo, N., G. Pietra, L.C. Sullivan, A.G. Brooks, T. Prezzemolo, M.P. La Manna, D. Di Liberto, S.A. Joosten, K.E. van Meijgaarden, P. Di Carlo, L. Titone, L. Moretta, M.C. Mingari, T.H. Ottenhoff, and F. Dieli. 2015. Human CD8 T lymphocytes recognize Mycobacterium tuberculosis antigens presented by HLA-E during active tuberculosis and express type 2 cytokines. *Eur J Immunol* 45:1069-1081.

Carbone, F.R., and M.J. Bevan. 1990. Class I-restricted processing and presentation of exogenous cell-associated antigen in vivo. *J Exp Med* 171:377-387.

Chang, C.H., J.D. Curtis, L.B. Maggi, Jr., B. Faubert, A.V. Villarino, D. O'Sullivan, S.C. Huang, G.J. van der Windt, J. Blagih, J. Qiu, J.D. Weber, E.J. Pearce, R.G. Jones, and E.L. Pearce. 2013. Posttranscriptional control of T cell effector function by aerobic glycolysis. *Cell* 153:1239-1251.

Chang, C.H., J. Qiu, D. O'Sullivan, M.D. Buck, T. Noguchi, J.D. Curtis, Q. Chen, M. Gindin, M.M. Gubin, G.J. van der Windt, E. Tonc, R.D. Schreiber, E.J. Pearce, and E.L. Pearce. 2015. Metabolic Competition in the Tumor Microenvironment Is a Driver of Cancer Progression. *Cell* 162:1229-1241.

Chaudhary, P.M., M. Eby, A. Jasmin, A. Bookwalter, J. Murray, and L. Hood. 1997. Death receptor 5, a new member of the TNFR family, and DR4 induce FADD-dependent apoptosis and activate the NF-kappaB pathway. *Immunity* 7:821-830.

Chen, H., C.I. Liakou, A. Kamat, C. Pettaway, J.F. Ward, D.N. Tang, J. Sun, A.A. Jungbluth, P. Troncoso, C. Logothetis, and P. Sharma. 2009. Anti-CTLA-4 therapy results in higher

CD4+ICOShi T cell frequency and IFN-gamma levels in both nonmalignant and malignant prostate tissues. *Proc Natl Acad Sci U S A* 106:2729-2734.

Chen, H., Z.M. Ndhlovu, D. Liu, L.C. Porter, J.W. Fang, S. Darko, M.A. Brockman, T. Miura, Z.L. Brumme, A. Schneidewind, A. Piechocka-Trocha, K.T. Cesa, J. Sela, T.D. Cung, I. Toth, F. Pereyra, X.G. Yu, D.C. Douek, D.E. Kaufmann, T.M. Allen, and B.D. Walker. 2012. TCR clonotypes modulate the protective effect of HLA class I molecules in HIV-1 infection. *Nat Immunol* 13:691-700.

Chen, L., and D.B. Flies. 2013. Molecular mechanisms of T cell co-stimulation and co-inhibition. *Nat Rev Immunol* 13:227-242.

Chen, S., L.F. Lee, T.S. Fisher, B. Jessen, M. Elliott, W. Evering, K. Logronio, G.H. Tu, K. Tsaparikos, X. Li, H. Wang, C. Ying, M. Xiong, T. VanArsdale, and J.C. Lin. 2015. Combination of 4-1BB agonist and PD-1 antagonist promotes antitumor effector/memory CD8 T cells in a poorly immunogenic tumor model. *Cancer Immunol Res* 3:149-160.

Chowdhury, D., and J. Lieberman. 2008. Death by a thousand cuts: granzyme pathways of programmed cell death. *Annu Rev Immunol* 26:389-420.

Cook, C.H., L. Chen, J. Wen, P. Zimmerman, Y. Zhang, J. Trgovcich, Y. Liu, and J.X. Gao. 2009. CD28/B7-mediated co-stimulation is critical for early control of murine cytomegalovirus infection. *Viral Immunol* 22:91-103.

Corn, R.A., M.A. Aronica, F. Zhang, Y. Tong, S.A. Stanley, S.R. Kim, L. Stephenson, B. Enerson, S. McCarthy, A. Mora, and M. Boothby. 2003. T cell-intrinsic requirement for NF-kappa B induction in postdifferentiation IFN-gamma production and clonal expansion in a Th1 response. *J Immunol* 171:1816-1824.

Cresswell, P., M.J. Turner, and J.L. Strominger. 1973. Papain-solubilized HL-A antigens from cultured human lymphocytes contain two peptide fragments. *Proc Natl Acad Sci U S A* 70:1603-1607.

Cubillos-Ruiz, J.R., P.C. Silberman, M.R. Rutkowski, S. Chopra, A. Perales-Puchalt, M. Song, S. Zhang, S.E. Bettigole, D. Gupta, K. Holcomb, L.H. Ellenson, T. Caputo, A.H. Lee, J.R. Conejo-Garcia, and L.H. Glimcher. 2015. ER Stress Sensor XBP1 Controls Anti-tumor Immunity by Disrupting Dendritic Cell Homeostasis. *Cell* 161:1527-1538.

Cui, H., Y. Hu, D. Guo, A. Zhang, Y. Gu, S. Zhang, C. Zhao, P. Gong, X. Shen, Y. Li, H. Wu, L. Wang, Z. Zhao, and H. Fan. 2018. DNA methyltransferase 3A isoform b contributes to repressing E-cadherin through cooperation of DNA methylation and H3K27/H3K9 methylation in EMT-related metastasis of gastric cancer. *Oncogene* 37:4358-4371.

Danilczyk, U.G., M.F. Cohen-Doyle, and D.B. Williams. 2000. Functional relationship between calreticulin, calnexin, and the endoplasmic reticulum luminal domain of calnexin. *J Biol Chem* 275:13089-13097.

de Kruijf, E.M., A. Sajet, J.G. van Nes, R. Natanov, H. Putter, V.T. Smit, G.J. Liefers, P.J. van den Elsen, C.J. van de Velde, and P.J. Kuppen. 2010. HLA-E and HLA-G expression in classical HLA class I-negative tumors is of prognostic value for clinical outcome of early breast cancer patients. *J Immunol* 185:7452-7459.

Depper, J.M., W.J. Leonard, C. Drogula, M. Kronke, T.A. Waldmann, and W.C. Greene. 1985. Interleukin 2 (IL-2) augments transcription of the IL-2 receptor gene. *Proc Natl Acad Sci U S A* 82:4230-4234.

Dick, T.P., T. Ruppert, M. Groettrup, P.M. Kloetzel, L. Kuehn, U.H. Koszinowski, S. Stevanovic, H. Schild, and H.G. Rammensee. 1996. Coordinated dual cleavages induced by the proteasome regulator PA28 lead to dominant MHC ligands. *Cell* 86:253-262.

Diedrich, G., N. Bangia, M. Pan, and P. Cresswell. 2001. A role for calnexin in the assembly of the MHC class I loading complex in the endoplasmic reticulum. *J Immunol* 166:1703-1709.

Diehn, M., R.W. Cho, N.A. Lobo, T. Kalisky, M.J. Dorie, A.N. Kulp, D. Qian, J.S. Lam, L.E. Ailles, M. Wong, B. Joshua, M.J. Kaplan, I. Wapnir, F.M. Dirbas, G. Somlo, C. Garberoglio, B. Paz, J. Shen, S.K. Lau, S.R. Quake, J.M. Brown, I.L. Weissman, and M.F. Clarke. 2009. Association of reactive oxygen species levels and radioresistance in cancer stem cells. *Nature* 458:780-783.

Djenidi, F., J. Adam, A. Goubar, A. Durgeau, G. Meurice, V. de Montpreville, P. Validire, B. Besse, and F. Mami-Chouaib. 2015. CD8+CD103+ tumor-infiltrating lymphocytes are tumor-specific tissue-resident memory T cells and a prognostic factor for survival in lung cancer patients. *J Immunol* 194:3475-3486.

Doherty, P.C., and R.M. Zinkernagel. 1975. A biological role for the major histocompatibility antigens. *Lancet* 1:1406-1409.

Dong, C., A.E. Juedes, U.A. Temann, S. Shresta, J.P. Allison, N.H. Ruddle, and R.A. Flavell. 2001. ICOS co-stimulatory receptor is essential for T-cell activation and function. *Nature* 409:97-101.

Dong, T., G. Stewart-Jones, N. Chen, P. Easterbrook, X. Xu, L. Papagno, V. Appay, M. Weekes, C. Conlon, C. Spina, S. Little, G. Screaton, A. van der Merwe, D.D. Richman, A.J.

McMichael, E.Y. Jones, and S.L. Rowland-Jones. 2004. HIV-specific cytotoxic T cells from long-term survivors select a unique T cell receptor. *J Exp Med* 200:1547-1557.

Douin-Echinard, V., S. Bornes, P. Rochaix, A.F. Tilkin, J.M. Peron, J. Bonnet, G. Favre, and B. Couderc. 2000. The expression of CD70 and CD80 by gene-modified tumor cells induces an antitumor response depending on the MHC status. *Cancer Gene Ther* 7:1543-1556.

Duhen, T., R. Duhen, R. Montler, J. Moses, T. Moudgil, N.F. de Miranda, C.P. Goodall, T.C. Blair, B.A. Fox, J.E. McDermott, S.C. Chang, G. Grunkemeier, R. Leidner, R.B. Bell, and A.D. Weinberg. 2018. Co-expression of CD39 and CD103 identifies tumor-reactive CD8 T cells in human solid tumors. *Nat Commun* 9:2724.

Early, P., H. Huang, M. Davis, K. Calame, and L. Hood. 1980. An immunoglobulin heavy chain variable region gene is generated from three segments of DNA: VH, D and JH. *Cell* 19:981-992.

Eivazova, E.R., S.A. Markov, I. Pirozhkova, M. Lipinski, and Y.S. Vassetzky. 2007. Recruitment of RNA polymerase II in the Ifng gene promoter correlates with the nuclear matrix association in activated T helper cells. *J Mol Biol* 371:317-322.

El-Asady, R., R. Yuan, K. Liu, D. Wang, R.E. Gress, P.J. Lucas, C.B. Drachenberg, and G.A. Hadley. 2005. TGF-{beta}-dependent CD103 expression by CD8(+) T cells promotes selective destruction of the host intestinal epithelium during graft-versus-host disease. *J Exp Med* 201:1647-1657.

El-Sahwi, K., S. Bellone, E. Cocco, F. Casagrande, M. Bellone, M. Abu-Khalaf, N. Buza, F.A. Tavassoli, P. Hui, D. Ruttinger, D.A. Silasi, M. Azodi, P.E. Schwartz, T.J. Rutherford, S. Pecorelli, and A.D. Santin. 2010. Overexpression of EpCAM in uterine serous

papillary carcinoma: implications for EpCAM-specific immunotherapy with human monoclonal antibody adecatumumab (MT201). *Mol Cancer Ther* 9:57-66.

Embgenbroich, M., and S. Burgdorf. 2018. Current Concepts of Antigen Cross-Presentation. *Front Immunol* 9:1643.

Enamorado, M., S. Iborra, E. Priego, F.J. Cueto, J.A. Quintana, S. Martinez-Cano, E. Mejias-Perez, M. Esteban, I. Melero, A. Hidalgo, and D. Sancho. 2017. Enhanced anti-tumour immunity requires the interplay between resident and circulating memory CD8(+) T cells. *Nat Commun* 8:16073.

Farrar, M.A., J. Fernandez-Luna, and R.D. Schreiber. 1991. Identification of two regions within the cytoplasmic domain of the human interferon-gamma receptor required for function. *J Biol Chem* 266:19626-19635.

Feinberg, A.P., M.A. Koldobskiy, and A. Gondor. 2016. Epigenetic modulators, modifiers and mediators in cancer aetiology and progression. *Nat Rev Genet* 17:284-299.

Ferlay, J., I. Soerjomataram, R. Dikshit, S. Eser, C. Mathers, M. Rebelo, D.M. Parkin, D. Forman, and F. Bray. 2015. Cancer incidence and mortality worldwide: sources, methods and major patterns in GLOBOCAN 2012. *Int J Cancer* 136:E359-386.

Ferrone, C., and G. Dranoff. 2010. Dual roles for immunity in gastrointestinal cancers. *J Clin Oncol* 28:4045-4051.

Feske, M., R.J. Nudelman, M. Medina, J. Lew, M. Singh, J. Couturier, E.A. Graviss, and D.E. Lewis. 2008. Enhancement of human antigen-specific memory T-cell responses by interleukin-7 may improve accuracy in diagnosing tuberculosis. *Clin Vaccine Immunol* 15:1616-1622.

Fos, C., A. Salles, V. Lang, F. Carrette, S. Audebert, S. Pastor, M. Ghiotto, D. Olive, G. Bismuth, and J.A. Nunes. 2008. ICOS ligation recruits the p50alpha PI3K regulatory subunit to the immunological synapse. *J Immunol* 181:1969-1977.

Fourcade, J., Z. Sun, M. Benallaoua, P. Guillaume, I.F. Luescher, C. Sander, J.M. Kirkwood, V. Kuchroo, and H.M. Zarour. 2010. Upregulation of Tim-3 and PD-1 expression is associated with tumor antigen-specific CD8+ T cell dysfunction in melanoma patients. *J Exp Med* 207:2175-2186.

Freedman, J.D., M.R. Duffy, J. Lei-Rossmann, A. Muntzer, E.M. Scott, J. Hagel, L. Campo, R.J. Bryant, C. Verrill, A. Lambert, P. Miller, B.R. Champion, L.W. Seymour, and K.D. Fisher. 2018. An Oncolytic Virus Expressing a T-cell Engager Simultaneously Targets Cancer and Immunosuppressive Stromal Cells. *Cancer Res* 78:6852-6865.

Friedline, R.H., D.S. Brown, H. Nguyen, H. Kornfeld, J. Lee, Y. Zhang, M. Appleby, S.D. Der, J. Kang, and C.A. Chambers. 2009. CD4+ regulatory T cells require CTLA-4 for the maintenance of systemic tolerance. *J Exp Med* 206:421-434.

Friedmann, M.C., T.S. Migone, S.M. Russell, and W.J. Leonard. 1996. Different interleukin 2 receptor beta-chain tyrosines couple to at least two signaling pathways and synergistically mediate interleukin 2-induced proliferation. *Proc Natl Acad Sci U S A* 93:2077-2082.

Fu, T., Q. He, and P. Sharma. 2011. The ICOS/ICOSL pathway is required for optimal antitumor responses mediated by anti-CTLA-4 therapy. *Cancer Res* 71:5445-5454.

Galon, J., A. Costes, F. Sanchez-Cabo, A. Kirilovsky, B. Mlecnik, C. Lagorce-Pages, M. Tosolini, M. Camus, A. Berger, P. Wind, F. Zinzindohoue, P. Bruneval, P.H. Cugnenc, Z. Trajanoski, W.H. Fridman, and F. Pages. 2006. Type, density, and location of

immune cells within human colorectal tumors predict clinical outcome. *Science* 313:1960-1964.

Gamper, C.J., A.T. Agoston, W.G. Nelson, and J.D. Powell. 2009. Identification of DNA methyltransferase 3a as a T cell receptor-induced regulator of Th1 and Th2 differentiation. *J Immunol* 183:2267-2276.

Ganesan, A.P., J. Clarke, O. Wood, E.M. Garrido-Martin, S.J. Chee, T. Mellows, D. Samaniego-Castruita, D. Singh, G. Seumois, A. Alzetani, E. Woo, P.S. Friedmann, E.V. King, G.J. Thomas, T. Sanchez-Elsner, P. Vijayanand, and C.H. Ottensmeier. 2017. Tissue-resident memory features are linked to the magnitude of cytotoxic T cell responses in human lung cancer. *Nat Immunol* 18:940-950.

Gao, X., Y. Zhu, G. Li, H. Huang, G. Zhang, F. Wang, J. Sun, Q. Yang, X. Zhang, and B. Lu. 2012. TIM-3 expression characterizes regulatory T cells in tumor tissues and is associated with lung cancer progression. *PLoS One* 7:e30676.

Garon, E.B., N.A. Rizvi, R. Hui, N. Leighl, A.S. Balmanoukian, J.P. Eder, A. Patnaik, C. Aggarwal, M. Gubens, L. Horn, E. Carcereny, M.J. Ahn, E. Felip, J.S. Lee, M.D. Hellmann, O. Hamid, J.W. Goldman, J.C. Soria, M. Dolled-Filhart, R.Z. Rutledge, J. Zhang, J.K. Lunceford, R. Rangwala, G.M. Lubiniecki, C. Roach, K. Emancipator, L. Gandhi, and K.-. Investigators. 2015. Pembrolizumab for the treatment of non-small-cell lung cancer. *N Engl J Med* 372:2018-2028.

Gauthier, L., S. Corgnac, M. Boutet, G. Gros, P. Validire, G. Bismuth, and F. Mami-Chouaib. 2017. Paxillin Binding to the Cytoplasmic Domain of CD103 Promotes Cell Adhesion and Effector Functions for CD8(+) Resident Memory T Cells in Tumors. *Cancer Res* 77:7072-7082.

Gebhardt, T., L.M. Wakim, L. Eidsmo, P.C. Reading, W.R. Heath, and F.R. Carbone. 2009. Memory T cells in nonlymphoid tissue that provide enhanced local immunity during infection with herpes simplex virus. *Nat Immunol* 10:524-530.

GeurtsvanKessel, C.H., M.A. Willart, L.S. van Rijt, F. Muskens, M. Kool, C. Baas, K. Thielemans, C. Bennett, B.E. Clausen, H.C. Hoogsteden, A.D. Osterhaus, G.F. Rimmelzwaan, and B.N. Lambrecht. 2008. Clearance of influenza virus from the lung depends on migratory langerin+CD11b- but not plasmacytoid dendritic cells. *J Exp Med* 205:1621-1634.

Giri, J.G., M. Ahdieh, J. Eisenman, K. Shanebeck, K. Grabstein, S. Kumaki, A. Namen, L.S. Park, D. Cosman, and D. Anderson. 1994. Utilization of the beta and gamma chains of the IL-2 receptor by the novel cytokine IL-15. *EMBO J* 13:2822-2830.

Gjerstorff, M.F., M.M. Relster, K.B. Greve, J.B. Moeller, D. Elias, J.N. Lindgreen, S. Schmidt, J. Mollenhauer, B. Voldborg, C.B. Pedersen, N.H. Bruckmann, N.E. Mollegaard, and H.J. Ditzel. 2014. SSX2 is a novel DNA-binding protein that antagonizes polycomb group body formation and gene repression. *Nucleic Acids Res* 42:11433-11446.

Gooden, M., M. Lampen, E.S. Jordanova, N. Leffers, J.B. Trimbos, S.H. van der Burg, H. Nijman, and T. van Hall. 2011. HLA-E expression by gynecological cancers restrains tumor-infiltrating CD8(+) T lymphocytes. *Proc Natl Acad Sci U S A* 108:10656-10661.

Gordon-Alonso, M., T. Hirsch, C. Wildmann, and P. van der Bruggen. 2017. Galectin-3 captures interferon-gamma in the tumor matrix reducing chemokine gradient production and T-cell tumor infiltration. *Nat Commun* 8:793.

Graham, J.B., A. Da Costa, and J.M. Lund. 2014. Regulatory T cells shape the resident memory T cell response to virus infection in the tissues. *J Immunol* 192:683-690.

Grell, M., G. Zimmermann, E. Gottfried, C.M. Chen, U. Grunwald, D.C. Huang, Y.H. Wu Lee, H. Durkop, H. Engelmann, P. Scheurich, H. Wajant, and A. Strasser. 1999. Induction of cell death by tumour necrosis factor (TNF) receptor 2, CD40 and CD30: a role for TNF-R1 activation by endogenous membrane-anchored TNF. *EMBO J* 18:3034-3043.

Greve, K.B., M. Pohl, K.E. Olsen, O. Nielsen, H.J. Ditzel, and M.F. Gjerstorff. 2014. SSX2-4 expression in early-stage non-small cell lung cancer. *Tissue Antigens* 83:344-349.

Grey, H.M., R.T. Kubo, S.M. Colon, M.D. Poulik, P. Cresswell, T. Springer, M. Turner, and J.L. Strominger. 1973. The small subunit of HL-A antigens is beta 2-microglobulin. *J Exp Med* 138:1608-1612.

Groettrup, M., S. Khan, K. Schwarz, and G. Schmidtke. 2001. Interferon-gamma inducible exchanges of 20S proteasome active site subunits: why? *Biochimie* 83:367-372.

Guasch, G., M. Schober, H.A. Pasolli, E.B. Conn, L. Polak, and E. Fuchs. 2007. Loss of TGFbeta signaling destabilizes homeostasis and promotes squamous cell carcinomas in stratified epithelia. *Cancer Cell* 12:313-327.

Hamid, O., C. Robert, A. Daud, F.S. Hodi, W.J. Hwu, R. Kefford, J.D. Wolchok, P. Hersey, R.W. Joseph, J.S. Weber, R. Dronca, T.C. Gangadhar, A. Patnaik, H. Zarour, A.M. Joshua, K. Gergich, J. Elassaiss-Schaap, A. Algazi, C. Mateus, P. Boasberg, P.C. Tumeh, B. Chmielowski, S.W. Ebbinghaus, X.N. Li, S.P. Kang, and A. Ribas. 2013. Safety and tumor responses with lambrolizumab (anti-PD-1) in melanoma. *N Engl J Med* 369:134-144.

Hansen, S.G., H.L. Wu, B.J. Burwitz, C.M. Hughes, K.B. Hammond, A.B. Ventura, J.S. Reed, R.M. Gilbride, E. Ainslie, D.W. Morrow, J.C. Ford, A.N. Selseth, R. Pathak, D. Malouli, A.W. Legasse, M.K. Axthelm, J.A. Nelson, G.M. Gillespie, L.C. Walters, S.

Brackenridge, H.R. Sharpe, C.A. Lopez, K. Fruh, B.T. Korber, A.J. McMichael, S. Gnanakaran, J.B. Sacha, and L.J. Picker. 2016. Broadly targeted CD8(+) T cell responses restricted by major histocompatibility complex E. *Science* 351:714-720.

He, J.S., D.E. Gong, and H.L. Ostergaard. 2010. Stored Fas ligand, a mediator of rapid CTL-mediated killing, has a lower threshold for response than degranulation or newly synthesized Fas ligand. *J Immunol* 184:555-563.

Herber, D.L., W. Cao, Y. Nefedova, S.V. Novitskiy, S. Nagaraj, V.A. Tyurin, A. Corzo, H.I. Cho, E. Celis, B. Lennox, S.C. Knight, T. Padhya, T.V. McCaffrey, J.C. McCaffrey, S. Antonia, M. Fishman, R.L. Ferris, V.E. Kagan, and D.I. Gabrilovich. 2010. Lipid accumulation and dendritic cell dysfunction in cancer. *Nat Med* 16:880-886.

Herndon, T.M., X.C. Shan, G.C. Tsokos, and R.L. Wange. 2001. ZAP-70 and SLP-76 regulate protein kinase C-theta and NF-kappa B activation in response to engagement of CD3 and CD28. *J Immunol* 166:5654-5664.

Hildner, K., B.T. Edelson, W.E. Purtha, M. Diamond, H. Matsushita, M. Kohyama, B. Calderon, B.U. Schraml, E.R. Unanue, M.S. Diamond, R.D. Schreiber, T.L. Murphy, and K.M. Murphy. 2008. Batf3 deficiency reveals a critical role for CD8alpha+ dendritic cells in cytotoxic T cell immunity. *Science* 322:1097-1100.

Hodi, F.S., M.C. Mihm, R.J. Soiffer, F.G. Haluska, M. Butler, M.V. Seiden, T. Davis, R. Henry-Spires, S. MacRae, A. Willman, R. Padera, M.T. Jaklitsch, S. Shankar, T.C. Chen, A. Korman, J.P. Allison, and G. Dranoff. 2003. Biologic activity of cytotoxic T lymphocyte-associated antigen 4 antibody blockade in previously vaccinated metastatic melanoma and ovarian carcinoma patients. *Proc Natl Acad Sci U S A* 100:4712-4717.

Hodi, F.S., S.J. O'Day, D.F. McDermott, R.W. Weber, J.A. Sosman, J.B. Haanen, R. Gonzalez, C. Robert, D. Schadendorf, J.C. Hassel, W. Akerley, A.J. van den Eertwegh, J. Lutzky, P. Lorigan, J.M. Vaubel, G.P. Linette, D. Hogg, C.H. Ottensmeier, C. Lebbe, C. Peschel, I. Quirt, J.I. Clark, J.D. Wolchok, J.S. Weber, J. Tian, M.J. Yellin, G.M. Nichol, A. Hoos, and W.J. Urba. 2010. Improved survival with ipilimumab in patients with metastatic melanoma. *N Engl J Med* 363:711-723.

Hombrink, P., C. Helbig, R.A. Backer, B. Piet, A.E. Oja, R. Stark, G. Brasser, A. Jongejan, R.E. Jonkers, B. Nota, O. Basak, H.C. Clevers, P.D. Moerland, D. Amsen, and R.A. van Lier. 2016. Programs for the persistence, vigilance and control of human CD8(+) lung-resident memory T cells. *Nat Immunol* 17:1467-1478.

Hoos, A., R. Ibrahim, A. Korman, K. Abdallah, D. Berman, V. Shahabi, K. Chin, R. Canetta, and R. Humphrey. 2010. Development of ipilimumab: contribution to a new paradigm for cancer immunotherapy. *Semin Oncol* 37:533-546.

Imboden, J.B., and J.D. Stobo. 1985. Transmembrane signalling by the T cell antigen receptor. Perturbation of the T3-antigen receptor complex generates inositol phosphates and releases calcium ions from intracellular stores. *J Exp Med* 161:446-456.

Isaacs, A., and J. Lindenmann. 1957. Virus interference. I. The interferon. *Proc R Soc Lond B Biol Sci* 147:258-267.

Ishida, Y., Y. Agata, K. Shibahara, and T. Honjo. 1992. Induced expression of PD-1, a novel member of the immunoglobulin gene superfamily, upon programmed cell death. *EMBO J* 11:3887-3895.

Iversen, T.Z., L. Engell-Noerregaard, E. Ellebaek, R. Andersen, S.K. Larsen, J. Bjoern, C. Zeyher, C. Gouttefangeas, B.M. Thomsen, B. Holm, P. Thor Straten, A. Mellemgaard,

M.H. Andersen, and I.M. Svane. 2014. Long-lasting disease stabilization in the absence of toxicity in metastatic lung cancer patients vaccinated with an epitope derived from indoleamine 2,3 dioxygenase. *Clin Cancer Res* 20:221-232.

Japp, A.S., M.A. Kursunel, S. Meier, J.N. Malzer, X. Li, N.A. Rahman, W. Jekabsons, H. Krause, A. Magheli, C. Klopf, A. Thiel, and M. Frentsch. 2015. Dysfunction of PSA-specific CD8+ T cells in prostate cancer patients correlates with CD38 and Tim-3 expression. *Cancer Immunol Immunother* 64:1487-1494.

Jenkins, M.R., A. Tsun, J.C. Stinchcombe, and G.M. Griffiths. 2009. The strength of T cell receptor signal controls the polarization of cytotoxic machinery to the immunological synapse. *Immunity* 31:621-631.

Jones, R.B., L.C. Ndhlovu, J.D. Barbour, P.M. Sheth, A.R. Jha, B.R. Long, J.C. Wong, M. Satkunarajah, M. Schweneker, J.M. Chapman, G. Gyenes, B. Vali, M.D. Hyrcza, F.Y. Yue, C. Kovacs, A. Sassi, M. Loutfy, R. Halpenny, D. Persad, G. Spotts, F.M. Hecht, T.W. Chun, J.M. McCune, R. Kaul, J.M. Rini, D.F. Nixon, and M.A. Ostrowski. 2008. Tim-3 expression defines a novel population of dysfunctional T cells with highly elevated frequencies in progressive HIV-1 infection. *J Exp Med* 205:2763-2779.

Jongbloed, S.L., A.J. Kassianos, K.J. McDonald, G.J. Clark, X. Ju, C.E. Angel, C.J. Chen, P.R. Dunbar, R.B. Wadley, V. Jeet, A.J. Vulink, D.N. Hart, and K.J. Radford. 2010. Human CD141+ (BDCA-3)+ dendritic cells (DCs) represent a unique myeloid DC subset that cross-presents necrotic cell antigens. *J Exp Med* 207:1247-1260.

Kabat, J., F. Borrego, A. Brooks, and J.E. Coligan. 2002. Role that each NKG2A immunoreceptor tyrosine-based inhibitory motif plays in mediating the human CD94/NKG2A inhibitory signal. *J Immunol* 169:1948-1958.

Kagi, D., B. Ledermann, K. Burki, P. Seiler, B. Odermatt, K.J. Olsen, E.R. Podack, R.M. Zinkernagel, and H. Hengartner. 1994. Cytotoxicity mediated by T cells and natural killer cells is greatly impaired in perforin-deficient mice. *Nature* 369:31-37.

Karyampudi, L., P. Lamichhane, J. Krempski, K.R. Kalli, M.D. Behrens, D.M. Vargas, L.C. Hartmann, J.M. Janco, H. Dong, K.E. Hedin, A.B. Dietz, E.L. Goode, and K.L. Knutson. 2016. PD-1 Blunts the Function of Ovarian Tumor-Infiltrating Dendritic Cells by Inactivating NF-kappaB. *Cancer Res* 76:239-250.

Kavanagh, B., A. Ko, A. Venook, K. Margolin, H. Zeh, M. Lotze, B. Schillinger, W. Liu, Y. Lu, P. Mitsky, M. Schilling, N. Bercovici, M. Loudovaris, R. Guillermo, S.M. Lee, J. Bender, B. Mills, and L. Fong. 2007. Vaccination of metastatic colorectal cancer patients with matured dendritic cells loaded with multiple major histocompatibility complex class I peptides. *J Immunother* 30:762-772.

Kawai, O., G. Ishii, K. Kubota, Y. Murata, Y. Naito, T. Mizuno, K. Aokage, N. Saijo, Y. Nishiwaki, A. Gemma, S. Kudoh, and A. Ochiai. 2008. Predominant infiltration of macrophages and CD8(+) T Cells in cancer nests is a significant predictor of survival in stage IV nonsmall cell lung cancer. *Cancer* 113:1387-1395.

Kayagaki, N., N. Yamaguchi, M. Nakayama, A. Kawasaki, H. Akiba, K. Okumura, and H. Yagita. 1999. Involvement of TNF-related apoptosis-inducing ligand in human CD4+ T cell-mediated cytotoxicity. *J Immunol* 162:2639-2647.

Kisielow, P., H.S. Teh, H. Bluthmann, and H. von Boehmer. 1988. Positive selection of antigen-specific T cells in thymus by restricting MHC molecules. *Nature* 335:730-733.

Klebanoff, C.A., L. Gattinoni, D.C. Palmer, P. Muranski, Y. Ji, C.S. Hinrichs, Z.A. Borman, S.P. Kerkar, C.D. Scott, S.E. Finkelstein, S.A. Rosenberg, and N.P. Restifo. 2011.

Determinants of successful CD8+ T-cell adoptive immunotherapy for large established tumors in mice. *Clin Cancer Res* 17:5343-5352.

Kloetzel, P.M. 2004. Generation of major histocompatibility complex class I antigens: functional interplay between proteasomes and TPPII. *Nat Immunol* 5:661-669.

Koguchi, K., D.E. Anderson, L. Yang, K.C. O'Connor, V.K. Kuchroo, and D.A. Hafler. 2006. Dysregulated T cell expression of TIM3 in multiple sclerosis. *J Exp Med* 203:1413-1418.

Komori, H.K., T. Hart, S.A. LaMere, P.V. Chew, and D.R. Salomon. 2015. Defining CD4 T cell memory by the epigenetic landscape of CpG DNA methylation. *J Immunol* 194:1565-1579.

Koopman, L.A., W.E. Corver, A.R. van der Slik, M.J. Giphart, and G.J. Fleuren. 2000. Multiple genetic alterations cause frequent and heterogeneous human histocompatibility leukocyte antigen class I loss in cervical cancer. *J Exp Med* 191:961-976.

Kuang, D.M., Q. Zhao, C. Peng, J. Xu, J.P. Zhang, C. Wu, and L. Zheng. 2009. Activated monocytes in peritumoral stroma of hepatocellular carcinoma foster immune privilege and disease progression through PD-L1. *J Exp Med* 206:1327-1337.

Kuiper, R.P., L.E. Vissers, R. Venkatachalam, D. Bodmer, E. Hoenselaar, M. Goossens, A. Haufe, E. Kamping, R.C. Niessen, F.B. Hogervorst, J.J. Gille, B. Redeker, C.M. Tops, M.E. van Gijn, A.M. van den Ouweland, N. Rahner, V. Steinke, P. Kahl, E. Holinski-Feder, M. Morak, M. Kloor, S. Stemmler, B. Betz, P. Hutter, D.J. Bunyan, S. Syngal, J.O. Culver, T. Graham, T.L. Chan, I.D. Nagtegaal, J.H. van Krieken, H.K. Schackert, N. Hoogerbrugge, A.G. van Kessel, and M.J. Ligtenberg. 2011. Recurrence and variability of germline EPCAM deletions in Lynch syndrome. *Hum Mutat* 32:407-414.

Kutlesa, S., J.T. Wessels, A. Speiser, I. Steiert, C.A. Muller, and G. Klein. 2002. E-cadherin-mediated interactions of thymic epithelial cells with CD103+ thymocytes lead to enhanced thymocyte cell proliferation. *J Cell Sci* 115:4505-4515.

Kwon, E.D., A.A. Hurwitz, B.A. Foster, C. Madias, A.L. Feldhaus, N.M. Greenberg, M.B. Burg, and J.P. Allison. 1997. Manipulation of T cell costimulatory and inhibitory signals for immunotherapy of prostate cancer. *Proc Natl Acad Sci U S A* 94:8099-8103.

Laoui, D., J. Keirsse, Y. Morias, E. Van Overmeire, X. Geeraerts, Y. Elkrim, M. Kiss, E. Bolli, Q. Lahmar, D. Sichien, J. Serneels, C.L. Scott, L. Boon, P. De Baetselier, M. Mazzone, M. Guilliams, and J.A. Van Ginderachter. 2016. The tumour microenvironment harbours ontogenically distinct dendritic cell populations with opposing effects on tumour immunity. *Nat Commun* 7:13720.

Lazetic, S., C. Chang, J.P. Houchins, L.L. Lanier, and J.H. Phillips. 1996. Human natural killer cell receptors involved in MHC class I recognition are disulfide-linked heterodimers of CD94 and NKG2 subunits. *J Immunol* 157:4741-4745.

Le Floc'h, A., A. Jalil, K. Franciszkiewicz, P. Validire, I. Vergnon, and F. Mami-Chouaib. 2011. Minimal engagement of CD103 on cytotoxic T lymphocytes with an E-cadherin-Fc molecule triggers lytic granule polarization via a phospholipase Cgamma-dependent pathway. *Cancer Res* 71:328-338.

Le Floc'h, A., A. Jalil, I. Vergnon, B. Le Maux Chansac, V. Lazar, G. Bismuth, S. Chouaib, and F. Mami-Chouaib. 2007. Alpha E beta 7 integrin interaction with E-cadherin promotes antitumor CTL activity by triggering lytic granule polarization and exocytosis. *J Exp Med* 204:559-570.

Leach, D.R., M.F. Krummel, and J.P. Allison. 1996. Enhancement of antitumor immunity by CTLA-4 blockade. *Science* 271:1734-1736.

Lee, N., M. Llano, M. Carretero, A. Ishitani, F. Navarro, M. Lopez-Botet, and D.E. Geraghty. 1998. HLA-E is a major ligand for the natural killer inhibitory receptor CD94/NKG2A. *Proc Natl Acad Sci U S A* 95:5199-5204.

Leone, P., E.C. Shin, F. Perosa, A. Vacca, F. Dammacco, and V. Racanelli. 2013. MHC class I antigen processing and presenting machinery: organization, function, and defects in tumor cells. *J Natl Cancer Inst* 105:1172-1187.

Levy, E.M., M. Bianchini, E.M. Von Euw, M.M. Barrio, A.I. Bravo, D. Furman, E. Domenichini, C. Macagno, V. Pinsky, C. Zucchini, L. Valvassori, and J. Mordoh. 2008. Human leukocyte antigen-E protein is overexpressed in primary human colorectal cancer. *Int J Oncol* 32:633-641.

Li, X., M.T. Lewis, J. Huang, C. Gutierrez, C.K. Osborne, M.F. Wu, S.G. Hilsenbeck, A. Pavlick, X. Zhang, G.C. Chamness, H. Wong, J. Rosen, and J.C. Chang. 2008. Intrinsic resistance of tumorigenic breast cancer cells to chemotherapy. *J Natl Cancer Inst* 100:672-679.

Lindstein, T., C.H. June, J.A. Ledbetter, G. Stella, and C.B. Thompson. 1989. Regulation of lymphokine messenger RNA stability by a surface-mediated T cell activation pathway. *Science* 244:339-343.

Ling, K.L., N. Dulphy, P. Bahl, M. Salio, K. Maskell, J. Piris, B.F. Warren, B.D. George, N.J. Mortensen, and V. Cerundolo. 2007. Modulation of CD103 expression on human colon carcinoma-specific CTL. *J Immunol* 178:2908-2915.

Linsley, P.S., W. Brady, L. Grosmaire, A. Aruffo, N.K. Damle, and J.A. Ledbetter. 1991. Binding of the B cell activation antigen B7 to CD28 costimulates T cell proliferation and interleukin 2 mRNA accumulation. *J Exp Med* 173:721-730.

Liston, A., S. Lesage, J. Wilson, L. Peltonen, and C.C. Goodnow. 2003. Aire regulates negative selection of organ-specific T cells. *Nat Immunol* 4:350-354.

Liu, Y., C. Ma, and N. Zhang. 2018. Tissue-Specific Control of Tissue-Resident Memory T Cells. *Crit Rev Immunol* 38:79-103.

Lowin, B., M. Hahne, C. Mattmann, and J. Tschopp. 1994. Cytolytic T-cell cytotoxicity is mediated through perforin and Fas lytic pathways. *Nature* 370:650-652.

Lyubchenko, T.A., G.A. Wurth, and A. Zweifach. 2001. Role of calcium influx in cytotoxic T lymphocyte lytic granule exocytosis during target cell killing. *Immunity* 15:847-859.

Ma, D., C. Jiang, X. Hu, H. Liu, Q. Li, T. Li, Y. Yang, and O. Li. 2014. Methylation patterns of the IFN-gamma gene in cervical cancer tissues. *Sci Rep* 4:6331.

Mackay, L.K., A. Rahimpour, J.Z. Ma, N. Collins, A.T. Stock, M.L. Hafon, J. Vega-Ramos, P. Lauzurica, S.N. Mueller, T. Stefanovic, D.C. Tscharke, W.R. Heath, M. Inouye, F.R. Carbone, and T. Gebhardt. 2013. The developmental pathway for CD103(+)CD8+ tissue-resident memory T cells of skin. *Nat Immunol* 14:1294-1301.

Madden, D.R., J.C. Gorga, J.L. Strominger, and D.C. Wiley. 1992. The three-dimensional structure of HLA-B27 at 2.1 A resolution suggests a general mechanism for tight peptide binding to MHC. *Cell* 70:1035-1048.

Malik, B.T., K.T. Byrne, J.L. Vella, P. Zhang, T.B. Shabaneh, S.M. Steinberg, A.K. Molodtsov, J.S. Bowers, C.V. Angeles, C.M. Paulos, Y.H. Huang, and M.J. Turk. 2017. Resident memory T cells in the skin mediate durable immunity to melanoma. *Sci Immunol* 2:

Martinez-Lorenzo, M.J., M.A. Alava, S. Gamen, K.J. Kim, A. Chuntharapai, A. Pineiro, J. Naval, and A. Anel. 1998. Involvement of APO2 ligand/TRAIL in activation-induced death of Jurkat and human peripheral blood T cells. *Eur J Immunol* 28:2714-2725.

Martini, M., M.G. Testi, M. Pasetto, M.C. Picchio, G. Innamorati, M. Mazzocco, S. Ugel, S. Cingarlini, V. Bronte, P. Zanovello, M. Krampera, F. Mosna, T. Cestari, A.P. Riviera, N. Brutti, O. Barbieri, L. Matera, G. Tridente, M. Colombatti, and S. Sartoris. 2010. IFN-gamma-mediated upmodulation of MHC class I expression activates tumor-specific immune response in a mouse model of prostate cancer. *Vaccine* 28:3548-3557.

Masopust, D., D. Choo, V. Vezys, E.J. Wherry, J. Duraiswamy, R. Akondy, J. Wang, K.A. Casey, D.L. Barber, K.S. Kawamura, K.A. Fraser, R.J. Webby, V. Brinkmann, E.C. Butcher, K.A. Newell, and R. Ahmed. 2010. Dynamic T cell migration program provides resident memory within intestinal epithelium. *J Exp Med* 207:553-564.

Massague, J. 2008. TGFbeta in Cancer. *Cell* 134:215-230.

Matter, A. 1979. Microcinematographic and electron microscopic analysis of target cell lysis induced by cytotoxic T lymphocytes. *Immunology* 36:179-190.

Menk, A.V., N.E. Scharping, R.S. Moreci, X. Zeng, C. Guy, S. Salvatore, H. Bae, J. Xie, H.A. Young, S.G. Wendell, and G.M. Delgoffe. 2018. Early TCR Signaling Induces Rapid Aerobic Glycolysis Enabling Distinct Acute T Cell Effector Functions. *Cell Rep* 22:1509-1521.

Meuer, S.C., K.A. Fitzgerald, R.E. Hussey, J.C. Hodgdon, S.F. Schlossman, and E.L. Reinherz. 1983. Clonotypic structures involved in antigen-specific human T cell function. Relationship to the T3 molecular complex. *J Exp Med* 157:705-719.

Milner, J.J., C. Toma, B. Yu, K. Zhang, K. Omilusik, A.T. Phan, D. Wang, A.J. Getzler, T. Nguyen, S. Crotty, W. Wang, M.E. Pipkin, and A.W. Goldrath. 2017. Runx3 programs CD8(+) T cell residency in non-lymphoid tissues and tumours. *Nature* 552:253-257.

Mittrucker, H.W., A. Kohler, T.W. Mak, and S.H. Kaufmann. 1999. Critical role of CD28 in protective immunity against Salmonella typhimurium. *J Immunol* 163:6769-6776.

Miyazaki, T., A. Kawahara, H. Fujii, Y. Nakagawa, Y. Minami, Z.J. Liu, I. Oishi, O. Silvennoinen, B.A. Witthuhn, J.N. Ihle, and et al. 1994. Functional activation of Jak1 and Jak3 by selective association with IL-2 receptor subunits. *Science* 266:1045-1047.

Monney, L., C.A. Sabatos, J.L. Gaglia, A. Ryu, H. Waldner, T. Chernova, S. Manning, E.A. Greenfield, A.J. Coyle, R.A. Sobel, G.J. Freeman, and V.K. Kuchroo. 2002. Th1-specific cell surface protein Tim-3 regulates macrophage activation and severity of an autoimmune disease. *Nature* 415:536-541.

Moore, L.D., T. Le, and G. Fan. 2013. DNA methylation and its basic function. *Neuropsychopharmacology* 38:23-38.

Mueller, D.L., S. Seiffert, W. Fang, and T.W. Behrens. 1996. Differential regulation of bcl-2 and bcl-x by CD3, CD28, and the IL-2 receptor in cloned CD4+ helper T cells. A model for the long-term survival of memory cells. *J Immunol* 156:1764-1771.

Muro, K., H.C. Chung, V. Shankaran, R. Geva, D. Catenacci, S. Gupta, J.P. Eder, T. Golan, D.T. Le, B. Burtness, A.J. McRee, C.C. Lin, K. Pathiraja, J. Lunceford, K. Emancipator, J. Juco, M. Koshiji, and Y.J. Bang. 2016. Pembrolizumab for patients with PD-L1-positive advanced gastric cancer (KEYNOTE-012): a multicentre, open-label, phase 1b trial. *Lancet Oncol* 17:717-726.

Nakajima, C., Y. Uekusa, M. Iwasaki, N. Yamaguchi, T. Mukai, P. Gao, M. Tomura, S. Ono, T. Tsujimura, H. Fujiwara, and T. Hamaoka. 2001. A role of interferon-gamma (IFN-gamma) in tumor immunity: T cells with the capacity to reject tumor cells are generated but fail to migrate to tumor sites in IFN-gamma-deficient mice. *Cancer Res* 61:3399-3405.

Nizard, M., H. Roussel, M.O. Diniz, S. Karaki, T. Tran, T. Voron, E. Dransart, F. Sandoval, M. Riquet, B. Rance, E. Marcheteau, E. Fabre, M. Mandavit, M. Terme, C. Blanc, J.B. Escudie, L. Gibault, F.L.P. Barthes, C. Granier, L.C.S. Ferreira, C. Badoual, L. Johannes, and E. Tartour. 2017. Induction of resident memory T cells enhances the efficacy of cancer vaccine. *Nat Commun* 8:15221.

Northrop, J.K., R.M. Thomas, A.D. Wells, and H. Shen. 2006. Epigenetic remodeling of the IL-2 and IFN-gamma loci in memory CD8 T cells is influenced by CD4 T cells. *J Immunol* 177:1062-1069.

O'Brien, S.M., A. Klampatsa, J.C. Thompson, M.C. Martinez, W.T. Hwang, A.S. Rao, J.E. Standalick, S. Kim, E. Cantu, L.A. Litzky, S. Singhal, E.B. Eruslanov, E.K. Moon, and S.M. Albelda. 2019. Function of Human Tumor-Infiltrating Lymphocytes in Early-Stage Non-Small Cell Lung Cancer. *Cancer Immunol Res* 7:896-909.

Oettinger, M.A. 2004. How to keep V(D)J recombination under control. *Immunol Rev* 200:165-181.

Okazaki, T., S. Chikuma, Y. Iwai, S. Fagarasan, and T. Honjo. 2013. A rheostat for immune responses: the unique properties of PD-1 and their advantages for clinical application. *Nat Immunol* 14:1212-1218.

Osta, W.A., Y. Chen, K. Mikhitarian, M. Mitas, M. Salem, Y.A. Hannun, D.J. Cole, and W.E. Gillanders. 2004. EpCAM is overexpressed in breast cancer and is a potential target for breast cancer gene therapy. *Cancer Res* 64:5818-5824.

Pallett, L.J., J. Davies, E.J. Colbeck, F. Robertson, N. Hansi, N.J.W. Easom, A.R. Burton, K.A. Stegmann, A. Schurich, L. Swadling, U.S. Gill, V. Male, T. Luong, A. Gander, B.R. Davidson, P.T.F. Kennedy, and M.K. Maini. 2017. IL-2(high) tissue-resident T cells in the human liver: Sentinels for hepatotropic infection. *J Exp Med* 214:1567-1580.

Pan, Y., T. Tian, C.O. Park, S.Y. Lofftus, S. Mei, X. Liu, C. Luo, J.T. O'Malley, A. Gehad, J.E. Teague, S.J. Divito, R. Fuhlbrigge, P. Puigserver, J.G. Krueger, G.S. Hotamisligil, R.A. Clark, and T.S. Kupper. 2017. Survival of tissue-resident memory T cells requires exogenous lipid uptake and metabolism. *Nature* 543:252-256.

Patsoukis, N., K. Bardhan, P. Chatterjee, D. Sari, B. Liu, L.N. Bell, E.D. Karoly, G.J. Freeman, V. Petkova, P. Seth, L. Li, and V.A. Boussiotis. 2015. PD-1 alters T-cell metabolic reprogramming by inhibiting glycolysis and promoting lipolysis and fatty acid oxidation. *Nat Commun* 6:6692.

Pauken, K.E., M.A. Sammons, P.M. Odorizzi, S. Manne, J. Godec, O. Khan, A.M. Drake, Z. Chen, D.R. Sen, M. Kurachi, R.A. Barnitz, C. Bartman, B. Bengsch, A.C. Huang, J.M. Schenkel, G. Vahedi, W.N. Haining, S.L. Berger, and E.J. Wherry. 2016. Epigenetic stability of exhausted T cells limits durability of reinvigoration by PD-1 blockade. *Science* 354:1160-1165.

Pauken, K.E., and E.J. Wherry. 2015. SnapShot: T Cell Exhaustion. *Cell* 163:1038-1038 e1031.

Pauls, K., M. Schon, R.C. Kubitza, B. Homey, A. Wiesenborn, P. Lehmann, T. Ruzicka, C.M. Parker, and M.P. Schon. 2001. Role of integrin alphaE(CD103)beta7 for tissue-specific epidermal localization of CD8+ T lymphocytes. *J Invest Dermatol* 117:569-575.

Pell, R., K. Oien, M. Robinson, H. Pitman, N. Rajpoot, J. Rittscher, D. Snead, C. Verrill, and U.K.N.C.R.I.C.-M.P.q.a.w. group. 2019. The use of digital pathology and image analysis in clinical trials. *J Pathol Clin Res* 5:81-90.

Penix, L.A., M.T. Sweetser, W.M. Weaver, J.P. Hoeffler, T.K. Kerppola, and C.B. Wilson. 1996. The proximal regulatory element of the interferon-gamma promoter mediates selective expression in T cells. *J Biol Chem* 271:31964-31972.

Phan, G.Q., J.C. Yang, R.M. Sherry, P. Hwu, S.L. Topalian, D.J. Schwartzentruber, N.P. Restifo, L.R. Haworth, C.A. Seipp, L.J. Freezer, K.E. Morton, S.A. Mavroukakis, P.H. Duray, S.M. Steinberg, J.P. Allison, T.A. Davis, and S.A. Rosenberg. 2003. Cancer regression and autoimmunity induced by cytotoxic T lymphocyte-associated antigen 4 blockade in patients with metastatic melanoma. *Proc Natl Acad Sci U S A* 100:8372-8377.

Piet, B., G.J. de Bree, B.S. Smids-Dierdorp, C.M. van der Loos, E.B. Remmerswaal, J.H. von der Thusen, J.M. van Haarst, J.P. Eerenberg, A. ten Brinke, W. van der Bij, W. Timens, R.A. van Lier, and R.E. Jonkers. 2011. CD8(+) T cells with an intraepithelial phenotype upregulate cytotoxic function upon influenza infection in human lung. *J Clin Invest* 121:2254-2263.

Podlaha, O., S. De, M. Gonen, and F. Michor. 2014. Histone modifications are associated with transcript isoform diversity in normal and cancer cells. *PLoS Comput Biol* 10:e1003611.

Powles, T., J.P. Eder, G.D. Fine, F.S. Braiteh, Y. Loriot, C. Cruz, J. Bellmunt, H.A. Burris, D.P. Petrylak, S.L. Teng, X. Shen, Z. Boyd, P.S. Hegde, D.S. Chen, and N.J. Vogelzang. 2014. MPDL3280A (anti-PD-L1) treatment leads to clinical activity in metastatic bladder cancer. *Nature* 515:558-562.

Price, D.A., T.E. Asher, N.A. Wilson, M.C. Nason, J.M. Brenchley, I.S. Metzler, V. Venturi, E. Gostick, P.K. Chattopadhyay, M. Roederer, M.P. Davenport, D.I. Watkins, and D.C. Douek. 2009. Public clonotype usage identifies protective Gag-specific CD8+ T cell responses in SIV infection. *J Exp Med* 206:923-936.

Purbhoo, M.A., D.H. Sutton, J.E. Brewer, R.E. Mullings, M.E. Hill, T.M. Mahon, J. Karbach, E. Jager, B.J. Cameron, N. Lissin, P. Vyas, J.L. Chen, V. Cerundolo, and B.K. Jakobsen. 2006. Quantifying and imaging NY-ESO-1/LAGE-1-derived epitopes on tumor cells using high affinity T cell receptors. *J Immunol* 176:7308-7316.

Qiu, J., M. Villa, D.E. Sanin, M.D. Buck, D. O'Sullivan, R. Ching, M. Matsushita, K.M. Grzes, F. Winkler, C.H. Chang, J.D. Curtis, R.L. Kyle, N. Van Teijlingen Bakker, M. Corrado, F. Haessler, F. Alfei, J. Edwards-Hicks, L.B. Maggi, Jr., D. Zehn, T. Egawa, B. Bengsch, R.I. Klein Geltink, T. Jenuwein, E.J. Pearce, and E.L. Pearce. 2019. Acetate Promotes T Cell Effector Function during Glucose Restriction. *Cell Rep* 27:2063-2074 e2065.

Qu, Y., G. Mu, Y. Wu, X. Dai, F. Zhou, X. Xu, Y. Wang, and F. Wei. 2010. Overexpression of DNA methyltransferases 1, 3a, and 3b significantly correlates with retinoblastoma tumorigenesis. *Am J Clin Pathol* 134:826-834.

Quinn, E., N. Hawkins, Y.L. Yip, C. Suter, and R. Ward. 2003. CD103+ intraepithelial lymphocytes--a unique population in microsatellite unstable sporadic colorectal cancer. *Eur J Cancer* 39:469-475.

Rabbitts, T.H., M.P. Lefranc, M.A. Stinson, J.E. Sims, J. Schroder, M. Steinmetz, N.L. Spurr, E. Solomon, and P.N. Goodfellow. 1985. The chromosomal location of T-cell receptor genes and a T cell rearranging gene: possible correlation with specific translocations in human T cell leukaemia. *EMBO J* 4:1461-1465.

Radvanyi, L.G., C. Bernatchez, M. Zhang, P.S. Fox, P. Miller, J. Chacon, R. Wu, G. Lizee, S. Mahoney, G. Alvarado, M. Glass, V.E. Johnson, J.D. McMannis, E. Shpall, V. Prieto, N. Papadopoulos, K. Kim, J. Homsi, A. Bedikian, W.J. Hwu, S. Patel, M.I. Ross, J.E. Lee, J.E. Gershenwald, A. Lucci, R. Royal, J.N. Cormier, M.A. Davies, R. Mansaray, O.J. Fulbright, C. Toth, R. Ramachandran, S. Wardell, A. Gonzalez, and P. Hwu. 2012. Specific lymphocyte subsets predict response to adoptive cell therapy using expanded autologous tumor-infiltrating lymphocytes in metastatic melanoma patients. *Clin Cancer Res* 18:6758-6770.

Reth, M. 1989. Antigen receptor tail clue. *Nature* 338:383-384.

Roberts, E.W., M.L. Broz, M. Binnewies, M.B. Headley, A.E. Nelson, D.M. Wolf, T. Kaisho, D. Bogunovic, N. Bhardwaj, and M.F. Krummel. 2016. Critical Role for CD103(+)/CD141(+) Dendritic Cells Bearing CCR7 for Tumor Antigen Trafficking and Priming of T Cell Immunity in Melanoma. *Cancer Cell* 30:324-336.

Robinson, J., A. Malik, P. Parham, J.G. Bodmer, and S.G. Marsh. 2000. IMGT/HLA database--a sequence database for the human major histocompatibility complex. *Tissue Antigens* 55:280-287.

Roose, J.P., M. Mollenauer, V.A. Gupta, J. Stone, and A. Weiss. 2005. A diacylglycerol-protein kinase C-RasGRP1 pathway directs Ras activation upon antigen receptor stimulation of T cells. *Mol Cell Biol* 25:4426-4441.

Rota, G., C. Niogret, A.T. Dang, C.R. Barros, N.P. Fonta, F. Alfei, L. Morgado, D. Zehn, W. Birchmeier, E. Vivier, and G. Guarda. 2018. Shp-2 Is Dispensable for Establishing T Cell Exhaustion and for PD-1 Signaling In Vivo. *Cell Rep* 23:39-49.

Rothstein, T.L., M. Mage, G. Jones, and L.L. McHugh. 1978. Cytotoxic T lymphocyte sequential killing of immobilized allogeneic tumor target cells measured by time-lapse microcinematography. *J Immunol* 121:1652-1656.

Ruffell, B., D. Chang-Strachan, V. Chan, A. Rosenbusch, C.M. Ho, N. Pryer, D. Daniel, E.S. Hwang, H.S. Rugo, and L.M. Coussens. 2014. Macrophage IL-10 blocks CD8+ T cell-dependent responses to chemotherapy by suppressing IL-12 expression in intratumoral dendritic cells. *Cancer Cell* 26:623-637.

Russell, S.M., A.D. Keegan, N. Harada, Y. Nakamura, M. Noguchi, P. Leland, M.C. Friedmann, A. Miyajima, R.K. Puri, W.E. Paul, and et al. 1993. Interleukin-2 receptor gamma chain: a functional component of the interleukin-4 receptor. *Science* 262:1880-1883.

Saias, L., A. Gomes, M. Cazales, B. Ducommun, and V. Lobjois. 2015. Cell-Cell Adhesion and Cytoskeleton Tension Oppose Each Other in Regulating Tumor Cell Aggregation. *Cancer Res* 75:2426-2433.

Sakuishi, K., L. Apetoh, J.M. Sullivan, B.R. Blazar, V.K. Kuchroo, and A.C. Anderson. 2010. Targeting Tim-3 and PD-1 pathways to reverse T cell exhaustion and restore anti-tumor immunity. *J Exp Med* 207:2187-2194.

Salmon, H., J. Idoyaga, A. Rahman, M. Leboeuf, R. Remark, S. Jordan, M. Casanova-Acebes, M. Khudoynazarova, J. Agudo, N. Tung, S. Chakarov, C. Rivera, B. Hogstad, M. Bosenberg, D. Hashimoto, S. Gnjatic, N. Bhardwaj, A.K. Palucka, B.D. Brown, J. Brody, F. Ginhoux, and M. Merad. 2016. Expansion and Activation of CD103(+)

Dendritic Cell Progenitors at the Tumor Site Enhances Tumor Responses to Therapeutic PD-L1 and BRAF Inhibition. *Immunity* 44:924-938.

Samten, B., J.C. Townsend, S.E. Weis, A. Bhoumik, P. Klucar, H. Shams, and P.F. Barnes. 2008. CREB, ATF, and AP-1 transcription factors regulate IFN-gamma secretion by human T cells in response to mycobacterial antigen. *J Immunol* 181:2056-2064.

Sandoval, F., M. Terme, M. Nizard, C. Badoual, M.F. Bureau, L. Freyburger, O. Clement, E. Marcheteau, A. Gey, G. Fraisse, C. Bouguin, N. Merillon, E. Dransart, T. Tran, F. Quintin-Colonna, G. Autret, M. Thiebaud, M. Suleman, S. Riffault, T.C. Wu, O. Launay, C. Danel, J. Taieb, J. Richardson, L. Zitvogel, W.H. Fridman, L. Johannes, and E. Tartour. 2013. Mucosal imprinting of vaccine-induced CD8(+) T cells is crucial to inhibit the growth of mucosal tumors. *Sci Transl Med* 5:172ra120.

Sansom, D.M. 2000. CD28, CTLA-4 and their ligands: who does what and to whom? *Immunology* 101:169-177.

Sargentini, V., S. Mariotti, S. Carrara, M.C. Gagliardi, R. Teloni, D. Goletti, and R. Nisini. 2009. Cytometric detection of antigen-specific IFN-gamma/IL-2 secreting cells in the diagnosis of tuberculosis. *BMC Infect Dis* 9:99.

Sathaliyawala, T., M. Kubota, N. Yudanin, D. Turner, P. Camp, J.J. Thome, K.L. Bickham, H. Lerner, M. Goldstein, M. Sykes, T. Kato, and D.L. Farber. 2013. Distribution and compartmentalization of human circulating and tissue-resident memory T cell subsets. *Immunity* 38:187-197.

Scarlett, U.K., M.R. Rutkowski, A.M. Rauwerdink, J. Fields, X. Escovar-Fadul, J. Baird, J.R. Cubillos-Ruiz, A.C. Jacobs, J.L. Gonzalez, J. Weaver, S. Fiering, and J.R. Conejo-

Garcia. 2012. Ovarian cancer progression is controlled by phenotypic changes in dendritic cells. *J Exp Med* 209:495-506.

Schneider, P., J.L. Bodmer, M. Thome, K. Hofmann, N. Holler, and J. Tschopp. 1997. Characterization of two receptors for TRAIL. *FEBS Lett* 416:329-334.

Sedy, J.R., M. Gavrieli, K.G. Potter, M.A. Hurchla, R.C. Lindsley, K. Hildner, S. Scheu, K. Pfeffer, C.F. Ware, T.L. Murphy, and K.M. Murphy. 2005. B and T lymphocyte attenuator regulates T cell activation through interaction with herpesvirus entry mediator. *Nat Immunol* 6:90-98.

Segal, N.H., A.R. He, T. Doi, R. Levy, S. Bhatia, M.J. Pishvaian, R. Cesari, Y. Chen, C.B. Davis, B. Huang, A.D. Thall, and A.K. Gopal. 2018. Phase I Study of Single-Agent Utomilumab (PF-05082566), a 4-1BB/CD137 Agonist, in Patients with Advanced Cancer. *Clin Cancer Res* 24:1816-1823.

Seidman, J.G., E.E. Max, and P. Leder. 1979. A kappa-immunoglobulin gene is formed by site-specific recombination without further somatic mutation. *Nature* 280:370-375.

Seliger, B., K. Schreiber, K. Delp, M. Meissner, S. Hammers, T. Reichert, K. Pawlischko, R. Tampe, and C. Huber. 2001. Downregulation of the constitutive tapasin expression in human tumor cells of distinct origin and its transcriptional upregulation by cytokines. *Tissue Antigens* 57:39-45.

Shen, C., T. Xu, Y. Wu, X. Li, L. Xia, W. Wang, K.A. Shahzad, L. Zhang, X. Wan, and J. Qiu. 2017. Frequency and reactivity of antigen-specific T cells were concurrently measured through the combination of artificial antigen-presenting cell, MACS and ELISPOT. *Sci Rep* 7:16400.

Shen, D.T., J.S. Ma, J. Mather, S. Vukmanovic, and S. Radoja. 2006. Activation of primary T lymphocytes results in lysosome development and polarized granule exocytosis in CD4+ and CD8+ subsets, whereas expression of lytic molecules confers cytotoxicity to CD8+ T cells. *J Leukoc Biol* 80:827-837.

Sheng, S.Y., Y. Gu, C.G. Lu, J.Y. Zou, H. Hong, and R. Wang. 2017. The distribution and function of human memory T cell subsets in lung cancer. *Immunol Res* 65:639-650.

Sheppard, K.A., L.J. Fitz, J.M. Lee, C. Benander, J.A. George, J. Wooters, Y. Qiu, J.M. Jussif, L.L. Carter, C.R. Wood, and D. Chaudhary. 2004. PD-1 inhibits T-cell receptor induced phosphorylation of the ZAP70/CD3zeta signalosome and downstream signaling to PKCtheta. *FEBS Lett* 574:37-41.

Shields, B.D., B. Koss, E.M. Taylor, A.J. Storey, K.L. West, S.D. Byrum, S.G. Mackintosh, R. Edmondson, F. Mahmoud, S.C. Shalin, and A.J. Tackett. 2019. Loss of E-Cadherin Inhibits CD103 Antitumor Activity and Reduces Checkpoint Blockade Responsiveness in Melanoma. *Cancer Res* 79:1113-1123.

Shim, E.K., S.H. Jung, and J.R. Lee. 2011. Role of two adaptor molecules SLP-76 and LAT in the PI3K signaling pathway in activated T cells. *J Immunol* 186:2926-2935.

Shuford, W.W., K. Klussman, D.D. Tritchler, D.T. Loo, J. Chalupny, A.W. Siadak, T.J. Brown, J. Emswiler, H. Raecho, C.P. Larsen, T.C. Pearson, J.A. Ledbetter, A. Aruffo, and R.S. Mittler. 1997. 4-1BB costimulatory signals preferentially induce CD8+ T cell proliferation and lead to the amplification in vivo of cytotoxic T cell responses. *J Exp Med* 186:47-55.

Siegel, P.M., and J. Massague. 2003. Cytostatic and apoptotic actions of TGF-beta in homeostasis and cancer. *Nat Rev Cancer* 3:807-821.

Skon, C.N., J.Y. Lee, K.G. Anderson, D. Masopust, K.A. Hogquist, and S.C. Jameson. 2013. Transcriptional downregulation of S1pr1 is required for the establishment of resident memory CD8+ T cells. *Nat Immunol* 14:1285-1293.

Slingluff, C.L., Jr., G.R. Petroni, K.A. Chianese-Bullock, M.E. Smolkin, S. Hibbitts, C. Murphy, N. Johansen, W.W. Grosh, G.V. Yamshchikov, P.Y. Neese, J.W. Patterson, R. Fink, and P.K. Rehm. 2007. Immunologic and clinical outcomes of a randomized phase II trial of two multipeptide vaccines for melanoma in the adjuvant setting. *Clin Cancer Res* 13:6386-6395.

Smith-Garvin, J.E., G.A. Koretzky, and M.S. Jordan. 2009. T cell activation. *Annu Rev Immunol* 27:591-619.

Spranger, S., R. Bao, and T.F. Gajewski. 2015. Melanoma-intrinsic beta-catenin signalling prevents anti-tumour immunity. *Nature* 523:231-235.

Stauber, D.J., E.W. Debler, P.A. Horton, K.A. Smith, and I.A. Wilson. 2006. Crystal structure of the IL-2 signaling complex: paradigm for a heterotrimeric cytokine receptor. *Proc Natl Acad Sci U S A* 103:2788-2793.

Strong, R.K., M.A. Holmes, P. Li, L. Braun, N. Lee, and D.E. Geraghty. 2003. HLA-E allelic variants. Correlating differential expression, peptide affinities, crystal structures, and thermal stabilities. *J Biol Chem* 278:5082-5090.

Suffia, I., S.K. Reckling, G. Salay, and Y. Belkaid. 2005. A role for CD103 in the retention of CD4+CD25+ Treg and control of Leishmania major infection. *J Immunol* 174:5444-5455.

Sun, L., G. Wu, J.K. Willson, E. Zborowska, J. Yang, I. Rajkarunanayake, J. Wang, L.E. Gentry, X.F. Wang, and M.G. Brattain. 1994. Expression of transforming growth factor beta

type II receptor leads to reduced malignancy in human breast cancer MCF-7 cells. *J Biol Chem* 269:26449-26455.

Surh, C.D., and J. Sprent. 1994. T-cell apoptosis detected in situ during positive and negative selection in the thymus. *Nature* 372:100-103.

Takahashi, T., T. Tagami, S. Yamazaki, T. Uede, J. Shimizu, N. Sakaguchi, T.W. Mak, and S. Sakaguchi. 2000. Immunologic self-tolerance maintained by CD25(+)CD4(+) regulatory T cells constitutively expressing cytotoxic T lymphocyte-associated antigen 4. *J Exp Med* 192:303-310.

Takeshita, T., H. Asao, K. Ohtani, N. Ishii, S. Kumaki, N. Tanaka, H. Munakata, M. Nakamura, and K. Sugamura. 1992. Cloning of the gamma chain of the human IL-2 receptor. *Science* 257:379-382.

Taylor, P.A., A. Panoskaltsis-Mortari, G.J. Freeman, A.H. Sharpe, R.J. Noelle, A.Y. Rudensky, T.W. Mak, J.S. Serody, and B.R. Blazar. 2005. Targeting of inducible costimulator (ICOS) expressed on alloreactive T cells down-regulates graft-versus-host disease (GVHD) and facilitates engraftment of allogeneic bone marrow (BM). *Blood* 105:3372-3380.

Teixeira, C., S.L. Stang, Y. Zheng, N.S. Beswick, and J.C. Stone. 2003. Integration of DAG signaling systems mediated by PKC-dependent phosphorylation of RasGRP3. *Blood* 102:1414-1420.

Tessmer, M.S., C. Fugere, F. Stevenaert, O.V. Naidenko, H.J. Chong, G. Leclercq, and L. Brossay. 2007. KLRG1 binds cadherins and preferentially associates with SHIP-1. *Int Immunol* 19:391-400.

Thiery, J., D. Keefe, S. Boulant, E. Boucrot, M. Walch, D. Martinvalet, I.S. Goping, R.C. Bleackley, T. Kirchhausen, and J. Lieberman. 2011. Perforin pores in the endosomal membrane trigger the release of endocytosed granzyme B into the cytosol of target cells. *Nat Immunol* 12:770-777.

Thomas, S., S.A. Xue, C.R. Bangham, B.K. Jakobsen, E.C. Morris, and H.J. Stauss. 2011. Human T cells expressing affinity-matured TCR display accelerated responses but fail to recognize low density of MHC-peptide antigen. *Blood* 118:319-329.

Thommen, D.S., V.H. Koelzer, P. Herzig, A. Roller, M. Trefny, S. Dimeloe, A. Kiialainen, J. Hanhart, C. Schill, C. Hess, S. Savic Prince, M. Wiese, D. Lardinois, P.C. Ho, C. Klein, V. Karanikas, K.D. Mertz, T.N. Schumacher, and A. Zippelius. 2018. A transcriptionally and functionally distinct PD-1(+) CD8(+) T cell pool with predictive potential in non-small-cell lung cancer treated with PD-1 blockade. *Nat Med* 24:994-1004.

Tomasec, P., V.M. Braud, C. Rickards, M.B. Powell, B.P. McSharry, S. Gadola, V. Cerundolo, L.K. Borysiewicz, A.J. McMichael, and G.W. Wilkinson. 2000. Surface expression of HLA-E, an inhibitor of natural killer cells, enhanced by human cytomegalovirus gpUL40. *Science* 287:1031.

Tomita, K., A. van Bokhoven, G.J. van Leenders, E.T. Ruijter, C.F. Jansen, M.J. Bussemakers, and J.A. Schalken. 2000. Cadherin switching in human prostate cancer progression. *Cancer Res* 60:3650-3654.

Topalian, S.L., F.S. Hodi, J.R. Brahmer, S.N. Gettinger, D.C. Smith, D.F. McDermott, J.D. Powderly, R.D. Carvajal, J.A. Sosman, M.B. Atkins, P.D. Leming, D.R. Spigel, S.J. Antonia, L. Horn, C.G. Drake, D.M. Pardoll, L. Chen, W.H. Sharfman, R.A. Anders,

J.M. Taube, T.L. McMiller, H. Xu, A.J. Korman, M. Jure-Kunkel, S. Agrawal, D. McDonald, G.D. Kollia, A. Gupta, J.M. Wigginton, and M. Sznol. 2012. Safety, activity, and immune correlates of anti-PD-1 antibody in cancer. *N Engl J Med* 366:2443-2454.

Trilling, M., V.T. Le, A. Zimmermann, H. Ludwig, K. Pfeffer, G. Sutter, G.L. Smith, and H. Hengel. 2009. Gamma interferon-induced interferon regulatory factor 1-dependent antiviral response inhibits vaccinia virus replication in mouse but not human fibroblasts. *J Virol* 83:3684-3695.

Tseng, D., J.P. Volkmer, S.B. Willingham, H. Contreras-Trujillo, J.W. Fathman, N.B. Fernhoff, J. Seita, M.A. Inlay, K. Weiskopf, M. Miyanishi, and I.L. Weissman. 2013. Anti-CD47 antibody-mediated phagocytosis of cancer by macrophages primes an effective antitumor T-cell response. *Proc Natl Acad Sci U S A* 110:11103-11108.

Tumeh, P.C., C.L. Harview, J.H. Yearley, I.P. Shintaku, E.J. Taylor, L. Robert, B. Chmielowski, M. Spasic, G. Henry, V. Ciobanu, A.N. West, M. Carmona, C. Kivork, E. Seja, G. Cherry, A.J. Gutierrez, T.R. Grogan, C. Mateus, G. Tomasic, J.A. Glaspy, R.O. Emerson, H. Robins, R.H. Pierce, D.A. Elashoff, C. Robert, and A. Ribas. 2014. PD-1 blockade induces responses by inhibiting adaptive immune resistance. *Nature* 515:568-571.

Ulbrecht, M., S. Martinozzi, M. Grzeschik, H. Hengel, J.W. Ellwart, M. Pla, and E.H. Weiss. 2000. Cutting edge: the human cytomegalovirus UL40 gene product contains a ligand for HLA-E and prevents NK cell-mediated lysis. *J Immunol* 164:5019-5022.

van Meijgaarden, K.E., M.C. Haks, N. Caccamo, F. Dieli, T.H. Ottenhoff, and S.A. Joosten. 2015. Human CD8+ T-cells recognizing peptides from Mycobacterium tuberculosis (Mtb) presented by HLA-E have an unorthodox Th2-like, multifunctional, Mtb

inhibitory phenotype and represent a novel human T-cell subset. *PLoS Pathog* 11:e1004671.

van Montfoort, N., L. Borst, M.J. Korrer, M. Sluijter, K.A. Marijt, S.J. Santegoets, V.J. van Ham, I. Ehsan, P. Charoentong, P. Andre, N. Wagtmann, M.J.P. Welters, Y.J. Kim, S.J. Piersma, S.H. van der Burg, and T. van Hall. 2018. NKG2A Blockade Potentiates CD8 T Cell Immunity Induced by Cancer Vaccines. *Cell* 175:1744-1755 e1715.

Vezys, V., P. Penaloza-MacMaster, D.L. Barber, S.J. Ha, B. Konieczny, G.J. Freeman, R.S. Mittler, and R. Ahmed. 2011. 4-1BB signaling synergizes with programmed death ligand 1 blockade to augment CD8 T cell responses during chronic viral infection. *J Immunol* 187:1634-1642.

Vidric, M., W.K. Suh, U. Dianzani, T.W. Mak, and T.H. Watts. 2005. Cooperation between 4-1BB and ICOS in the immune response to influenza virus revealed by studies of CD28/ICOS-deficient mice. *J Immunol* 175:7288-7296.

Wajant, H., K. Pfizenmaier, and P. Scheurich. 2003. Tumor necrosis factor signaling. *Cell Death Differ* 10:45-65.

Wang, B., S. Wu, H. Zeng, Z. Liu, W. Dong, W. He, X. Chen, X. Dong, L. Zheng, T. Lin, and J. Huang. 2015. CD103+ Tumor Infiltrating Lymphocytes Predict a Favorable Prognosis in Urothelial Cell Carcinoma of the Bladder. *J Urol* 194:556-562.

Wang, C., A.J. McPherson, R.B. Jones, K.S. Kawamura, G.H. Lin, P.A. Lang, T. Ambagala, M. Pellegrini, T. Calzascia, N. Aidarus, A.R. Elford, F.Y. Yue, E. Kremmer, C.M. Kovacs, E. Benko, C. Tremblay, J.P. Routy, N.F. Bernard, M.A. Ostrowski, P.S. Ohashi, and T.H. Watts. 2012. Loss of the signaling adaptor TRAF1 causes CD8+ T cell dysregulation during human and murine chronic infection. *J Exp Med* 209:77-91.

Webb, J.R., K. Milne, P. Watson, R.J. Deleeuw, and B.H. Nelson. 2014. Tumor-infiltrating lymphocytes expressing the tissue resident memory marker CD103 are associated with increased survival in high-grade serous ovarian cancer. *Clin Cancer Res* 20:434-444.

Weissmann, S., P.A. Cloos, S. Sidoli, O.N. Jensen, S. Pollard, and K. Helin. 2018. The Tumor Suppressor CIC Directly Regulates MAPK Pathway Genes via Histone Deacetylation. *Cancer Res* 78:4114-4125.

White, G.P., P.M. Watt, B.J. Holt, and P.G. Holt. 2002. Differential patterns of methylation of the IFN-gamma promoter at CpG and non-CpG sites underlie differences in IFN-gamma gene expression between human neonatal and adult CD45RO- T cells. *J Immunol* 168:2820-2827.

Yewdell, J.W., and S.M. Haeryfar. 2005. Understanding presentation of viral antigens to CD8+ T cells in vivo: the key to rational vaccine design. *Annu Rev Immunol* 23:651-682.

Youngblood, B.A., H. Ghoniem, A. Moustaki, P. Dogra, H.A. Abdelsamed, and Y. Fan. 2017. Tumor infiltrating T cells acquire exhaustion-associated epigenetic programs. *The Journal of Immunology* 198:56.56-56.56.

Yu, C.I., C. Becker, Y. Wang, F. Marches, J. Helft, M. Leboeuf, E. Anguiano, S. Pourpe, K. Goller, V. Pascual, J. Banchereau, M. Merad, and K. Palucka. 2013. Human CD1c+ dendritic cells drive the differentiation of CD103+ CD8+ mucosal effector T cells via the cytokine TGF-beta. *Immunity* 38:818-830.

Yu, X., K. Harden, L.C. Gonzalez, M. Francesco, E. Chiang, B. Irving, I. Tom, S. Ivelja, C.J. Refino, H. Clark, D. Eaton, and J.L. Grogan. 2009. The surface protein TIGIT suppresses T cell activation by promoting the generation of mature immunoregulatory dendritic cells. *Nat Immunol* 10:48-57.

Zaugg, K., Y. Yao, P.T. Reilly, K. Kannan, R. Kiarash, J. Mason, P. Huang, S.K. Sawyer, B. Fuerth, B. Faubert, T. Kalliomaki, A. Elia, X. Luo, V. Nadeem, D. Bungard, S. Yalavarthi, J.D. Growney, A. Wakeham, Y. Moolani, J. Silvester, A.Y. Ten, W. Bakker, K. Tsuchihara, S.L. Berger, R.P. Hill, R.G. Jones, M. Tsao, M.O. Robinson, C.B. Thompson, G. Pan, and T.W. Mak. 2011. Carnitine palmitoyltransferase 1C promotes cell survival and tumor growth under conditions of metabolic stress. *Genes Dev* 25:1041-1051.

Zhang, C., Y. Peng, P. Hublitz, H. Zhang, and T. Dong. 2018. Genetic abrogation of immune checkpoints in antigen-specific cytotoxic T-lymphocyte as a potential alternative to blockade immunotherapy. *Sci Rep* 8:5549.

Zhang, L., T.F. Gajewski, and J. Kline. 2009. PD-1/PD-L1 interactions inhibit antitumor immune responses in a murine acute myeloid leukemia model. *Blood* 114:1545-1552.